

Mechanistic studies on quadruple hydrogen bonding systems

Citation for published version (APA):

Greef, de, T. F. A. (2009). *Mechanistic studies on quadruple hydrogen bonding systems*. [Phd Thesis 1 (Research TU/e / Graduation TU/e), Chemical Engineering and Chemistry]. Technische Universiteit Eindhoven. <https://doi.org/10.6100/IR640448>

DOI:

[10.6100/IR640448](https://doi.org/10.6100/IR640448)

Document status and date:

Published: 01/01/2009

Document Version:

Publisher's PDF, also known as Version of Record (includes final page, issue and volume numbers)

Please check the document version of this publication:

- A submitted manuscript is the version of the article upon submission and before peer-review. There can be important differences between the submitted version and the official published version of record. People interested in the research are advised to contact the author for the final version of the publication, or visit the DOI to the publisher's website.
- The final author version and the galley proof are versions of the publication after peer review.
- The final published version features the final layout of the paper including the volume, issue and page numbers.

[Link to publication](#)

General rights

Copyright and moral rights for the publications made accessible in the public portal are retained by the authors and/or other copyright owners and it is a condition of accessing publications that users recognise and abide by the legal requirements associated with these rights.

- Users may download and print one copy of any publication from the public portal for the purpose of private study or research.
- You may not further distribute the material or use it for any profit-making activity or commercial gain
- You may freely distribute the URL identifying the publication in the public portal.

If the publication is distributed under the terms of Article 25fa of the Dutch Copyright Act, indicated by the "Taverne" license above, please follow below link for the End User Agreement:

www.tue.nl/taverne

Take down policy

If you believe that this document breaches copyright please contact us at:

openaccess@tue.nl

providing details and we will investigate your claim.

Mechanistic Studies on Quadruple Hydrogen Bonding Systems

PROEFSCHRIFT

ter verkrijging van de graad van doctor
aan de Technische Universiteit Eindhoven,
op gezag van de Rector Magnificus,
prof.dr.ir. C.J. van Duijn, voor een commissie
aangewezen door het College voor Promoties
in het openbaar te verdedigen
op maandag 16 februari 2009 om 16.00 uur

door

Tom Franciscus Antonius de Greef

geboren te Eindhoven

Dit proefschrift is goedgekeurd door de promotoren:

prof.dr. E.W. Meijer

en

prof.dr. R.P. Sijbesma

This research has been financially supported by the Netherlands Organization for Scientific Research, Chemical Sciences (NWO-CW).

Omslagontwerp: Paul Bos (ICMS animatie studio)

Druk: Gildeprint, Enschede.

A catalogue record is available from the Eindhoven University of Technology
Library

ISBN: 978-90-386-1514-1

"It is not order only, but unexpected order, that has value."

Henri Poincaré

Table of contents

Chapter 1

Supramolecular polymerization processes

1.1	Introduction	2
1.2	Isodesmic Polymerizations	4
	1.2.1 Definition and covalent counterpart	
	1.2.2 Physical aspects	
	1.2.3 Examples	
1.3	Ring-Chain supramolecular polymerizations	8
	1.3.1 Definition and covalent counterpart	
	1.3.2 Physical aspects	
	1.3.3 Examples	
1.4	Cooperative supramolecular polymerizations	15
	1.4.1 Definition and covalent counterpart	
	1.4.2 Physical aspects	
	1.4.3 Examples	
1.5	Conclusion and discussion	24
1.6	Aim and outline of this thesis	24
1.7	References	26

Chapter 2

Increasing selectivity in complementary quadruple hydrogen bonding

2.1	Introduction	32
2.2	Synthesis, self-assembly and tautomeric preference of various UPy derivatives	35
2.3	Screening the fidelity of hetero-complexation with 2,7-diamido-1,8-naphthyridine	40
2.4	Evaluation of dimerization constant and association constant of dibutyl-amino substituted UPy dimer with 2,7-diamido-1,8-naphthyridine	
2.5	Self-sorting in mixtures of DDAA and DADA hydrogen bonding units	44
2.6	Conclusions and discussion	47
2.7	Experimental section	49
2.8	Appendices	56
2.9	References	59

Chapter 3

The influence of selectivity on the supramolecular polymerization of AB type polymers capable of both A·A and A·B interactions

3.1	Introduction	64
3.2	Synthesis of AB monomers	66
3.3	Capillary viscosity measurements on AB monomers	67
3.4	¹ H-NMR and DOSY measurements	68
3.5	Theoretical model and simulations	69
3.6	Effect of A·A dimerization on the polydispersity	74
3.7	Discussion and conclusion	76
3.8	Experimental section	77
3.9	Appendices	82
3.10	References	88

Chapter 4

Kinetics of complementary quadruple hydrogen bonded dimers

4.1	Introduction	92
4.2	Kinetics of keto dimers	93
4.3	Kinetics of enol dimers	98
4.4	Kinetic product formation in mixtures of hydrogen bonded dimers	100
4.5	Summary and conclusions	102
4.6	Experimental section	102
4.7	Appendices	104
4.8	References	109

Chapter 5

Self-assembly of UPy dimers into one-dimensional stacks via lateral hydrogen bonding in solution

5.1	Introduction	114
5.2	Design and synthesis	115
5.3	Self-assembly of UPy-urea and UPy-urethane dimers in CDCl ₃	117
5.4	Heteromeric self-assembly of UPy / UPy-urea dimers in CDCl ₃	122
5.6	Discussion and conclusion	127
5.7	Experimental section	129
5.8	Appendices	140
5.9	References	148

Chapter 6

The influence of polar side chains on the thermodynamics of UPy based self-assemblies in apolar solvents

6.1	Introduction	152
6.2	The effect of ethylene oxide chains on UPy based self-assemblies	153
	6.2.1 Synthesis and design	
	6.2.2 Assessment of dimerization strength using ¹ H-NMR	
	6.2.3 Infrared spectroscopy	
	6.2.4 UV-Vis spectroscopy	
	6.2.5 How is the association constant with 2,7-diamido-1,8-naphthyridine affected?	
	6.2.6 Discussion and conclusion: the effect of short EO chains on the thermodynamics of UPy dimers in CDCl ₃	
6.3	The effect of polyacrylates on UPy based self-assemblies	167
	6.3.1 Synthesis and UPy dimerization strength	
	6.3.2 Hetero-dimerization strength	
6.4	The effect of ethylene oxide chains on the self-association of UPy-urea dimers in CDCl ₃	172
6.5	Discussion and conclusion	173
6.6	Experimental section	173
6.7	Appendices	186
6.8	References	189
	Summary	193
	Curriculum Vitae	195
	Dankwoord	197

1

Supramolecular polymerization processes

Abstract

The assembly of small and large natural molecules into larger structures plays an important role in various chemical, biological and physical processes. Synthetic supramolecular polymers aim to mimic the behaviour of their natural counterparts. Supramolecular polymers are defined as polymeric arrays of monomer units that are brought together by reversible and highly directional secondary interactions, resulting in polymeric properties in dilute and concentrated solution as well as in the bulk. The assembling of these one-dimensional systems produces equilibrium polymers in which the length distribution and average chain length is a function of both concentration and temperature. Their growth may occur by a step-by-step process akin to polycondensation, and by cooperative processes such as helical growth or ring-chain equilibria. In this chapter, the growth mechanisms of supramolecular polymers are critically reviewed and compared to the growth mechanisms of covalent polymers.

Part of this work has been published:

de Greef, T. F. A.; Meijer, E. W. *Nature* **2008**, 453, 171-173.

1.1 Introduction

The self-assembly of molecules to form large clusters under equilibrium conditions is a general phenomenon found widely in chemistry, physics and biology. Examples found in each field are ubiquitous and include living ionic polymerizations¹, the formation of molecular Bose–Einstein condensates² and the self-assembly of clathrin proteins³ during endocytosis. When the interaction between the monomers is generated by weak, reversible non-covalent, but highly directional, forces and those result in high-molecular weight, one-dimensional polymers under dilute conditions, the self-assembly is classified as a supramolecular polymerization process. Based on the current level of understanding, three different classification schemes for supramolecular polymers can be constructed.

Consider the supramolecular polymerization of ditopic monomers in solution leading to large one-dimensional polymers, the formation of which is driven by the reversible association of two end-groups, A and B. The two end-groups can be either connected via a (polymeric) spacer or they can be directly connected, as is the case in the self-assembly of disclike monomers. The reversible interaction can either occur between two self-complementary end-groups ($A = B$) or between two complementary end-groups ($A \neq B$). Using this notation, supramolecular polymerizations can be classified according to three different schemes: 1) the physical nature of the non-covalent force that lies at the origin of the reversible interaction 2) the type of monomer(s) used, and 3) the evolution of the energy of the system at equilibrium as a function of monomer conversion. In principle a fourth classification scheme based on the dimensionality of the aggregate is also possible. However, the addition of a second and third dimension will result in additional interaction energies and hence will directly influence the free energy of the self-assembled polymer as the concentration (or another thermodynamic force) is changed.

Previously, the physical nature of the various types of interactions that act as driving forces for the formation of large supramolecular assemblies has been extensively reviewed and their possible directional character was discussed.⁴ Examples of these interaction include: hydrogen bonds, π - π interactions, hydrophobic interactions and metal-ligand binding.

In the second classification scheme two groups are defined. The first class involves a *single* monomer containing either self-complementary or complementary end-group interactions. Examples of this include the supramolecular polymerization of an A_2 monomer in solution in which the reversible $A \cdot A$ interaction is self-complementary. Another example in this group is the supramolecular polymerization of an AB type monomer in which the reversible $A \cdot B$ interaction is complementary in nature. The

second class involves *two* different bifunctional monomers containing only one type of interaction. Examples of the second group include the supramolecular polymerization of an A_2 monomer with a B_2 monomer driven by a complementary $A \cdot B$ interaction.

The third classification scheme is based on the evolution of the energy of the system (consisting of monomer and polymer) as the monomer conversion, x (defined as the fraction of monomers present in reversible polymers), goes from zero ($x = 0$) to full conversion ($x = 1$). By introducing the concept of conversion a fundamental difference between covalent polymer chemistry and supramolecular polymer chemistry can be understood. Polymerization reactions involving covalent bond formation mostly occur under kinetic control as the potential barrier for back reaction (depolymerization) reaction is often much larger than for the forward reaction. As a result, dilution (or heating) of the polymerized material does not necessarily result in a change in the degree of conversion. This situation is very much different in supramolecular polymerizations where, due to thermodynamic equilibrium, the extent of reaction x is directly coupled to thermodynamic forces such as concentration, temperature and pressure. Several mechanisms are operative by which supramolecular polymers can grow into long polymers as the concentration of monomer or the temperature of the solution is changed. In this chapter the three major growth mechanisms (Scheme 1.1) available to supramolecular polymers in dilute solution will be discussed. An important physical aspect shared by two of these mechanisms is that they exhibit a critical point in their self-assembly pathway, characterized by a rapid change in the extent of polymerization.⁵

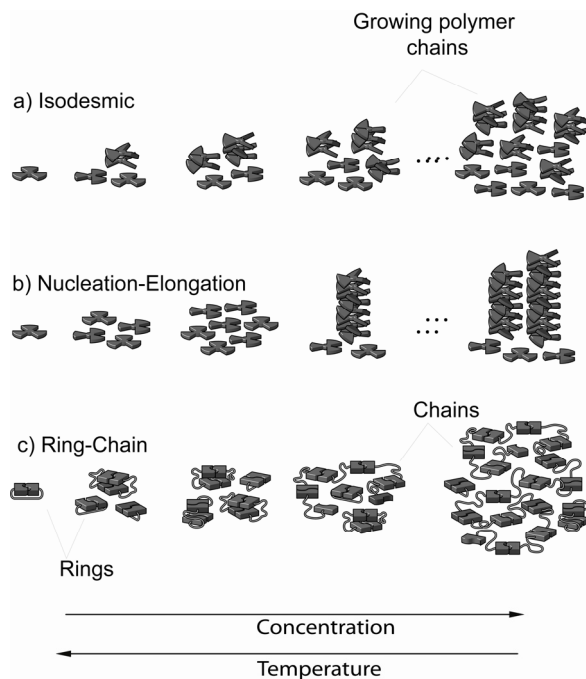
Based on the third scheme, three different types of supramolecular polymerizations are considered: isodesmic, ring-chain and nucleated (cooperative) supramolecular polymerizations. In the remaining part of this Chapter, a literature survey has been conducted and several examples of each type of supramolecular polymerization will be given.

1.2 Isodesmic Polymerizations

1.2.1 Definition and covalent counterpart

The first class of supramolecular polymerizations is represented by the reversible formation of a single non-covalent bond that is *identical* at all steps of the polymerization process (Scheme 1.1a). This implies that the reactivity of the end groups during the supramolecular polymerization process does not change due to neighbouring group effects or additional interaction energies between non-adjacent sites. In addition, an isodesmic supramolecular polymerization is characterized by the absence of cyclic

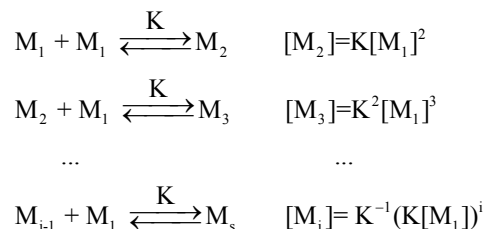
intermediates during the self-assembly pathway. The equivalent in covalent chemistry is a step-by-step polycondensation that obeys Flory's "principle of equal reactivity"⁶ and in which intramolecular cyclisation reactions do not occur (*vide infra*). An example of such a polymerization is the polycondensation of sebacoyl chloride ($\text{Cl-OC}(\text{CH}_2)_8\text{CO-Cl}$) with 1,10-decamethylene glycol ($\text{HO}-(\text{CH}_2)_{10}\text{-OH}$) in dioxane. Kinetic measurements on this polycondensation have shown that the reactivity of the functional groups is indeed independent of the degree of polymerization.⁷ Furthermore, when the polycondensation is conducted at very high concentrations or in the bulk, cyclisation during the reaction is considered to be almost negligible as the smallest cycle that can be formed is a cyclic 20-mer.⁸



Scheme 1.1: Graphical representation of the various growth mechanisms by which a monomer can polymerize into a supramolecular polymer: a) Isodesmic self-assembly. b) Nucleated self-assembly. c) Ring-chain mediated self-assembly.

1.2.2 Physical aspects

An isodesmic (after iso meaning equal, desmic meaning bond) supramolecular polymerization of a ditopic monomer in dilute solution is characterized by a single binding constant (K) for each reversible step in the assembly pathway.⁹ The successive addition of monomer to the growing chain leads to a constant decrease in the free energy, indicative of a non-cooperative process. The general scheme of such a supramolecular polymerization can be written as:



Due to the equivalence of each step during the polymerization, isodesmic supramolecular polymerizations are characterized by the absence of a critical concentration or critical temperature for self-assembly.⁹⁻¹⁵ As a result of this absence, the concentration of polymeric species rises gradually as the concentration of ditopic monomer in dilute solution is increased or the temperature of the solution is lowered. To illustrate this important fact, Figure 1.1a displays the mole fraction of self-assembled material, ϕ , as a function of the dimensionless concentration K^*C_t (with C_t defined as the total concentration of monomer and ϕ defined as $(C_t - M_1)/C_t$). Similar plots of polymerized material as a function of temperature reveal the same gradual transitions.^{12,13} This gradual transition is also observed when the weight and number average degree of polymerization are plotted as a function of the dimensionless concentration (Figure 1.1b).¹⁶ These plots immediately reveal a major drawback of supramolecular polymerizations occurring via an isodesmic, one-dimensional growth mechanism. Only at very high values of K^*C_t supramolecular polymers with a high degree of polymerization (DP) are obtained (Figure 1b). Hence, in order to obtain supramolecular polymers with high DP in dilute solutions ($C_t < 1$ M), a high value of the equilibrium constant K is needed ($K > 10^6$ M⁻¹).

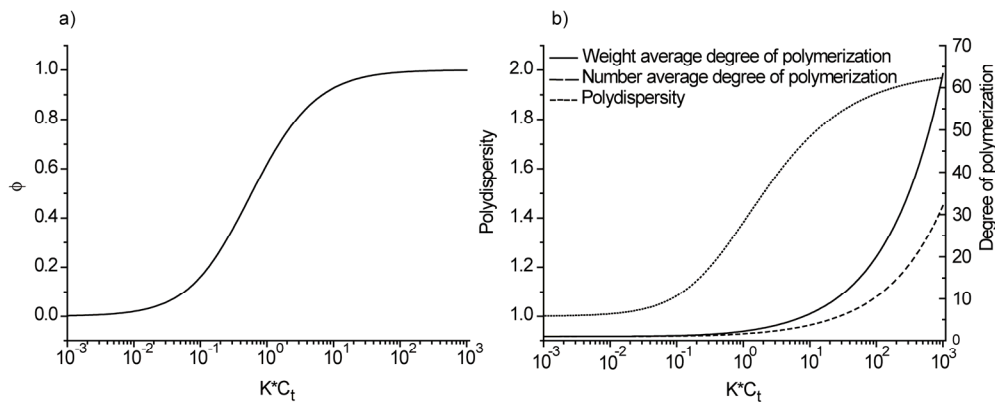


Figure 1.1: a) Mole fraction of self-assembled material, ϕ , as a function of the dimensionless concentration K^*C_t . b) Weight and number average degree of polymerization and polydispersity as a function of the dimensionless concentration.

Further analysis of this mechanism shows that the polydispersity index at equilibrium, characteristic of the width of the molecular weight distribution, rises steadily to a value

of 2 as the product K^*C_t is increased. Additionally, the size distribution of the polymers in the high molecular weight limit corresponds to a broad exponential distribution.^{10,12} In a recent paper Douglas and Freed have shown that the specific heat capacity C_v as a function of temperature shows a broad transition for an isodesmic polymerization whereas for cooperative polymerizations the specific heat shows a much sharper transition (*vide infra*).¹⁷

1.2.3 Examples

Previously, the self-assembly of C_3 -symmetric acylated 3,3'-diamino-2,2'-bipyridine disc **1** into helical columnar stacks, both in the liquid crystalline state and in dilute alkane solvents (Figure 1.2), has been studied.¹⁸⁻²⁰ In dodecane, chiral **1a** shows a very strong negative Cotton effect associated with the π - π^* absorption band of the bipyridine moiety. Heating of dilute dodecane solutions of **1a** results in a gradual decrease of the Cotton effect reflecting a shift in the equilibrium from long helical columns to short, disordered stacks (Figure 1.2c).²¹ The monotonic decrease in Cotton effect upon increasing the temperature is indicative for an isodesmic growth mechanism, although care must be exercised upon drawing a firm conclusion based on such a small amount of data points.

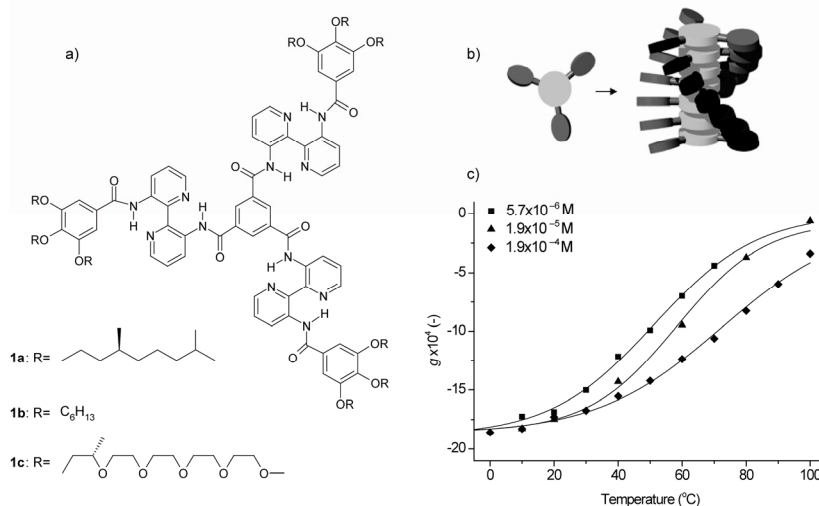


Figure 1.2: a) Chemical structure of C_3 -symmetric 3,3'-diamino-2,2'-bipyridine discs **1a**, **1b** and **1c**. b) Schematic representation of the self-assembly of **1** into helical columnar stacks. c) Temperature dependence of the Cotton effect of **1b** in dodecane expressed as the anisotropy factor g .

In light of this, these experiments have been re-evaluated using a larger amount of data points which indeed has revealed that the self-assembly process of the monomeric discs into the helical stacks is best described by an isodesmic growth mechanism with an association constant of 10^7 M^{-1} in hexane.²² Although the formation of a helical structure

is often associated with a cooperative growth mechanism²³ it appears from these experiments, conducted in apolar solvents, that the contact energy between non-adjacent units is too low for a cooperative process to occur. Sergeant and Soldiers experiments²⁴, implying the control of the movements of large numbers of cooperative achiral units (the soldiers) by a few chiral units (the sergeants), in dilute hexane solutions of **1a** and **1b** show a strong cooperative transfer of chirality in the mixed helical columns.¹⁸ A cooperative length of approximately 80 molecules was determined from these experiments which shows that the isodesmic build-up of the helical columns is completely decoupled from the strong cooperative transfer of chirality in mixed columns of **1a** and **1b**.

A clear-cut example of an isodesmic self-assembly is the supramolecular polymerization of bifunctional 2-ureido-pyrimidinone (UPy) derivatives. The ureido-pyrimidinone unit displays a very strong self-complementary quadruple hydrogen-bonding array in which the donor (D) and acceptors (A) are either arranged in a **DDAA** array or in a **DADA** array (Figure 1.3a) depending on the nature of the substituent of the pyrimidinone ring.^{25,26} As a result of the high number of attractive secondary interactions, the **DDAA** array of the 2-ureido-4[1*H*]-pyrimidinone dimer displays²⁷ a K_{dim} of $6 \times 10^7 \text{ M}^{-1}$ in CHCl_3 and is therefore ideally suited to create high molecular weight supramolecular polymers via an isodesmic growth mechanism. Bifunctional derivative **2**, containing two ureido-pyrimidinone units tethered with an aliphatic hexyl spacer yields viscous solutions in CHCl_3 at concentration as low as 40 mM. The observed viscous behaviour is a direct result of the formation of long supramolecular chains in solutions by reversible hydrogen-bonding. Titration of monofunctional stopper **3** to solutions of supramolecular polymer $[\mathbf{2}]_n$ in CHCl_3 results in a monotonic decrease of the specific viscosity (Figure 1.3b) as a result of a concomitant decrease in the average degree of polymerization.²⁸ Fitting of the specific viscosity as a function of **3** assuming an isodesmic polymerization of **2** resulted in an estimated DP of 700. Additionally, these experiments highlight the reversibility inherent in supramolecular polymers.

Detailed analysis of the supramolecular polymerization process of UPy derivative **2** has shown that at very low concentrations (<1 mM) the solution contains a significant amount of rings. Further analysis of the supramolecular polymerization process of bifunctional UPy derivatives with conformationally restricted spacers reveal that in some cases significant amounts of macrocyclic polymers are formed, even at high concentrations. The formation of supramolecular rings from linear supramolecular polymers will be the subject of discussion of the next section.

Examples of other isodesmic supramolecular polymerizations include the self-assembly of phenylacetylene macrocycles and perylene-bisimides in dilute solution as reported by Moore²⁹ and Würthner³⁰ respectively.

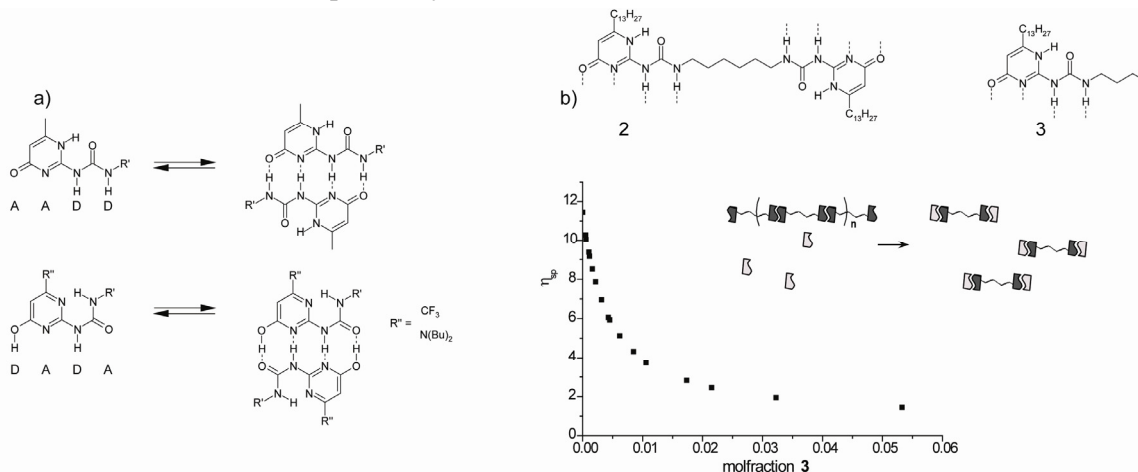


Figure 1.3: a) Dimerization of ureido-pyrimidinones via a self-complementary DDAA or DADA array (R' denotes any aliphatic tail). b) Effect of the addition of supramolecular "stopper" 3 on the specific viscosity of a 40 mM solution of 2 in CHCl_3 .

1.3 Ring-Chain supramolecular polymerizations

1.3.1 Definition and covalent counterpart

The second class of supramolecular polymerizations is represented by the reversible polymerization of a ditopic monomer in which each linear aggregate (including the monomer) in the assembly pathway is in equilibrium with its cyclic counterpart. The products of most step growth covalent polymerizations, whether under kinetic or under thermodynamic control, usually contain a few percent by weight of macrocyclic oligomers. An example of a covalent polymerization in which oligomeric rings are formed under kinetic control is the polycondensation of triethylene glycol (TEG) /hexamethylene-diisocyanate in the bulk at elevated temperatures.³¹ If the linkages in the chain of a step growth polymer are reversibly broken and reformed, an equilibrium is set up between oligomeric rings and linear chains. An archetype of a ring-chain equilibrium under thermodynamic control is the equilibrium polymerization of sulphur, which has first been theoretically modelled by Gee.³² This equilibrium polymerization starts at elevated temperatures by ring-opening of the eight-membered sulfur ring to form a diradical chain which further reacts to form long polymeric chains. Other examples of covalent polycondensations under thermodynamic control are the cyclo-oligomerization of lactones under the influence of the catalytic system 2,2-dibutyl-1,3,2-

dioxastannolane/dibutyltin dichloride (DOS/DTC)³³ and the entropically driven ring-opening-metathesis polymerization of macrocyclic olefins.³⁴

In contrast to covalent polymerizations, macrocyclisation reactions in supramolecular polymerizations always occur under thermodynamic control due to the fast association and dissociation of the reversible interaction.

1.3.2 Physical aspects

Theoretical distributions of cyclic and linear products in thermodynamically controlled macrocyclisations have first been described by Jacobson and Stockmayer (JS),³⁵ who pointed out the existence of a critical concentration, below which the system is composed of cyclic products only and above which the concentration of cyclic species remains constant and excess monomer produces linear species only. This model was later extended by Flory³⁶ into a more realistic model, which also included end-to-end conformation effects. Ercolani extended the treatment of JS to describe the distribution of cyclic oligomers under dilute conditions and a wide range of association constants (Figure 1.4).^{37,39} He pointed out that the phenomenon of a critical concentration is only manifested when the intermolecular association constant is sufficiently high ($> 10^5 \text{ M}^{-1}$).

As most supramolecular polymerizations occur in relatively dilute solutions, the model proposed by Ercolani is eminently suited to describe the equilibrium between cyclic and linear species in these equilibrium polymerizations.

In contrast to an isodesmic polymerization which is characterized by a single thermodynamic constant, the ring-chain model developed by Ercolani is characterized by two distinct thermodynamic constants (Figure 1.4a) i.e. the intermolecular binding constant (K_{inter}) and the intramolecular binding constant for i -th ring closure ($K_{\text{intra}(i)}$).

An important parameter in any ring-chain equilibrium is the effective molarity (EM_i), defined as:

$$\text{EM}_i = \frac{K_{\text{intra}(i)}}{K_{\text{inter}}} \quad (1)$$

When all cycles are considered strainless (i.e. the linker that connects the two end groups and the end group itself are considered flexible) and obey Gaussian statistics, the EM_i (and hence the $K_{\text{intra}(i)}$) values for $i > 1$ can be conveniently written as a function of EM_1 .³⁷

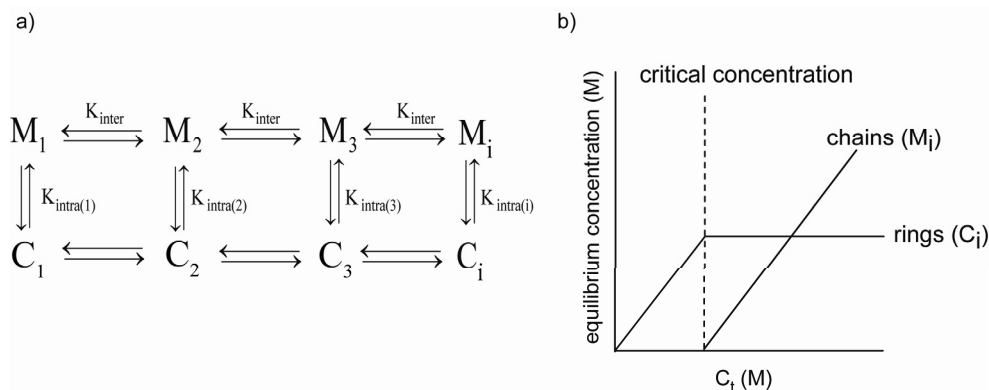


Figure 1.4: a) Schematic display of a general ring-chain equilibrium defined by the intermolecular association constant K_{inter} (M^{-1}) and the intramolecular, dimensionless association constant for i -th ring closure, $K_{intra(i)}$. b) The relation between the total concentration of a ditopic monomer in dilute solution (C_t) and the equilibrium concentration of chains and rings in a ring-chain equilibrium displaying a critical concentration.

The presence of a critical concentration in supramolecular ring-chain polymerizations leads to characteristic features not present in isodesmic supramolecular polymerizations. To illustrate this, the fraction of monomer present in linear species together with the weight and number average degree of polymerizations (DP_w and DP_n) for a general ring-chain equilibrium assuming strainless cycles was calculated for various values of $K_{intra(1)}$ and a value of K_{inter} of $10^6 M^{-1}$.³⁸ As the value of $K_{intra(1)}$ increases the transition between cyclic and linear material at the critical concentration becomes much sharper as is evident from Figure 1.5a. Furthermore, both number- and weight average degrees of polymerization abruptly increase once the total concentration (C_t) exceeds EM_1 , while the sharpness of the transition depends on the value of $K_{intra(1)}$. This situation is in contrast with an isodesmic polymerization in which the DP rises gradually as the concentration is increased. At high total concentration, isodesmic and ring-chain equilibria become indistinguishable and both the number and weight average degree of polymerization are equal at a given concentration far above EM_1 (Figure 1.5 b and c).

Recent Monte-Carlo simulations on ring-chain equilibria in which hydrogen bonds were used as the reversible interaction have shown that the critical concentration is strongly influenced by the rigidity of the spacer. From these studies it was found that the critical concentration decreases in the order rigid < semi-flexible < flexible when all other factors such as spacer length and interaction energy between the end-groups are considered constant.⁴⁰ For semiflexible and rigid polymers, the probability to find spacer ends within a bonding distance is smaller than for flexible polymers which results in a decrease in the total fraction of rings.

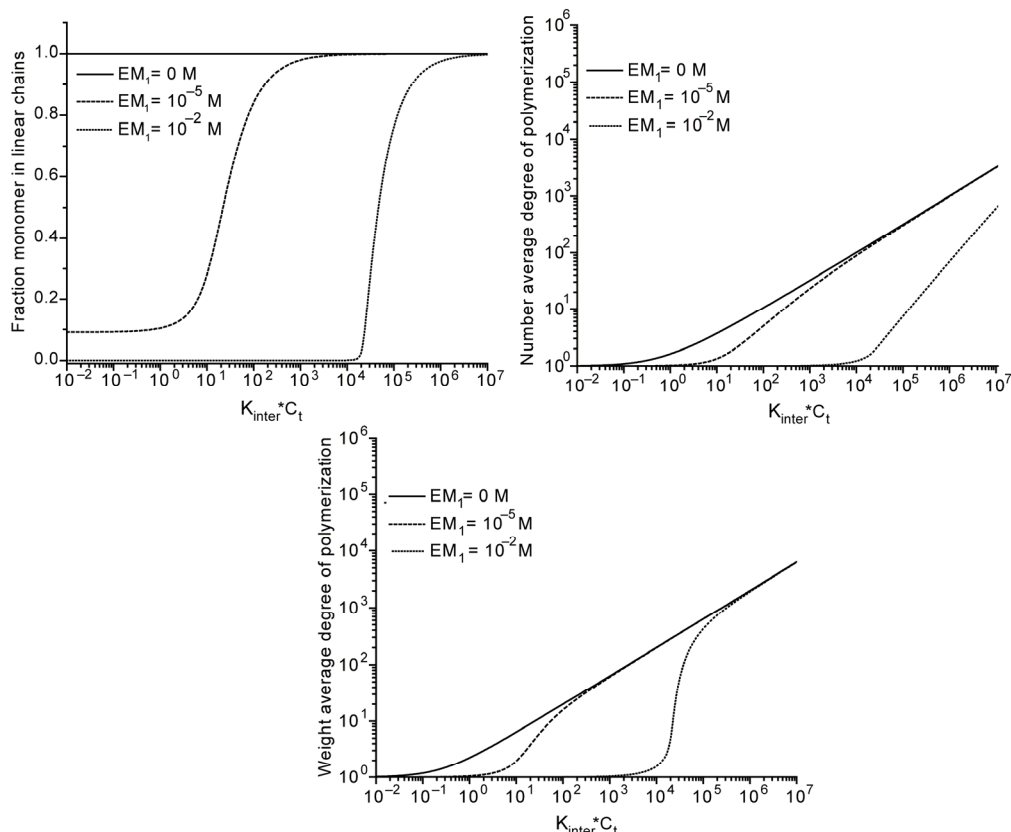


Figure 1.5: a) Fraction of monomer present in linear species as a function of the dimensionless concentration $K_{inter} * C_t$ for various values of EM_1 and a fixed value of K_{inter} ($10^6 M^{-1}$). b) Number averaged degree of polymerization as a function of the dimensionless concentration $K_{inter} * C_t$ for various values of EM_1 and a fixed value of K_{inter} ($10^6 M^{-1}$). c) Weight averaged degree of polymerization as a function of the dimensionless concentration $K_{inter} * C_t$ for various values of EM_1 and a fixed value of K_{inter} ($10^6 M^{-1}$).

It is important to realize that ring-chain equilibria also exhibit a critical temperature (T_c) as has first been shown by Gee³² and later by Tobolsky and Eisenberg⁴¹ and Harris⁴² for the equilibrium polymerization of sulfur. At this critical temperature there is a transition in the equilibrium between cyclic species and high molecular weight chains. Two limiting cases can be distinguished. In the first case, there exists a ceiling temperature *above* which high molecular-weight polymer is thermodynamically unstable with respect to cyclic monomer; in the other case there exists a floor temperature *below* which high-molecular weight polymer is thermodynamically unstable with respect to cyclic monomer. The concept of a floor and ceiling temperature was developed by Dainton and Ivin⁴³ to describe the propagation step of a general equilibrium polymerization. Polymerization reactions which have negative enthalpy (H) and entropy (S) changes associated with their propagation steps are characterized by a ceiling temperature, while polymerizations in which the change in enthalpy and entropy of propagation are

positive exhibit a floor temperature below which polymerization is not possible. The fact that such a temperature exists is a direct result of the fact that polymerization is a chemical aggregation process. A close analogy can be drawn to phase transitions, for example a solid cannot be obtained from a liquid unless the temperature is below the freezing point of the liquid.⁴³ Solid, liquid and freezing point are physical analogues of polymer, monomer and ceiling temperature.

Most examples of covalent ring-opening polymerizations involve the opening of strained rings. Such polymerizations are mainly enthalpy driven and hence display a ceiling temperature above which virtually all species are cyclic (examples are the cationic polymerization of tetrahydrofuran and dioxolane). However, in some cases, ring opening polymerizations can be driven by a gain in entropy and display a floor temperature. Examples of entropy-driven ring-opening polymerizations are the ring-opening polymerization of cyclic S₈ in liquid sulfur⁴² and the ring-opening-metathesis polymerization of strainless, macrocyclic olefins.³⁴

Although the theory of Dainton and Ivin⁴³ provides an accurate thermodynamic description of the *cause* of a ceiling or floor temperature (change in enthalpy *vs.* change in entropy) it does not yield any indication on the *sharpness* of this transition. Tobolsky and Eisenberg^{41, 44} first showed that the transition between cyclic and linear polymers can be extremely sharp at the critical temperature. In their theoretical investigations on the ring-chain equilibrium of cyclic S₈ in liquid sulfur they elegantly showed that the sharpness of this transition is dependent on the ratio of the inter and intramolecular equilibrium constants. Interestingly, Wheeler⁴⁵ and co-workers have shown that the ring-chain theory of Tobolsky and Eisenberg can be considered as a mean field approximation for a second order phase transition in the Ehrenfest sense. The phase transition approach has many advantages compared to the simple equilibrium approach as it presents a far more general framework based on formalisms developed for phase transitions in magnets, simple fluids and covalent polymers.^{46a} In covalent polymer science second-order transitions in the Ehrenfest sense have appeared in a number of different problems: (1) the helix-random coil transition in DNA, (2) the isolated polymer adsorbed to a surface, (3) the glass transition and (4) the collapse transition.⁴⁷ In all cases, the polymeric phase transition is characterized by a discontinuity in the heat-capacity at the critical temperature. Indeed, experimental data acquired by Greer and Wheeler on the thermal polymerization of cyclic sulfur has shown that the heat capacity exhibits a λ -like anomaly at the critical temperature while the density does not display a discontinuity, both features characteristic of a second order phase transition.^{17,45,46}

1.3.3 Examples

Bifunctional ureido-pyrimidinone derivatives equipped with an unsubstituted hexane spacer can self-assemble in dilute solutions to form high-molecular weight linear chains via an isodesmic supramolecular polymerization. On the other hand, exclusive formation of cyclic dimers, both in the solid state and in dilute solutions is observed for a bifunctional UPy derivative based on a rigid *m*-xylylene linker.⁴⁸ The dominant formation of cyclic dimers in this supramolecular polymerization can directly be attributed to the very rigid pre-organized nature of the linker. Further analysis of the supramolecular polymerization process revealed that solutions of bifunctional UPy molecules in CHCl₃ always contain a certain amount of cyclic species in equilibrium with high molecular weight chains (Figure 1.6b). It was anticipated that selective pre-organization toward cyclic species could be achieved by conformational effects in the spacer unit. To this end, a series of bifunctional UPy derivatives with several substituted linear spacers was synthesized (Figure 1.6a). Because the resonances corresponding to cyclic UPy dimers are in slow exchange on the ¹H-NMR timescale with the signals of the linear UPy chains, ¹H-NMR spectroscopy proved to be a convenient technique to quantify the critical concentration⁴⁹ for all UPy derivatives (Figure 1.6c). Indeed, the high binding constant of the UPy quadruple hydrogen bond array results in a true critical concentration as is predicted by theory.^{49,50} Using ¹H-NMR spectroscopy in combination with Ubbelohde viscometry, estimates for the critical concentration for a family of closely related bifunctional UPy derivatives in CDCl₃ could be obtained (Figure 1.7a).

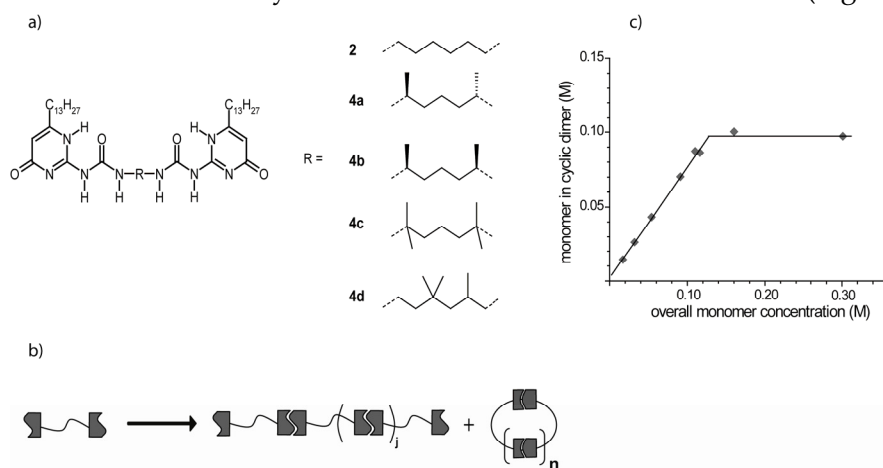


Figure 1.6: a) Bifunctional ureido-pyrimidinone derivatives equipped with a variety of short C₆ and C₅ spacers. b) Schematic representation of the supramolecular polymerization of a bifunctional UPy monomer into linear chains and cycles. c) Concentration of monomer in cyclic dimers determined by ¹H-NMR for various concentrations of **4c** in CDCl₃.

At low concentrations all compounds formed cyclic dimers in solution while at higher concentration linear polymers were formed. Whereas the critical concentration of **2** is estimated to be lower than 1 mM, the critical concentration of **4a** is almost 300 mM. The differences in critical concentration of **2**, **4a-c** are also reflected in the concentration dependent specific viscosity of solutions of these compound in CHCl_3 (Figure 1.7a, inset).

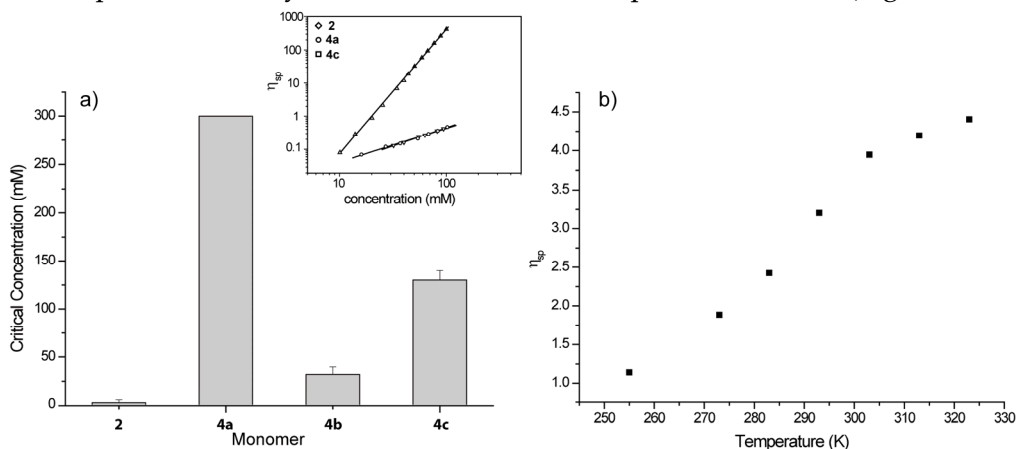


Figure 1.7: a) Critical concentration of UPy derivatives **2**, **4a-c** in CDCl_3 solution as determined by $^1\text{H-NMR}$ analysis. The inset shows the concentration dependent specific viscosity of chloroform solutions of **2**, **4a** and **4c** vs. the concentration (293 K). b) Specific viscosity of a 0.145 M solution of **4d** as a function of temperature.

While solutions of **2** are extremely viscous at a concentration of 75 mM, solutions of **4a** and **4c** at this concentration are much less viscous due to the higher fraction of small cycles at this concentration.

From these results it is apparent that substitution of the alkyl linker with methyl groups next to the UPy moieties strongly increases the concentration of cyclic dimers formed in solution. This change in critical concentration has been attributed to a shift in the equilibrium between the different *anti* and *gauche* conformations of the linker, resulting in a preferred conformation in which the methyl groups are in *anti* organization with respect to the rest of the linker. In this way the UPy end-groups become preorganized for cyclic dimer formation which in turn results in a significant rise in the critical concentration. This example clearly shows that conformational control in the spacer unit provides an attractive way to tune the equilibrium between cycles and linear chains in hydrogen-bonded assemblies.

As already stated, ring-chain equilibria can exhibit either a floor or a ceiling temperature. In analogy with covalent ring-opening polymerizations, supramolecular ring-chain equilibria are also capable of displaying a floor or ceiling temperature. If the formation of supramolecular polymers from supramolecular rings in enthalpically favoured ($\Delta H <$

0) and the transition from cyclic to polymeric species results in a loss of entropy ($\Delta S < 0$) a supramolecular ring-chain equilibrium will exhibit a ceiling temperature. In contrast, if the formation of supramolecular polymers from supramolecular rings is enthalpically unfavorable ($\Delta H > 0$) and the transition from cyclic to polymeric species is driven by a gain of entropy ($\Delta S > 0$) a supramolecular ring-chain equilibrium will exhibit a floor temperature. A remarkable example of an entropically driven supramolecular ring opening polymerization is displayed by bifunctional UPy monomer **4d**. Upon heating of solutions of **4d** in CHCl_3 the viscosity of the solution dramatically increases corresponding to a shift in the equilibrium toward linear chains at higher temperatures.⁵¹ Further analysis of the temperature dependence of the ring-chain equilibrium for other bifunctional UPy derivatives (**2**, **4b** and **4c**) has shown that the critical concentration decreases upon an increase of the temperature, indicative of an enthalpically driven supramolecular ring-opening polymerization.⁵²

Recently the supramolecular polymerization of an AB type ditopic monomer in dilute CHCl_3 solutions was also investigated.⁵³ In this case, the reversible AB interaction is based on the strong complementary quadruple hydrogen bond array between the hydrogen-bonding acceptor-donor-donor-acceptor (**ADDA**) array of 2-ureido-6[1H]pyrimidinone with the complementary **DAAD** array of 2,7-diamido-1,8-naphthyridine ($K_a = 6 \times 10^6 \text{ M}^{-1}$ in CHCl_3).⁵⁴ Using concentration dependent $^1\text{H-NMR}$ and viscosity measurements a sharp transition from cyclic species at low concentrations to linear species at high concentrations was observed. This example clearly shows that intramolecular cyclization plays a crucial role when strong binding units are used to construct supramolecular polymers. This notion is further strengthened by the large body of experimental evidence found in literature on ring formation in different supramolecular polymerizations.⁵⁵

A long standing, unanswered question is whether the mechanism by which cyclic species are in equilibrium with linear supramolecular polymers can be regarded as a true ring-opening mechanism or resembles an open-chain association model. In the first mechanism, the free end-groups of the supramolecular polymer directly attack the binding sites present in cyclic species whether in the second mechanism the cycles first open before associating with the free end-groups of the supramolecular polymer.

1.4 Cooperative supramolecular polymerizations

1.4.1 Definition and covalent counterpart

The third class of supramolecular polymerization of a ditopic monomer into linear, one-dimensional aggregates is characterized by a so-called cooperative mechanism where

the polymerization process can be divided in two stages. In each stage the non-covalent bond formation is governed by a constant equilibrium constant (Scheme 1.1b). For cooperative polymerizations, below a critical length of the polymer n , *i.e.* the nucleus size, monomer addition to the growing polymer is thermodynamically unfavourable, resulting in a relatively small equilibrium constant K_i , with $i \leq n$. It is only when the polymer has reached the critical nucleus size that addition becomes more favourable and the equilibrium constant K_j (with $j > n$) increases compared to K_i . Consequently, for cooperative processes a ratio of K_i/K_j that is smaller than unity is observed. In contrast, in an anticooperative polymerization, this ratio of K_i/K_j exceeds unity. It should be noted that the formation of the nucleus occurs via homogeneous nucleation, *i.e.* it is formed out of monomers, and is not due to an external impurity or surface effects (heterogeneous nucleation).

Two general classes of cooperativity can be distinguished: electronic and structural cooperativity. In the first case electronic properties, such as bond polarizability or hydrogen bond strength, change during polymerization, resulting in a growing polymer that is more susceptible to chain growth compared to the monomer. In classical covalent polymerizations characterized by irreversible bond formation, the electronic cooperative mechanism has been observed for polycondensation reactions that do not obey Flory's "principle of equal reactivity"⁶, but in which the reactivity of the polymer end groups become more reactive than the monomer and in which the reaction of monomers with each other is prevented. An example of such a polymerization is the polycondensation of phenyl 4-(alkylamino)-benzoate in the presence of phenyl 4-nitrobenzoate as initiator and a base in THF.⁵⁶ Due to the abstraction of the proton from the amino group of the monomer (phenyl 4-(alkylamino)-benzoate) by the base, the reactivity of the phenyl ester moiety is deactivated, which prevents monomers reacting with each other. The anion produced by proton abstraction from the monomer will only react with initiator, leading to an activated monomer which possesses a more reactive phenyl ester moiety compared to the anionic monomer. As a result, only activated monomer will react resulting in a chain growth polymerization.

In the case of structural cooperativity, initial polymerization is thermodynamically unfavourable and polymerization becomes favourable only when the growing polymer has reached a critical length at which, due to a conformational or structural change in the growing polymer, additional interactions stabilize the nucleus, transforming the nucleus into a more ordered conformation. In this respect structural cooperativity is distinctly different from electronic cooperativity where no transition from a disordered assembly to an ordered nucleus is observed.

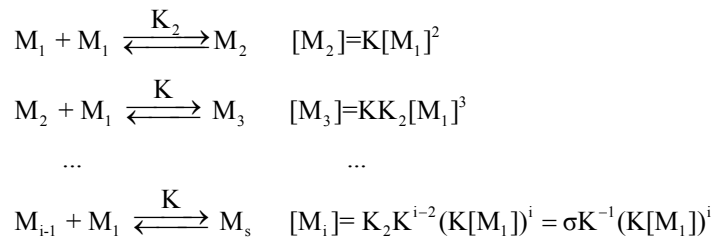
Structural cooperativity was mainly applied to describe reversible protein aggregation; two notable examples being the self-assembly of the tobacco mosaic virus (TMV)⁵⁷ and the polymerization of G-actin into fibrous F-actin.⁵⁸

In classical covalent polymerizations structural cooperativity has been observed for the acid-initiated polymerization of isocyanides to form a helical polymer. For this polymerization, a mechanism was proposed in which an initial helical oligomer needs to be formed which then acts as a template for the incorporation of subsequent monomeric units.⁵⁹ Nakano *et al.* reported the asymmetric, anionic polymerization of triphenyl methyl methacrylate initiated by 9-fluorenyllithium, in the presence of chiral ligands, to form a one-handed helical polymer.⁶⁰ They observed that the reactivity of each oligomer anion depended on the degree of polymerization, which was correlated to the specific conformation of the oligomer anions. Only when a stable helical conformation of the oligomer was formed, which occurred for a DP of 7–9 units, further monomer addition occurred more readily.

In supramolecular polymerization processes, structural cooperativity has hitherto received relatively little attention. First of all this is because, strictly speaking, linear, one-dimensional supramolecular polymers cannot display structural cooperativity, as these polymers ‘by definition’ cannot display the structural change, required for activation, without losing their one-dimensional character. As a result, so far researchers have mainly relied on the isodesmic model to analyze their data.

1.4.2 Physical aspects

To allow for cooperativity, the isodesmic model can be modified to include a second equilibrium constant that differs from the first one. One approach is to assume that the dimerization step has a different equilibrium constant than the other constants, which can be schematically represented by:^{11,16}



Where K_2 represents the equilibrium constant of dimerization and K represents the equilibrium constant for all following steps. As a measure for the degree of cooperativity the parameter σ can be defined as the ratio of K_2/K which is smaller than unity for a cooperative process and larger than unity for an anti-cooperative process. Although this

model is limited to cooperative systems where activation occurs already at the dimer stage, it has the advantage that it can be solved analytically. Using this K_2 - K model, characteristic features of cooperative supramolecular polymerizations can be understood. Figure 1.8a, displays the mole fraction of self-assembled material, ϕ , as a function of the dimensionless concentration $K \cdot C_t$ for three different values for σ (with C_t defined as the total concentration of monomer and ϕ defined as $(C_t - M_1)/C_t$). Increasing the cooperativity (*i.e.* smaller values of σ) has a clear influence on the growth profile of the polymeric species. Whereas for the isodesmic growth ($\sigma = 1$) a gradual increase in polymeric species is observed with increasing concentration (see Figure 1.1), for the cooperative systems, below a (critical) dimensionless concentration of 1, hardly any polymeric species are formed. Only when the concentration is raised beyond the critical concentration rapid chain growth occurs and all monomers are converted into long polymeric species over a relatively small concentration range (Figure 1.8b). Another remarkable feature of cooperative polymerization is its bimodal mass distribution which is the result of the presence of (non-activated) monomers and activated polymers that have rapidly elongated after activation (Figure 1.8c). Consequently, compared to the isodesmic system, cooperative polymerization processes will lead to polymers with a larger polydispersity, but more interesting also to polymers with a higher degree of polymerization. That is, higher DPs can be obtained not only by increasing K , but also by decreasing the ratio K_2/K .

Interestingly, the curves shown in Figure 1.8a,b for the cooperative polymerization according to the K_2 - K model show a strong resemblance to the curves obtained for the AB polymerization with cycle formation, as shown in Figure 1.5 in the previous section. This resemblance is a result of the fact that in the initial stages of both polymerizations the (cyclic) monomers are lower in energy compared to the next oligomers that will be formed during the polymerization. Hence, in both models a sharp transition in the fraction of polymerized material accompanied by a rapid increase in DP is observed once critical conditions are reached.

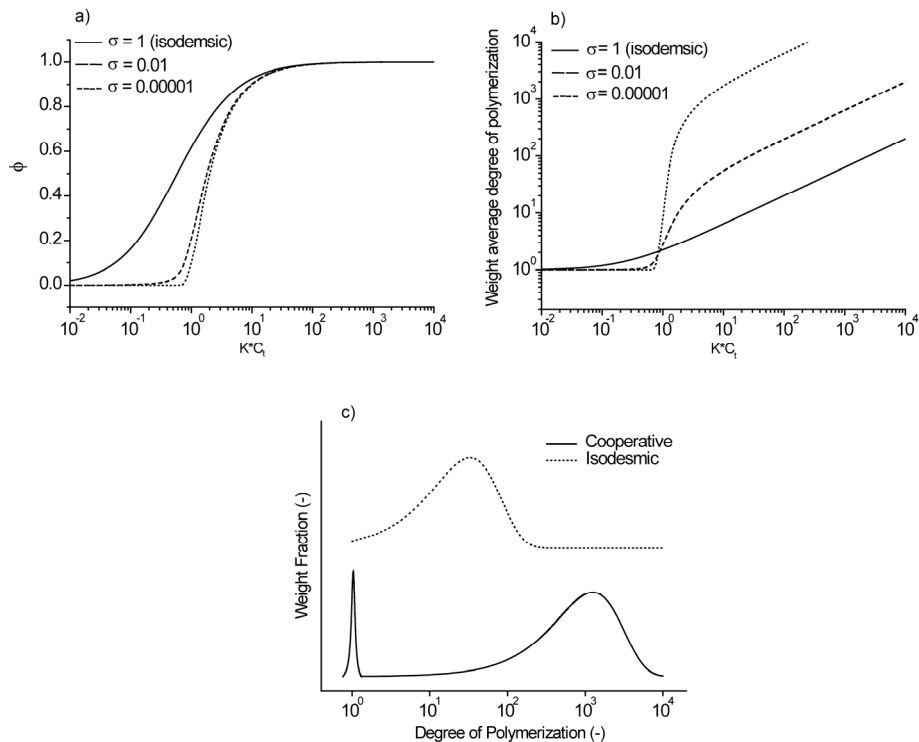


Figure 1.8: a) Mole fraction of self-assembled material, ϕ , as a function of the dimensionless concentration K^*C_i for 3 values of σ . b) Weight-averaged degree of polymerization as a function of the dimensionless concentration for 3 values of σ (K_2/K). c) Schematic representation of the molecular weight distribution for an isodesmic aggregation mechanism and a cooperative aggregation mechanism.

The above K_2 - K model can be used to obtain thermodynamic constants of supramolecular polymerization processes, provided it is known *a priori* that the size of the nucleus is two. Goldstein and Stryer have generalized this model for cooperative polymerization processes using a variable nucleus size.⁶¹

An alternative model was developed to investigate cooperative polymerization processes based on temperature controlled self-assembly instead of a concentration driven supramolecular polymerization.^{62,63} This model, derived by Van der Schoot,¹² is based on a model developed by Oosawa and Kasai to describe the cooperative, helical aggregation of actin.⁶⁴ In this model two equilibrium constants are defined, *i.e.* the dimensionless activation equilibrium constant K_a that describes the equilibrium between the monomer and nucleus, and the elongation equilibrium constant K_e (M^{-1}) for the subsequent polymerization steps beyond this critical size (Figure 1.9).

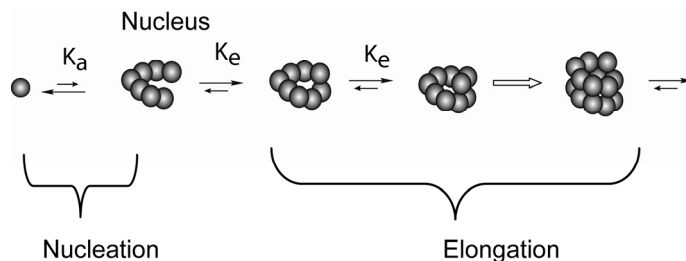


Figure 1.9: Schematic representation of a helical polymerization with a nucleus size of 7 units. The pre-nucleus equilibria are governed by the nucleation constant K_a while the post-nucleation steps are governed by the elongation constant K_e

As the temperature is the variable, the equilibrium constants are no longer constant during the supramolecular polymerization, but are influenced by the change in temperature. Two temperature regimes can be distinguished, which are separated by the elongation temperature, T_e . Above the elongation temperature, most of the molecules in the system are in an inactive state (nucleation regime) which means that the equilibria governed by K_a lie almost completely to the left (Figure 1.9). At the elongation temperature activation occurs, meaning that the pre-nucleation equilibria are shifted to the right resulting in formation of the high energy nucleus. Below the elongation temperature, rapid growth of the polymer takes place (elongation regime). With this model similar polymerization characteristics can be observed as for the K_2 -K model. However, as the elongation equilibrium constant K_e is no longer constant, we consider the enthalpy release ΔH_e to be constant during elongation and use it as a parameter in the model. Figure 1.10a shows the fraction of polymerized material, ϕ , for 4 values of K_a as a function of the normalized temperature (T/T_e), in which ϕ is described by two different equations, one valid for $T > T_e$ and one valid for $T < T_e$.

Similar as for the K_2 -K model, for low values of K_a , *i.e.* for a high degree of cooperativity, hardly any polymeric species are present at temperatures above T_e and the fraction polymerized material grows sharply below T_e . This behaviour resembles a true second order phase transition in the limit $K_a \rightarrow 0$.^{12,17,45a} At the critical point the number averaged degree of polymerization, counted over all polymerizing species is proportional to $K_a^{-1/3}$. The number-averaged degree of polymerization in Figure 1.10b at temperatures below T_e starts to show an exponential growth while the DP becomes proportional to $K_a^{-0.5}$. That is, higher DPs can be reached when the cooperativity is increased, as was also observed in the K_2 -K model. Similarly, a higher enthalpy release ΔH_e in the elongation regime, corresponding to a higher K_e , will lead to more rapid chain growth (Figure 1.10c) and higher DPs (Figure 1.10d), as was also observed for the K_2 -K model.

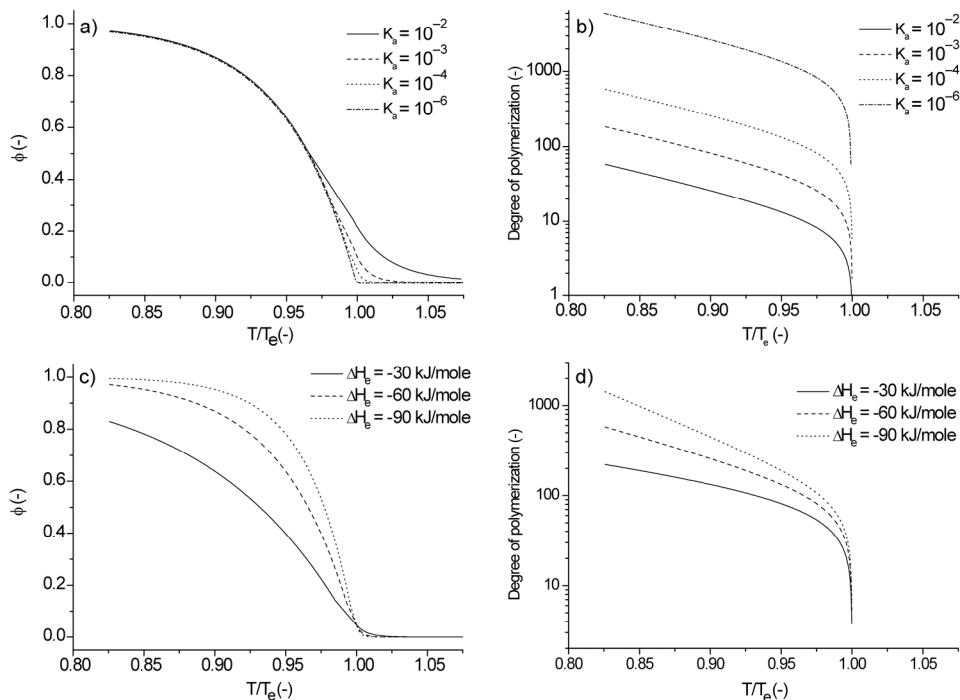


Figure 1.10: Mole fraction of self-assembled material, ϕ , (a) and number-averaged degree of polymerization (b) as a function of the dimensionless temperature T/T_e for 4 values of K_a , with $\Delta H_e = -60$ kJ/mole. Mole fraction of self-assembled material, ϕ , (c) and number-averaged degree of polymerization (d) as a function of the dimensionless temperature for 3 values of ΔH_e , with $K_a = 10^{-4}$.

1.4.3 Examples

In supramolecular polymerizations electronic cooperativity has been observed for a number of self-assembling systems, driven by hydrogen bonding^{64,65} and aromatic interactions.^{29b,66} Often electronic effects are most pronounced in the first association step, *i.e.* the dimerization step. Once the dimer is formed the (electronic) properties of the dimer change, making addition of the next monomer more (un)favourable. For example, Bouteiller and coworkers have described the cooperative supramolecular polymerization for both N,N' -disubstituted ureas, as well as bis-ureas, which both form linear chains due to bifurcated hydrogen bonds.^{64,65} For these derivatives it was found that the formation of higher oligomers was favored relative to the formation of dimers (*i.e.* $K_2 < K$), which was explained by the polarization of the urea function prior to dimerization.⁶⁷ Although Bouteiller and coworkers used the K_2 - K model for their analysis, they also commented that this model is an approximation because the

association constants for the formation of trimers and higher oligomers are probably not strictly equal to each other.⁶⁵

Zhao and Moore have described the self-association behaviour of phenylene ethynylene based macrocycles containing two imine bonds.^{29b} In acetone an anticooperative aggregation was observed that could be analyzed with the K_2 -K model. Electrostatic (dipole-dipole) interactions between the two monomeric components were proposed to be responsible for enhanced strength of dimerization and unfavourable formation of longer aggregates.

Previously the self-assembly of chiral C_3 -symmetrical trialkylbenzene-1,3,5-tricarboxamide **5** into helical columnar stacks in both the liquid crystalline state and in dilute alkane solutions was reported (Figure 1.11a).^{63,68-71}

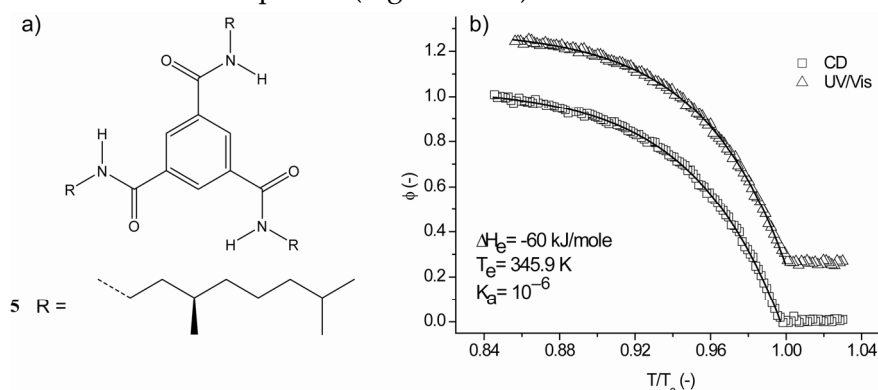


Figure 1.11: a) Chemical structure of C_3 -symmetrical trialkylbenzene-1,3,5-tricarboxamide **5**. b) Mole fraction of self-assembled material, ϕ , as a function of the dimensionless temperature T/T_e , based on CD and UV/vis absorption (at 223 nm) of a 2.1×10^{-5} M solution of **5** in heptane. The solid lines are the corresponding fits of the data using the model for the elongation regime. The UV/vis absorption-based data are shown with a 0.25 offset.

Recently, temperature dependent spectroscopic measurements were employed to describe the cooperative self-assembly mechanism of **5** using the model developed by Van der Schoot.¹² By monitoring the CD and UV/vis absorption at a wavelength characteristic for aggregation, the fraction of polymerized material, ϕ , as a function of temperature could be determined (Figure 1.11b). Both spectroscopic techniques revealed an identical transition, suggesting that the monomers are in equilibrium with chiral stacks and no achiral intermediate stacks are formed during self-assembly. Fitting of the data resulted for the cooperative self-assembly of **5** in an enthalpy release, ΔH_e , of -60 kJ/mol and a K_a value of 10^{-6} . Based on this K_a value a number average degree of polymerization of 100 was determined at the elongation temperature whereas a DP of 6000 was determined at room temperature. Remarkably, replacing the chiral alkyl side

chains with achiral octyl tails was found to significantly influence the supramolecular polymerization as is evident by its higher enthalpy release (-70 kJ/mole) and lower K_a value (10^{-4}). It is believed that the origin of this cooperativity is electronic and is related to the orientation of the dipoles which change during aggregation and thereby influence the intermolecular hydrogen bonding strength.^{72,73}

Remarkably, bipyridinyl-based C_3 -symmetrical discs **1a** and **1b**, in which only intramolecular hydrogen bonds are present, self-assemble *via* an isodesmic growth mechanism, whereas C_3 -symmetrical disc **5**, capable of forming intermolecular hydrogen bonds displays a highly cooperative self-assembly mechanism. In contrast to its aliphatic analogs **1a** and **1b**, the self-assembly mechanism of bipyridinyl-based C_3 -symmetrical **1c**, equipped at the periphery with chiral, hydrophilic oligo(ethylene oxide) side chains is highly cooperative in polar solvents.^{74,75} In *n*-butanol these molecules self-assemble in helical, columnar structures via non-helical intermediate oligomeric assemblies and the transition from non-helical to helical structures was found to be a highly cooperative process. The results for these related C_3 -symmetrical discs show that relatively small changes in structure or solvent can have large effects on the self-assembly pathway.

A cooperative self-assembly mechanism was also observed for chiral oligo(*p*-phenylenevinylene) (OPV) derivative **6** (Figure 1.12a) equipped with an ureidotriazine unit designed for self-complementary four-fold hydrogen bonding.⁶² In apolar solution these π -conjugated chromophores can be present in two different states; *i.e.* discrete monomeric or hydrogen-bonded dimeric species at high temperature and helical aggregates at low temperature.^{76,77} The hydrogen-bonded dimers have been studied in detail with scanning tunneling microscopy (STM)^{76,78} and $^1\text{H-NMR}$ spectroscopy,⁷⁶ whereas the fibrillar structural dimensions have been measured by small angle neutron scattering (SANS) and atomic force microscopy (AFM).⁷⁷

Due to the π -conjugated chromophore and the presence of enantiomerically pure side chains, a combination of spectroscopic techniques (UV/vis, circular dichroism (CD) and fluorescence) could be used probe the different stages in the supramolecular polymerization of **6** as a function of temperature. Different spectroscopic techniques revealed different transitions in the supramolecular polymerization of **6**. By combining all spectroscopic data it proved possible to identify the different stages in the hierarchical self-assembly pathway of **6** into fibrillar structures upon cooling a solution of molecularly dissolved monomers at high temperature (Figure 1.12b,c). At first, the monomers form dimers via quadruple hydrogen bonding which then aggregate via an isodesmic pathway into short, disordered stacks. Upon further cooling, the molecules in the pre-aggregates become more restricted in their relative positions, characterized by

the abrupt change at $T_e = 328$ K in the UV/vis absorption at 335 nm and in the fluorescence spectra.

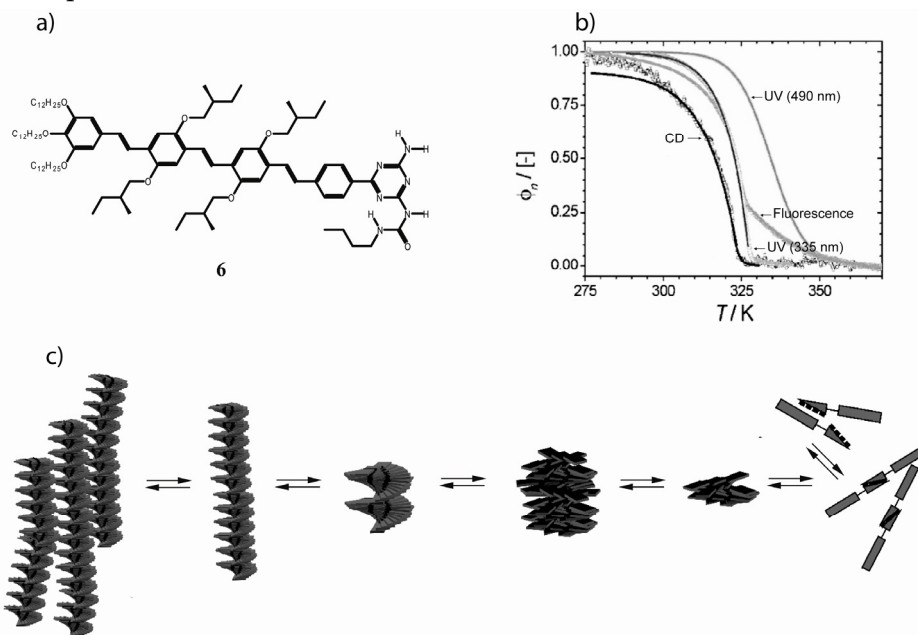


Figure 1.12: a) Chemical structure of chiral oligo(*p*-phenylenevinylene) derivative **6**. b) Mole fraction of self-assembled material, ϕ , as a function of the temperature as determined by UV/vis, fluorescence and CD spectroscopy for a 1.1×10^{-5} M solution in dodecane). c) Schematic representation of the self-assembly process for **6**.

This cooperative transition is close to the onset of chiroptical activity in the pre-aggregates, where helix formation transforms the pre-aggregate into a chiral nucleus. The value of DP_n , averaged over all polymerizing species, at the elongation temperature was determined to be 30. Tentatively, this value was assigned to the size of the nucleus as this number corresponds to the number of dimers required to complete one helical pitch⁷⁹ which suggest that in this case structural cooperativity plays a dominant role. However, care must be taken in this analysis as these two numbers (size of the nucleus and DP_n averaged over all polymerizing species at T_e) are not necessarily equal to each other. Based on the best fitted value of K_a a stack length of approximately 500 units was determined at room temperature in good agreement with the length determined in solution by small angle neutron scattering.⁷⁷

Comparing the cooperative self-assembly mechanisms of C₃-symmetrical disc **5** and OPV derivative **6**, it is clear that the self-assembly of **6** is considerably more complicated and involves multiple assembly steps. Most likely this is related to the more intricate structure that is possible for the OPV derivative **6** which involves hydrogen-bonded dimers and conformational changes in the π -conjugated backbone.

1.5 Conclusion and discussion

The development of useful models to understand one-dimensional self-assembly of molecules into large fibrils is a particularly important topic in material science and biophysics. Nucleation dependent (cooperative) self-assembly underpins the pathology of neurodegenerative disorders such as Alzheimer's disease⁸⁰ and plays a fundamental role in actin polymerization. Moreover, cooperativity provides a switching mechanism for many biological processes that are essential to living systems.⁸¹⁻⁸³

Future research on supramolecular polymers will undoubtedly show the relation between cooperative self-assembly and the macroscopic properties of the resulting materials.

1.6 Aim and outline of this thesis

The aim of this thesis is to investigate the various supramolecular polymerization processes of quadruple hydrogen bonding based supramolecular system. Special attention is paid to the various growth mechanisms that govern the formation of supramolecular assemblies based on quadruple hydrogen bonding. Using a wide variety of analytical techniques, this thesis aims to unambiguously assign one of three major growth mechanisms to each newly synthesized supramolecular assembly discussed in this thesis.

In self-assembly, the initial differences and/or relationships among the components that encode the global structure of the assembled whole is crucial in determining the composition of the final equilibrium mixture. Understanding the mechanisms by which high-fidelity recognition is accomplished in complex mixtures of supramolecular assemblies is important for the development of functional nano-medicines⁸⁴ where multiple self-assemblies need to operate simultaneously without being affected by the presence of other self-assembling components in the mixture. Therefore, throughout this thesis, selectivity in mixtures of various quadruple hydrogen bonding assemblies will be probed using a variety of techniques.

Finally, the kinetic characterization of supramolecular assemblies is an important tool to elucidate the mechanism by which these self-assemblies are formed. Therefore, it is tried to complement the thermodynamic studies with kinetic studies at various concentrations wherever possible. More importantly, the kinetic study of multi-component, supramolecular assemblies can lead to a rational design of supramolecular assemblies operating under kinetic control as will be shown in chapter 4.

In chapter 2 various novel 2-ureido-pyrimidinone (UPy) units capable of quadruple hydrogen bonding will be synthesized and their preferred tautomeric form will be determined using ¹H-NMR, FTIR and X-ray diffraction. In search for a more selective

ureido-pyrimidinone for hetero-complexation with 2,7-diamino-1,8-naphthyridine (NaPy) the novel 2-ureido-pyrimidinones will be screened for their binding affinity with 2,7-diamino-1,8-naphthyridine.

In chapter 3, the influence of the increased fidelity towards hetero-complexation with NaPy will be examined by studying the concentration dependent supramolecular polymerization of two AB monomers capable of both reversible A·A (UPy·UPy) and A·B (UPy·NaPy) interactions. In this chapter, a new theoretical model will be developed that mathematically captures the ring-chain equilibrium of these compounds. Chapter 4 deals with the complexation kinetics of UPy dimers with 2,7-diamino-1,8-naphthyridine. In this chapter a mechanism is presented by which UPy dimers associate with NaPy. Furthermore, kinetic self-sorting in a three-component supramolecular system is reported.

The self-assembly of dimeric UPy-urea model compounds into one dimensional stacks both in the apolar solvent heptane and the more polar solvent CDCl₃ is discussed in chapter 5. These model compounds are equipped with a soluble wedge attached to the distal urea functionality and substituted with a chiral citronellol group at the pyrimidinone ring. Chapter 6 deals with the dramatic influence of polar side chains on the dimerization constant of UPy based supramolecular assemblies. In this chapter, evidence is presented which shows that short ethylene glycol chains have a large influence on the dimerization constant of UPy based supramolecular systems. Furthermore, it is shown that a similar effect is observed in UPy substituted polyacrylates in which the effect is dependent on the length of the spacer unit used to connect the polyacrylate to the pyrimidinone ring.

1.7 References

- 1) a) Examples: anionic polymerization of α -methyl styrene: Worsfold, D. J.; Bywater, S. J. *Polym. Sci.* **1957**, 26, 299. b) Cationic polymerization of THF in benzene: Leonard, J.; Maheux, D. J. *Macromol. Sci., Part A: Pure Appl. Chem.* **1973**, 7, 1421.
- 2) a) Jochim, S.; Bartenstein, M.; Altmeyer, A.; Hendl, G.; Riedl, S.; Chin, C.; Denschlag, H. J.; Grimm, R. *Science* **2003**, 302, 2101.
- 3) Brodsky, F. M.; Chen, C. Y.; Knuehl, C.; Towler, M. C.; Wakeham, D. E. *Annu. Rev. Cell. Dev. Biol.* **2001**, 17, 517.
- 4) Brunsveld, L.; Folmer, B. J. B.; Meijer, E. W.; Sijbesma, R. P. *Chem. Rev.* **2001**, 101, 4071.
- 5) This behaviour is also observed in solutions of surfactants in equilibrium with micelles where only above a certain threshold concentration (critical micelle concentration) self-assembly occurs. This phenomenon is described by the classical Debye model which can be written as an equilibrium between m identical surfactants, M , and the fully assembled micelle M_m : $mM \rightleftharpoons M_m$ in which m is often taken as a measure of cooperativity, see: Debye, P. J. W. *Ann. N.Y. Acad. Sci.* **1949**, 51, 575.

- 6) Flory, P. J. *Principles of Polymer Chemistry*; Ithaca, NY: Cornell University Press 1953.
- 7) Ueberreiter, K.; Engel, M. *Makromol. Chem.* **1977**, *178*, 2257.
- 8) This is further supported by a patent of Flory which describes the polycondensation of 1,10-decamethylene glycol with sebacoyl chloride. After reaction of the bifunctional monomers in the bulk a highly viscous material is obtained which corresponds with linear polyesters of high molecular weight: Flory, P. J. Leunter, F. S. US 2589687, 1952.
- 9) This mechanism is also named the multistage open association model (MSOA): Ciferri, A. *J. Macromol. Rapid Commun.* **2002**, *23*, 511.
- 10) Henderson, J. R. *Phys. Rev. E* **1997**, *55*, 5731.
- 11) Martin, R. B. *Chem. Rev.* **1996**, *96*, 3043.
- 12) van der Schoot, P. P. A. M. *Theory of Supramolecular Polymerization in Supramolecular Polymers*; Second Edition; Taylor & Francis Group 2005.
- 13) Dudowicz, J.; Freed, K. F.; Douglas, J. F. *J. Chem. Phys.* **2003**, *119*, 12645.
- 14) Mukerjee, P.; Ghosh, A. K. *J. Am. Chem. Soc.* **1970**, *92*, 6408.
- 15) Connors, K. A. *Binding Constants, The Measurement of Molecular Complex Stability*; John Wiley & Sons, Inc. 1987.
- 16) For the equations: Zhao, D. Moore, J. S. *Org. Biomol. Chem.* **2003**, *1*, 3471.
- 17) Douglas, J. F.; Dudowicz, J.; Freed, K. F. *J. Chem. Phys.* **2008**, *128*, 224901.
- 18) Palmans, A. R. A.; Vekemans, J. A. J. M.; Havinga, E. E.; Meijer, E. W. *Angew. Chem. Int. Ed.* **1997**, *36*, 2648.
- 19) Palmans, A. R. A.; Vekemans, J. A. J. M.; Fischer, H.; Hikmet, R. A.; Meijer, E. W. *Chem. Eur. J.* **1997**, *3*, 300.
- 20) Palmans, A. R. A.; Vekemans, J. A. J. M.; Hikmet, R. A.; Fischer, H.; Meijer, E. W. *Adv. Mater.* **1998**, *10*, 873.
- 21) Palmans, A. R. A. *Thesis: Supramolecular structures based on the intramolecular H-bonding in the 3,3'-di(acylamino)-2,2'-bipyridine unit*; Eindhoven University of Technology: Eindhoven **1997**.
- 22) Smulders, M. M. J.; Palmans, A. R. A.; Meijer, E. W. *Unpublished results*.
- 23) Saroff, H. A.; Kiefer, J. E. *Biopolymers* **1999**, *49*, 425.
- 24) Green, M. M.; Peterson, N. C.; Sato, T.; Teramoto, A.; Cook, R.; Lifson, S. *Science* **1995**, *268*, 1860.
- 25) Beijer, F. H.; Sijbesma, R. P.; Kooijman, H.; Spek, A. L.; Meijer, E. W. *J. Am. Chem. Soc.* **1998**, *120*, 6761.
- 26) de Greef, T. F. A.; Ligthart, G. B. W. L.; Lutz, M.; Spek, A. L.; Meijer, E. W.; Sijbesma, R. P. *J. Am. Chem. Soc.* **2008**, *130*, 5479.
- 24) Söntjens, S. H. M.; Sijbesma, R. P.; van Genderen, M. H. P.; Meijer, E. W. *J. Am. Chem. Soc.* **2000**, *122*, 7487.
- 28) Sijbesma, R. P.; Beijer, F. H.; Brunsveld, L.; Folmer, B. J. B.; Hirschberg, J. H. K. K.; Lange, R. F. M.; Lowe, J. K. L.; Meijer, E. W. *Science* **1997**, *278*, 1601.
- 29) a) Lahiri, S.; Thompson, J. L.; Moore, J. S. *J. Am. Chem. Soc.* **2000**, *122*, 11315. b) Zhao, D.; Moore, J. S. *J. Org. Chem.* **2002**, *67*, 3548.
- 30) Würthner, F.; Thalacker, C.; Diele, S.; Tschierske, C. *Chem. Eur. J.* **2001**, *7*, 2245.
- 31) Kricheldorf, H. R.; Schwarz, G. *Macromol. Rapid Commun.* **2003**, *24*, 359.
- 32) Gee, G. *Trans. Faraday Soc.* **1952**, *48*, 515.
- 33) Roelens, S.; Dalla Cort, A.; Mandolini, L. *J. Org. Chem.* **1992**, *57*, 1472.
- 34) Hodge, P.; Kamau, S. D. *Angew. Chem. Int. Ed.* **2003**, *42*, 2412.

- 35) Jacobson, H.; Stockmayer, W. H. *J. Chem. Phys.* **1950**, *18*, 1600.
- 36) Flory, P. J.; Suter, U. W.; Mütter, M. J. *Am. Chem. Soc.* **1976**, *98*, 5733.
- 37) Ercolani, G.; Mandolini, L.; Mencarelli, P.; Roelens, S. *J. Am. Chem. Soc.* **1993**, *115*, 3901.
- 38) In the simulations we have assumed an infinite number of linear species. The first 500 linear oligomers are in equilibrium with their corresponding cyclic counterpart. For details of these simulations and the corresponding equations see Chapter 3.
- 39) Ercolani, G.; Di Stefano, S. *J. Phys. Chem. B* **2008**, *112*, 4662.
- 40) Chen, C.-C.; Dormidontova, E. E. *Macromolecules* **2004**, *37*, 3905.
- 41) Tobolsky, A. V.; Eisenberg, A. *J. Am. Chem. Soc.* **1959**, *81*, 780.
- 42) Harris, R. E. *J. Phys. Chem.* **1970**, *74*, 3102.
- 43) Dainton, F. S.; Ivin, K. J. *Quart. Rev.* **1958**, *12*, 61.
- 44) Tobolsky, A. V.; Eisenberg, A. *J. Colloid Sci.* **1962**, *17*, 49.
- 45) a) Wheeler, J. C.; Kennedy, S. J.; Pfeuty, P. *Phys. Rev. Lett.* **1980**, *45*, 1748. b) Petschek, R. G.; Pfeuty, P.; Wheeler, J. C. *Phys. Rev. A* **1986**, *34*, 2391. c) Wheeler, J. C.; Pfeuty, P. *Phys. Rev. A* **1981**, *24*, 1050.
- 46) a) Greer, S. C. *Annu. Rev. Phys. Chem.* **2002**, *53*, 173. b) Greer, S. C. *J. Phys. Chem. B* **1998**, *102*, 5412. c) Greer, S. C. *Adv. Chem. Phys.* **2007**, 261.
- 47) a) Di Marzio, E. A. *Macromolecules* **1984**, *17*, 969 and references therein. b) Di Marzio, E. A. *Prog. Polym. Sci.* **1999**, *24*, 329.
- 48) Folmer, B. J. B.; Sijbesma, R. P.; Kooijman, H.; Spek, A. L.; Meijer, E. W. *J. Am. Chem. Soc.* **1999**, *121*, 9001.
- 49) Söntjens, S. H. M.; Sijbesma, R. P.; van Genderen, M. H. P.; Meijer, E. W. *Macromolecules* **2001**, *34*, 3815.
- 50) ten Cate, A. T.; Kooijman, H.; Spek, A. L.; Sijbesma, R. P.; Meijer, E. W. *J. Am. Chem. Soc.* **2004**, *126*, 3801.
- 51) Folmer, B. J. B.; Sijbesma, R. P.; Meijer, E. W. *J. Am. Chem. Soc.* **2001**, *123*, 2093.
- 52) ten Cate, A. T.; Sijbesma, R. P. *Macromol. Rapid Commun.* **2002**, *23*, 1094.
- 53) Scherman, O. A.; Ligthart, G. B. W. L.; Sijbesma, R. P.; Meijer, E. W. *Angew. Chem. Int. Ed.* **2006**, *45*, 2072.
- 54) a) Corbin, P. S.; Zimmerman, S. C. *J. Am. Chem. Soc.* **1998**, *120*, 9710. b) Wang, X.-Z.; Li, X.-Q.; Shao, X.-B.; Zhao, X.; Deng, P.; Jiang, X.-K.; Li, Z.-T.; Chen, Y.-Q. *Chemistry* **2003**, *9*, 2904.
- 55) a) Cantrill, S. J.; Youn, G. J.; Stoddart, J. F. *J. Org. Chem.* **2001**, *66*, 6857. b) Miyauchi, M.; Takashima, Y.; Yamaguchi, H.; Harada, A. *J. Am. Chem. Soc.* **2005**, *127*, 2984. c) Fernández, G.; Pérez, E. M.; Sánchez, L.; Martín, N. *Angew. Chem. Int. Ed.* **2007**, *46*, 1. d) Yamaguchi, N.; Nagvekar, D. S.; Gibson, H. W. *Angew. Chem. Int. Ed.* **1998**, *37*, 2361. e) Abed, S.; Boileau, S.; Bouteiller, L. *Macromolecules* **2000**, *33*, 8479.
- 56) Yokozawa, T.; Asai, T.; Sugi, R.; Ishigooka, S.; Hiraoka, S. *J. Am. Chem. Soc.* **2000**, *122*, 8313.
- 57) Klug, A. *Philos. Trans. R. Soc. London Ser. B* **1999**, *354*, 531.
- 58) Kasai, M.; Asakura, S.; Oosawa, F. *Biochim. Biophys. Acta* **1962**, *57*, 22.
- 59) Metselaar, G. A.; Cornelissen, J. J. L. M.; Rowan, A. E. Nolte, R. J. M. *Angew. Chem. Int. Ed.* **2005**, *44*, 1990.
- 60) Nakano, T.; Okamoto, Y.; Hatada, K. *J. Am. Chem. Soc.* **1992**, *114*, 1318.
- 61) Goldstein, R. F.; Stryer, L. *Biophys. J.* **1986**, *50*, 583.
- 62) Jonkheijm, P.; van der Schoot, P. P. A. M.; Schenning, A. P. H. J.; Meijer, E. W. *Science* **2006**, *313*, 80.
- 63) Smulders, M. M. J.; Schenning, A. P. H. J.; Meijer, E. W. *J. Am. Chem. Soc.* **2008**, *130*, 606.
- 64) Simic, V.; Bouteiller, L.; Jalabert, M. *J. Am. Chem. Soc.* **2003**, *125*, 13148.

- 65) Lortie, F.; Boileau, S.; Bouteiller, L. *Chem. Eur. J.* **2003**, *9*, 3008.
- 66) Arnaud, A.; Belleney, J.; Boué, F.; Bouteiller, L.; Carrot, G.; Wintgens, V. *Angew. Chem. Int. Ed.* **2004**, *43*, 1718.
- 67) Masunov, A.; Dannenberg, J. J. *J. Phys. Chem. B* **2000**, *104*, 806.
- 68) Brunsveld, L.; Schenning, A. P. H. J.; Broeren, M. A. C.; Janssen, H. M.; Vekemans, J. A. J. M.; Meijer, E. W. *Chem. Lett.* **2000**, 292.
- 69) van Gorp, J. J.; Vekemans, J. A. J. M.; Meijer, E. W. *J. Am. Chem. Soc.* **2002**, *124*, 14759.
- 70) Wilson, A. J.; Masuda, M.; Sijbesma, R. P.; Meijer, E. W. *Angew. Chem. Int. Ed.* **2005**, *44*, 2275.
- 71) Wilson, A. J.; van Gestel, J.; Sijbesma, R. P.; Meijer, E. W. *Chem. Commun.* **2006**, 4404.
- 72) Sakamoto, A.; Ogata, D.; Shikata, T.; Urakawa, O.; Hanabusa, K. *Polymer* **2006**, *47*, 956.
- 73) Rochefort, A.; Bayard, É.; Hadj-Messaoud, S. *Adv. Mater.* **2007**, *19*, 1992.
- 74) van der Schoot, P. P. A. M.; Michels, M. A. J.; Brunsveld, L.; Sijbesma, R. P.; Ramzi, A. *Langmuir* **2000**, *16*, 10076.
- 75) Brunsveld, L.; Zhang, H.; Glasbeek, M.; Vekemans, J. A. J. M.; Meijer, E. W. *J. Am. Chem. Soc.* **2000**, *122*, 6175.
- 76) Schenning, A. P. H. J.; Jonkheijm, P.; Peeters, E.; Meijer, E. W. *J. Am. Chem. Soc.* **2001**, *123*, 409.
- 77) Jonkheijm, P.; Hoeben, F. J. M.; Kleppinger, R.; van Herrikhuizen, J.; Schenning, A. P. H. J.; Meijer, E. W. *J. Am. Chem. Soc.* **2003**, *125*, 15941.
- 78) Gesquiere, A.; Jonkheijm, P.; Hoeben, F. J. M.; Schenning, A. P. H. J.; de Feyter, S.; de Schryver, F. C.; Meijer, E. W. *Nano Lett.* **2004**, *4*, 1175.
- 79) Beljonne, D.; Hennebicq, E.; Daniel, C.; Herz, L. M.; Silva, C.; Scholes, G. D.; Hoeben, F. J. M.; Jonkheijm, P.; Schenning, A. P. H. J.; Meskers, S. C. J.; Phillips, R. T.; Friend, R. H.; Meijer, E. W. *J. Phys. Chem. B* **2005**, *109*, 10594.
- 80) Jarrett, J. T.; Lansbury, P. T. *Cell* **1993**, *73*, 1055.
- 81) Royer, W. E.; Zhu, H.; Gorr, T. A.; Flores, J. F.; Knapp, J. E. *J. Biol. Chem.* **2005**, *280*, 27477.
- 82) Nam, Y.; Sliz, P.; Pear, W. S.; Aster, J. C.; Blacklow, S. C. *Proc. Natl. Acad. Sci. U.S.A.* **2007**, *104*, 2103.
- 83) Iber, D.; Clarkson, J.; Yudkin, M. D.; Campbell, I. D. *Nature* **2006**, *441*, 371.
- 84) Cao, R.; Villalonga, R.; Fragoso, A. *IEE Proceedings - Nanobiotechnology* **2005**, *152*, 1

2

Increasing selectivity in complementary quadruple hydrogen bonding

Abstract

Various novel 2-ureido-pyrimidinone (UPy) units, capable of quadruple hydrogen bonding via DDAA and DADA hydrogen bonding arrays, have been synthesized and their ability to form strong hetero-complexes with 2,7-diamido-1,8-naphthyridine (NaPy) has been investigated using UV spectral changes as a convenient probe. From these titrations it is apparent that substitution of the pyrimidinone ring with an electron donating dibutyl amino group results in an increased fidelity for hetero-complexation. Using a combination of X-ray crystallography, NOESY experiments and FT-IR spectroscopy the existence of the DADA array of the heterocycle in its pyrimidin-4-ol tautomeric form was verified both in solution and in the solid state. The dimerization constant of this novel UPy unit is 70 times lower compared to the dimerization constant of 2-ureido-pyrimidinones substituted with alkyl groups at the C₆ position of the pyrimidinone ring. As a result of the diminished dimerization constant ($K_{dim} = 9 \times 10^5 \text{ M}^{-1}$, CDCl₃) and high association constant with NaPy ($6 \times 10^5 \text{ M}^{-1}$), the fidelity of UPy·Napy recognition is increased considerably compared to previous systems.

Part of this work has been published:

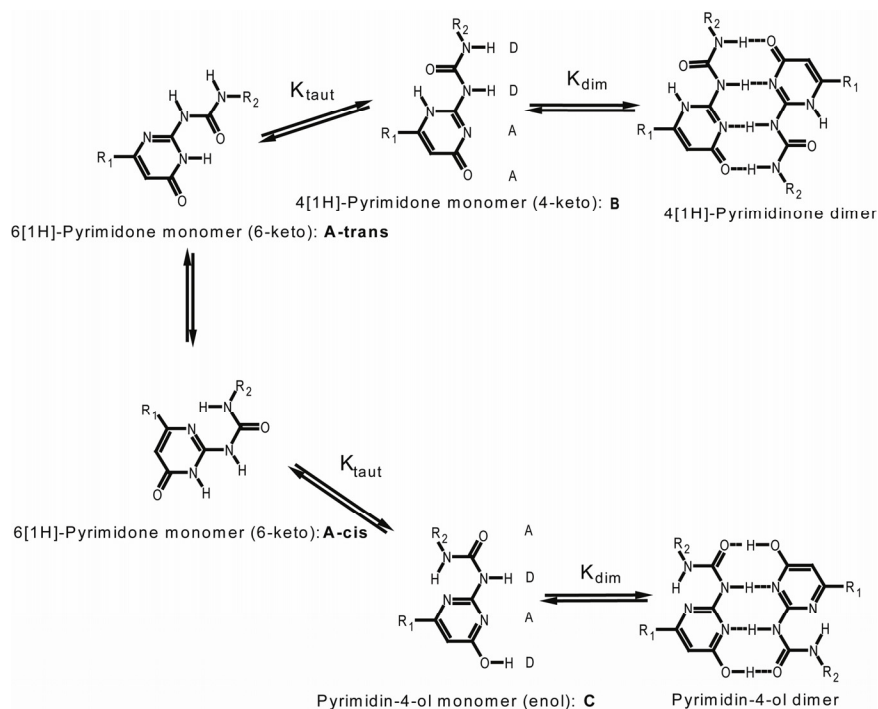
de Greef, T. F. A.; Ligthart, G. B. W. L.; Lutz, M.; Spek, A. L.; Meijer, E. W.; Sijbesma, R. P. *J. Am. Chem. Soc.* **2008**, *130*, 5479-5486.

2.1 Introduction

Due to the ease of synthetic accessibility and high dimerization constant ($K_{\text{dim}} = 6 \times 10^7 \text{ M}^{-1}$, CDCl_3), the ureido-pyrimidinone (UPy) **DDAA** module¹ has found widespread use in the design of novel supramolecular materials² where it serves as a physical chain-extending and cross-linking moiety. Recently, supramolecular materials based on the quadruple hydrogen bonding ureido-pyrimidinone moiety have been used as biocompatible scaffolds³ holding potential use in tissue engineering applications.

An important feature of the ureido-pyrimidinone unit is its ability to adopt various tautomeric forms (Scheme 2.1). The prototropy of the pyrimidinone ring is mainly dictated by substituent effects (R_1 and R_2), concentration and polarity of the solvent. In the polar aprotic solvent DMSO the UPy unit exists in the 6[1H]-pyrimidinone monomeric form. The urea group in the 6[1H]-pyrimidinone monomer can either adopt a *cisoid, transoid* (**A-cis**) or a *transoid, transoid* (**A-trans**) conformation. For ureido-pyrimidinones substituted with methyl groups ($R_1 = R_2 = \text{CH}_3$), gas phase calculations⁴ at the MP2 6-31+G* level of theory suggest that the *transoid, transoid* conformer is lower in energy compared to the *cisoid, transoid* conformer. In less polar solvents, such as CDCl_3 or toluene, a mixture of the 4[1H]-pyrimidinone form **B** (4-keto) and pyrimidin-4-ol **C** (enol) are observed which dimerize via a **DDAA** and **DADA** array respectively. Substitution of the pyrimidinone ring with electron withdrawing 6-substituents (R_1) like nitrophenyl- and trifluoro groups results in formation of a **DADA** type dimer.⁵ Hailes⁶ and co workers reported that substitution of the pyrimidinone ring at the C_6 position with an electron donating *p*-aminophenyl group also leads to preference for a pyrimidin-4-ol **DADA** dimer in DMSO while in CDCl_3 approximately 40% of the material is dimerized via a **DADA** hydrogen bonding array and the remaining material is dimerized via the 4[1H]-pyrimidinone **DDAA** dimer.

On the basis of differences in secondary interactions⁷ dimers of **DADA** arrays are predicted to be less stable than **DDAA** dimers, although the exact value of the dimerization constant for the **DADA** array has never been reported. Recently, high level DFT calculations at the B3LYP/6-311++G(d,p) level have indeed shown that the **DADA** hydrogen bonding array is less stable than a **DDAA** hydrogen bonding array.⁸ This reduction in self-dimerization is caused by the fact that the individual hydrogen bonds in a **DADA** hydrogen bonding array cannot simultaneously adopt their optimal geometrical arrangements.



Scheme 2.1: Equilibrium between different tautomeric forms of the UPy unit and between its monomeric and dimeric forms.

Based on these examples it is thus concluded that substitution of the pyrimidinone ring by inductive electron withdrawing ($R_1 = \text{CF}_3$, p-nitrophenyl) as well as electron donating substituents ($R_2 = \text{p-aminophenyl}$) lead to the preferred formation of **DADA** type dimers. The existence of multiple tautomeric equilibria makes it difficult to predict the properties of ureido-pyrimidinone based supramolecular materials⁹ and efforts have been made to reduce the numbers of tautomers by prototropic degeneracy.¹⁰ On the other hand, the prototropy of the pyrimidinone ring allows the UPy unit to selectively form strong heterodimers in its *cisoid*, *transoid* 6[1H] tautomeric form via a hydrogen bonding **ADDA** array with the **DAAD** array of 2,7-diamido-1,8-naphthyridine.^{11,12} The equilibrium between UPy monomer, UPy dimer and UPy·NaPy heterocomplex is strongly concentration dependent (Figure 1).¹³ For the case of UPy **1** ($R_1 = \text{CH}_3$, $R_2 = \text{C}_4\text{H}_9$) which dimerizes via a **DDAA** hydrogen bonding array ($K_{\text{dim}} = 6 \times 10^7 \text{ M}^{-1}$ in CHCl_3), the hetero-association constant (K_a) with NaPy **2** ($R_3 = \text{C}_{11}\text{H}_{23}$) has been determined to be $5 \times 10^6 \text{ M}^{-1}$ in CHCl_3 using UV-Vis spectroscopy.¹³ Using the high strength and selectivity of the UPy·NaPy heterodimer various supramolecular architectures have been developed. For example the formation of supramolecular block-copolymers based on bifunctional UPy and NaPy telechelic polymers, prepared by ring-opening metathesis polymerization (ROMP), was studied in solution as well as in the solid state.¹⁴ Investigation of the solid state structures of these copolymers by tapping mode AFM

provided evidence of microphase-separated morphologies. Very recently, supramolecular graft copolymers based on the UPy·NaPy heterodimer have been prepared and their supramolecular grafting has been studied¹⁵ with a variety of techniques.

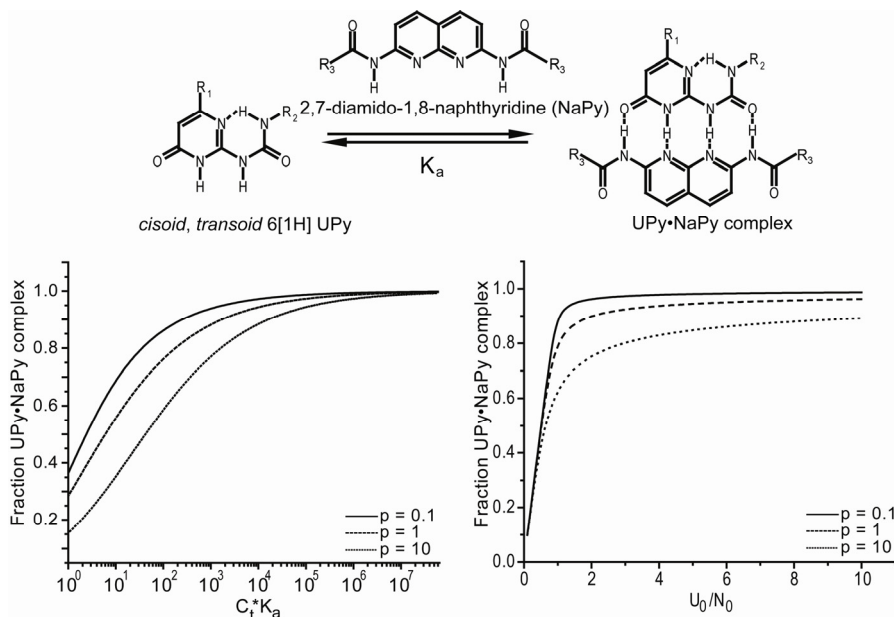


Figure 2.1: Concentration dependent selectivity for different values of the dimensionless binding constant p (defined as K_{dim} / K_a) in mixtures of UPy dimer, UPy monomer and UPy·NaPy hetero-complex. a) Fraction of UPy·NaPy hetero-complex vs. dimensionless concentration (defined as $C_t \cdot K_a$, with C_t the total concentration) in a 1:1 mixture of UPy and NaPy for several values of p and a value of K_a of 10^6 M^{-1} . b) Fraction of UPy·NaPy hetero-complex as a function of the UPy to NaPy ratio in a $2.5 \times 10^{-5} \text{ M}$ solution of NaPy for several different values of p and a value of K_a of 10^6 M^{-1} .

However, a major drawback of the current UPy·NaPy system is the higher dimerization constant of the UPy dimer compared to the association constant of the UPy·NaPy hetero-complexation as this results in “self-stoppered” behavior in AB type supramolecular polymerizations (Chapter 3) and a low propensity for alternation in A_2 - B_2 type supramolecular polymerizations. An approach to increase the propensity for alternation in A_2 - B_2 supramolecular polymerizations introduced by Zimmerman is the use of a guanosine urea derivative (UG) which only weakly self-associates ($K_{dim} = 200 \text{ M}^{-1}$) but has a high association constant with 2,7-diamido-1,8-naphthyridine.^{16,17} Due to the low dimerization constant of the urea-guanosine analogue the fidelity of the UG·NaPy recognition process is greatly improved compared to that of UPy·NaPy complex **1.2**. However, a major drawback of the system as introduced by Zimmerman is the formation of multimeric UG assemblies which can lead to uncontrolled cross-linking in

supramolecular polymerizations. Therefore, in this chapter attempts will be made to synthesize several new UPy derivatives with various electron donating and electron accepting groups attached to the C₆ position. The tautomeric preference of these compounds will be investigated using a variety of techniques and subsequently the fidelity²² of hetero-complex formation with NaPy will be screened using UV-Vis titrations.

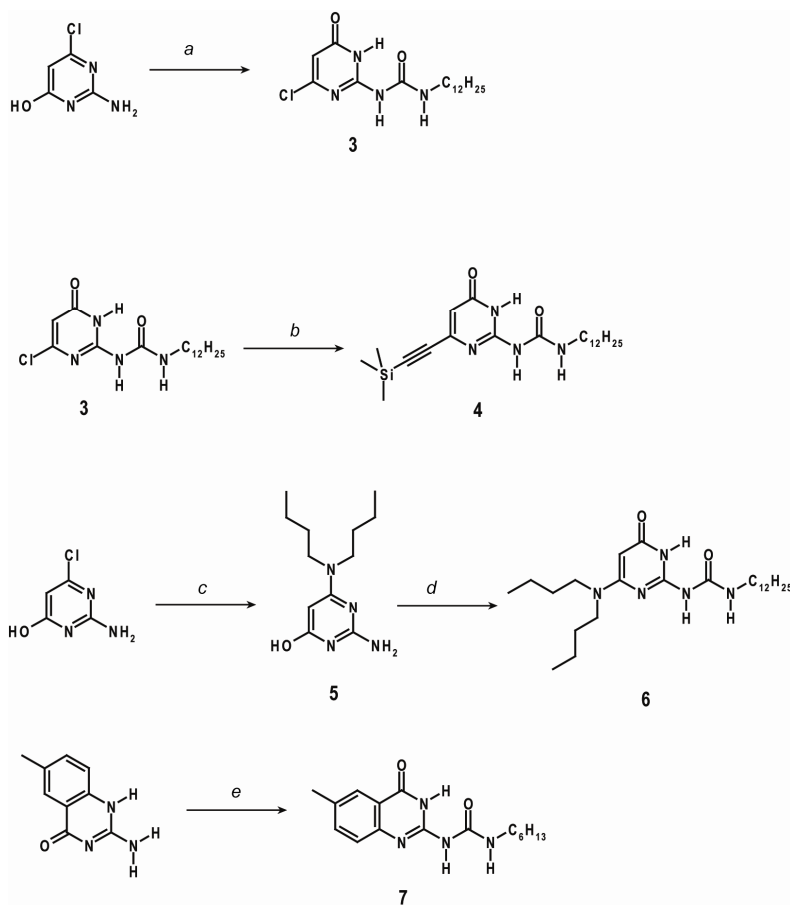
2.2 Synthesis, self-assembly and tautomeric preference of various UPy derivatives

The synthetic routes towards the various C₆ substituted 2-ureido-pyrimidinones are depicted in Scheme 2.2. Synthesis of chloro-substituted UPy **3** could be achieved by reaction of dodecyl isocyanate with anhydrous 2-amino-6-chloro-4-pyrimidinol at elevated temperatures in ortho-dichlorobenzene. Purified chloro substituted ureido-pyrimidinone **3** was subjected to Stille coupling with 1-tributylstannyl-2-trimethylsilylacetylene resulting in TMS protected UPy **4** bearing an electron donating acetylene group at the C₆ position of the pyrimidinone ring. Nucleophilic aromatic substitution of 2-amino-6-chloro-4-pyrimidinol hydrate with dibutylamine at elevated temperatures and subsequent reaction of the resulting isocytosine **5** with dodecyl isocyanate resulted in UPy **6** bearing an electron donating amino group at the C₆ position of the pyrimidinone ring. Finally, UPy **7** was obtained by reaction of hexyl isocyanate with commercially available 2-amino-6-methyl-4(3*H*)-quinazolone in DMF.

The self-assembly of these compounds was further probed by ¹H-NMR, FTIR and X-ray analysis. The ¹H-NMR spectra of UPy compounds **3**, **4**, **6** and **7** in CDCl₃ at a concentration of 10 mM clearly show three sharp resonances in the downfield region (> 9 ppm) of the spectrum indicative of hydrogen bonding induced dimerization. Table 2.1 summarizes the ¹H chemical shifts of the three hydrogen bonded NH protons as well as the ¹H chemical shift of the alkylidene proton and the ¹³C chemical shift of alkylidene carbon of the novel synthesized UPy compounds.

For comparison, the chemical shift data of trifluoro substituted UPy **8**, methyl substituted UPy **1** and phenyl substituted UPy **9** are also included. Previously, UPy **8** was shown to dimerize via its **DADA** array both in solution (CDCl₃ and toluene-d₈) and in the solid state. Comparison of the chemical shift data of **8** with the chemical shift data of **3** in CDCl₃ clearly shows that the latter dimerizes via a **DADA** array in which the heterocycle adopts the pyrimidin-4-ol tautomeric form. This was further confirmed by FTIR measurements in the solid state and in dilute solution (10⁻³ M in CDCl₃) which shows the presence of characteristic bands at 2550 cm⁻¹ and 3245 cm⁻¹ previously

assigned to the pyrimidin-4-ol tautomeric form.⁵ ¹H-NMR and FTIR analysis of 2-ureidoquinazolone derivative **7** showed that it dimerizes via a **DDAA** array in CDCl₃. Remarkably, this compound also exists as a dimer in the more polar solvent DMF-d₆ as is evident by three sharp NH resonances at a concentration of 40 mM as observed by ¹H-NMR.



Scheme 2.2: Synthesis of various C₆ substituted 2-ureido-pyrimidinones: a) *n*-dodecylisocyanate, *ortho*-dichlorobenzene, 18 h, 150 °C, 28%; b) 1-tributylstannyl-2-trimethylsilylacetylene, Pd₂(dba)₃, P(*t*-Bu)₃, toluene, 20 h, 70-100 °C, 40%; c) dibutylamine, ethylene glycol, 5 h, 135 °C, 65%; d) *n*-dodecylisocyanate, pyridine, 12 h, 90 °C, 30%; e) *n*-hexylisocyanate, DMF/NMP, 20 h, 100 °C, 53%.

However, the dimerization constant of **7** in DMF-d₆ was not further determined. Next, the tautomeric preference of **6** was investigated in CDCl₃. From the comparison (Table 2.1) of the chemical shifts of **6** to those of UPy dimers substituted with weakly electron donating groups (**1** and **9**) and strong electron-withdrawing groups (**3** and **8**) in CDCl₃ the dramatic influence of the electron donating amino group can be readily observed. For example, pronounced differences in chemical shift can be observed for the most downfield proton, corresponding to the intramolecular hydrogen bonded NH proton in

the 4[1H]-pyrimidinone tautomer or the intermolecular hydrogen bonded OH proton in the pyrimidin-4-ol tautomer.

Table 2.1: ^1H and ^{13}C NMR chemical shifts (in ppm) of various UPy dimers measured in CDCl_3 at a concentration of 10 mM and a temperature of 25 °C.

Compound	$^{13}\text{C}^{\text{a}}$	^1H				
	C_5	NH/OH	NH	NH	$\text{C}_5\text{-H}$	
1 ($\text{R}_1 = \text{Me}$, $\text{R}_2 = \text{C}_4\text{H}_9$)	105	13.14	11.86	10.14	5.82	
3 ($\text{R}_1 = \text{Cl}$, $\text{R}_2 = \text{C}_{12}\text{H}_{25}$)	101	13.84	11.15	9.21	6.36	
4 ($\text{R}_1 = \text{C}_2\text{Si}(\text{Me})_3$, $\text{R}_2 = \text{C}_{12}\text{H}_{25}$)	keto	112	13.10	11.65	9.95	6.11
	enol ^{b)}	-	13.76	11.08	9.65	6.41
6 ($\text{R}_1 = \text{N}(\text{Bu})_2$, $\text{R}_2 = \text{C}_{12}\text{H}_{25}$)	79	12.60	11.22	9.58	5.33	
7 ($\text{R}_2 = \text{C}_6\text{H}_{13}$)	-	13.43	11.95	10.19	-	
	DMF- d_6^{c}	-	11.9	9.5	7.91	-
8 ($\text{R}_1 = \text{CF}_3$, $\text{R}_2 = \text{C}_4\text{H}_9$)	100	14.30	11.14	9.30	6.64	
9 ($\text{R}_1 = \text{Ph}$, $\text{R}_2 = \text{C}_4\text{H}_9$)	keto	104	13.92	12.04	10.21	6.35
	enol	-	13.60	11.30	10.0	6.70

^{a)} Determined by gHMQC ^{b)} Present in 5% as determined by integration. ^{c)} 40 mM

This proton in **6** is observed at 12.6 ppm while it takes a value of 13.4 ppm in **1** and 14.3 ppm in **8**. This strong upfield shift suggests substantial weakening¹⁷ of the corresponding hydrogen bond in dimeric **6** as compared to the same hydrogen bond present in dimers of **1** and **8**.

To gain further insight into the tautomeric preference of **6**, 2D transverse-ROESY spectroscopy was performed in toluene- d_8 (Figure 2.2). In CDCl_3 , the ^1H -NMR signals of H_a and H_e could not be resolved due to similar shielding constants of H_a and H_e . However, it was found that in toluene- d_8 an aromatic solvent induced chemical shift (ASIS) occurred¹⁸, inducing a difference in chemical shift between protons H_a and H_e , therefore allowing for the unambiguous assignment¹⁹ of the tautomeric form adopted in

this solvent. The key ROe contacts are drawn in Figure 2.2 and suggest hydrogen bonding via a **DADA** array in toluene- d_8 . The distance between H_a and H_c in the corresponding 4[1H]-pyrimidinone dimer is well over 5.5 Å, too large to give a ROe crosspeak of significant intensity.²⁰

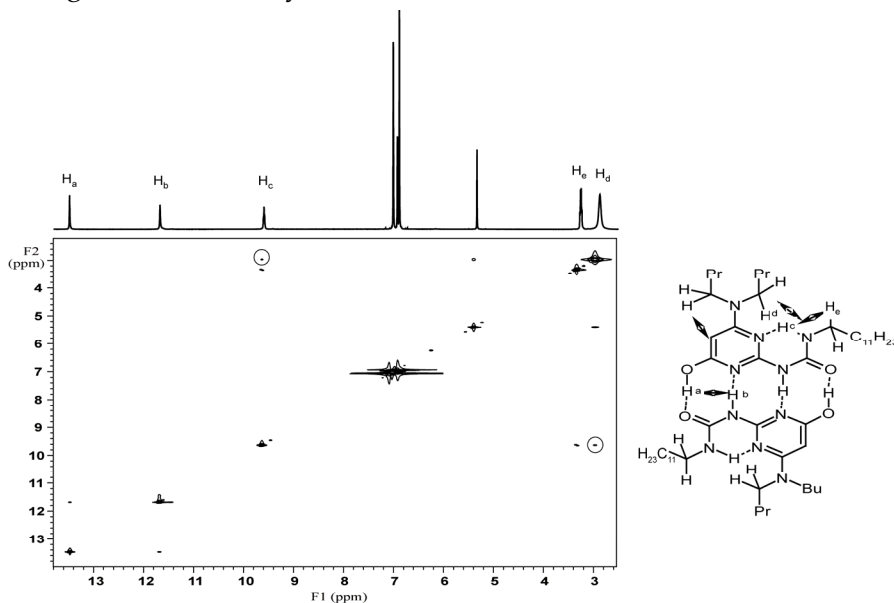


Figure 2.2: Key ROe contacts observed for **6** in toluene- d_8 (mixing time 100 ms) at 25 °C.

As is the case for UPy **6** in toluene- d_8 only a single set of signals is observed for UPy **3** in $CDCl_3$ suggesting that in this solvent **6** adopts only one tautomeric form. The tautomerization equilibrium constant of isocytosines are known to be solvent dependent²¹ and previously it was found⁵ that the pyrimidin-4-ol tautomer is slightly favored over the 4[1H]-pyrimidinone tautomer in more apolar solvents such as toluene. To our knowledge, there is no example of complete switching of the **DADA** hydrogen bonding array in toluene- d_8 to the **DDAA** form in $CDCl_3$. However, to assure that the **DADA** array is also maintained in $CDCl_3$, FT-IR experiments were performed on crystals of **6** (*vide infra*) and a solution of **6** in $CDCl_3$ (10^{-3} M). The solid state FT-IR spectra of dimers of **6** shows the characteristic peak pattern for dimers that exist in the pyrimidin-4-ol tautomeric form (see Appendix A).⁵ Notably, an absorption peak above 3215 cm^{-1} (intramolecular N-H...N) and an absorption peak at 2600 cm^{-1} (O-H...O=C) were found, indicative for pyrimidin-4-ol dimers. The FT-IR spectrum of UPy **6** in $CDCl_3$ is a superposition of the spectrum obtained on the crystalline material with the only difference being broadening of the absorption peak at 2600 cm^{-1} . These findings indicate that the **DADA** array is also maintained in the solid state and in the more polar solvent $CDCl_3$.

The crystal structure of dimeric **6** obtained from a saturated solution in acetone (Figure 2.3) shows that the molecules are indeed present in the pyrimidin-4-ol form. The urea functionality is in a *cisoid*, *transoid* conformation and an intramolecular hydrogen bond is present from the urea N-H to the pyrimidine nitrogen. As was previously found for **8** and **9**, the pyrimidinol units are dimerized via the **DADA** array. The OH...O hydrogen bonds are short (2.58 Å) while the NH...N distance is larger (2.98 Å). These distances are exactly similar to the hydrogen bond lengths found in pyrimidinol type dimers present in crystals of **9**. However, in the case of **9** it was found that roughly 50% dimerizes via the pyrimidinol tautomer in toluene-*d*₈ while the remaining material is present in the 4[1*H*]-pyrimidinone dimeric form. Remarkably, for **6** there is no indication for the formation of 4[1*H*]-pyrimidinone dimers in this solvent.

Table 2.2: Selected bond distances (Å), angles (deg) and dihedral angles (deg) for UPy **6**.

Compound	N-H...N distance	N-H...N angle	O-H...O distance	O-H...O angle	Sum of angles around N(24)	N(1)-C(6)- N(24)-C(29)
6	2.98	176	2.58	169	359.4	4.74

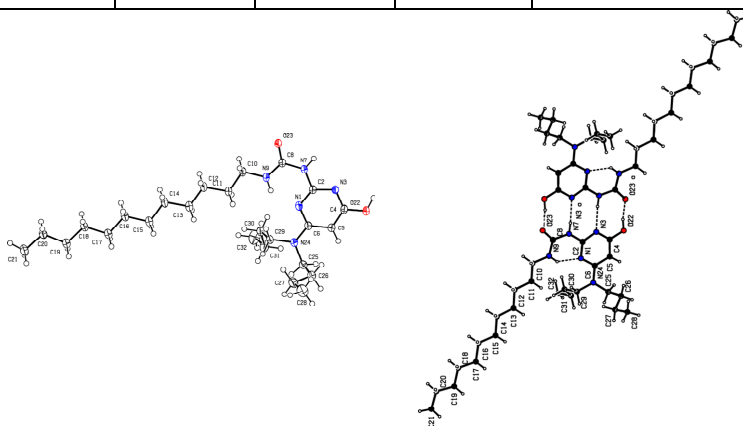


Figure 2.3: ORTEP diagram of the monomer geometry of **6** in the crystal. Ellipsoids represent 50% probability. PLUTON representation of the dimer geometry of **6** in the crystal.

Closer inspection of the crystal structure (Table 2.2) reveals that the sum of angles around N(24) in **6** is 359.4° suggesting almost full sp² hybridization and therefore complete delocalization of the nitrogen free electron pair into the pyrimidinone ring. The angle between the plains spanned by the aromatic ring and C(25)-C(29)-N(24) is 6.2°. These findings suggest that the stability of the **DADA** array is mainly due to an increase in hydrogen bonding acceptor strength of N(1) and N(3). This conclusion is supported

by the more downfield chemical shifts of both NH hydrogen bonds in dimeric **6** as compared the chemical shift of the dimer of trifluoro derivative **8** (Table 2.1).

2.3 Screening the fidelity of hetero-complexation with 2,7-diamido-1,8-naphthyridine

The hetero-association of UPy compounds **3**, **4**, **6**, **7**, **8**, **9** with 2,7-diamido-1,8-naphthyridine **10** (Figure 2.4) was probed by UV-Vis titrations at a concentration of 2.5×10^{-5} M in CHCl_3 at 25 °C. Upon addition of UPy to a solution of NaPy in CHCl_3 the absorption intensity at 355 nm increased (Figure 2.4a) while the absorption intensity at 347 nm decreases. A similar red shift upon formation of a hydrogen bonded anthyridine based **DDD-AAA** dimer has been recently reported by Leigh and co-workers.²¹

The ratio of the two absorptions *vs.* the amount of added UPy provides a qualitative tool to probe the fidelity²² of UPy-NaPy complex formation. As can be observed from Figure 2.1b for a high fidelity UPy-NaPy system, full complexation of dimeric UPy with NaPy into the UPy-NaPy hetero-complex already occurs at 2 eq of added UPy while for lower fidelity systems, 4–10 equivalents are required in order to induce full hetero-complexation.

As can be observed from Figure 2.4b the fidelity of the UPy-NaPy hetero-complex is the highest for UPy dimer **6** bearing an electron donating dibutyl-amino group at the C₆ position of the pyrimidinone ring.

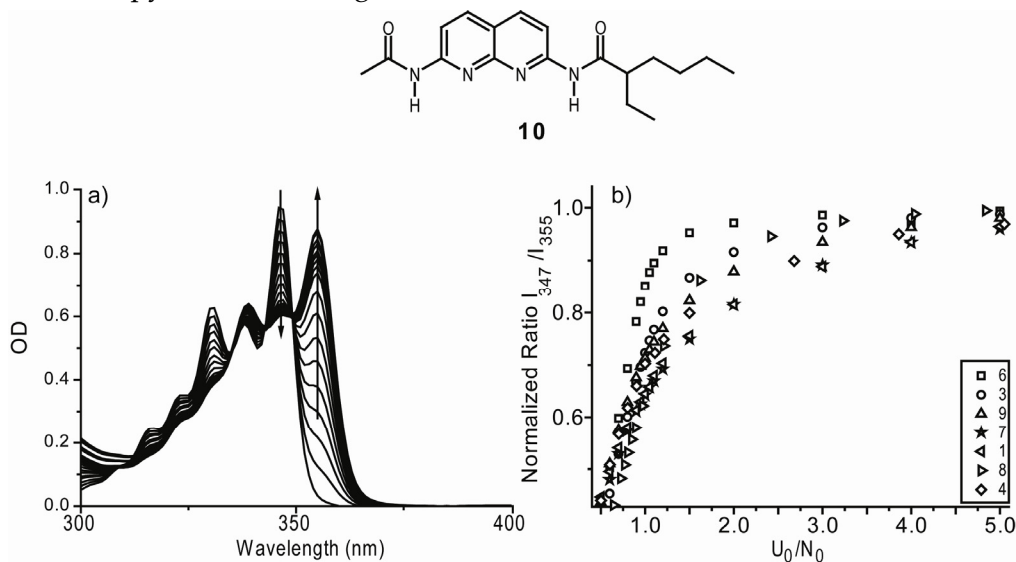


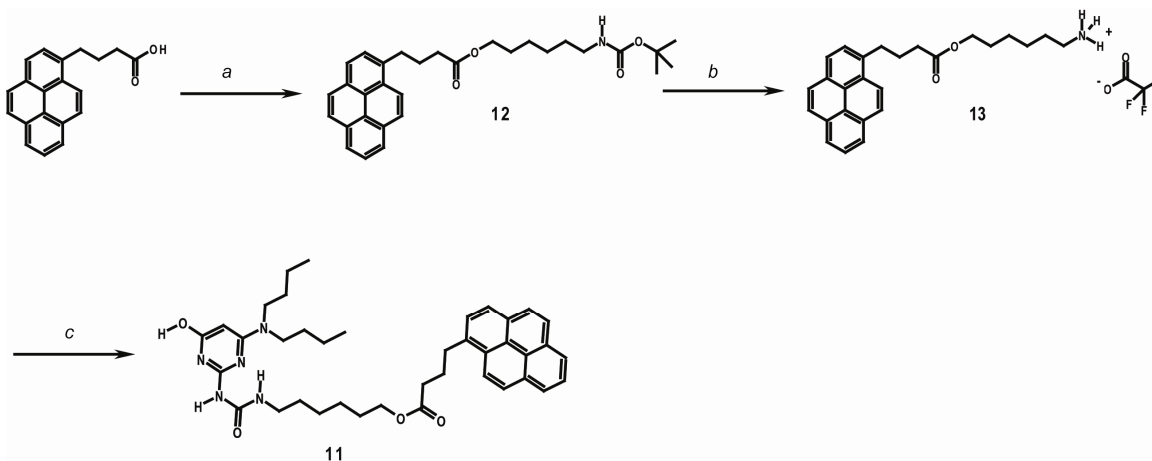
Figure 2.4: a) UV-visible spectra of a 2.5×10^{-5} M solution of **10** in CHCl_3 upon addition of UPy **6** at 25 °C. b) Change in normalized absorbance²³ as a function of the ratio UPy/NaPy for various ureido-pyrimidinones **3**, **4**, **6**, **7**, **8**, **9** added to NaPy **10**.

Upon addition of only 2 eq of UPy **6**, the normalized absorbance is already maximized while for methyl-substituted UPy **1** ($K_{\text{dim}} = 6 \times 10^7 \text{ M}^{-1}$ in CHCl_3) even the addition of 5 eq of **1** does not lead to a saturated signal, indicating that full conversion of dimeric **1** into **1·10** has not yet occurred at this concentration. From these experiments it can be further concluded that all ureido-pyrimidinones dimerizing via the weaker **DADA** hydrogen bonding array (UPy **3**, **6** and **8**) show increased fidelity of UPy·NaPy hetero-complexation compared to ureido-pyrimidinones dimerizing via the much stronger **DDAA** array (UPy **1** and **7**).

2.4 Evaluation of dimerization constant and association constant of dibutyl-amino substituted UPy dimer with 2,7-diamido-1,8-naphthyridine

Based on the previous UV-Vis titrations, the fidelity of UPy·NaPy hetero-complex formation is the highest for dibutyl-amino substituted UPy dimer **6·6**. To allow for a more quantitative treatment, the dimerization constant of **6** and the association constant of **6** with NaPy were assessed. $^1\text{H-NMR}$ dilution experiments performed on UPy dimer **6·6** up onto a final concentration of 0.1 mM did not result in the appearance of new signals nor did any significant shift occur. Under the assumption that at least 10% dissociation is required to be observable at this concentration, a lower limit on the dimerization constant can be placed: $K_{\text{dim}} > 4.5 \times 10^5 \text{ M}^{-1}$. To more accurately establish the dimerization constant of dibutylamino substituted 2-ureido-pyrimidinols, pyrene labeled compound **11** was synthesized and studied by fluorescence spectroscopy. Pyrene is highly fluorescent and is known to form an excimer species in solution, with a fluorescence band well separated from the monomer fluorescence. By attachment of the pyrene probe to the 2-ureido-pyrimidinol part excimer species within the dimerized complex can be followed as a function of concentration. This method has been previously used to find accurate values of the dimerization strength of methyl substituted 2-ureido-pyrimidinones^{1b}, ureidodeazapterin²⁴ and more recently to probe the dimerization constant of α,γ -cyclic peptides in CHCl_3 .²⁵

As a control experiment, a fluorescence spectrum was obtained at a concentration of 10^{-6} M of **11** in the presence of a 1000 fold excess of non-pyrene functionalized **6**. The fluorescence spectrum did not show any emission bands corresponding to excimer or exciplex, indicating that intramolecular exciplex formation with the dibutylamino groups does not occur.



Scheme 2.3: Synthesis of pyrene labeled dibutyl-amino substituted UPy **11**: a) 1-ethyl-3-(3-dimethylaminopropyl)carbodiimide hydrochloride, 4-dimethylaminopyridine, 6-(Boc-amino)-1-hexanol, dichloromethane, 24 h, 0-25 °C, 57%; b) trifluoroacetic acid, dichloromethane, 4 h, room temperature, 76%; c) Extraction (0.1 M NaOH/ dichloromethane followed by drying with MgSO₄ and addition of di-*t*-butyltricarboxylate at room temperature, then 2-amino-6-(dibutylamino) 4-pyrimidinol, pyridine, 15 h, 90 °C, 8%.

The dimerization constant (K_{dim}) of **11** obtained in freshly opened CHCl₃ ([water] = 10 mM) was determined to be $9 (\pm 2) \times 10^5 \text{ M}^{-1}$ (Figure 2.5) at 25 °C a value roughly 70 times lower than the value reported for the K_{dim} of UPy **1**. The difference in the dimerization constant between **11** and a pyrene derivative of **1** is mainly caused by the greater number of repulsive secondary interactions in **DADA** dimers compared to **DDAA** dimers.⁷ Using a recently published empirical model²⁶ a K_{dim} value of $1 \times 10^6 \text{ M}^{-1}$ was calculated for **6**, in close agreement²⁷ with the experimentally determined value. The application of pyrene chromophores for analysis of aggregation phenomena ought to be approached with caution because they are not passive fluorescence probes.²⁸ For example, Jones and co-workers determined the excimer formation constant of 4-(1-pyrene)butanoate in H₂O to be $1 \times 10^4 \text{ M}^{-1}$.²⁹ However, their study also showed that the driving force for this interaction is mainly hydrophobic and the excimer formation constant rapidly decreased upon addition of an organic co-solvent, such as CHCl₃.

In order to determine the association constant of UPy **6** with NaPy **2** ($R_3 = \text{C}_{11}\text{H}_{23}$), spectrophotometric titrations were employed. Upon addition of UPy dimer **6** to a solution of NaPy **2** ($2.5 \times 10^{-5} \text{ M}$) in CHCl₃ the absorption intensity at 355 nm increased. The absorbance at 355 nm as a function of added **6** could be fitted with a 1:1 binding model accompanied by dimerization of one of the components.

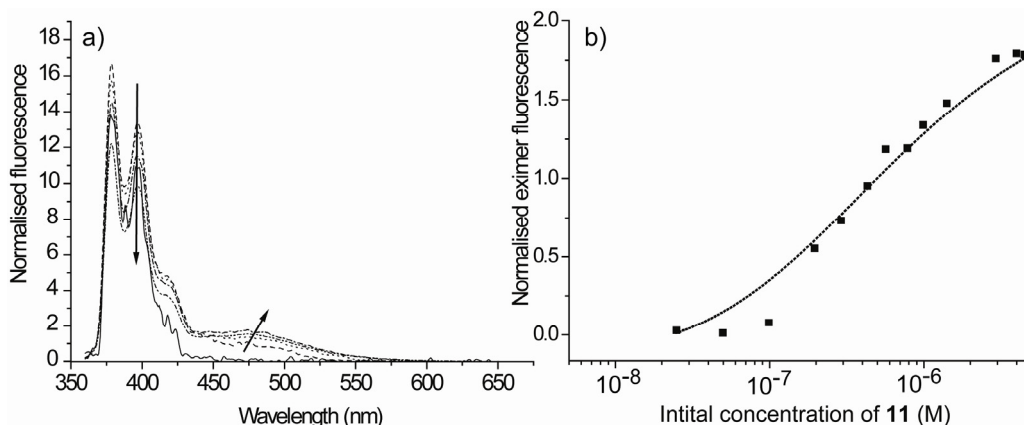


Figure 2.5: a) Normalized excimer fluorescence (defined as the integrated intensity divided by the concentration of **11**) at several concentrations of **11** in CHCl_3 at 25 °C. The arrow indicates an increase in concentration of **11** and hence an increase in intra-dimer excimer species. b) Plot of the normalized excimer fluorescence as a function of concentration. The dashed line represents the best-fit value of ($R^2 = 0.98$) K_{dim} using a monomer-dimer binding isotherm.

Assuming a K_{dim} of $9 \times 10^5 \text{ M}^{-1}$ the association constant (K_{a}) of the UPy·NaPy heterodimer (as well as the extinction coefficient at the absorption maximum (ϵ_{nu})) can be obtained (see Appendix B). Curve fitting gave a K_{a} of **6·2** of $6 (\pm 0.5) \times 10^6 \text{ M}^{-1}$ at 25 °C in CHCl_3 , a value close to the association constant of **1·2** ($5 (\pm 0.6) \times 10^6 \text{ M}^{-1}$). To investigate the influence of the lowered K_{dim} of **6** on the selectivity of UPy·NaPy complex formation, the fraction of **6·2** in a 1:1 mixture was measured with $^1\text{H-NMR}$ in CDCl_3 at several concentrations and compared with the concentration dependent formation of **1·2**. As can be readily observed from Figure 2.6, the fraction of **6·2** at lower concentration is higher than the fraction of **1·2**, indicating that hetero-association of dimeric **6** with **2** is more selective than hetero-association of dimeric **1** with **2**. The calculated values, based on the experimentally determined values of K_{dim} and K_{a} correspond well with the measured fractions as determined by $^1\text{H-NMR}$.

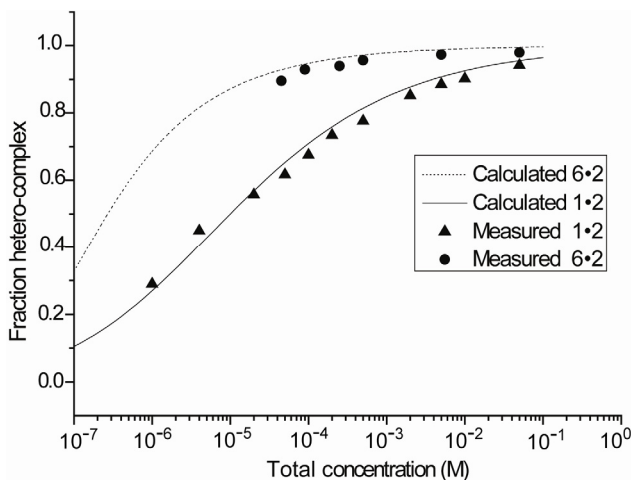


Figure 2.6: Measured value of the fraction of UPy·NaPy complex in a 1:1 mixture for 6•2 and 1•2 in CDCl₃ at 25 °C. Lines are calculated values from experimentally determined K_a and K_{dim} values.

2.5 Self-sorting in mixtures of DDAA and DADA hydrogen bonding units

Self-sorting, the mutual recognition of complementary components within a mixture is common in nature but is still relatively rare in synthetic supramolecular systems. For example, a survey of the various proteins found in *E. coli* shows that homo-oligomeric proteins are present in a much larger amount compared to hetero-oligomeric proteins.³¹ In synthetic supramolecular systems, self-sorting can lead to multiple self-assemblies capable of operating simultaneously and orthogonally within a complex mixture.^{32,33}

As has been proposed by Isaacs, self-sorting systems can be subdivided into thermodynamic self-sorting systems and kinetic self-sorting systems.³³ A system is defined as a thermodynamic self-sorting system if it has attained thermodynamic equilibrium and displays self-sorting. Thermodynamic self-sorting in supramolecular assemblies has been realized by engineering different local interactions within the various possible supramolecular aggregates. For example, different hydrogen bonding patterns³⁴, different metal-ligand pairs³⁵, different solvophobic interactions³⁶ and even a difference in geometry³⁷ or chirality³⁸ between various supramolecular complexes can be used to induce thermodynamic self-sorting.

Previously, it was shown that in a mixture containing two different 2-ureido-pyrimidinone units both dimerizing via the strong DDAA array, a statistical mixture of homo and hetero dimers was formed.³⁹ Triggered by the difference in arrangement of donor and acceptor units between DDAA and DADA hydrogen bonding arrays, 1:1 mixtures of **1** with **3**, **6** or **8** at a total concentration of 10 mM in CDCl₃ were probed for their ability to selectively self-sort into their homomeric components (Figure 2.7). The ¹H-NMR spectra of mixtures of two ureido-pyrimidinone derivatives at low

concentration indeed shows slowly exchanging hetero-dimers in equilibrium with their homo-dimers in all cases (Figure 2.7). The process of exchange leads to a mixture in which the homo-dimers of **1** (**DDAA** hydrogen bonding array) and the homo-dimers of **3**, **6** or **8** (**DADA** hydrogen bonding array) are present in a much larger amount than their hetero-dimers (**1·3**, **1·6** and **1·8** respectively). Closer inspection of the $^1\text{H-NMR}$ traces reveal the formation of two distinct hetero-dimers in a total amount of approximately 15% in all three cases. For example, for the 1:1 mixture of dibutyl-amino substituted UPy **6** and methyl substituted UPy **1** one hetero-dimer adopts a **DDAA** hydrogen bonding array in which **6** adopts the keto tautomeric form while the other hetero-dimer adopts a **DADA** hydrogen bonding array in which **1** adopts the enol tautomeric form.

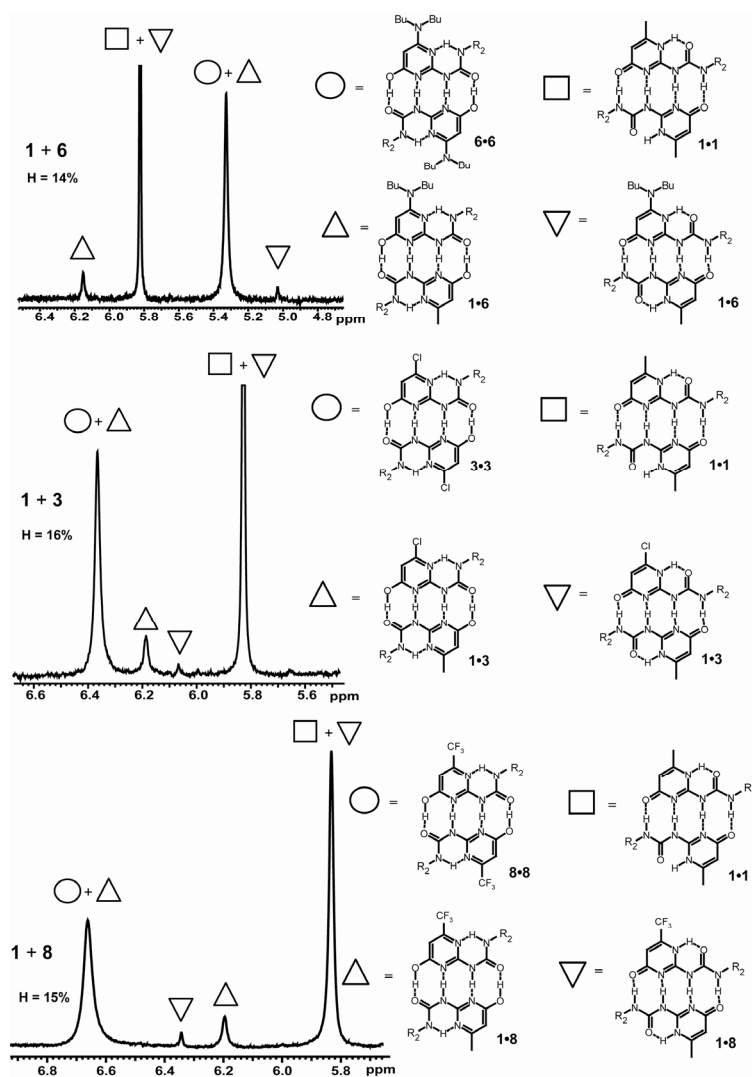


Figure 2.7: $^1\text{H-NMR}$ spectra of a 10 mM equimolar CDCl_3 solution of **1** with either **3**, **6** or **8** at 25 °C.

Characterization of the two hetero-dimers was performed by performing the same experiment using a derivative of **1** lacking the proton at the alkylidene position (see Appendix C).

From these experiments it becomes clear that the self-sorting process is driven by difference between the equilibrium constants for homomeric versus heteromeric aggregation. The smaller equilibrium constant of the hetero-dimers most probably finds its origin in the fact that in each of the two hetero-dimers one of the UPy units needs to adopt a wrong tautomeric form. In order to allow for a more quantitative discussion a model was developed, based on a previously published model by Isaacs^{33a}, for a simple two component system as described in Figure 2.8a comprising monomer (A and B), homodimers (A_2 and B_2) and one hetero-dimer (AB) whose equilibria are governed by three equilibrium constant (K_{AA} , K_{BB} , K_{AB}).

The values for the total concentrations of A and B (5 mM each) and values of K_{AA} ($6 \times 10^7 \text{ M}^{-1}$) and K_{BB} ($9 \times 10^5 \text{ M}^{-1}$) were fixed as outlined in Figure 2.8b (see Appendix C for the description of the computer program). Figure 2.8d shows a plot of the mole fraction versus K_{AB} . For low values of K_{AB} ($0 < K_{AB} < 10^5 \text{ M}^{-1}$) self-sorting is highly effective and the homo dimers are present in an amount greater than 98%. When K_{AB} is 10-fold lower than the dimerization constant of the weakest binding monomer B, the fraction of hetero-dimer starts to increase while at high values of K_{AB} ($> 10^8 \text{ M}^{-1}$) the fidelity of hetero-dimerization is almost 100%.

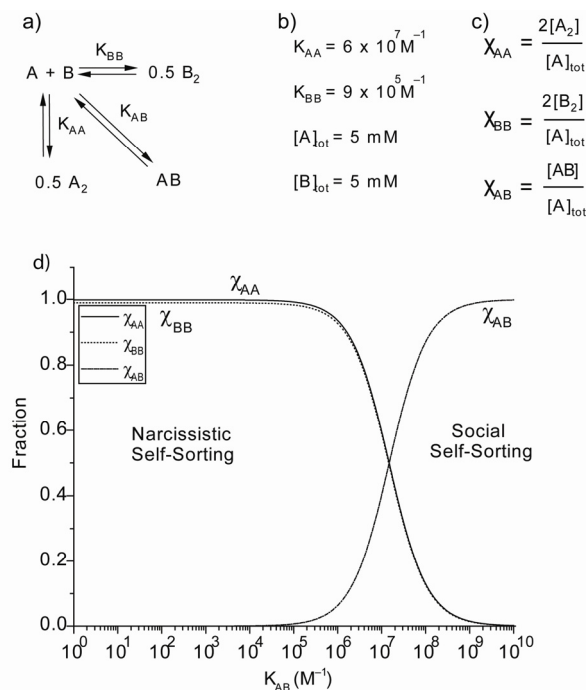


Figure 2.8: Degree of self-sorting in a two component mixture as a function of K_a : a) equilibria present b) constraints imposed c) mole fraction definitions d) a plot of the mole fraction versus K_{AB} .

2.6 Conclusions and discussion

In this chapter, several new ureido-pyrimidinone derivatives were synthesized with both electron-withdrawing and electron donating substituents attached to the C₆ position of the pyrimidinone ring. Previously, it was reported that electron withdrawing substituents such as CF₃ attached to the C₆ position of the pyrimidinone ring favor the exclusive formation of the pyrimidin-4-ol **DADA** dimer. This preference was explained by Beijer³⁹ by considering the fact that the enol and keto tautomers are in equilibrium with the same protonated species (Figure 2.9). The tautomeric equilibrium can be deduced from the relative acidities of the two hydrogen atoms that can be lost from the common cation: if the OH proton is more acidic than the NH proton this proton will be abstracted more easily and the 4[1H]-pyrimidinone tautomer results while if the NH proton is more acidic the pyrimidin-4-ol tautomer will be formed.

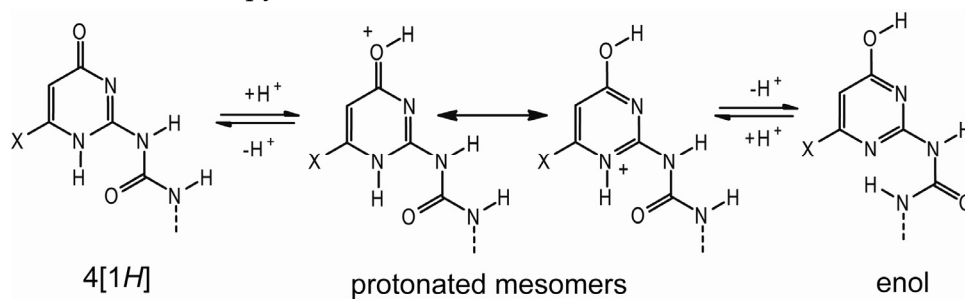


Figure 2.9: Explanation for the preference for the pyrimidin-4-ol tautomer (enol) over the 4[1H]-pyrimidinone with electron withdrawing 6-position substituents.

Hence, if X is an electron withdrawing group the acidity of the *ortho* NH proton is increased considerably relative to the OH proton at the *meta* position resulting in a preference for the pyrimidin-4-ol tautomeric form. Indeed for an inductive electron withdrawing group such as chlorine, the pyrimidin-4-ol **DADA** dimer of **3** is present as the only species in both CDCl₃ as well as in toluene. These findings are in agreement with the results reported by Katritzky⁴⁰ who found that chlorine atoms α to the nitrogen atom in the analogous 4-pyridone system displace the tautomeric equilibrium of pyridones almost completely in favor of the hydroxypyridine form in solvents of low dielectric constant. However, this hypothesis does not explain the preference of the pyrimidin-4-ol tautomer when an electron-donating dialkyl amino substituent, such as is found in **6**, is employed. For electron-donating groups at the 6 position, the *ortho* NH becomes less acidic which should result in an increased preference of the 4[1H]-pyrimidinone tautomer in sharp contrast to the experimental results.

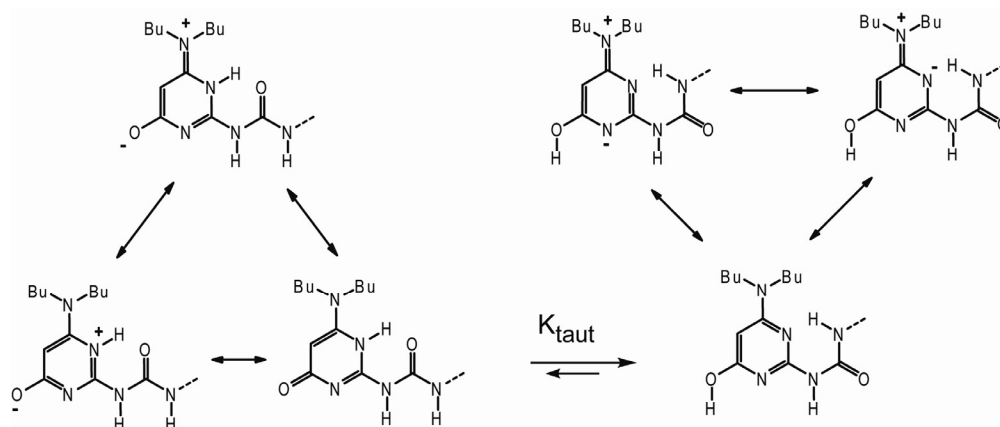


Figure 2.10: Explanation for the preference for the pyrimidin-4-ol tautomer (enol) over the 4[1H]-pyrimidinone with an electron donating dibutyl-amino substituent.

The preferred formation of the pyrimidin-4-ol tautomer in **6** may therefore be due a combination of several factors: 1) Higher basicity of the oxygen atom with respect to N1 and N3. 2) A more pronounced aromatic stabilization of the pyrimidin-4-ol with respect to the pyrimidinone tautomer⁶ and a favorable intramolecular hydrogen bond between the urea side chain and N1 (Figure 2.10). 3) Steric hindrance of the NH proton in the keto 4[1H] tautomer with the dibutylamino substituent at the C₆ position of the pyrimidinone ring.

The fact that **6** dimerizes via a **DADA** hydrogen bonding array in solution results in a considerable loss in dimerization strength compared to UPy compounds dimerizing via the **DDAA** hydrogen bonding array. Quite conveniently, the large drop in K_{dim} results in an increase in fidelity with respect to hetero-association with 2,7-diamido-1,8-naphthyridine as the K_a of UPy·NaPy formation is not influenced by the substitution with an electron-donating substituent. The effect of the increased fidelity on the supramolecular polymerization of an AB monomer capable of both A·B and A·A interactions will be the subject of the next chapter.

Driven by the mismatch in the pattern of hydrogen bond donors and acceptors and high tautomerization energies, effective self-sorting in mixtures of 4[1H]-pyrimidinone and pyrimidin-4-ol dimers is observed. For example, in 1:1 solutions of methyl substituted UPy **1** and dibutyl-amino UPy **6**, only 15% of the material is present in the hetero-dimer **1·6**. This amount can most probably be reduced even further by employing an UPy derivative with a higher tautomerization energy compared to UPy **1**. Previous results³⁹ have shown that substitution of the ureido substituent with a phenyl group ($R_1 = C_{13}H_{27}$, $R_2 = C_6H_5$) leads to an increase of the pyrimidinone tautomer with respect to the pyrimidin-4-ol tautomer compared to its aliphatic counterpart **1**. Further research in this

area can lead to a new class of supramolecular polymers in which orthogonal operating hydrogen bonding units can be used to create novel material properties. Currently, the design of orthogonal interactions within supramolecular materials relies on the simultaneous use of two different non-covalent interactions i.e. hydrogen bonding in combination with ionic interactions or metal ligand coordination.⁴¹ Only recently, self-sorting of competitive hydrogen bonding units has been used to construct orthogonal interactions within supramolecular graft co-polymers.⁴²

2.7 Experimental section

General Methods

All chemicals were purchased from Aldrich, Acros or Alfa Aesar and were used as received unless otherwise noted. 1-Tributylstannyl-2-trimethylsilylacetylene was ordered from TCI Europe Organic Chemicals. Toluene was distilled from sodium/potassium/benzophenone. CDCl₃ was dried over 4 Å molsieves 2 days before use and anhydrous pyridine was obtained from Aldrich. All reactions were followed by thin-layer chromatography (precoated 0.25 mm silica gel plates from Merck), and silica gel column chromatography was carried out with silica gel 60 (mesh 70-230). ¹H-NMR and ¹³C-NMR spectra were recorded on a 400 MHz NMR (Varian Mercury, 400 MHz for ¹H-NMR and 100 MHz for ¹³C-NMR), a 300 MHz NMR (Varian Gemini, 300 MHz for ¹H-NMR and 75 MHz for ¹³C-NMR) or 500 MHz NMR (Varian Unity Inova, 500 MHz for ¹H-NMR and 125 MHz for ¹³C-NMR). Proton chemical shifts are reported in ppm downfield from tetramethylsilane (TMS). The following splitting patterns are designated as s, singlet; d, doublet; t, triplet; q, quartet; b, broad; m, multiplet. Carbon chemical shifts are reported downfield from TMS using the resonance of the deuterated solvent as the internal standard.

Matrix assisted laser desorption/ionization mass-time of flight (MALDI-TOF) were obtained using a PerSeptive Biosystems Voyager-DE PRO spectrometer using an acid α -cyanohydroxycinnamic acid (CHCA) or a neutral 2-[(2E)-3-(4-*tert*-butylphenyl)-2-methylprop-2-enylidene]malononitrile (DCTB) matrix. Infrared (IR) spectra were recorded on a Perkin Elmer Spectrum One FT-IR spectrometer with a Universal ATR sampling Accessory. Solutions of **3**, **6** and **7** in CDCl₃ (10⁻³ M) were loaded between a pair of KBr windows using a 5 mm Teflon spacer contained in a demountable liquid cell. Elemental analysis was performed on a Perkin Elmer 2400 series II CHNS/O Analyzer. Melting points were determined on a Büchi Melting Point B-540 apparatus. 2,7-Diamido-1,8-naphthyridines **2** and **10** were synthesized according to the method of Lighthart et al.⁴³ 2-Ureido-pyrimidinones **1**, **8** and **9** were synthesized according to Beijer.⁵ 2-ureido-pyrimidinone **15** was synthesized according to Söntjens.⁴⁴

Synthesis of 1-(4-chloro-6-hydroxypyrimidin-2-yl)-3-dodecylurea (**3**)

Before the reaction, 2-amino-6-chloro-4-pyrimidinol hydrate was dried extensively (2 days) over P₂O₅ under dynamic vacuum followed by several co-evaporations with *p*-xylol. 2.34 g (16 mmol) of dried 2-amino-6-chloro-4-pyrimidinol and 5 mL of dodecyl isocyanate (1.35 eq) were added to

48 mL of *o*-dichlorobenzene (ODCB) and heated to 150 °C for 18 h under an atmosphere of argon. After 18 hours the homogeneous solution was cooled slowly to room temperature after which a precipitate was formed. The precipitate was collected by vacuum filtration and washed with 100 mL of boiling CHCl₃. The CHCl₃, containing the desired compound, was evaporated *in vacuo* and the resulting solid was subsequently recrystallized from 50 mL of acetonitrile after which the resulting precipitate was washed with cold acetone resulting in an off white solid. Further purification consists of repetitive recrystallizations from 40 mL of CHCl₃ at -20 °C resulting in 2.0 g (5.6 mmol, yield 28%) of **3** as an off white solid, mp 197 °C (degr.). ¹H-NMR (CDCl₃): δ = 13.84 (s, 1H, OH), 11.15 (s, 1H, NH), 9.21 (s, 1H, NH), 6.36 (s, 1H, C₁-H), 3.38 (t, 2H, CH₂C₁₁H₂₃), 1.64-1.26 (m, 20H, -CH₂-), 0.88 (t, 3H, CH₃). ¹³C-NMR (CDCl₃): δ = 171.9 (C₂), 159.7, 156.8, 156.3, 101.4 (C₁), 40.1, 31.9, 29.6, 29.5, 29.33, 29.28, 29.23, 26.9, 22.7, 14.1 (CH₃). IR (ATR): ν = 3245, 3148, 3031, 2917, 2849, 2580, 1679, 1607, 1564, 1531, 1477, 1458, 1388, 1360, 1326, 1291, 1281, 1256, 1134, 1062, 994, 968, 921 cm⁻¹. MALDI-TOF-MS (m/z): calcd: 356.2 obs: 357.14 (MH⁺), 379.13 (MNa⁺). Anal. Calcd for C₁₇H₂₉N₄O₂Cl: C 57.21, H 8.19, N 15.70 found C 57.14, H 8.67, N 15.63.

Synthesis of 1-dodecyl-3-(4-oxo-6-((trimethylsilyl)ethynyl)-1,4-dihydropyrimidin-2-yl)urea (**4**)

0.1 g of (0.28 mmol) of 1-(4-chloro-6-hydroxypyrimidin-2-yl)-3-dodecylurea **3** was dissolved in 2.4 mL of distilled toluene in an oven dried Schlenk tube under an atmosphere of argon. Then Pd₂(dba)₃ (12.4 mg, 0.014 mmol, 5 mol%) and P(*t*-Bu)₃ (33 μL of a 1.73 M stock solution in distilled toluene, 0.056 mmol, 20 mol%) were added and the solution was degassed by repetitive cycles of freeze-pump-thaw. The temperature of the solution was raised to 70 °C and 163 mg of 1-tributylstannyl-2-trimethylsilylacetylene (0.16 g, 0.42 mmol, 1.5 eq) was added in a single portion under a constant stream of argon. The solution was heated at 100 °C for 20 h and subsequently cooled to room temperature after which ethyl acetate was added and the solution was filtered over silica and evaporated *in vacuo*. Column chromatography using a gradient of 0-2% EtOH/CHCl₃ resulted in a black solid after evaporated *in vacuo* which was further purified by recrystallization from a minimal amount of 1:1 ethyl acetate/pentane resulting in 45 mg (0.11 mmol, 40% yield) of **4** as a off white solid, mp 95-97 °C. ¹H-NMR (CDCl₃): δ = 13.10 (s, 1H, NH), 11.65 (s, 1H, NH), 9.95 (s, 1H, NH), 6.1 (s, 1H, C₁-H), 3.25 (t, 2H, CH₂C₁₁H₂₃), 1.61-1.25 (m, 20H, -CH₂-), 0.88 (t, 3H, CH₃), 0.26 (s, 9H, Si(CH₃)₃). ¹³C-NMR (CDCl₃): δ = 172.0, 156.2, 154.6, 131.9, 112.1 (C₁), 104.8, 94.6, 40.1, 31.9, 29.64, 29.58, 29.49, 29.34, 26.9, 22.7, 14.1 (CH₃), -0.7 (Si(CH₃)₃). IR (ATR): ν = 3216, 2958, 2919, 2851, 1695, 1649, 1582, 1524, 1469, 1403, 1323, 1295, 1252, 1167, 1131, 1011, 950, 846 cm⁻¹. MALDI-TOF-MS (m/z): calcd: 418.27 found: 419.25 (MH⁺), 441.25 (MNa⁺). Anal. Calcd for C₂₂H₃₈N₄O₂Si: C 63.12, H 9.15, N 13.38 found C 63.17, H 9.44, N 13.36.

Synthesis of 2-amino-6-(dibutylamino) 4-pyrimidinol (**5**)

10 g (68.7 mmol) 2-amino-6-chloro-4-pyrimidinol hydrate (H₂O 5-15%) was dissolved in 170 mL ethylene glycol and 30 mL dibutylamine (178 mmol) was added. The solution was heated for 5 h at 135 °C after which it was allowed to cool room temperature. The solution was dumped into 666 mL of a saturated aqueous solution of NH₄Cl and extracted three times with 700 mL ethyl acetate. The combined organic layers were evaporated *in vacuo* to a volume of 700 mL and extracted with 500 mL of a saturated aqueous solution of NaHCO₃ and 700 mL brine. The organic

layer was dried with magnesium sulfate, filtered and evaporated *in vacuo*. The slightly yellow solid was treated with 50 mL boiling acetonitrile after which everything dissolved. Upon cooling of the solution a precipitate was formed which was filtrated and washed with 10 mL pentane resulting in a white residue containing the desired compound. This process was repeated twice affording 10.69 g (44.85 mmol, yield 65%) of 2-amino-6-(dibutylamino) 4-pyrimidinol as a white solid, mp 161 °C. ¹H-NMR (CDCl₃): δ = 12.01 (s, 1H, OH), 5.32 (s, 2H, NH₂), 4.8 (s, 1H, C₁-H), 3.30 (b, 4H, N(-CH₂)₂), 1.54-1.49 (m, 4H, N(-CH₂-CH₂)₂), 1.32-1.26 (m, 4H, N(-CH₂-CH₂-CH₂)₂), 0.94-0.91 (t, 6H, CH₃). ¹³C-NMR (CDCl₃): δ = 165.8 (C₂), 163.6, 154.4, 76.3 (C₁). 48.1, 29.6, 20.1, 13.9. IR (ATR): ν = 3317, 3166, 2956, 2930, 2871, 2730, 1586, 1558, 1490, 1453, 1369, 1331, 1288, 1161, 1110, 1075, 1028, 969, 782, 750 cm⁻¹. MALDI-TOF-MS (m/z): calcd: 238.18 obs: 239.17 (MH⁺). Anal. Calcd for C₁₂H₂₂N₄O: C 60.48, H 9.3, N 23.51 found C 60.24, H 9.17, N 23.45.

Synthesis of 1-(4-(dibutylamino)-6-hydroxypyrimidin-2-yl)-3-dodecylurea (6)

A suspension of 1 g (4.2 mmol) 2-amino-6-(dibutylamino) 4-pyrimidinol and 1.2 mL of dodecyl isocyanate (4.98 mmol, 1.2 eq) in 5 mL of dry pyridine was heated under argon at 90 °C for 12 h. After cooling the solution was evaporated to dryness. Upon addition of 20 mL diethyl ether a white precipitate was formed which was filtered off. The filtrate was evaporated *in vacuo* and further purified by column chromatography (SiO₂ 3:1 (v/v) cyclohexane/ ethylacetate) resulting in a sticky off white solid. Recrystallization of the sticky solid in 20 mL of acetone at 0 °C resulted in precipitation of **6** as an amorphous white powder which was subsequently dried *in vacuo*, mp 87 °C. Yield: 30% ¹H-NMR (CDCl₃): δ 12.61 (s, 1H, OH), 11.21 (s, 1H, NH), 9.58 (s, 1H, NH), 5.32 (s, 1H, C₁-H), 3.3-3.0 (b, 6H, N(-CH₂)₂ and CH₂-C₁₁H₂₃), 1.61-1.55(m, 6H, N(-CH₂-CH₂)₂ and CH₂CH₂C₁₀H₂₁), 1.39-1.25 (m, 22H, CH₂), 0.98-0.94 (t, 6H, CH₃), 0.89-0.86 (t, 3H, CH₃). ¹³C-NMR (CDCl₃): δ = 170.9, 162.5, 157.4, 157.0, 78.7 (C₁), 50.0, 40.0, 31.9, 30.3, 29.6, 29.4, 29.3, 27.0, 22.7, 20.4, 14.1 (CH₃), 14.0 (CH₃). IR (ATR): ν = 3218, 3127, 3019, 2955, 2922, 2852, 2548 (O-H ::O=C hydrogen bond), 1674, 1613, 1559, 1524, 1504, 1454, 1445, 1369, 1321, 1282, 1252, 1206, 1147, 1111, 1061, 987, 891, 795, 692 cm⁻¹. MALDI-TOF-MS (m/z): calcd: 449.38 obs: 450.25 (MH⁺). Anal. Calcd for C₂₅H₄₇N₅O₂: C 66.78, H 10.54, N 15.57 found C 67.20, H 10.65, N 15.70.

Synthesis of 1-hexyl-3-(6-methyl-4-oxo-1,4-dihydroquinazolin-2-yl)urea (7)

To a suspension of 0.51 g (2.92 mmol) of 2-amino-6-methyl-4(3H)-quinazolone, 12 mL dimethylformamide and 1 ml of N-methylpyrrolidone was added 0.62 mL of hexylisocyanate (0.48 mg, 3.8 mmol). The suspension was heated at 100 °C for 20 h under an atmosphere of argon after which the solution became clear. After cooling to room temperature, 30 mL of a 1:1 mixture of diethylether/pentane was added and the precipitate was filtered and washed with 30 mL of pentane and 30 mL of acetone respectively. After drying of the residue it was treated with 400 mL of hot CHCl₃ which was subsequently evaporated *in vacuo* resulting in 0.34 g (yield: 53%) of **7** as a white solid, mp 250-255 °C (degr.). ¹H-NMR (CDCl₃): 13.43 (1, 1H, NH), 11.95 (s, 1H, NH), 10.19 (s, 1H, NH), 8.0 (s, 1H, C₁₈-H), 7.47 (d, 1H, C₁₆-H), 7.16 (d, 1H, C₁₅-H), 3.35 (t, 2H, CH₂), 2.45 (s, 3H, CH₃), 1.70-1.32 (m, 8H, CH₂), 0.9 (t, 3H, CH₃). ¹³C-NMR (CDCl₃): δ = 171.2, 156.9, 154.4, 136.0, 135.3, 135.1, 127.2, 118.2, 116.5, 40.2, 31.6, 29.4, 26.7, 22.6, 21.0, 14.1. IR (ATR): ν = 3211, 2961, 2949, 2925, 2851, 1692, 1636, 1446, 1307, 1263, 1219, 1206, 1128, 1040, 999, 923, 817 cm⁻¹. MALDI-TOF-MS

(m/z): calcd: 302.17 obs: 303.12 (MH⁺). Anal. Calcd for C₁₆H₂₂N₄O₂: C 63.56, H 7.33, N 18.53 found C 63.17, H 7.33, N 18.63.

Synthesis of 6-(tert-butoxycarbonylamino)hexyl 4-(pyren-1-yl)butanoate (**12**)

Under argon, a mixture of 1 g 4-(1-pyrenyl)butyric acid (3.47 mmol) and 70 mg of DMAP (0.57 mmol) in 70 mL of distilled dichloromethane was cooled to 0 °C followed by addition of 724 mg of 1-ethyl-3-(3-dimethylaminopropyl)carbodiimide hydrochloride (3.77 mmol). The mixture was stirred for 1 h at this temperature after which 828 mg of 6-(boc-amino)-1-hexanol (3.81 mmol) dissolved in 20 mL distilled dichloromethane was added dropwise. The mixture was allowed to come to room temperature and was stirred for an additional 16 h. The solution was diluted with 120 mL dichloromethane and extracted two times with 0.02 M aqueous HCl. The aqueous layer was back extracted with 100 mL dichloromethane and the combined organic layers were extracted two times with 300 mL saturated aqueous NaHCO₃ solution and one time with 350 mL brine. The organic layer was dried with magnesium sulfate, filtered and evaporated *in vacuo*. The resulting yellow oil was further purified by column chromatography (SiO₂, 20% ethyl acetate/heptane) followed by additional column chromatography (SiO₂, DCM) resulting in 955 mg (1.96 mmol) of **12** as a sticky white solid, mp 71 °C. Yield: 57%. ¹H-NMR (CDCl₃): δ 8.30-7.84 (m, 9H, PyrH), 4.53 (s, 1H, NH), 4.07 (t, 2H, COO-CH₂), 3.38 (t, 2H, CH₂-COOCH₂), 3.08 (m, 2H, CH₂NH), 2.46 (t, 2H, Pyr-CH₂CH₂), 2.20 (m, 2H, CH₂-CH₂-COOCH₂-), 1.62-1.56 (m, 2H, COOCH₂CH₂), 1.46-1.26 (m, 13H) ppm. ¹³C-NMR (CDCl₃): 173.5, 156.0, 135.7, 131.4, 130.9, 128.7, 127.5, 127.4, 127.3, 126.7, 125.8, 125.1, 125.0, 124.9, 124.81, 124.78, 124.76, 123.3, 79.0, 64.4, 40.5, 33.9, 32.8, 30.0, 28.6, 28.5, 26.8, 26.4, 25.6 ppm. IR (ATR): ν = 3374, 3041, 2933, 2861, 1701, 1509, 1454, 1390, 1365, 1246, 1162, 1144, 908, 728 cm⁻¹. MALDI-TOF-MS (m/z): calcd: 487.28 obs: 487.17 (M⁺). Anal. Calcd for C₃₁H₃₇NO₄: C 76.36, H 7.65, N 2.87 found C 75.99, H 7.58, N 2.75

Synthesis of 6-(4-(pyren-1-yl)butanoyloxy)hexan-1-aminium (isolated as TFA salt) (**13**)

To a stirred solution of 6-(tert-butoxycarbonylamino)hexyl 4-(pyren-1-yl)butanoate (1.56 g, 3.20 mmol) in 67 mL of dry dichloromethane under argon was added 7 mL trifluoroacetic acid dropwise (10.75 g, 94.4 mmol). The solution was stirred for an additional 4 h after which it was concentrated *in vacuo*. All traces of trifluoroacetic acid were removed by flushing several times with 10 mL of acetonitrile followed by flushing with diethyl ether which resulted in solidification of the product. Finally, addition of 20 mL diethyl ether to the white solid resulted in a suspension that was filtrated and washed with 10 mL of cold acetone. Drying of the residue resulted in 1.22 g of **13** (2.42 mmol) as a white solid, 118 °C (degr.). Yield: 76%. ¹H-NMR (CDCl₃): δ 8.30-7.84 (m, 9H, PyrH), 7.84 (b, 3H, NH₃⁺), 3.98 (t, 2H, COOCH₂), 3.32 (t, 2H, CH₂-COOCH₂), 2.80 (b, 2H, CH₂-NH₃⁺), 2.40 (t, 2H, Pyr-CH₂CH₂), 2.14 (tt, 2H, CH₂-CH₂-COOCH₂-), 1.52-1.25 (m, 8H, CH₂) ppm. ¹³C-NMR (CDCl₃): 173.8, 135.6, 131.3, 130.8, 129.9, 128.7, 127.4, 127.33, 127.27, 126.7, 125.8, 125.0, 124.93, 124.89, 124.76, 124.73, 123.22, 64.1, 39.7, 33.8, 32.7, 28.1, 27.2, 26.7, 25.6, 25.1 ppm. IR (ATR): ν (cm⁻¹) = 3041, 2939, 2865, 1725, 1674, 1529, 1460, 1431, 1418, 1345, 1306, 1242, 1199, 1178, 1132, 841, 798, 721 cm⁻¹. MALDI-TOF-MS (m/z): calcd: 388.22 obs: 388.10 (M⁺). Anal. Calcd for C₃₁H₃₇NO₄: C 67.05, H 6.03, N 2.79 found C 67.19, H 6.00, N 2.83

Synthesis of 6-(3-(4-(dibutylamino)-6-hydroxypyrimidin-2-yl)ureido)hexyl4-(pyren-1-yl)butanoate (11)

A suspension of 1 g of 6-(4-(pyren-1-yl)-butanoyloxy) hexan-1-aminium (2.05 mmol) in 400 mL distilled dichloromethane was extracted with 1 L 0.1 M NaOH. The aqueous layer was back extracted with 100 mL distilled dichloromethane and the combined organic layers were extracted with 500 mL brine. The organic layer was dried extensively with magnesium sulfate, filtered and evaporated *in vacuo* to a volume of 10 mL. Under argon, this solution was rapidly injected into a solution of 720 mg di-*t*-butyltricarboxylate in 100 mL distilled dichloromethane. The solution immediately showed gas evolution (CO₂) indicating the formation of the isocyanate. The solution was stirred for 1 h after which it was added dropwise, under an atmosphere of argon, to a solution of 0.5 g of 2-amino-6-(dibutylamino) 4-pyrimidinol (2.09 mmol) in 40 mL dry pyridine at 90 °C. The mixture was stirred for an additional 16 h at this temperature after which all pyridine was removed *in vacuo*. After removal of all pyridine, 20 mL of CHCl₃ was added and the suspension was filtered over a 1.0 µm PTFE filter. The filtrate was evaporated *in vacuo* and extensively purified by column chromatography (SiO₂, 25-35% acetone/CHCl₃) resulting in 102 mg (0.16 mmol) of **11** as a white solid, mp 148 °C. Yield: 8%. ¹H-NMR (CDCl₃): 12.58 (OH), 11.18 (N₉H), 9.56 (N₁₃H), 8.30-7.84 (m, 9H, PyrH), 5.30 (s, 1H, C₁H), 4.08 (t, 2H, COOCH₂), 3.38 (t, 2H, CH₂-COOCH₂), 3.30 (m, 2H, NH-CH₂), 3.25 (b, 4H, N(-CH₂)₂), 2.45 (t, 2H, Pyr-CH₂CH₂), 2.19 (m, 2H, 2H, CH₂-CH₂-COOCH₂), 1.65-1.20 (m, 16H, -CH₂-), 0.92 (t, 6H, CH₃) ppm. ¹³C-NMR (CDCl₃): 173.5 (C₂₃), 170.5 (C₂), 162.4, 157.6, 156.8, 135.7, 131.4, 130.9, 129.9, 128.7, 127.4, 127.3, 126.7, 125.8, 125.06, 124.96, 124.85, 124.77, 124.73, 124.6, 123.3, 78.7, 64.4, 49.0, 39.8, 33.9, 32.8, 30.2, 29.8, 28.6, 26.8, 26.6, 25.7, 20.3, 13.9 ppm. IR (ATR): ν (cm⁻¹) = 3220, 3123, 3038, 2955, 2932, 2596 (O-H ::O=C hydrogen bond), 1731, 1675, 1615, 1561, 1524, 1508, 1444, 1370, 1321, 1281, 1250, 1205, 1160, 1145, 987, 845 cm⁻¹ MALDI-TOF-MS (m/z): calcd: 651.37 obs: 651.34 (M⁺). Anal. Calcd for C₃₉H₄₉N₅O₄: C 71.86, H 7.58, N 10.74 found C 72.15, H 7.47, N 10.84.

X-ray crystal structure determination of 6

C₂₅H₄₇N₅O₂, Fw = 449.68, colourless plate, 0.33 x 0.30 x 0.09 mm³, triclinic, P $\bar{1}$ (no. 2), a = 10.3030(2), b = 10.9384(2), c = 14.1351(3) Å, α = 93.0804(6), β = 109.5916(7), γ = 114.8871(9)°, V = 1325.56(5) Å³, Z = 2, D_x = 1.127 g/cm³, μ = 0.072 mm⁻¹. 31497 Reflections were measured on a Nonius Kappa CCD diffractometer with rotating anode (graphite monochromator, λ = 0.71073 Å) up to a resolution of (sin θ/λ)_{max} = 0.65 Å⁻¹ at a temperature of 150(2) K. An absorption correction was not considered necessary. 6043 Reflections were unique (R_{int} = 0.0545), of which 4318 were observed [I > 2σ(I)]. The structure was solved with Direct Methods using the program SHELXS-97.⁴⁵ The structure was refined with SHELXL-97 against F² of all reflections. Non hydrogen atoms were refined with anisotropic displacement parameters. All hydrogen atoms were located in difference Fourier maps. N-H and O-H hydrogen atoms were refined freely with isotropic displacement parameters, C-H hydrogen atoms were refined with a riding model. 304 Parameters

were refined with no restraints. R1/wR2 [$I > 2\sigma(I)$]: 0.0474/0.1129. R1/wR2 [all refl.]: 0.0769/0.1266. $S = 1.027$. Residual electron density between -0.28 and 0.19 $e/\text{\AA}^3$. Geometry calculations and checking for higher symmetry was performed with the PLATON program.⁴⁶

UV-Vis titrations

UV/Vis spectra were recorded using 1 cm path length cells on a Perkin Elmer Lambda 40P equipped with a PTP-1 Peltier temperature control system. A series of spectra were obtained by the addition of μL amounts of a stock solution containing 25.7 μM of **10** and 300 μM UPy **1**, **3**, **4**, **6**, **7**, **8**, **9** in CHCl_3 to a cell containing 2.0 mL of a 25.7 μM solution of 2,7-diamido-1,8-naphthyridine **10**. All obtained traces were base-line corrected.

Fluorescence measurements

Fluorescence spectra were recorded on a Perkin-Elmer LS 50B luminescence spectrometer. The slit size was set to 8 nm x 8 nm and the scan speed was set to a value of 600 nm/min. For all measurements a fresh opened bottle of spectroscopic grade CHCl_3 was used (Aldrich). Each fluorescence spectrum was normalized to the concentration after which the pyrene excimer band was integrated from 475 nm to 600 nm and the integral fitted to a monomer-dimer equilibrium.^{1b} All spectra were measured in air, at equilibrium oxygen concentration. This leads to slow photo-oxidation of the pyrene moiety, but prevents change in concentration of oxygen during the measurement, influencing the kinetics of excited state decay.

Two dimensional NMR

All two dimensional NMR spectra were recorded on a 500 MHz NMR (Varian Unity Inova) by means of a 5 mm $^1\text{H}/\text{X}$ Inverse Detection probe equipped with gradient capabilities at 25 °C. Deuterated chloroform was de-acidified and dried by passing it through a column of activated basic alumina (type I). Solutions used for ROE measurements were degassed by a repetitive freeze-pump-thaw procedure. For all measurements the 90° ^1H pulse width was calibrated (4.8 μs at a transmitter power of 59 dB).

2D transverse ROESY experiments were performed with a relaxation delay time of 3 s and a mixing time of 100 ms using a spin-lock field of 8000 Hz (32.9 μs duration). All 2D-data were collected in the phase-sensitive mode using the States-Haberkmorn method. A total of 400 FIDs of 2K complex data points were collected in t_2 with 16 scans per increment and zero-filling was applied in both dimensions before Fourier transformation. These data was then processed with a cosine squared window function in both dimensions.

Gradient selective HMQC (gHMQC) experiments were performed using a relaxation delay time of 1 s, a sweep width of 8000 Hz for proton dimension and 21362 Hz for the carbon dimension. All 2D-data were collected in the phase-sensitive mode using the States-Haberkmorn method. A total of 300 FIDs of 2K complex data points were collected in t_2 with 16 scans per increment. The $^1\text{J}_{\text{C-H}}$ coupling constant was set to 160 Hz. TANGO gradient suppression was applied to filter residual ^1H coupled to ^{13}C . Processing was done after Gaussian apodization in both dimensions.

Calibration of the decoupler pulse widths and decoupler strength was achieved by using the standard Varian calibration procedure (page 59, Unity Inova acceptance test procedures) on the ^{13}C enriched methyl iodide sample.

Computational procedure for determining K_a using Uv-Vis titrations at a single wavelength

A script was written in Matlab 7.0.4. The input data consists of the analytical concentrations of UPy (U0), NaPy (N0), the observed absorptions ($A^{\lambda_{\text{obs}}}$) at a single wavelength, the extinction coefficient of free ureido-pyrimidinone, ϵ^{λ_u} (in $\text{L}\cdot\text{mol}^{-1}\cdot\text{cm}^{-1}$), the extinction coefficient of free N, ϵ^{λ_N} (in $\text{L}\cdot\text{mol}^{-1}\cdot\text{cm}^{-1}$) at the corresponding wavelength and an experimentally determined value of K_{dim} (in M^{-1}). Starting with a trial value of K_a the program calculates the concentration UPy·NaPy (UN), free NaPy (N), free UPy (U) and UPy (U₂) dimer using the mass balance equations as developed in reference 30. The absorption at a single wavelength for a given cuvette length (l) is then calculated as: $A^{\lambda_{\text{cal}}} = l \cdot (\epsilon^{\lambda_{\text{NU}}}[\text{UN}] + \epsilon^{\lambda_{\text{N}}}[\text{N}] + \epsilon^{\lambda_{\text{U}}}[\text{U} + \text{U}_2])$ using a trial value of ϵ_{UN} . Least squares optimization of this function using the Levenberg-Marquardt method is then performed until K_a (M^{-1}) and $\epsilon^{\lambda_{\text{UN}}}$ ($\text{L}\cdot\text{mol}^{-1}\cdot\text{cm}^{-1}$) become constant within the desired accuracy (0.0001%).

Sample preparation for ^1H -NMR studies

Equimolar mixtures of **1** and **3**, **6** or **8** were prepared by weighing the calculated amounts of their components into 5 ml screw cap vials followed by addition of CDCl_3 (0.6 mL).

Computer simulations for two component mixture

All simulations were performed on a PC running Scientist 3.0 (MicroMath Scientific Software, Salt Lake City, Utah) under Windows XP.

2.8 Appendices

Appendix A

FT-IR measurements on **6** in the solid state and in solution (both at room temperature).

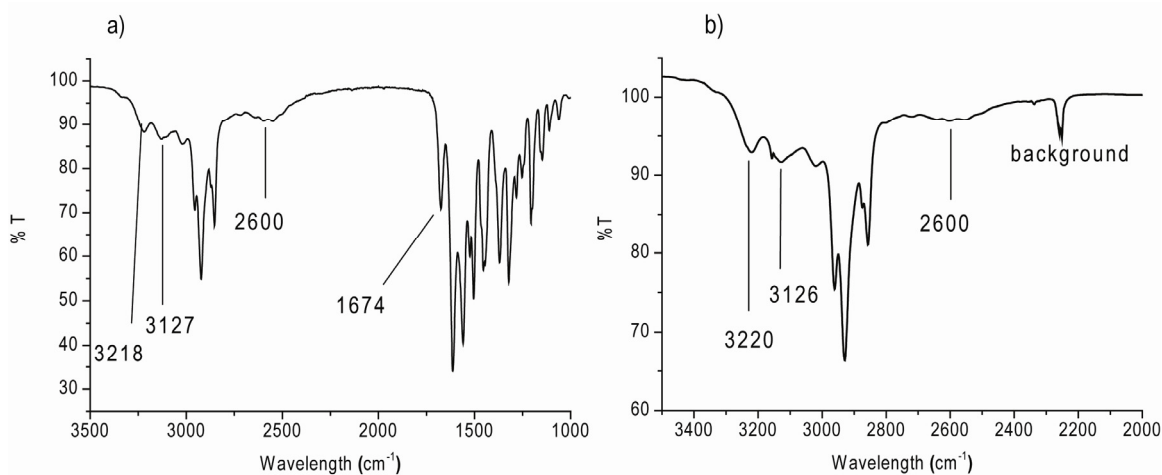


Figure A1: a) FT-IR spectrum of crystals of compound **6**. b) FT-IR spectrum of a 10⁻³ M solution of **6** in CDCl₃.

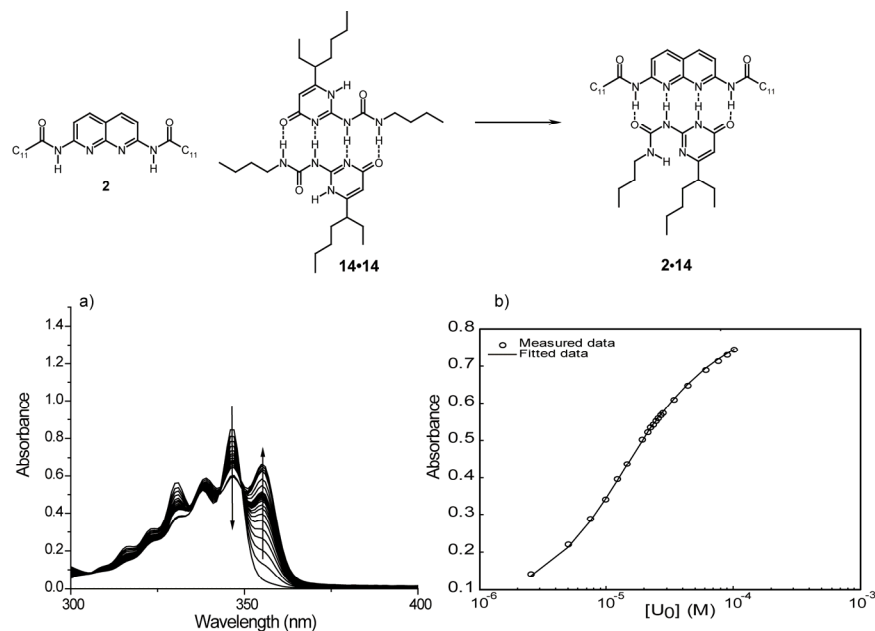
Appendix B
UV-Vis titrations and K_a determination.


Figure A2: a) Changes in the absorbance of a solution of a $2.53 \times 10^{-5} \text{ M}$ solution of **2** upon addition of aliquots of **14** in CHCl_3 at 25°C . b) Plot of absorbance at 355 nm for a solution containing $2.53 \times 10^{-5} \text{ M}$ **2** vs. concentration of **14** in CHCl_3 . The curve represents the best fit of the data ($K_a = 5 (+/- 0.2) \times 10^6 \text{ M}^{-1}$) to the 1:1 binding model with one component self-associating.

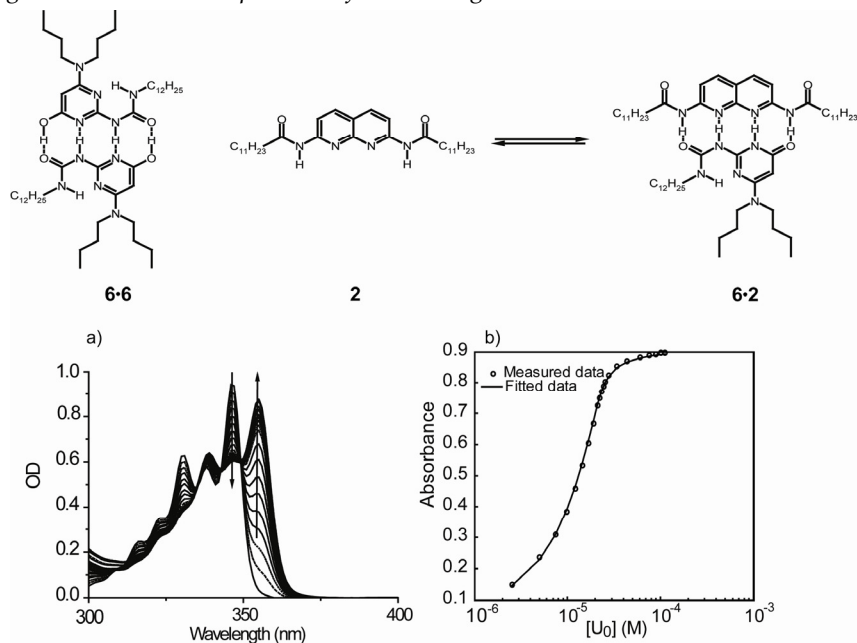


Figure A3: a) Changes in the absorbance of a solution of a $2.53 \times 10^{-5} \text{ M}$ solution of **2** upon addition of aliquots of **6** in CHCl_3 at 25°C . b) Plot of absorbance at 355 nm for a solution containing $2.53 \times 10^{-5} \text{ M}$ **2** vs. concentration of **6** in CHCl_3 . The curve represents the best fit of the data ($K_a = 6 (+/- 0.5) \times 10^6 \text{ M}^{-1}$) to the 1:1 binding model with one component self-associating.

Appendix C

Characterization of the two hetero-dimers using blocked UPy derivative 15.

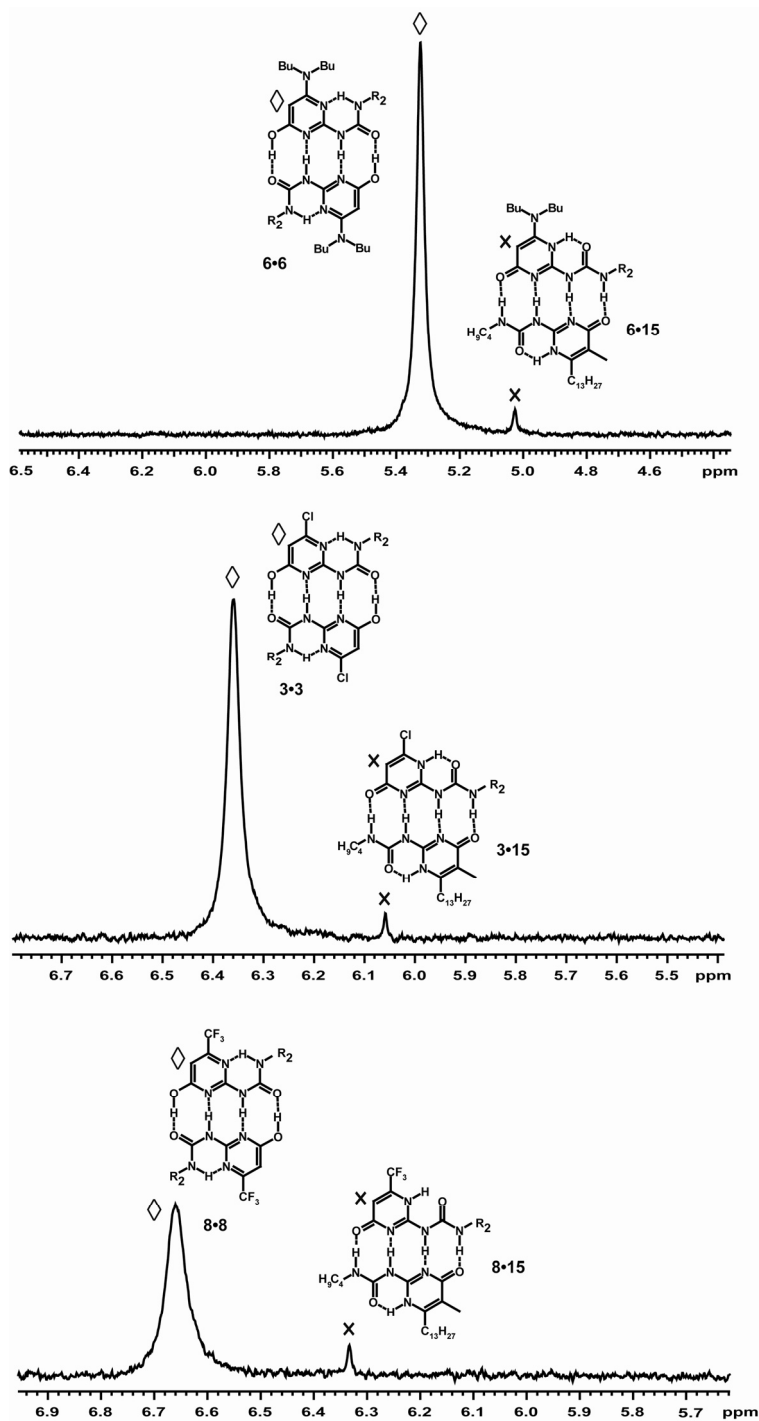


Figure A4: $^1\text{H-NMR}$ spectra of equimolar mixtures of 15 and 6, 3 or 8 in CDCl_3 at a total concentration of 10 mM and a temperature of 25 $^\circ\text{C}$.

Appendix D

Scientist 3.0 model for a two component mixture as a function of K_a .

```
// Micromath Scientist Model File
IndVars: Kab
DepVars: ChiAA, ChiAB, ChiBA, ChiAfree, ChiBB, ChiBfree, ChiABtot
Params: Kaa, Kbb, Btot, Atot
Kaa=ConcAA/(ConcAfree*ConcAfree)
Kbb=ConcBB/(ConcBfree*ConcBfree)
Kab=ConcAB/(ConcAfree*ConcBfree)
ChiAA=(2*ConcAA)/(Atot)
ChiAB=ConcAB/Atot
ChiBA=ConcAB/Btot
ChiAfree=ConcAfree/Atot
ChiBB=(2*ConcBB)/(Btot)
ChiBfree=ConcBfree/Btot
ChiABtot=ConcAB/(Atot+Btot)
Atot=ConcAB+ConcAfree+(2*ConcAA)
Btot=ConcAB+ConcBfree+(2*ConcBB)
0<ConcAfree<Atot
0<ConcBfree<Btot
```

2.9 References

- 1) a) Sijbesma, R. P.; Beijer, F. H.; Brunsveld, L.; Folmer, B. J. B.; Hirschberg, J. H. K. K.; Lange, R. F. M.; Lowe, J. K. L.; Meijer, E. W. *Science* **1997**, *278*, 1601.
b) Söntjens, S. H. M.; Sijbesma, R. P.; van Genderen, M. H. P.; Meijer, E. W. *J. Am. Chem. Soc.* **2000**, *122*, 7487.
- 2) a) Folmer, B. J. B.; Sijbesma, R. P.; Versteegen, R. M.; van der Rijt, J. A. J.; Meijer, E. W. *Adv. Mater.* **2000**, *12*, 874. b) Kautz, H.; van Beek, D. J. M.; Sijbesma, R. P.; Meijer, E. W. *Macromolecules* **2006**, *39*, 4265.
- 3) a) Dankers, P. Y. W.; Harmsen, M. C.; Brouwer, L. A.; Van Luyn, M. J. A.; Meijer, E. W. *Nat. Mater.* **2005**, *4*, 568. b) Dankers, P. Y. W.; Zhang, Z.; Wisse, E.; Grijpma, D. W.; Sijbesma, R. P.; Feijen, J.; Meijer, E. W. *Macromolecules* **2006**, *39*, 8763.
- 4) Park, T.; Todd, E. M.; Nakashima, S.; Zimmerman, S. J. *Am. Chem. Soc.* **2005**, *127*, 18133.
- 5) Beijer, F. H.; Sijbesma, R. P.; Kooijman, H.; Spek, A. L.; Meijer, E. W. *J. Am. Chem. Soc.* **1998**, *120*, 6761.
- 6) Lafitte, V. G. H.; Aliev, A. E.; Hailes, H. C.; Bala, K.; Holdings, P. *J. Org. Chem.* **2005**, *70*, 2701.
- 7) a) Jorgensen, W. L.; Pranata, J. *J. Am. Chem. Soc.* **1990**, *112*, 2008. b) Pranata, J.; Wierschke, S. G.; Jorgensen, W. L. *J. Am. Chem. Soc.* **1991**, *113*, 2810. c) Quinn, J. R.; Zimmerman, S. C.; Del Bene, J. E.; Shavitt, I. *J. Am. Chem. Soc.* **2007**, *129*, 934.
- 8) Dong, H.; Hua, W.; Li, S. *J. Phys. Chem. A* **2007**, *111*, 2941.
- 9) Schnell, I.; Langer, B.; Sontjens, S. H. M.; Sijbesma, R. P.; van Genderen, M. H. P.; Spiess, H. W. *Phys. Chem. Chem. Phys.* **2002**, *4*, 3750.
- 10) a) Baruah, P. K.; Gonnade, R.; Phalgune, U. D.; Sanjayan, G. J. *J. Org. Chem.* **2005**, *70*, 6467.

- 11) Wang, X.-Z.; Li, X.-Q.; Shao, X.-B.; Zhao, X.; Deng, P.; Jiang, X.-K.; Li, Z.-T.; Chen, Y.-Q. *Chem. Eur. J.* **2003**, *9*, 2904.
- 12) Corbin, P. S.; Zimmerman, S. C. *J. Am. Chem. Soc.* **1998**, *120*, 9710.
- 13) Ligthart, G. B. W. L.; Ohkawa, H.; Sijbesma, R. P.; Meijer, E. W. *J. Am. Chem. Soc.* **2005**, *127*, 810.
- 14) Scherman, O. A.; Ligthart, G. B. W. L.; Ohkawa, H.; Sijbesma, R. P.; Meijer, E. W. *Proc. Natl. Acad. Sci. USA* **2006**, *103*, 11850.
- 15) Ohkawa, H.; Ligthart, G. B. W. L.; Sijbesma, R. P.; Meijer, E. W. *Macromolecules* **2007**, *40*, 1453.
- 16) Park, T. ; Todd, E. M.; Nakashima, S.; Zimmerman, S.C. *J. Am. Chem. Soc.* **2005**, *127*, 18133.
- 17) For a discussion on the correlation between hydrogen bond strength and ¹H-NMR chemical shift value see: Del Bene, J. E.; Perera, S. A.; Bartlett, R. J. *J. Phys. Chem. A.* **1999**, *103*, 8121.
- 18) Stamm, H.; Jaekel, H. *J. Am. Chem. Soc.* **1989**, *111*, 6544.
- 19) Proton H_d and H_e could be unambiguously assigned by a gCOSY experiment in toluene-d₈ in which a crosspeak was observed between H_e and H_c. Furthermore, the ROE data could also correspond to the 6[1H] trans tautomer. However, this possibility was ruled out based on the large dimerization constant of the complex. Zimmerman and co workers (see: Ong, H. C.; Zimmerman, S. C. *Org. Lett.* **2006**, *8*, 1589) found that complexes that dimerize via the 6[1H] *transoid* tautomer have dimerization constants of less than 1000 M⁻¹.
- 20) Neuhaus, D.; Williamson, M. P.; *The Nuclear Overhauser Effect in Structural and Conformational Analysis*, 2nd ed.; Wiley-VCH: New York, 2000.
- 21) Djurdjevic, S.; Leigh, D. A.; McNab, H.; Parsons, S; Teobaldi, G.; Zerbetto, F. *J. Am. Chem. Soc.* **2007**, *129*, 476.
- 22) Fidelity is defined by the following equation:
Fidelity =
$$\frac{\text{total concentration of desired complexes}}{\text{total concentration of all complexes}} \quad (1)$$

In the case where the UPy·NaPy complex is the desired compound, fidelity is defined as:
Fidelity =
$$\frac{[\text{UPy}\cdot\text{NaPy}]}{[\text{UPy}_2] + [\text{UPy}] + [\text{NaPy}] + [\text{UPy}\cdot\text{NaPy}]} \quad (2)$$

See: Todd, E. M.; Quinn, J. R.; Park, T.; Zimmerman, S. C. *Isr. J. Chem.* **2005**, *45*, 381.
- 23) The normalized absorbance is calculated as the absorbance at λ = 355 nm divided by the absorbance at λ = 347 nm normalized against the absorbance at λ = 355 nm upon addition of 10 equivalents of UPy.
- 24) Corbin, P. S.; Lawless, L. J.; Li, Z.; Ma, Y.; Witmer, M.J.; Zimmerman, S. C.; *Proc. Natl. Acad. Sci. USA* **2002**, *99*, 5099.
- 25) Brea, R. J.; Vázquez, M. E.; Mosquera, M.; Castedo, L.; Granja, J. R. *J. Am. Chem. Soc.* **2007**, *129*, 1653.
- 26) Quinn, J. R.; Zimmerman, S. C.; Del Bene, J. E.; Shavitt, I. *J. Am. Chem. Soc.* **2007**, *129*, 934.
- 27) Because the model does not specifically consider OH··O hydrogen bonds the two OH··O hydrogen bonds in **62** were treated as NH··O hydrogen bonds.
- 28) Jones II, G.; Vullev, V. I. *Org. Lett.* **2001**, 2457.
- 29) Jones II, G.; Vullev, V. I. *J. Phys. Chem. A* **2001**, *105*, 6402.
- 30) For details of the fitting procedure: de Greef, T. F. A.; Ligthart, G. B. W. L.; Lutz, M.; Spek, A. L.; Meijer, E. W.; Sijbesma, R. P. *J. Am. Chem. Soc.* **2008**, *130*, 5479.

- 31) For a review regarding the preference for homomeric aggregates in natural systems, see: Goodsell, D. S.; Olson, A. J. *Annu. Rev. Biophys. Biomol. Struct.* **2000**, *29*, 105.
- 32) Lehn, J.-M. *Science* **2002**, *295*, 2400.
- 33) a) Wu, A.; Isaacs, L. *J. Am. Chem. Soc.* **2003**, *125*, 4831. b) Mukhopadhyay, P.; Wu, A.; Isaacs, L. *J. Org. Chem.* **2004**, *69*, 6157. c) Ghosh, S.; Wu, A.; Fettinger, J. C.; Zavalij, P. Y.; Isaacs, L. *J. Org. Chem.* **2008**, *73*, 5915.
- 34) a) Wu, A.; Chakraborty, A.; Fettinger, J. C.; Flowers II, R. A.; Isaacs, L. *Angew. Chem., Int. Ed.* **2002**, *41*, 4028. b) Jolliffe, K. A.; Timmerman, P.; Reinhoudt, D. N. *Angew. Chem., Int. Ed. Engl.* **1999**, *38*, 933. c) Cai, M.; Shi, X.; Sidorov, V.; Fabris, D.; Lam, Y.-F.; Davis, J. T. *Tetrahedron* **2002**, *58*, 661. d) Barrett, E. S.; Dale, T. J.; Rebek, J. Jr. *J. Am. Chem. Soc.* **2008**, *130*, 2344. e) Braekers, D.; Peters, C.; Bogdan, A.; Rudzevich, Y.; Boehmer, V.; Desreux, J. F. *J. Org. Chem.* **2008**, *73*, 701. f) Plutowski, U.; Jester, S. S.; Lenhert, S.; Kappes, M. M.; Richert, C. *Adv. Mater.* **2007**, *19*, 1951.
- 35) a) Taylor, P. N.; Anderson, H. L. *J. Am. Chem. Soc.* **1999**, *121*, 11538. b) Krämer, R.; Lehn, J.-M.; Marquis-Rigault, A. *Proc. Natl. Acad. Sci. U.S.A.* **1993**, *90*, 5394. c) Yamanaka, M.; Yamada, Y.; Sei, Y.; Yamaguchi, K.; Kobayashi, K. *J. Am. Chem. Soc.* **2006**, *128*, 1531.
- 36) a) Bilgiçer, B.; Xing, X.; Kumar, K. *J. Am. Chem. Soc.* **2001**, *123*, 11815. b) Schnarr, N. A.; Kennan, A. J. *J. Am. Chem. Soc.* **2003**, *125*, 667.
- 37) a) He, Y.; Tian, Y.; Chen, Y.; Ribbe, A. E.; Mao, C. *Chem. Commun.* **2007**, 165. b) Zheng, Y.-R.; Yang, H.-B.; Northrop, B. H.; Ghosh, K.; Stang, P. J. *Inorg. Chem.* **2008**, *47*, 4706.
- 38) Hwang, I.-W.; Kamada, T.; Ahn, T. K.; Ko, D. M.; Nakamura, T.; Tsuda, A.; Osuka, A.; Kim, D. *J. Am. Chem. Soc.* **2004**, *126*, 16187.
- 39) Beijer, F. H. *Thesis: Cooperative Multiple Hydrogen Bonding in Supramolecular Chemistry*; Eindhoven University of Technology: Eindhoven (The Netherlands), **1998**.
- 40) Katritzky, A. R.; Rowe, J. D.; Roy, S. K. *J. Chem. Soc. (B)* **1967**, 758.
- 41) a) Pollino, J. M.; Stubbs, L. P.; Weck, M. *J. Am. Chem. Soc.* **2004**, *126*, 563. b) Pollino, J. M.; Stubbs, L. P.; Weck, M. *Macromolecules* **2003**, *36*, 2230. c) South, C. R.; Burd, C.; Weck, M. *Acc. Chem. Res.* **2007**, *40*, 63. d) Hoogenboom, R.; Fournier, D.; Schubert, U. S. *Chem. Commun.* **2008**, 155.
- 42) a) Burd, C.; Weck, M. *Macromolecules*, **2005**, *38*, 7225. b) Khan, M. K.; Sundararajan, P. R. *J. Phys. Chem. B* **2008**, *112*, 4223.
- 43) Ligthart, G. B. W. L.; Ohkawa, H.; Sijbesma, R. P.; Meijer, E. W. *J. Org. Chem.*, **2006**, *71*, 375.
- 44) Söntjens, S. H. M. *Thesis: Dynamics of Quadruply Hydrogen-bonded Systems*, Eindhoven University of Technology: Eindhoven (The Netherlands), **2002**.
- 45) Sheldrick, G.M. (1997). SHELXS-97. Program for crystal structure solution. University of Göttingen, Germany.
- 46) Spek, A.L. *J. Appl. Cryst.* **2003**, *36*, 7.

3

The influence of selectivity on the supramolecular polymerization of AB type polymers capable of both A·A and A·B interactions

The supramolecular polymerization of two AB type monomers capable of hydrogen bond mediated A·B hetero-coupling and A·A homo-coupling is discussed. The AB-type supramolecular polymerization is based on the strong interaction between self-dimerizing 2-ureido-pyrimidinone (UPy) and 2,7-diamido-1,8-naphthyridine (NaPy). In an effort to reduce the “self-stoppered” effect that is inherently present in these supramolecular polymerizations, the UPy unit in one of the two AB monomers is substituted with a dibutylamino group. As discussed in Chapter 2, the dimerization constant of this novel UPy unit is lower than ureido-pyrimidinones substituted with aliphatic groups at the 6 position of the pyrimidinone ring, while the hetero-dimerization strength with NaPy is retained. Unexpectedly, the increased selectivity towards hetero-association not only influences the concentration dependent degree of polymerization due to the reduction of the “self-stoppered” effect but also has a pronounced effect on the ring-chain equilibrium by increasing the tendency to cyclize. In order to quantitatively explain the results, a model was developed that accurately predicts the degree of polymerization by taking into account homo and hetero-dimerization as well as cyclization. Finally, molecular weight distributions for non-cyclizing AB supramolecular polymerizations with and without a reversible A·A interaction are calculated. It is found that the molecular weight distribution becomes narrower when A·A interactions are present.

This work has been published:

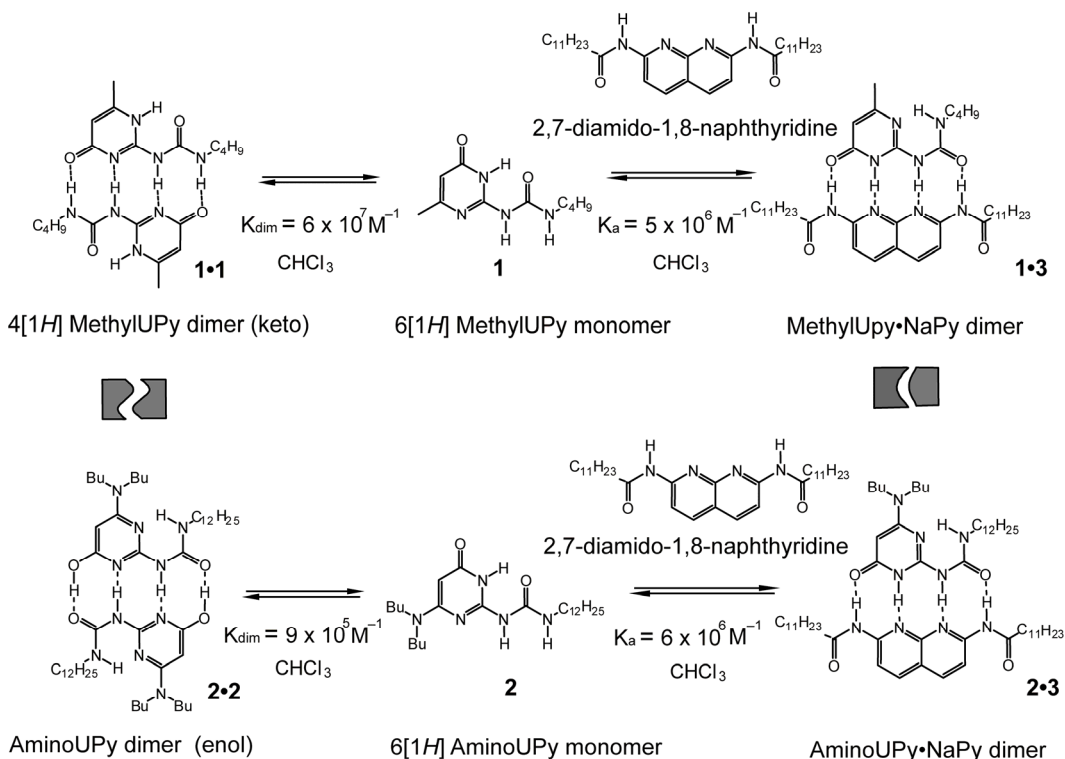
de Greef, T. F. A.; Ercolani, G.; Ligthart, G. B. W. L.; Meijer, E. W.; Sijbesma, R. P. J. *Am. Chem. Soc.* **2008**, *130*, 13755-13764.

3.1 Introduction

The combination of supramolecular chemistry and polymer science has led to the development of supramolecular polymers in which the individual monomeric units are held together by strong, directional and reversible non-covalent interactions.¹ Arrays of hydrogen bonds, being inherently dynamic and displaying tunable association strengths, constitute an important building block for supramolecular polymer based materials.² The majority of supramolecular polymers has been constructed using a mixture of AA and BB ditopic molecules with complementary hydrogen-bonding functionalities.³ In such systems, high molecular weight polymer is only obtained at the exact equivalence point ($c_{AA} = c_{BB}$) because a stoichiometric imbalance rapidly leads to a diminished degree of polymerization.^{3a} In an attempt to avoid the need for stoichiometric balance, supramolecular polymers using AA and BB ditopic monomers in which both A·A homo-dimerization and A·B hetero-association occurs have been described.⁴ In this setup, the A·A interaction is based on the strong dimerization of methyl-substituted 2-ureido-4[1*H*]-pyrimidinone **1** (UPy; $K_{dim} = 6 \times 10^7 \text{ M}^{-1}$ in CHCl_3) while the A·B interaction is based on the strong interaction between methyl-substituted 2-ureido-6[1*H*]-pyrimidinone **1** and 2,7-diamido-1,8-naphthyridine (UPy·NaPy, $K_a = 5 \times 10^6 \text{ M}^{-1}$ in CHCl_3 , see Scheme 3.1). Using this approach, high degrees of polymerization were obtained using mixtures of AA and BB ditopic monomers if $c_{AA} > c_{BB}$, while chain shortening occurs if $c_{AA} < c_{BB}$ because the excess of B units act as chain stoppers.

An alternative way to address the problem of stoichiometric imbalance in supramolecular polymerizations is the use of an AB-type monomer.⁵ Recently an AB type monomer was synthesized based on the previously described UPy·NaPy motif using selective olefin-metathesis chemistry.⁶ Concentration dependent ¹H-NMR and viscosity measurements indicated a transition from cyclic species at low concentrations to linear species at high concentrations.

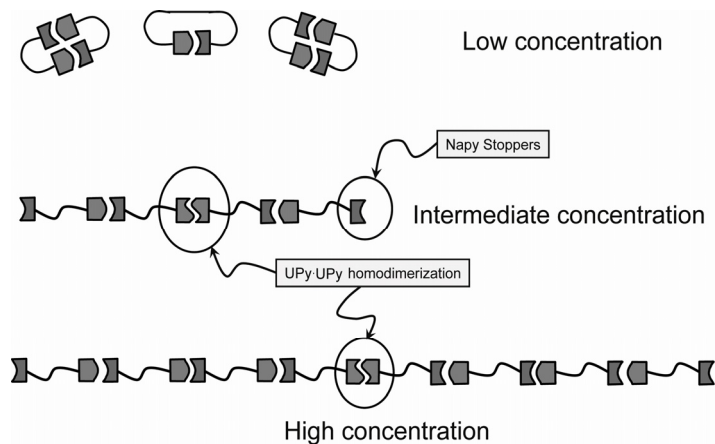
In supramolecular polymers based on the current UPy·Napy system (**1·3**) a major drawback is the incomplete selectivity of 2-ureido-4[1*H*]-pyrimidinone dimerization relative to association of 2-ureido-6[1*H*]-pyrimidinone with 2,7-diamido-1,8-naphthyridine (NaPy) because this results in self-stoppered behavior in both AB and A₂-B₂ supramolecular polymerizations.^{4,6} The self-stoppered behavior in supramolecular AB polymerizations using the current UPy·NaPy system is a result of the formation of free NaPy end-groups (Scheme 3.2) due to the formation of UPy·UPy bonds even at high concentrations.



Scheme 3.1: Equilibrium between methyl-substituted UPy dimer **1·1** (Donor-Donor-Acceptor-Acceptor hydrogen bonding array) and 2,7-diamido-1,8-naphthyridine **3** (top) and equilibrium between dibutylamino-substituted UPy dimer **2·2** (Donor-Acceptor-Donor-Acceptor hydrogen bonding array) and 2,7-diamido-1,8-naphthyridine **3** (bottom).

As the NaPy end groups hardly self-dimerize⁷ ($K_{dim} < 10 M^{-1}$ in CDCl₃), chain growth is effectively limited at high concentrations. An approach to reduce this self-stoppered effect in A₂-B₂ supramolecular polymerizations introduced by Zimmerman is the use of a guanosine urea derivative (UG) which only weakly self-associates ($K_{dim} = 200 M^{-1}$) but has a high association constant with 2,7-diamido-1,8-naphthyridine ($\approx 5 \times 10^7 M^{-1}$).⁸

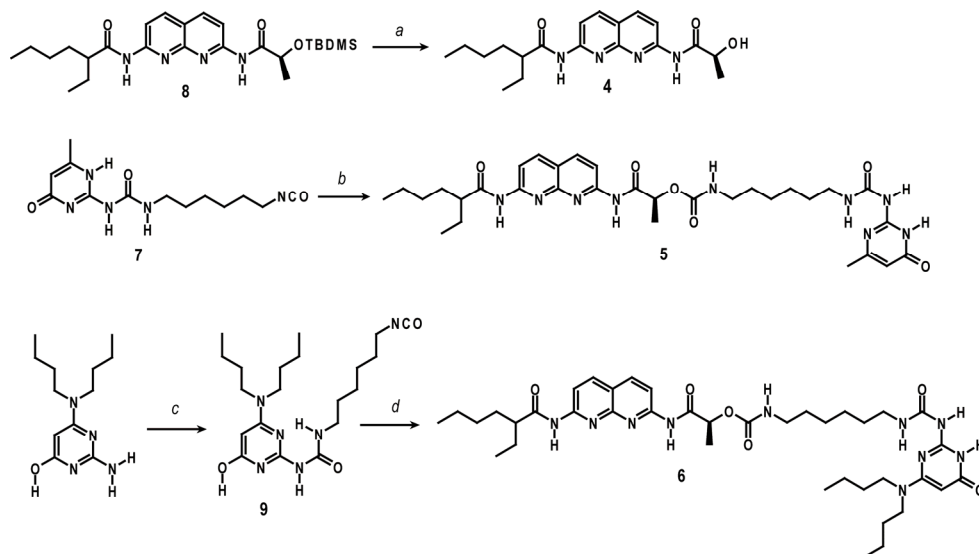
In chapter 2 a novel ureido-pyrimidinone unit (**2**) was synthesized substituted with a dibutylamino group at the C₆ position of the pyrimidinone ring. Thermodynamic analysis of its homo-dimerization and hetero-complexation with NaPy reveal that this UPy shows an increased fidelity for hetero-complexation compared to methyl-substituted UPy **1**. For an AB-type polymerization with both A·A homo and A·B hetero-coupling, the increased fidelity of hetero-complex formation will reduce the “self-stoppered” effect thereby increasing the degree of polymerization. In this chapter, two AB-type monomers are synthesized, differing in the nature of their UPy end group, and their supramolecular polymerization is studied in solution using a variety of techniques (viscometry, ¹H-NMR, DOSY).



Scheme 3.2: Schematic representation of the supramolecular polymerization of an UPy·NaPy AB type monomer in solution at various concentrations illustrating the “self-stoppered” effect. Due to the high dimerization constant of the methyl-substituted UPy unit a significant amount of chains containing free NaPy end groups are formed which limits the degree of polymerization.

3.2 Synthesis of AB monomers

To investigate the influence of the increased fidelity on the supramolecular polymerization of an AB monomer in solution, two different AB monomers (**5** and **6**, see Scheme 3.3) were synthesized. The two AB monomers differ in the nature of the UPy end-groups but have the same NaPy unit incorporated. AB monomer **5** has a methyl-substituted UPy end group for which the K_{dim} was previously determined to be $6 \times 10^7 \text{ M}^{-1}$ in CHCl_3 . The second AB monomer **6**, has a dibutylamino-substituted UPy end group with a K_{dim} of $9 \times 10^5 \text{ M}^{-1}$. To ensure a fair comparison between the two different AB monomers it is of crucial importance to include the same linker between the hydrogen bonding groups because conformational constraints in the linker can influence the equilibrium between cycles and linear species.⁹ Synthesis of UPy·NaPy monomer **5** could be achieved in one step by reaction of 2,7-diamido-1,8-naphthyridine alcohol **4** with UPy isocyanate **7**. The synthesis of **4** could be achieved by deprotection of the TBDMS group of 2,7-diamido-1,8-naphthyridine **8** which was synthesized according to a previously established route.¹⁰ The synthesis of AB monomer **6** was achieved in two steps starting from 2-amino-6-(dibutylamino) 4-pyrimidinol (see Chapter 2). Reaction of this compound with 1,6-diisocyanatohexane resulted in isocyanate synthon **9** which was subsequently reacted with **4**, affording AB monomer **6**. Purification of AB monomers **5** and **6** was critical and was achieved via column chromatography and precipitation in MeOH. The purity of **5** and **6** was checked with Size Exclusion Chromatography (SEC) using THF as the eluent.



Scheme 3.3: Synthesis of UPy-NaPy AB monomers **5** and **6**: a) triethylamine trihydrofluoride, THF, 4 h, room temperature, 86%; b) **4**, dibutyl tin laureate, CHCl₃, 20 h, 60 °C, 67%; c) 1,6-diisocyanato-hexane, 1 h, 60 °C, 16 %; d) **4**, dibutyl tin laureate, CHCl₃, 4 days, 60 °C, 49%.

The purity of the UPy-NaPy AB monomer **5** was determined to be 98% while the SEC trace of the UPy-NaPy AB monomer **6** did not reveal any impurity (purity > 99%, see Appendix A).

3.3 Capillary viscosity measurements on AB monomers

A double logarithmic plot of specific viscosity (η_{sp}) versus concentration of **5** and **6** in CHCl₃ yields a linear relationship well above the critical polymerization concentration (CPC).¹¹ The CPC for monomer **6** has a value of ≈ 0.13 M in CHCl₃ as evidenced by the clear change of slope occurring at this concentration. In the case of monomer **5**, the change of slope is less sharp but approximately occurs in the same concentration region.

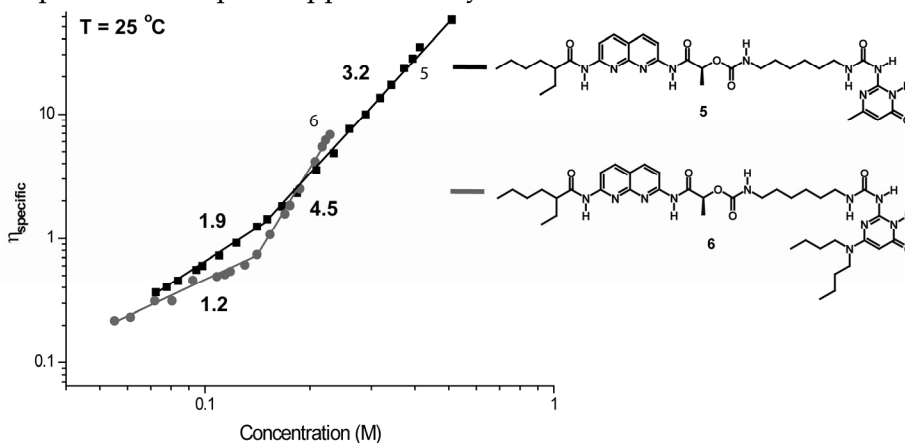


Figure 3.1: Solution viscosities of UPy-NaPy monomers **5** and **6** in CHCl₃ at 25 °C.

Surprisingly, up to concentrations well above the CPC the specific viscosity of **5** is higher than the specific viscosity of **6**. Hence, in this concentration region the system with the lowest selectivity displays the strongest effects of supramolecular polymerization. Only at concentrations above 0.2 M, the specific viscosity of **6** surpasses that of **5**. Furthermore, the slope of **6** above the CPC is higher than the slope of **5**, indicating a stronger concentration dependence of supramolecular polymerization of **6**. The lower specific viscosity of **6** just around the CPC and the higher slope above the CPC suggests that cycles are more abundant in solutions of **6** than in solutions of **5**. To find more evidence for this hypothesis $^1\text{H-NMR}$ dilution experiments and diffusion ordered spectroscopy (DOSY) were performed to probe the nature and sizes of the aggregates in solutions of **5** and **6** in CDCl_3 at various concentrations.

3.4 $^1\text{H-NMR}$ and DOSY measurements

$^1\text{H-NMR}$ spectra at several concentrations of **5** and **6** were taken in CDCl_3 . Figure 3.2 displays the partial $^1\text{H-NMR}$ of **5** and **6** in the region where the hydrogen bonding NH protons resonate. At low concentrations of **5** and **6** (1 mM), the downfield region clearly shows five sharp resonances, indicative of the five hydrogen bonds (four intermolecular and one intramolecular) being present in the UPy-NaPy **ADDA-DAAD** hydrogen bonded complex. At higher concentrations of **5** (> 50 mM, Figure 3.2a), additional signals corresponding to the hydrogen bonding **DDAA** array (UPy-UPy dimer) are observed. Previously, the increase in fraction of UPy-UPy homo-dimer to UPy-NaPy hetero-dimer for a similar molecule was attributed to ring opening of small cyclic species at higher concentrations.⁶ A further increase in concentration of **5** only results in changes in the signals corresponding to the two naphthyridine amide protons (11.4 and 11.8 ppm) due to a concomitant change in exchange dynamics between homo and hetero hydrogen bonding complexes at higher concentrations.

Due to the increased selectivity for hetero-complexation, no signals corresponding to dibutylamino-substituted UPy homo dimer were detected at any concentration of **6** in CDCl_3 .¹² At a concentration of 50 mM of **6** in CDCl_3 (Figure 3.2b), the downfield region of the $^1\text{H-NMR}$ spectrum displayed a large number of resonances, most probably originating from cyclic species. A further increase in concentration of **6** up to 179 mM resulted in four broad NH resonances due to the fast exchange of the two non-equivalent naphthyridine amide protons at high concentrations. This fast exchange results in a broad NH resonance centered at 12.0 ppm.

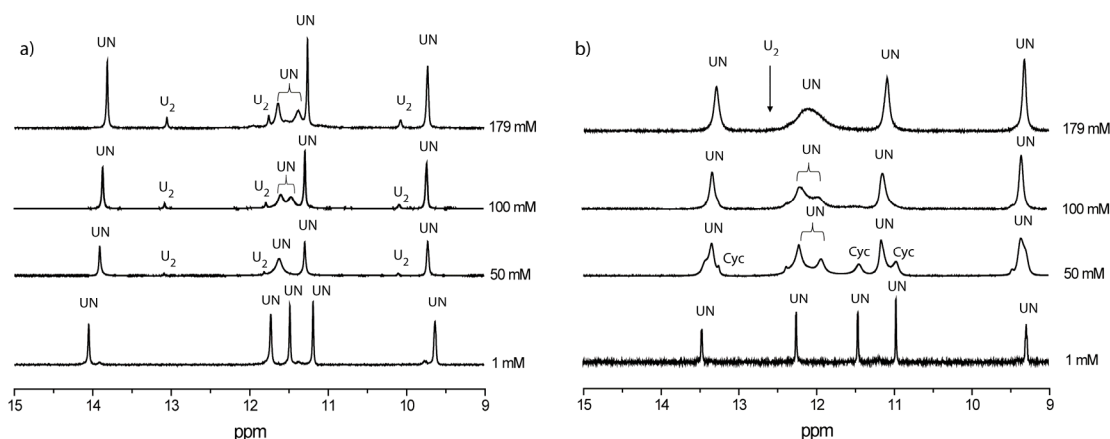


Figure 3.2: Partial ^1H -NMR spectra of the AB monomers at different concentrations in CDCl_3 . a) Methyl substituted UPy-NaPy monomer **5**. b) Dibutylamino-substituted UPy-NaPy monomer **6**. The abbreviations UN, U_2 and Cyc are used to denote signals arising from UPy-NaPy heterocomplex, UPy homo-dimer and cyclic material respectively. At the lowest concentration (1 mM) all monomers in solutions of **5** and **6** in CDCl_3 are incorporated in cycles.

Diffusion ordered ^1H -NMR spectroscopy (DOSY) is a convenient method to probe the dimensions of polydisperse supramolecular aggregates provided that the chemical shifts of the different aggregates are in slow exchange both on the ^1H -NMR as well as on the DOSY timescale.¹³ The 2D DOSY spectrum of **5** at a concentration of 100 mM displays two sets of signals with different diffusion coefficients (Figure 3.3a). The diffusion coefficient of the signals originating from UPy-UPy homo-dimers are smaller than the diffusion constant of the UPy-NaPy indicating that the UPy-UPy homo dimers are part, on average, of an aggregate with a larger hydrodynamic radius. Because of the absence of signals belonging to UPy-UPy homo dimer, all the proton signals in the 2D DOSY spectrum of **6** (Figure 3.3b) have the same diffusion constant. Although accurate calculations on the sizes of the different aggregates are difficult to make due to the possibility of fast exchange on the DOSY time scale^{13e}, the fact that the signals belonging to the UPy-UPy hydrogen bonds in **5** have a lower diffusion constant than the signals belonging to the UPy-NaPy hydrogen bonds is strong evidence that at this concentration cycle formation plays a dominant role (*vide infra*).

3.5 Theoretical model and simulations

Scheme 3.4 schematically displays the supramolecular polymerization of an AB monomer in solution capable of both reversible A-B hetero-coupling (equilibrium constant K_a) and A-A homo-coupling (equilibrium constant K_{dim}). Two different linear

species can be formed: an i-meric linear chain with two NaPy chains ends and containing one reversible A·A (UPy·UPy) bond (chains M_i), and an i-meric linear chain with both a UPy (A) and a NaPy (B) chain end and containing only reversible A·B (UPy·NaPy) bonds (chains L_i). Due to the high association constant of hetero-bond formation (K_a) and the low dimerization constant of the NaPy chain ends⁷, only the linear chains with both a UPy and a NaPy chain end (L_i) are in direct equilibrium with cyclic species (equilibrium constant $K_{(intra)i}$).

This model for the supramolecular polymerization of **5** and **6** in solution allows us to explain the lower diffusion constant of the UPy·UPy signals as measured with DOSY on the 100 mM solution of **5** in $CDCl_3$. At this concentration below the CPC, the chains containing a single UPy·UPy bond (M_i type chains) cannot form cyclic species and hence will be much larger than the small cycles formed from the L_i type chains. Because the linker connecting the UPy and NaPy groups in both AB monomers **5** and **6** is equal and the association constants of **1·3** and **2·3** are nearly identical, it is straightforward to rationalize the influence of K_{dim} on the equilibrium between cycles and linear chains. Due to the higher K_{dim} of methyl-substituted UPy **1**, the fraction of linear chains with two NaPy chains ends (M_i) is higher in the supramolecular polymerization of **5** than **6**.

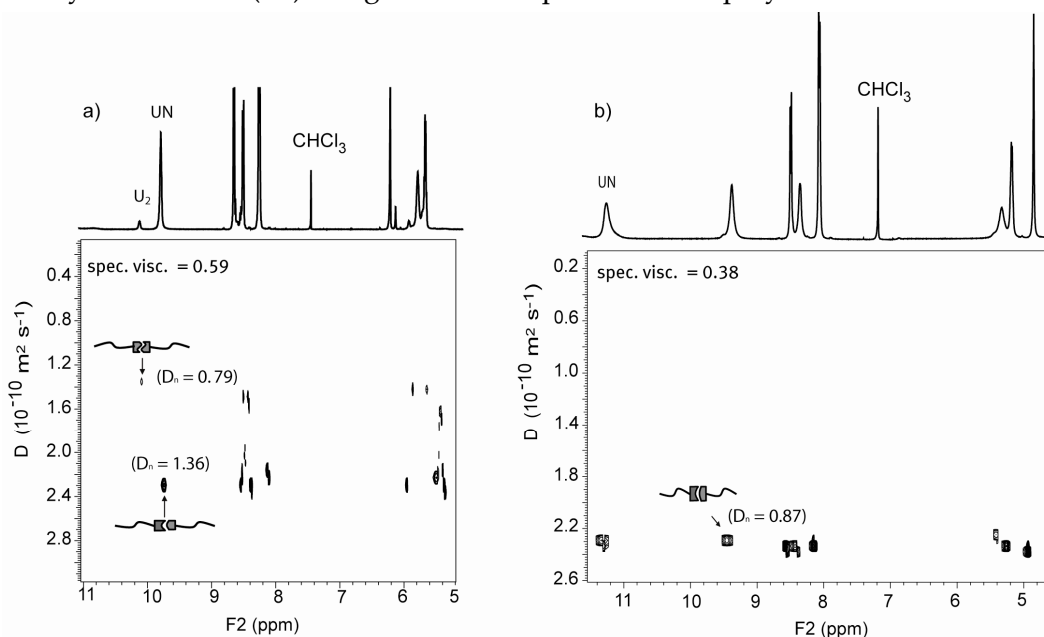


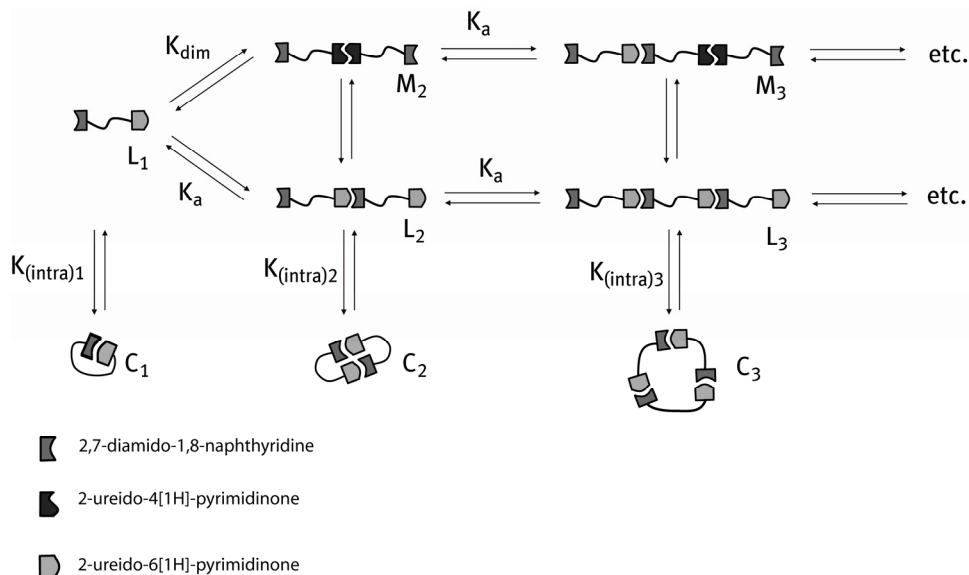
Figure 3.3: 2D-DOSY spectra at a concentration of 100 mM in $CDCl_3$ ($T = 25$ °C). a) Methyl-substituted UPy·NaPy monomer **5**. b) Dibutylamino-substituted UPy·NaPy monomer **6**. The values in parentheses are the viscosity normalized diffusion constants.¹⁴

As a result, the fraction of cyclic species of **5** at a given concentration below the CPC is lower compared to the fraction of cyclic species in the supramolecular polymerization of

6. The higher fraction of cyclic species will result in a lower degree of polymerization of **6** below the CPC. Above the CPC, when additional monomer is added to linear species, the higher fraction of chains M_i in the supramolecular polymerization of **5** will result in a slower growth of the linear polymers due to the “self-stoppered” effect of the two NaPy chain ends. Hence, above the CPC, the degree of polymerization of **6** will increase faster than the degree of polymerization of **5** due to the higher fraction of M_i chains in the latter.

To gain a more quantitative insight into the effects of K_a , K_{dim} , and $K_{(intra)i}$ on the fraction of the various species and the degree of polymerization, a mathematical model was developed based on a previously published model for the ring-chain equilibrium of an AB monomer in solution capable of only A·B interactions.¹¹

The previous model was based on the concept of effective molarity which is a measure of the ease of formation of a given cyclic oligomer and is defined as $EM_i = K_{(intra)i}/K_a$.



Scheme 3.4: Linear (M_i and L_i type chains) vs. cyclic species (C_i) present in the supramolecular polymerization of an AB monomer in solution capable of both A·B hetero-coupling and A·A homo-coupling. Due to the non-associating NaPy end groups, only linear species with one NaPy and one UPy end group (L_i type chains) are able to form cycles. L_1 and all other L_i type oligomers implicitly contain all tautomeric forms of the free UPy end group.

Under the assumption that all the rings, including the smaller ones, are strainless and follow the Jacobson–Stockmayer equation, *i.e.* $EM_i = EM_1 i^{-5/2}$, the following expression can be deduced (see Appendix B) that links the total AB monomer concentration C and the equilibrium constants K_a , K_{dim} , EM_1 to the structural characteristics of the system as schematically drawn in Scheme 3.4.

$$C = \underbrace{\frac{1}{K_a} \frac{x}{(1-x)^2}}_{L_i \text{ type chains}} + \underbrace{\frac{2K_{\text{dim}}}{K_a^2} \frac{x^2}{(1-x)^3}}_{M_i \text{ type chains}} + \underbrace{EM_1 \sum_{i=1}^{\infty} i^{-3/2} x^i}_{\text{rings}} \quad (1)$$

The three terms in the right-hand side of eq (1) represent the amount of monomer, in concentration units, that, at equilibrium, went into L_i chains, M_i chains, and rings, respectively. All of them are expressed as a function of x , namely the extent of heterocoupling reaction in the linear fraction. To more quantitatively understand the development of the viscosity as a function of concentration, expressions for the weight and average degree of polymerization were also derived.

The number average degree of polymerization (DP_n) is defined by eq (2).

$$DP_n = \frac{\sum_{i=1}^{\infty} iN_i}{\sum_{i=1}^{\infty} N_i} \quad (2)$$

where N_i is the number of molecules of a given i -mer. The numerator of eq (2) is proportional to the initial monomer concentration, C , whereas the denominator is proportional to the summation of the molar concentrations of all the i -mers. In other words eq (2) can be rewritten as eq (3).

$$DP_n = \frac{C}{\sum_{i=1}^{\infty} [L_i] + \sum_{i=2}^{\infty} [M_i] + \sum_{i=1}^{\infty} [C_i]} \quad (3)$$

The first two sums in the denominator can be evaluated using standard expressions for infinite converging series while the last sum can be numerically evaluated for finite-sized systems (see Appendix B). The weight average degree of polymerization (DP_w) is defined by eq (4).

$$DP_w = \frac{\sum_{i=1}^{\infty} i^2 N_i}{\sum_{i=1}^{\infty} i N_i} \quad (4)$$

The numerator of eq (4) is proportional to the summation of the molar concentrations of all the i -mers multiplied by i^2 , whereas the denominator is proportional to the initial monomer concentration, C . In other words, eq (4) can be rewritten as eq (5).

$$DP_w = \frac{\sum_{i=1}^{\infty} i^2 [L_i] + \sum_{i=2}^{\infty} i^2 [M_i] + \sum_{i=1}^{\infty} i^2 [C_i]}{C} \quad (5)$$

Again, the first two sums can be evaluated using standard mathematical expression for infinite series while the last sum can be approximated numerically.

Finally, the polydispersity index is defined as:

$$\text{PDI} = \frac{\text{DP}_w}{\text{DP}_n} \quad (6)$$

Using the mass balance eq (1) and the expressions for the weight average degree of polymerization (eq (3) and eq (5)) the fraction of cycles, fraction of linear species and the weight and number average degree of polymerization can be calculated given values of K_{dim} , K_a and EM_1 . Although the developed model assumes that all cycles are strainless, in reality the first few oligomeric rings will be strained. However, it is stressed that the goal of the numerical simulations is to reveal the differences in the supramolecular polymerizations of both AB monomers based on the difference in dimerization constant of the UPy-UPy interaction. The value for EM_1 was set to 0.1 M to reproduce the experimental viscosity data.

Figure 3.4 displays the results of the calculations of the fraction of monomer incorporated in the various chains and rings as a function of the concentration of monomer using the experimentally determined thermodynamic parameters for **5** and **6**. As can be observed, there are some differences in the composition of the mixture between the more (**6**) and less (**5**) hetero-selective system. For example the concentration at which the fraction with only of cycles becomes significantly smaller than 1 is lower for the less hetero-selective system due to the lower fraction of L_i type chains, although this feature cannot be clearly detected from the plots in Figure 3.4.

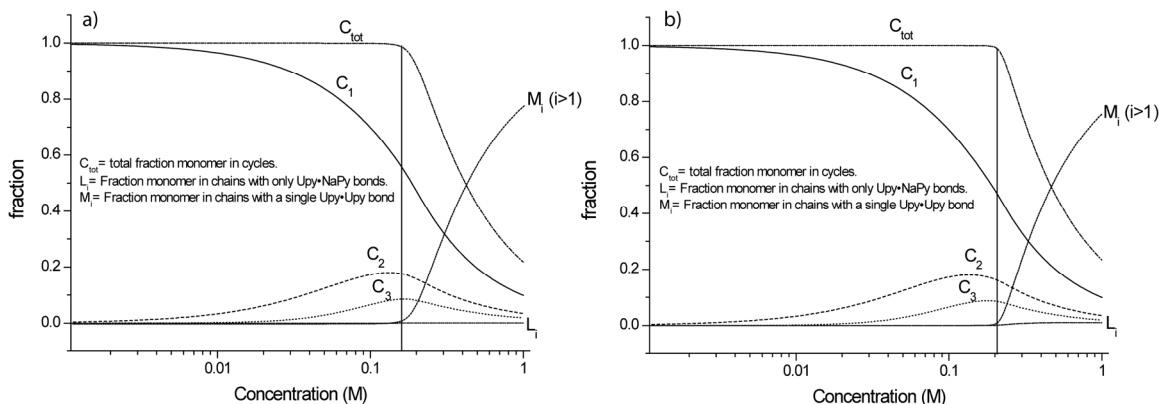


Figure 3.4: Calculations of the fraction of monomer in cyclic oligomers (C_1 , C_2 and C_3), total fraction of monomer present in cycles (C_{tot}) and total fraction of monomer present in linear chains containing only UPy-NaPy bonds (L_i type chains) or containing a single UPy-UPy bond (M_i type chains) as a function of concentration for $\text{EM}_1 = 0.1$ M. a) $K_a = 6 \times 10^6 \text{ M}^{-1}$, $K_{\text{dim}} = 6 \times 10^7 \text{ M}^{-1}$ corresponding to the thermodynamic parameters of methyl-substituted UPy-NaPy monomer **5**. b) $K_a = 6 \times 10^6 \text{ M}^{-1}$, $K_{\text{dim}} = 9 \times 10^5 \text{ M}^{-1}$ corresponding to the thermodynamic parameters of dibutylamino-substituted UPy-NaPy monomer **6**.

Simulations of the weight average degree of polymerization *vs.* concentration for both systems reveal large differences in the growth of supramolecular polymer as the concentration is increased. At concentrations slightly above the effective molarity of the first ring closure, the weight average degree of polymerization for all *i*-mers of the less hetero-selective system starts to increase while the weight average degree of polymerization for the more hetero-selective system is not increasing. Only at concentrations well above (>0.22 M) the effective molarity of the first cyclization, the weight average degree of polymerization of the more hetero-selective system starts to increase (Figure 3.5) and increases much faster compared to the less hetero-selective system because of the higher fraction of L_i type chains. In the intermediate concentration regime (between 0.15 and 0.25 M), the DP_w of the oligomeric and polymeric chains of the less hetero-selective system is higher. These simulations illustrate, from a theoretical point of view¹⁵, the experimental results obtained from the capillary viscosity measurements where a similar crossover region is observed at roughly a concentration of 0.2 M (see Figure 3.1).

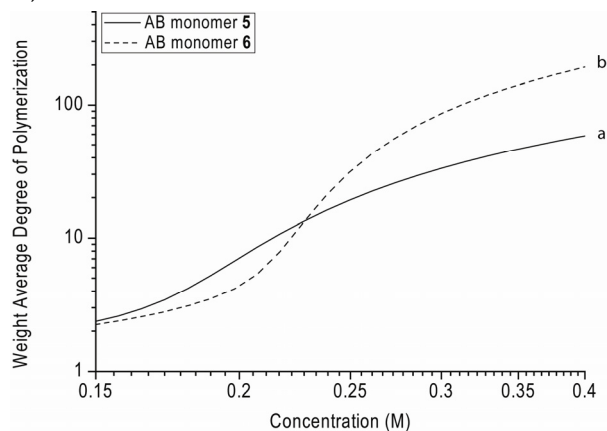


Figure 3.5: Simulation of the weight average degree of polymerization *vs.* total concentration of AB monomer for $EM_1 = 0.1$ M and a) $K_a = 5 \times 10^6$ M^{-1} , $K_{dim} = 6 \times 10^7$ M^{-1} corresponding to the thermodynamic parameters of methyl-substituted UPy·NaPy monomer 5. b) $K_a = 6 \times 10^6$ M^{-1} , $K_{dim} = 9 \times 10^5$ M^{-1} corresponding to the thermodynamic parameters of dibutylamino-substituted UPy·NaPy monomer 6.

3.6 Effect of A·A dimerization on the polydispersity

The mathematical model allows for the determination of the polydispersity index at equilibrium. For an isodesmic equilibrium polymerization in the absence of cyclization, characterized by a single elongation constant (K_a), the polydispersity index approaches 2 as the concentration of AB becomes high.¹⁶ Indeed for $K_{dim} = 0$ the model predicts that the polydispersity index becomes 2 at high values of the dimensionless concentration $K_a \cdot C$ (Figure 3.6a). However, if the AB monomer is also capable of A·A interactions the

polydispersity drops to a limiting value of 1.5 (see Appendix C for the derivation). The drop in polydispersity is accompanied with a lower weight average degree of polymerization compared to the situation in which no A·A interaction is present (Figure 3.6b).

The first question that arises from these simulations is why homo-coupling results in a lower limiting *PDI* value at high concentrations. This question can be answered by calculating the polydispersity index for the individual M_i and L_i type chains. For the L_i type chains the following expression can be derived (see Appendix C):

$$PDI = 1 + x \quad (7)$$

Indeed, as x goes to 1, the polydispersity index goes to 2 in accordance with the standard theory for step polymerizations as derived by Flory.¹⁷

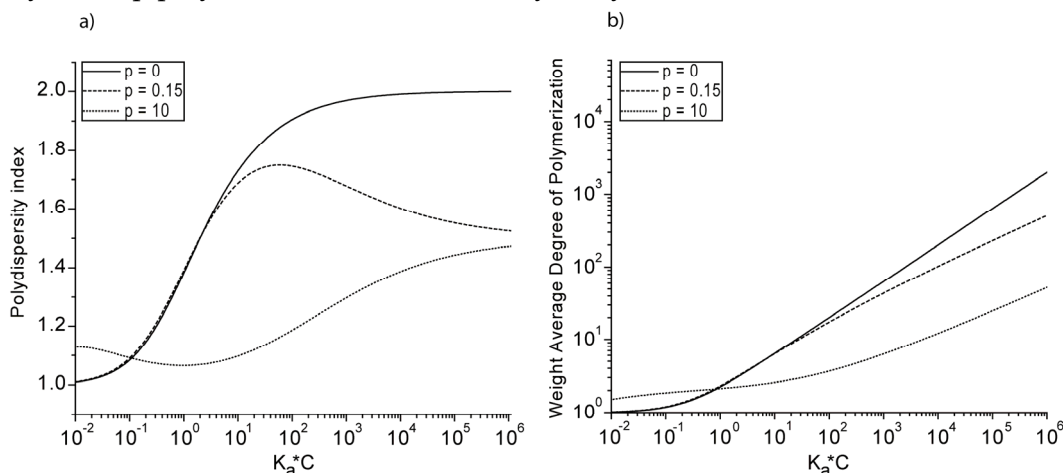


Figure 3.6: a) Calculation of the polydispersity index vs. dimensionless concentration ($K_a \cdot C$) for a supramolecular AB type monomer for several values of the dimensionless binding constant p (defined as K_{dim} / K_a) and $EM_1 = 0$. b) Calculation of the weight-average degree of polymerization vs. dimensionless concentration for a supramolecular AB type monomer for several values of the dimensionless binding constant p (defined as K_{dim} / K_a) and $EM_1 = 0$

For the M_i type chains the following expression can be derived (see supporting info) that links the polydispersity index to the extent of the reaction (x):

$$PDI = \frac{2+x}{2} \quad (8)$$

In contrast to the L_i type chains, the polydispersity index for the M_i type chains goes to 1.5 as $x \rightarrow 1$ in accordance with the limiting PDI for a multichain AB polycondensation containing a small amount of bifunctional initiator.¹⁸ For the general case of an f -functional monomer ($R-A_f$) present in low amount in a multichain AB polycondensation, Flory¹⁹ derived the following approximate expression for the polydispersity index for high molecular weight chains in the limit $x \rightarrow 1$.

$$PDI = 1 + \frac{1}{f} \quad (9)$$

The effect of the reversible AA interaction has an equivalent effect on the polydispersity as the addition of a bifunctional RA₂ initiator in low amounts in a covalent multichain AB polymerization. Hence, the narrower distribution is the direct result of the linking of two statistically independent L_i polymer chains via the reversible A·A interaction.

Now that the origin of the reduced polydispersity index is understood in terms of the differences in the polydispersity index of the two different chains, the question arises why the equilibrium shifts to M_i type chains at the expense of L_i type chains when the concentration is increased. This shift can be understood by further examination of eq 1. In this mass balance equation, the first and the second term represent the amount of monomer that has gone into the L_i and M_i type oligomers, respectively (the third term, representing the cyclic oligomers, is ignored because of the assumption that no rings are formed). The total concentration of L_i type oligomers is proportional to $x/(1-x)^2$ whereas the M_i oligomers are proportional to $x^2/(1-x)^3$, thus, as x approaches 1 (or equivalently the concentration is increased), the concentration of M_i oligomers increases much more rapidly than that of L_i type oligomers. Hence, the change of *PDI* from 2 to 1.5 is a consequence of the shift of equilibrium in favor of the M_i type oligomers.

Although equations 7 and 8 only apply for the case when cycle formation is neglected ($EM_1 = 0$) it has the advantage that they can be derived in a rather straightforward way. However, when cycle formation is taken into account it proved difficult to derive analytical expressions analogous to equations 7 and 8. However, calculation of the polydispersity index as a function of monomer concentration, taken into account cycle formation³⁷, shows that the molecular weight distribution becomes extremely broad around concentrations close to the effective molarity of first ring closure (EM_1). The broad distribution is the direct result of the fact that at these concentrations the solution consists of small cycles and long polymeric chains (Appendix D). Further examination of these graphs shows that the polydispersity index goes to 1.5 if $p > 0$ and $C \gg EM_1$ indicating that the above treatment is still valid when cycle formation is taken into account although only at high values of x .

3.7 Discussion and conclusion

In this chapter, the formation of linear supramolecular polymers, in equilibrium with cyclic intermediates of heteroditopic UPy·NaPy, AB-type monomers capable of complementary as well as self-complementary interactions, has been studied. In the efforts to reduce the “self-stoppered” effect that is inherently present in these

supramolecular polymerizations, two different UPy·NaPy monomers were synthesized and their concentration dependent supramolecular polymerization was studied using Ubbelohde viscometry, diffusion ordered spectroscopy (DOSY) and ¹H-NMR. Surprisingly, the UPy·NaPy monomer which was anticipated to exhibit the lowest amount of “self-stoppered” behavior showed the lowest degree of polymerization below the critical concentration, suggesting that cycle formation was enhanced by the increased fidelity for hetero-complexation. In order to theoretically illustrate the results a previous model for the ring-chain equilibrium of an AB monomer in solution was extended to include reversible A·A interaction. Simulations have shown that the value of K_{dim} significantly affects the extent of cyclization. For UPy·NaPy AB type monomers, the fraction of cycles just above the critical polymerization concentration is lower when the dimerization constant of the UPy is increased. More importantly, the growth of linear high molecular weight material far above the CPC has a stronger concentration dependence when the UPy dimerization constant is lower than K_a as in the case of UPy·NaPy monomer **6**, ultimately resulting in a higher degree of polymerization compared to UPy·NaPy monomer **5**.

Theoretical analysis of the polydispersity index at equilibrium when cyclization is negligible reveals that the presence of the reversible A·A interactions plays a crucial role in narrowing the molecular weight distribution. The continuous quest to obtain polymeric architectures with low polydispersities in covalent polymerization has resulted in a wealth of novel living polymerization techniques in the last few decades (*i.e.* ATRP, RAFT, NMP). In sharp contrast, the development of supramolecular polymeric architectures with low polydispersities has achieved much less attention with the exception of a few cases.²⁰

3.8 Experimental section

General Methods

See General Methods Chapter 2. Analytical gel permeation chromatography (GPC) was carried out in THF on two PL Gel single pore size (100 Å) 30 cm columns, with a particle size of 3 μm (Polymer Labs) connected in series with a SPD-M10Avp photodiode array UV/Vis detector (Shimadzu) measuring between 250 and 370 nm.

7-(2-(*tert*-Butyldimethylsilyloxy)propanoylamino)-2-(2-ethylhexanoylamino)-1,8-naphthyridine was synthesized according to Ligthart et al.¹⁰ 2-(6-isocyanatohexylamino carbonylamino)-6-methyl-4[1H]pyrimidinone was synthesized according to Folmer et al.²¹

Synthesis of 7-(2-hydroxypropanoylamino)-2-(2-ethylhexanoylamino)-1,8-naphthyridine (4)

To a solution of 7-(2-(tert-butyltrimethylsilyloxy)propanoylamino)-2-(2-ethylhexanoylamino)-1,8-naphthyridine (**8**, 0.72 g, 1.52 mmol) in 6 mL distilled tetrahydrofuran (THF) was added a solution of triethylamine trihydrofluoride (0.50 g, 3.05 mmol) in 1.5 mL of distilled THF. The solution was stirred for 4 h at room temperature after which the solution was evaporated *in vacuo* and 20 mL CHCl₃ was added. The solution was washed with H₂O (1 x 10 mL), a saturated solution of NaHCO₃ (2 x 20 mL), H₂O (2 x 20 mL) and finally with brine (1 x 20 mL). The organic solution was dried over Na₂SO₄, filtered and evaporated *in vacuo*. Column chromatography (SiO₂ 2% MeOH/CHCl₃) resulted in 470 mg of pure 7-(2-hydroxypropanoylamino)-2-(2-ethylhexanoylamino)-1,8-naphthyridine as a white solid, mp 191 °C (degr.). Yield: 86%. ¹H-NMR (CDCl₃): δ 9.77 (s, 1H, NH), 8.74 (b, 1H, NH), 8.46 (d, 2H, naphthyridine-H), 8.08 (d, 2H, naphthyridine-H), 5.85 (b, 1H, OH), 4.68 (q, 1H, CH(OH)), 2.35 (m, 1H, CH(CH₂)₂), 1.80-1.33 (m, 11H, CH₂ and CH₃), 0.97 (t, 3H, CH₃), 0.87 (t, 3H, CH₃) ppm. ¹³C-NMR (CDCl₃): δ 176.1, 175.9, 154.2, 153.4, 153.3, 139.3, 138.9, 118.4, 113.9, 113.2, 69.2, 50.6, 32.4, 32.3, 29.8, 29.7, 26.0, 22.76, 22.72, 20.71, 13.9, 12.0 ppm. IR (ATR): ν (cm⁻¹) = 3365, 3309, 2961, 2932, 2873, 2860, 1705, 1686, 1537, 1502, 1459, 1382, 1312, 1286, 1173, 1136, 1120, 855. MALDI-TOF-MS (m/z): calcd: 358.20 obs: 359.15 (MH⁺). Anal. Calcd for C₁₉H₂₆N₄O₃: C 63.67, H 7.31, N 15.63 found C 63.62, H 7.33, N 15.63.

Synthesis of MethylUPy-NaPy AB monomer (5)

To a solution of 2-(6-isocyanatohexylaminocarbonylamino)-6-methyl-4[1H]pyrimidinone (**7**, 155 mg, 0.53 mmol) and 7-(2-hydroxypropanoylamino)-2-(2-ethylhexanoylamino)-1,8-naphthyridine (**4**, 180 mg, 0.50 mmol) in 4 mL CHCl₃ was added two drops of DBTDL (dibutyltin dilaurate). The solution was stirred for 20 h at 60 °C under an atmosphere of argon. The solution was evaporated *in vacuo* and the product was purified by column chromatography (SiO₂, 10-30% acetone/ CHCl₃). The resulting solid was further purified by precipitation by addition of 15 mL MeOH to a concentrated solution of **5** in CHCl₃ at 0 °C. Extensive drying *in vacuo* resulted in 220 mg of **5** as a white solid, mp: 158-160 °C (degr.) Yield: 67%. ¹H-NMR (CDCl₃, 100 mM): δ 13.92 (s, 1H, NH), 11.62 (b, 2H, NH), 11.3 (s, 1H, NH), 9.73 (s, 1H, NH), 8.54 (d, 1H, naphthyridine-H), 8.36 (d, 1H, naphthyridine-H), 8.12 (d, 2H, naphthyridine-H), 5.96 (s, 1H, C=CH), 5.50 (b, 1H, CH₂NH), 5.34 (q, 1H, CHOCO), 3.5-3.1 (m, 4H, CONHCH₂), 2.65 (m, 1H, CH(CH₂)₂), 2.25 (s, 3H, CH₃), 1.78-1.30 (m, 19H, CH₂ + CH₃), 0.95 (t, 3H, CH₃), 0.85 (t, 3H, CH₃) ppm. ¹³C-NMR (CDCl₃): δ 177.4, 172.1, 164.9, 164.7, 155.6, 155.5, 155.2, 154.9, 153.7, 150.3, 139.2, 118.1, 115.6, 115.5, 105.8, 70.9, 48.7, 40.7, 39.6, 32.3, 32.3, 29.7, 29.1, 26.3, 26.1, 26.0, 24.0, 22.81, 22.78, 18.0, 14.0, 11.9 ppm. IR (ATR): ν (cm⁻¹) = 3333, 3183, 2933, 2860, 1697, 1675, 1623, 1610, 1536, 1504, 1459, 1385, 1309, 1281, 1251, 1174, 1141, 1094, 1048, 970, 853. MALDI-TOF-MS (m/z): calcd: 651.34 obs: 652.27 (MH⁺), 674.27 (MNa⁺), 690.21 (MK⁺). Anal. Calcd. for C₃₂H₄₅N₉O₆: C 58.97, H 6.96, N 19.34 found: C 58.55, H 6.99, N 19.42.

Synthesis of 2-(6-isocyanatohexylaminocarbonylamino)- 6-(dibutylamino) 4-pyrimidinol (9)

A solution of 3.04 g (12.75 mmol) of 2-amino-6-(dibutylamino) 4-pyrimidinol and 30 mL (31.2 g, 185.5 mmol) 1,6-diisocyanatohexane (HDI) was heated to 60 °C and stirred for 1 h. The solution was cooled to room temperature and 7 mL of acetonitrile was added. To this solution, 300 mL of pentane was added and the solution was stirred for half a minute. Upon standing, the solution

separated into two layers. The upper layer (containing HDI and pentane) was decanted and the process was repeated an additional two times. After the third decantation step, 40 mL of acetonitrile was added and the solution was cooled to $-40\text{ }^{\circ}\text{C}$. Upon cooling a white solid precipitated which was collected by vacuum filtration. The residue was washed several times with 100 mL pentane and dried extensively *in vacuo* resulting in 850 mg of a white solid. mp $96\text{--}100\text{ }^{\circ}\text{C}$ Yield: 16%. $^1\text{H-NMR}$ (CDCl_3): δ 12.60 (s, 1H, OH), 11.25 (s, 1H, NH), 9.63 (s, 1H, NH), 5.33 (s, 1H, aromatic-H), 3.40 (m, 8H, $\text{N}(-\text{CH}_2)_2 + \text{CONHCH}_2 + \text{CH}_2\text{NCO}$), 1.61-1.31 (m, 18H, CH_2), 0.96 (t, 6H, CH_3) ppm. $^{13}\text{C-NMR}$ (CDCl_3): δ 170.8, 162.4, 157.5, 157.0, 121.9, 78.7, 49.0, 42.9, 39.7, 31.2, 30.2, 29.8, 26.33, 26.29, 13.96 ppm. IR (ATR): ν (cm^{-1}) = 3221, 3126, 2958, 2933, 2862, 2270, 1675, 1617, 1561, 1508, 1455, 1371, 1322, 1283, 1252, 1206, 1148, 1099, 1062, 987. MALDI-TOF-MS (m/z): calcd: 406.26 obs: 407.17 (MH^+). Anal. Calcd. for $\text{C}_{20}\text{H}_{34}\text{N}_6\text{O}_3$: C 59.09, H 8.43, N 20.67 found: C 59.09, H 8.43, N 20.72.

Synthesis of dibutylamino substituted UPy·NaPy AB monomer (6)

To a solution of 2-(6-isocyanatohexylaminocarbonylamino)-6-(dibutylamino)-4-pyrimidinol (732.2 mg, 1.81 mmol) and 7-(2-hydroxypropanoylamino)-2-(2-ethylhexanoylamino)-1,8-naphthyridine (591.0 mg, 1.65 mmol) in 13 mL CHCl_3 was added two drops of DBTDL (dibutyltin dilaurate). The solution was stirred for 4 days at $60\text{ }^{\circ}\text{C}$ after it was cooled to room temperature. The solution was evaporated *in vacuo* and purified using column chromatography (SiO_2 , 5-20% acetone / CHCl_3). Precipitation in cold methanol (100 mL) followed by filtration and extensive drying *in vacuo* resulted in 619 mg of a white solid, mp $142\text{--}146\text{ }^{\circ}\text{C}$. Yield: 49%. $^1\text{H-NMR}$ (CDCl_3 , 1 mM): δ 13.48 (s, 1H, NH), 12.25 (s, 1H, NH), 11.47 (s, 1H, NH), 10.96 (s, 1H, NH), 9.30 (s, 1H, NH), 8.53 (d, 1H, naphthyridine-H), 8.33 (d, 1H, naphthyridine-H), 8.13 (d, 2H, naphthyridine-H), 5.45 (b, 1H, NH), 5.38 (q, 1H, CHOCO), 5.09 (s, 1H, $\text{C}=\text{CH}$), 3.54-3.19 (m, 8H, $\text{N}(-\text{CH}_2)_2 + \text{CONHCH}_2 + \text{CH}_2\text{NCO}$), 2.76 (m, 1H, $\text{CH}(\text{CH}_2)_2$), 1.77-1.26 (m, 27H, CH_2 and CH_3), 0.97 (m, 9H, CH_3), 0.85 (m, 3H, CH_3). $^{13}\text{C-NMR}$ (CDCl_3): 177.8, 172.3, 165.0, 161.0, 155.8, 155.6, 155.5, 155.1, 153.7, 149.8, 139.1, 139.0, 118.0, 115.9, 115.5, 79.4, 70.5, 49.5, 48.5, 48.4, 40.8, 32.4, 29.7, 29.2, 26.1, 22.9, 22.8, 20.3, 18.0, 14.0, 13.9, 11.9 ppm. IR (ATR): ν (cm^{-1}) = 3234, 3125, 2958, 2931, 2872, 2861, 1697, 1650, 1628, 1609, 1560, 1523, 1504, 1461, 1430, 1381, 1309, 1281, 1247, 1217, 1176.4, 1140, 1124, 1094, 1047, 852, 748 cm^{-1} . MALDI-TOF-MS (m/z): calcd: 765.46, obs: 765.4 (MH^+). Anal. Calcd. for $\text{C}_{39}\text{H}_{60}\text{N}_{10}\text{O}_6$: C 61.24, H 7.91, N 18.31 found: C 60.77 H 7.78 N 18.41.

Viscosity measurements

Solution viscosities were measured using Schott-Geräte Ubbelohde microviscometers (type 53810 / I) with suspended level bulb in automated setups with Schott-Geräte AVS/S measurement tripods and AVS 350 measurement devices. The micro-viscometers were thermostated in a water bath at $25.00 (\pm 0.01)\text{ }^{\circ}\text{C}$. Samples were filtered over $1.0\text{ }\mu\text{m}$ PTFE filters before measurement. Specific viscosities were corrected using the appropriate Hagenbach correction factors. The specific viscosity at each concentration of **5** or **6** was determined from an average of 5 (high concentrations) or 10 (low concentrations) individual measurements.

¹H-NMR measurements

¹H-NMR dilution experiments on **5** and **6** in CDCl₃ were performed on a Varian Unity Inova, 500 MHz equipped with a 5mm ¹H/X Inverse Detection probe equipped with gradient capabilities at 25 °C. Both AB monomers were dried over P₂O₅ under dynamic vacuum for at least a period of 12 hours to remove any trace amounts of water. Dry CDCl₃ used for the dilution studies was obtained by adding oven dried molecular sieves (4 Å) 48 hours prior to the measurements.

Diffusion ordered spectroscopy (DOSY)

2D-DOSY experiments on **5** and **6** in CDCl₃ were performed on a Varian Unity Inova, 500 MHz equipped with a 5 mm ¹H/X Inverse Detection probe equipped with gradient capabilities (Performa II/III, maximum gradient strength of 70 gauss/cm) at 25 °C. Both AB monomers were dried over P₂O₅ under dynamic vacuum for at least a period of 12 hours to remove any trace amounts of water. Dry CDCl₃ used for the dilution studies was obtained by adding oven dried molecular sieves (4 Å) 48 hours prior to the measurements. The NMR tubes (5 mm) used for the studies were dried over P₂O₅ under high vacuum. Samples were not spinning during the measurements. A 5-min temperature calibration period was provided prior to analysis. The DOSY bipolar pulse pair stimulated echo with convection compensation (Dbppste_cc) sequence²² was used for the determination of the self-diffusion of the different components. Temperature calibration was achieved by observing the temperature dependent chemical-shift separation between the OH and CH₃ resonance in methanol. In all experiments the 90° pulse widths were determined. Firstly, the strength of the B₀ field gradient was calibrated by measuring the self-diffusion coefficient of the residual HDO signal in a 1% D₂O sample, at 25 °C (D(H₂O) = 19 × 10⁻¹⁰ m²/s).²³ The experimental diffusion data can be obtained using the Stejskal–Tanner equation:

$$I(G) = I(0) \exp(-D \gamma^2 \delta^2 (G)^2 (\Delta - \delta/3 - \tau/2))$$

In which $I(G_a)$ represents the experimental signal intensity, $I(0)$ the initial signal intensity, γ_h is the magnetogyric ratio for ¹H, τ the time interval between the bipolar pulse pair, δ the length of the pulsed field gradient and Δ the diffusion period. Using this equation it is possible to determine D from a plot of $\ln(I(G)/I(0))$ vs. G^2 . In a typical experiment, 32 transients (with a recycle delay of 3 s per transient) for each of the 100 steps were recorded with increasing gradient strength (ranging from an initial value of 1.085 G/cm⁻¹ to 32.55 G/cm⁻¹), where gradient pulse duration, diffusion delay and maximum gradient strength were adjusted at each concentration in order to obtain an 80% reduction of the signal at the highest gradient strength. At each concentration the 90° ¹H pulse width was calibrated at a transmitter power of 58 dB.

Computational procedure for simulation of ring-chain equilibrium

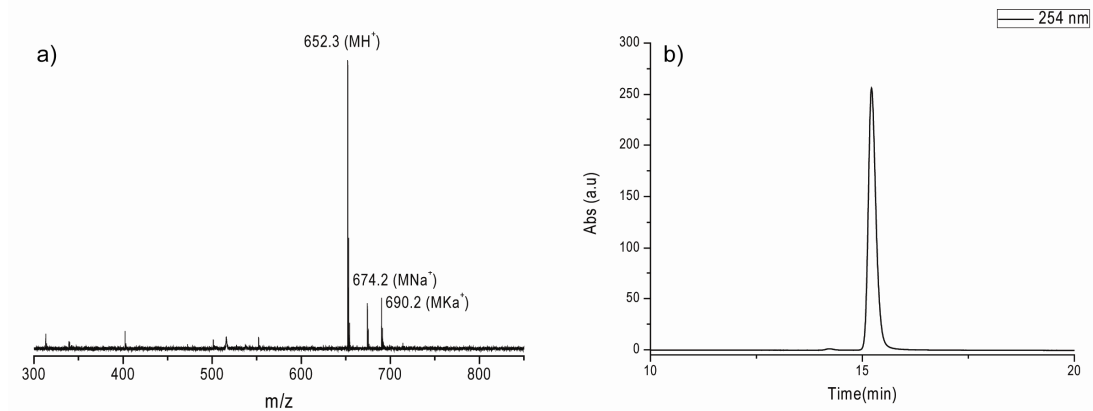
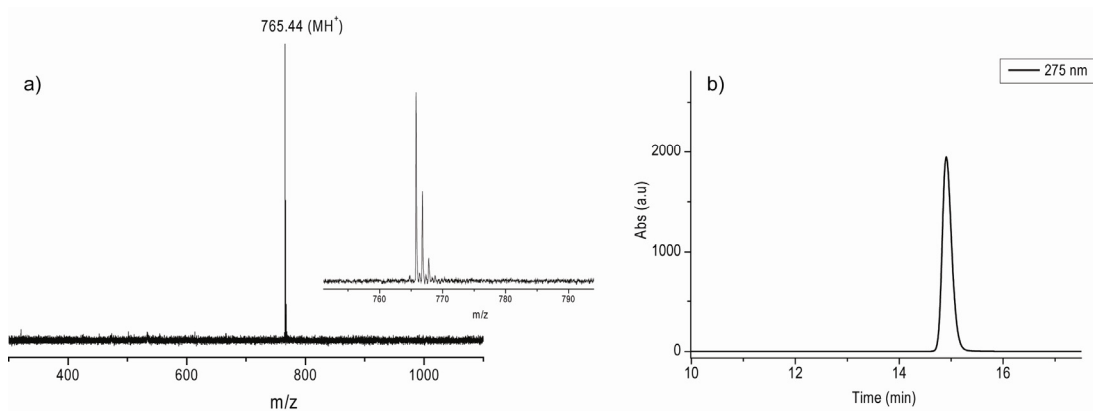
A computer script was written using Matlab R2007B. The input consists of a vector of initial concentrations, K_{dim} , K_a and the effective molarity of the first cyclization (EM₁). Using a combination of bisection, secant, and inverse quadratic interpolation methods present in the

Matlab script *fzero*, equation (1) was solved for x at each initial monomer concentration C . Instead of evaluating the sum in equation (1) from 1 to infinity it was evaluated to ring sizes up to 100. For each resulting value of x both the weight average degree of polymerization (DP_w) and the number average degree of polymerization (DP_n) was calculated using the expressions developed in Appendix B.

3.9 Appendices

Appendix A

Characterization of AB monomers 5 and 6.

**Figure A1:** a) Maldi-TOF MS of 5. b) GPC trace of 5 in THF.**Figure A2:** a) Maldi-TOF MS of 6. b) GPC trace of 6 in THF.

Appendix B

Derivation of eq 1 and expressions for eq 3 and 5.

Consider a bifunctional monomer bearing two different functional groups at its ends (A—B). Two reversible reactions are allowed: the hetero-coupling between –A and –B groups, and the homo-coupling between two –A groups. The following quantities can be defined.

C = initial monomer concentration in mol L⁻¹

C' = monomer concentration that has gone into the linear fraction at equilibrium in mol L⁻¹

C'' = monomer concentration that has gone into the cyclic fraction at equilibrium in mol L⁻¹

K_a = reference equilibrium constant for intermolecular hetero-coupling in mol⁻¹ L

K_{dim} = reference equilibrium constant for intermolecular homo-coupling in mol⁻¹ L

x = extent of hetero-coupling reaction in the linear fraction

y = extent of homo-coupling reaction in the linear fraction

L_i = i -meric chain made of AB hetero-bonds only (i running from 1 to ∞)

M_i = i -meric chain with one AA homo-bond (i running from 2 to ∞). Note that M_i accounts for all the isomeric chains differing for the position of the AA homo-bond along the chain.

C_i = i -meric ring (i running from 1 to ∞).

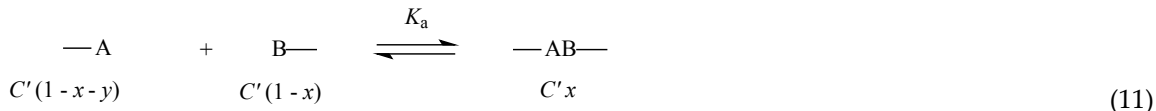
$K_{(intra)i}$ = equilibrium constant for the cyclization of L_i to yield C_i . Note that M_i chains cannot undergo cyclization because they have –B groups at both ends.

EM_i = effective molarity relative to the ease of formation of the i -meric ring. It is defined as the ratio $K_{(intra)i} / K_a$

When equilibrium is attained, the initial monomer concentration, C , is partitioned into the fractions of linear and cyclic oligomers. Indicating the monomer concentration that has gone into linears and cyclics as C' and C'' , respectively, eq (10) holds.

$$C = C' + C'' \quad (10)$$

Now, we concentrate on the equilibria occurring in the linear fraction. We assume that the thermodynamic reactivities of end groups related to hetero- and homo- couplings, as given by the constants K_a and K_{dim} , respectively, are independent of the length of the chain (principle of equal thermodynamic reactivity). Accordingly the intermolecular reactions of –A and –B groups can be treated collectively by considering the two equilibria below:



From the definition of the equilibria (11) and (12), eqs. (13) and (14), respectively, are easily obtained:

$$C' = \frac{x}{K_a(1-x-y)(1-x)} \quad (13)$$

$$C' = \frac{y}{2K_{\text{dim}}(1-x-y)^2} \quad (14)$$

Equating eq (13) with eq (14) and solving for y , eq (15) is obtained.

$$y = \frac{2K_{\text{dim}}x(1-x)}{2K_{\text{dim}}x + K_a(1-x)} \quad (15)$$

Substituting eq (15) into eq (13), eq (16) is obtained.

$$C' = \frac{1}{K_a} \frac{x}{(1-x)^2} + \frac{2K_{\text{dim}}}{K_a^2} \frac{x^2}{(1-x)^3} \quad (16)$$

By comparing eq (13) with eq (16), it appears that, when y tends to 0, eq (13) reduces to the first term of eq (16). Thus the meaning of the two terms in eq (16) is obvious: they represent the amount of monomer that has gone into L_i and M_i chains, respectively. In other words, eqs (17) and (18) hold.

$$\sum_{i=1}^{\infty} i[L_i] = \frac{1}{K_a} \frac{x}{(1-x)^2} \quad (17)$$

$$\sum_{i=2}^{\infty} i[M_i] = \frac{2K_{\text{dim}}}{K_a^2} \frac{x^2}{(1-x)^3} \quad (18)$$

Now consider the infinite McLaurin expansion series shown in eq (19)

$$\frac{x}{(1-x)^2} = \sum_{i=1}^{\infty} ix^i \quad (19)$$

it is evident, by substituting eq (19) into eq (17), that eq (20) holds.

$$[L_i] = \frac{x^i}{K_a} \quad (20)$$

Analogously, by considering the infinite McLaurin expansion series shown in eq (21)

$$\frac{x^2}{(1-x)^3} = \frac{1}{2} \sum_{i=2}^{\infty} i(i-1)x^i \quad (21)$$

it is evident, by substituting eq (21) into eq (18), that eq (22) holds.

$$[M_i] = \frac{K_{\text{dim}}}{K_a^2} (i-1)x^i \quad (22)$$

Now, let us concentrate on the cyclic fraction. Consider the equilibrium of cyclization of a chain L_i to yield the corresponding cyclic oligomer C_i



Considering that $K_{(\text{intra})i} = EM_i K_a$, from the definition of the equilibrium (23), eq (24) is easily obtained.

$$[C_i] = EM_i K_{\text{AB}} [L_i] \quad (24)$$

If we assume that all the rings are large enough to follow the Jacobson–Stockmayer equation (eq (25)).

$$EM_i = EM_1 i^{-5/2} \quad (25)$$

we can substitute eqs (25) and (20) into eq (24) to obtain eq (26).

$$[C_i] = EM_1 i^{-5/2} x^i \quad (26)$$

Then the cyclic fraction will be given by eq (27).

$$C'' = \sum_{i=1}^{\infty} i [C_i] = EM_1 \sum_{i=1}^{\infty} i^{-3/2} x^i \quad (27)$$

Considering eqs (10), (16), and (27), eq (1) is easily obtained.

$$C = \frac{1}{K_a} \frac{x}{(1-x)^2} + \frac{2K_{\text{dim}}}{K_a^2} \frac{x^2}{(1-x)^3} + EM_1 \sum_{i=1}^{\infty} i^{-3/2} x^i \quad (1)$$

Calculation of DP_n and DP_w

The number average degree of polymerization (DP_n) is defined by eq (2).

$$DP_n = \frac{\sum_{i=1}^{\infty} i N_i}{\sum_{i=1}^{\infty} N_i} \quad (2)$$

where N_i is the number of molecules of a given i -mer. Now the numerator of eq (2) is proportional to the initial monomer concentration, C , whereas the denominator is proportional to the summation of the molar concentrations of all the i -mers. In other words eq (2) can be rewritten as eq (3).

$$DP_n = \frac{C}{\sum_{i=1}^{\infty} [L_i] + \sum_{i=2}^{\infty} [M_i] + \sum_{i=1}^{\infty} [C_i]} \quad (3)$$

The following sum will be useful to evaluate the first two sums appearing in the denominator of eq (3)

$$\sum_{i=1}^{\infty} x^i = \frac{x}{(1-x)} \quad (28)$$

Let us consider the first of the three sums appearing in the denominator of eq (3). Taking into account eqs (20) and (28), eq (29) is easily obtained

$$\sum_{i=1}^{\infty} [L_i] = \frac{1}{K_a} \frac{x}{(1-x)} \quad (29)$$

As to the second sum, considering eqs (22), (19), and (28), eq (30) is obtained

$$\sum_{i=2}^{\infty} [M_i] = \frac{K_{\text{dim}}}{K_a^2} \left(\sum_{i=1}^{\infty} i x^i - \sum_{i=1}^{\infty} x^i \right) = \frac{K_{\text{dim}}}{K_a^2} \frac{x^2}{(1-x)^2} \quad (30)$$

As to the third sum, considering eq (24), eq (31) is obtained

$$\sum_{i=1}^{\infty} [C_i] = EM_1 \sum_{i=1}^{\infty} i^{-5/2} x^i \quad (31)$$

Let us consider, now, the weight average degree of polymerization (DP_w) which is defined by eq (4).

$$DP_w = \frac{\sum_{i=1}^{\infty} i^2 N_i}{\sum_{i=1}^{\infty} i N_i} \quad (4)$$

The numerator of eq (4) is proportional to the summation of the molar concentrations of all the i -mers multiplied by i^2 , whereas the denominator is proportional to the initial monomer concentration, C . In other words, eq (4) can be rewritten as eq (5):

$$DP_w = \frac{\sum_{i=1}^{\infty} i^2 [L_i] + \sum_{i=2}^{\infty} i^2 [M_i] + \sum_{i=1}^{\infty} i^2 [C_i]}{C} \quad (5)$$

Let us consider separately the three sums appearing in the numerator of eq (5). As to the first one, considering eq (20), eq (32) is obtained:

$$\sum_{i=1}^{\infty} i^2 [L_i] = \frac{1}{K_a} \sum_{i=1}^{\infty} i^2 x^i = \frac{1}{K_a} \frac{x(1+x)}{(1-x)^3} \quad (32)$$

As to the second one, considering eq (22), eq (33) is obtained:

$$\sum_{i=2}^{\infty} i^2 [M_i] = \frac{K_{dim}}{K_a^2} \left(\sum_{i=1}^{\infty} i^3 x^i - \sum_{i=1}^{\infty} i^2 x^i \right) = \frac{K_{dim}}{K_a^2} \frac{2x^2(2+x)}{(1-x)^4} \quad (33)$$

As to the third one, considering eq (26), eq (34) is obtained:

$$\sum_{i=1}^{\infty} i^2 [C_i] = EM_1 \sum_{i=1}^{\infty} i^{-1/2} x^i \quad (34)$$

Appendix C

Mathematical treatment of limit PDI value for a supramolecular AB polymerization with reversible A·A and A·B bond formation.

The value of DP_n and DP_w are given by eqs (35) and (36), respectively:

$$DP_n = \frac{K_a x(1-x) + 2K_{dim} x^2}{(1-x)[K_a x(1-x) + K_{dim} x^2]} \quad (35)$$

$$DP_w = \frac{K_a x(1-x)(1+x) + 2K_{dim} x^2(2+x)}{(1-x)[K_a x(1-x) + 2K_{dim} x^2]} \quad (36)$$

These equations are easily obtained by considering eqs (1), (3), (29), (30), (5), (32), and (33), under the assumption that no rings are formed.

The value of PDI is given by the ratio of eq (36) to eq (35):

$$PDI = \frac{[K_a x(1-x)(1+x) + 2K_{dim} x^2(2+x)][K_a x(1-x) + K_{dim} x^2]}{[K_a x(1-x) + 2K_{dim} x^2]^2} \quad (37)$$

Let us consider the limit behavior of eq (37) when x tends to 1 in two separate steps. In the first step, let us substitute 1 for x in eq (37) with the exception of the terms $(1-x)$ that are left unaltered. Accordingly, eq (37) becomes:

$$PDI = \frac{[2K_a(1-x) + 6K_{dim}][K_a(1-x) + K_{dim}]}{[K_a(1-x) + 2K_{dim}]^2} \quad (38)$$

Let us consider the case in which there is hetero-coupling only. By substituting $K_{dim} = 0$ into eq (38), the value of $PDI = 2$ is obtained, as expected.

Considering now the case in which homo-coupling is also possible ($K_{dim} > 0$) and substituting 1 for x in eq 4, the value of $PDI = 1.5$ is obtained. Of course the lower the value of K_{dim} , the higher the concentration of AB monomer necessary to reach this value of PDI . For very small K_{dim} values, on increasing the monomer concentration, the value of PDI will increase up to a value very close to 2 and then will slowly decrease up to reach the limit value of 1.5. We will now consider the expressions for the two different linear chains, i.e. chains consisting of only AB interactions (L_i type chains) and chains containing a single AA interaction (M_i type chains). For the L_i type chains, the following equations hold:

$$DP_n = \frac{1}{1-x} \quad (39)$$

$$DP_w = \frac{1+x}{1-x} \quad (40)$$

$$PDI = 1+x \quad (7)$$

Eq 39 is obtained as the ratio of eq (17) to eq (29); eq (40) is obtained as the ratio of eq (32) to eq (17); eq (7) is obtained as the ratio of eq (40) to eq (39).

For the M_i type chains, the following equations hold

$$DP_n = \frac{2}{1-x} \quad (41)$$

$$DP_w = \frac{2+x}{1-x} \quad (42)$$

$$PDI = \frac{2+x}{2} \quad (8)$$

Eq 41 is obtained as the ratio of eq (18) to eq (30); eq (42) is obtained as the ratio of eq (33) to eq (18); eq (8) is obtained as the ratio of eq (42) to eq (41).

Considering eqs (7) and (8), it is evident that the limit PDI of L_i type chains is 2 whereas the limit PDI of M_i type chains is 1.5.

Appendix D

Calculations of limit PDI value for a supramolecular AB polymerization with reversible A·A and A·B bond formation taking into account cyclization.

As explained in the main text, the presence of cyclics greatly increases the PDI value at equilibrium at concentrations close to the effective molarity of first ring closure (EM_1). This increase in PDI value is a direct result of the fact that around this concentration the system consists of small cyclic species²⁴ which are in equilibrium with long chains. Because an analytical expression such as eq 37 is much harder to derive when rings are taken into account we decided to calculate the PDI value for several values of p assuming an EM_1 value of 0.1 (Figure A3a).

At intermediate dimensionless concentrations close to $K_a \cdot EM_1$ (which by definition equals $K_{intra(1)}$) the PDI value as calculated using eqs 1, 3, 29, 30, 5, 32, and 33 starts to increase rapidly due to the simultaneous present of small cyclics and large polymeric species. However, as can be clearly seen from the expansion (Figure A3b) at high values of $K_a \cdot C$ the PDI value goes to 1.5 only if $p > 0$.

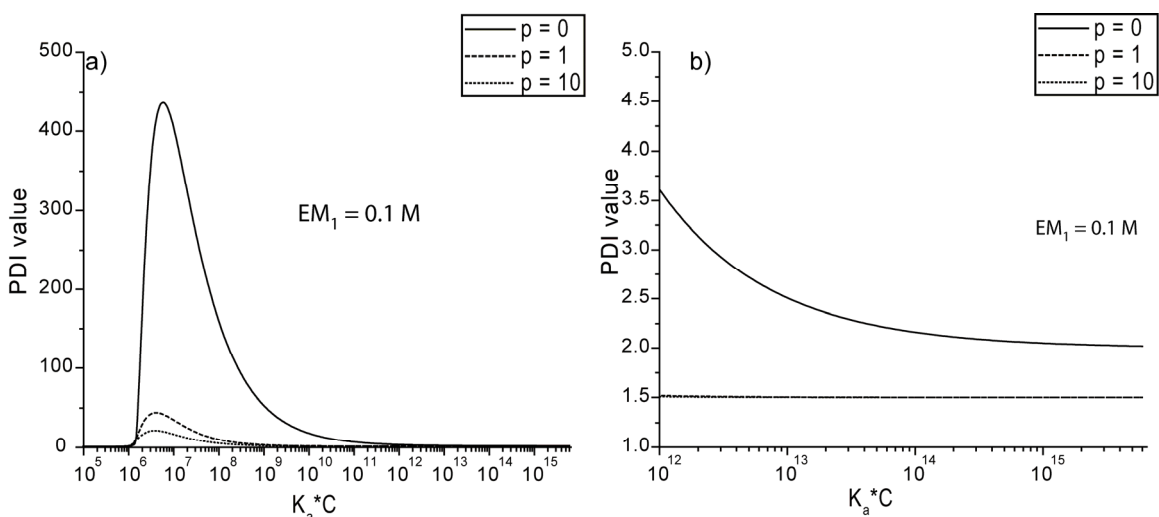


Figure A3: a) Calculation of the polydispersity index vs. dimensionless concentration ($K_a \cdot C$) for a supramolecular type AB monomer for several values of the dimensionless binding constant p (defined as K_{dim}/K_a) and $EM_1 = 0.1 \text{ M}$. b) Expansion of Figure A3a at high values of the dimensionless concentration $K_a \cdot C$.

3.10 References

- Brunsveld, L.; Folmer, B. J. B.; Meijer, E. W.; Sijbesma, R. P. *Chem. Rev.* **2001**, *101*, 4071.
 - Corbin, P. S.; Zimmerman, S. C. In *Supramolecular Polymers*; Ciferri, A., Ed.; M. Dekker: New York, 2000; 147.
 - Ciferri, A. *J. Macromol. Sci. Polym. Rev.* **2003**, *43*, 271.
 - Lehn, J.-M. *Polym. Int.* **2002**, *51*, 825.
 - Wilson, A. J. *Soft. Matter*, **2007**, *3*, 409.
 - Bouteiller, L. *Adv. Polym. Sci.* **2007**, *207*, 79.
 - Serpe, M. J.; Craig, S. L. *Langmuir* **2007**, *23*, 1626.
 - Harada, A.; Hashidzume, A.; Takashima, Y. *Adv. Polym. Sci.* **2006**, *201*, 1.
 - Huang, F.; Nagvekar, D. S.; Zhou, X.; Gibson, H. W. *Macromolecules* **2007**, *40*, 356.
 - Hunter, C. A.; Tomas, S. *J. Am. Chem. Soc.* **2006**, *128*, 8975.
 - Kitagishi, H.; Oohora, K.; Yamaguchi, H.; Sato, H.; Matsuo, T.; Harada, A.; Hayashi, T. *J. Am. Chem. Soc.* **2007**, *129*, 10326.
 - Soto Tellini, V. H.; Jover, A.; Garcia, J. C.; Galantini, L.; Meijide, F.; Tato, J. V. *J. Am. Chem. Soc.* **2006**, *128*, 5728.
 - de Greef, T. F. A.; Meijer, E. W. *Nature* **2008**, *453*, 171.
- Sijbesma, R. P.; Beijer, F. H.; Brunsveld, L.; Folmer, B. J. B.; Hirschberg, J. H. K. K.; Lange, R. F. M.; Lowe, J. K. L.; Meijer, E. W. *Science* **1997**, *278*, 1601.
- Selected publications: a) Berl, V.; Schmutz, M.; Krische, M. J.; Khoury, R. G.; Lehn, J. M. *Chem. Eur. J.* **2002**, *8*, 1227. b) Binder, W. H.; Bernstoff, C.; Kluger, L.; Petraru, L.; Kunz, M. J. *Adv. Mater.* **2005**, *17*, 2824. c) Castellano, R. K.; Clark, R.; Craig, S. L.; Nuckolls, C.; Rebek, J. Jr. *Proc. Natl. Acad. Sci. USA* **2000**, *97*, 12418.
- Ligthart, G. B. W. L.; Ohkawa, H.; Sijbesma, R. P.; Meijer, E. W. *J. Am. Chem. Soc.* **2005**, *127*, 810.
- Other examples of AB type polymerizations: a) Cantrill, S. J.; Youn, G. J.; Stoddart, J. F. *J. Org. Chem.* **2001**, *66*, 6857. b) Miyauchi, M.; Takashima, Y.; Yamaguchi, H.; Harada, A. *J. Am. Chem. Soc.* **2005**, *127*, 2984. c) Fernández, G.; Pérez, E. M.; Sánchez, L.; Martín, N. *Angew. Chem. Int. Ed.* **2007**, *46*, 1. d) Yamaguchi, N.; Nagvekar, D. S.; Gibson, H. W. *Angew. Chem. Int. Ed.* **1998**, *37*, 2361. e) Ikeda, M.; Nobori, T.; Schmutz, M.; Lehn, J.-M.

- Chem. Eur. J.* **2005**, *11*, 662. f) Lortie, F.; Boileau, S.; Bouteiller, L. *Chem. Eur. J.* **2003**, *9*, 3008. g) Sakamoto, A.; Ogata, D.; Shikata, T.; Hanabusa, K. *Macromolecules* **2005**, *38*, 8983. h) Sakamoto, A.; Ogata, D.; Shikata, T.; Urakawa, O.; Hanabusa, K. *Polymer* **2006**, *47*, 956.
- 6) Scherman, O. A.; Ligthart, G. B. W. L.; Sijbesma, R. P.; Meijer, E. W. *Angew. Chem. Int. Ed.* **2006**, *45*, 2072.
- 7) Corbin, P. S.; Zimmerman, S. C. *J. Am. Chem. Soc.* **1998**, *120*, 9710.
- 8) a) Park, T.; Zimmerman, S. C. *J. Am. Chem. Soc.* **2006**, *128*, 13986. b) Park, T.; Zimmerman, S. C.; Nakashima, S. *J. Am. Chem. Soc.* **2005**, *127*, 6520. c) Park, T.; Todd, E. M.; Nakashima, S.; Zimmerman, S. C. *J. Am. Chem. Soc.* **2005**, *127*, 18133. d) Park, T.; Zimmerman, S. C. *J. Am. Chem. Soc.* **2006**, *128*, 11582. e) Park, T.; Zimmerman, S. C. *J. Am. Chem. Soc.* **2006**, *128*, 14236.
- 9) ten Cate, A. T.; Kooijman, H.; Spek, A. L.; Sijbesma, R. P.; Meijer, E. W. *J. Am. Chem. Soc.* **2004**, *126*, 3801.
- 10) Ligthart, G. B. W. L.; Ohkawa, H.; Sijbesma, R. P.; Meijer, E. W. *J. Org. Chem.* **2006**, *71*, 375.
- 11) Ercolani, G.; Mandolini, L.; Mencarelli, P.; Roelens, S. *J. Am. Chem. Soc.* **1993**, *115*, 3901.
- 12) A solution of 1.05 eq of **2** and 1 eq of **3** in CDCl₃ (total concentration 20 mM) revealed dibutylamino UPy homo dimer **2·2** and dibutylamino-substituted UPy·NaPy hetero-dimer **2·3** to be in slow exchange on the ¹H-NMR timescale. The signals of the three NH protons of the hydrogen bonded dimer **2·2** resonate at 12.60, 11.22, and 9.58 ppm.
- 13) a) Brand, T.; Cabrita, E. J.; Berger, S. *Prog. Nucl. Magn. Reson. Spectrosc.* **2005**, *46*, 159. b) Cohen, Y. Avram, L.; Frish, L. *Angew. Chem., Int. Ed.* **2005**, *44*, 520. c) Johnson, C. S. *Prog. Nucl. Magn. Reson. Spectrosc.* **1999**, *34*, 203. d) Johnson, C. S. *J. Magn. Reson., Ser. A* **1993**, *102*, 214. e) Cabritta, E. J.; Berger, S.; Bräuer, P.; Kärger, J. *J. Magn. Res.* **2002**, *157*, 124.
- 14) The normalized diffusion constant was calculated using the measured specific viscosity of solutions of **5** and **6** and the measured value of the diffusion constant: $D_n = D_{meas} \eta_{mean}$.
- 15) Previously, it was shown that the specific viscosity of supramolecular polymers scales with the degree of polymerization according to an empirical power law: $\eta_{sp} = K \cdot DP^\alpha$. For UPy based polymers, α was determined to be 0.78 (see ref 2). Therefore, the calculated plots of the weight average degree of polymerization are a good representation of the development of the viscosity as a function of concentration.
- 16) Zhao, D.; Moore, J. S. *Org. Biomol. Chem.* **2003**, *1*, 3471.
- 17) Flory, P. J. *Principles of Polymer Chemistry*; Ithaca, NY: Cornell University Press 1953.
- 18) Odian, G. *Principles of Polymerization*; New York: McGraw-Hill 1991.
- 19) Schaeffgen, J. R.; Flory, P. J. *J. Am. Chem. Soc.* **1948**, *70*, 2709.
- 20) Todd, E. M.; Zimmerman, S. C. *J. Am. Chem. Soc.* **2007**, *129*, 14534.
- 21) Folmer, B. J. B.; Sijbesma, R. P.; Versteegen, R. M.; van der Rijt, J. A. J.; Meijer, E. W. *Adv. Mater.* **2000**, *12*, 874.
- 22) Jerschow, A.; Muller, N. *J. Magn. Reson.* **1997**, *125*, 372.
- 23) Longworth, L. G. *J. Phys. Chem.* **1960**, *64*, 1914.
- 24) In the calculations, only rings containing up to 100 monomeric units were included. Calculations including larger rings (up to 500) showed similar results.

4

Kinetics of complementary quadruple hydrogen bonded dimers

Abstract

The kinetics of association of ureido-pyrimidinone (U) dimers, either present in the 4[1H]-keto form or in the pyrimidin-4-ol form, with 2,7-diamido-1,8-naphthyridine (N) into a complementary hetero-dimer have been investigated. The formation of hetero-dimers with 2,7-diamido-1,8-naphthyridine from pyrimidin-4-ol dimers is much faster than from 4[1H]-pyrimidinone dimers. Using a combination of simple measurements and simulations, evidence for a bimolecular tautomerization step is presented. Finally, the acquired kinetic knowledge of the different pathways leading from ureido-pyrimidinone homodimers to ureido-pyrimidinone:diamido-naphthyridine (U·N) heterodimers allows the prediction and observation of kinetically determined ureido-pyrimidinone heterodimers which slowly convert back to the corresponding homo-dimers.

Part of this work has been published:

de Greef, T. F. A.; Ligthart, G. B. W. L.; Lutz, M.; Spek, A. L.; Meijer, E. W.; Sijbesma, R. P. *J. Am. Chem. Soc.* **2008**, *130*, 5479-5486.

4.1 Introduction

The role of kinetic control in self-assembly processes has recently attracted considerable interest. The formation of kinetically determined self-assemblies has been observed in systems of large polydisperse aggregates¹ as well as in discrete multi-component supramolecular assemblies.² Although the physical basis of self-assembly under thermodynamic control is well understood³, a theoretical description of the formation of supramolecular assemblies under kinetic control is less well developed. The lack of theory makes it more difficult to analyze and understand the role of subtle effects, such as solvent shells surrounding the periphery of large supramolecular aggregates in mixed solvent (good/poor) compositions and the effect of fast cooling on the formation of supramolecular assemblies. Despite the lack of theory⁴, the formation of kinetically controlled supramolecular products can lead to supramolecular systems displaying highly desirable features such as chiro-optical memory⁵ and dynamic chiral amplification.⁶ Furthermore, it is expected that an increase in the number of weak secondary interactions in a given supramolecular assembly will lead to a larger number of kinetically controlled products. Therefore, the characterization of both the ground state–ground state as well as the ground state–transition state energy differences of novel supramolecular assemblies can establish the generality of the transient formation of supramolecular complexes and provides an understanding of how the phenomenon of kinetic recognition is used in Nature to enhance biochemical specificity.⁷

The kinetics of supramolecular assemblies are closely connected to the macroscopic properties of the resulting supramolecular materials. Supramolecular polymers⁸⁻¹⁶ based on reversible interactions between arrays of hydrogen bonds localized at the end groups of polymeric spacers, have attracted interest as a new powerful tool towards functional materials. In supramolecular polymer-based materials, stress relaxation during network deformation mainly occurs by the kinetic creation and annihilation of the reversible defining interaction.^{16,17} As has been elegantly shown by Craig¹⁸, the dynamic relaxation rates of supramolecular polymer-based networks are often comparable to the dissociation rate constant of the defining non-covalent interaction. Based on the previously discussed mechanism of stress-relaxation in supramolecular polymer based networks, the creation of a kinetically stable non-covalent interaction instead of the expected thermodynamically formed interaction can lead to unexpected dynamical mechanical properties. For a rational design of supramolecular polymer-based materials, characterization of rate constants and determination of the complexation mechanism of novel developed supramolecular modules¹⁹ is an important task.

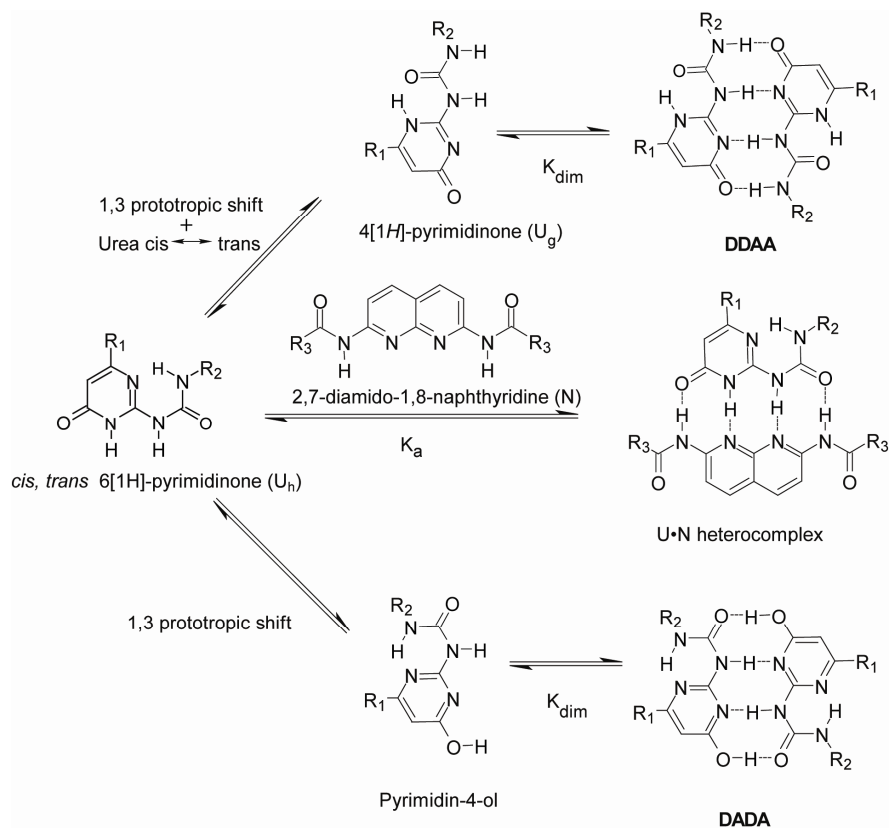
In the previous Chapter, the thermodynamics of complementary quadruple hydrogen bond interactions between 2,7-diamido-1,8-naphthyridine (N) and 2-ureido-pyrimidinone (U), which is also able to form homodimers (U₂), was investigated and their use as supramolecular polymers was discussed. In this Chapter, the association kinetics of 2,7-diamido-1,8-naphthyridine (N) with the dimerizing tautomers of 2-ureido-4[1H]-pyrimidinone and 2-ureido-pyrimidin-4-ol will be investigated. Although several pathways for the exchange of U₂ dimers with N may be postulated, the focus will be primarily on dissociative pathways in which U·N complexation starts with the dissociation of U₂ into the respective monomeric forms, since kinetic measurements on the exchange of U·U homo- and heterodimers, present in their 4[1H]-keto tautomeric form,²⁰ have shown that this is a dissociative process.

Scheme 4.1 displays the elementary steps by which either 2-ureido-4[1H]-pyrimidinone dimers or 2-ureido-pyrimidin-4-ol dimers can associate with 2,7-diamido-1,8-naphthyridine. The key reaction step during the formation of the U·N hetero-complex from the corresponding U₂ homo-dimers is in both cases a [1,3] prototropic shift resulting in the formation of the *cisoid*, *transoid* 2-ureido-6[1H]-pyrimidinone monomer. The [1,3] prototropic shift of nitrogen-containing acyclic and heterocyclic compounds has been a subject of intense research²¹ in the last few years. Considerable evidence, mainly from computational studies, has emerged, indicating that the lowest energy pathway for the [1,3] prototropic shift in such compounds proceeds via an intermolecular (dimeric, trimeric, oligomeric) proton transfer instead of a stepwise intramolecular proton transfer.²²⁻²⁵

In this Chapter the mechanism of U·N complexation (*intermolecular vs. intramolecular* tautomerization) is investigated using a combination of UV-Vis and ¹H-NMR spectroscopy.

4.2 Kinetics of keto dimers

¹H-NMR spectroscopy was used to monitor the formation of U·N hetero-complex **1·2** from ureido-pyrimidinone dimer **1·1** in toluene-d₈ (present for 90% as keto dimers and 10% as enol dimers in this solvent) upon the addition of equimolar amounts of diamido-naphthyridine **2** (Figure 4.1). To rule out a solvent-assisted tautomerization pathway it was chosen to perform the equilibration experiments in toluene-d₈, an apolar solvent, which lacks any acidic hydrogens or basic sites.



Scheme 4.1: Proposed intermediates in the exchange of the different tautomeric forms of ureido-pyrimidinone dimers with 2,7-diamido-1,8-naphththyridine. The substituents R_1 , R_2 and R_3 can be any functional group.

Upon rapid injection of 50 μL of a 200 mM solution of **1** in toluene- d_8 to 1 mL of a 10 mM solution of **2** the equilibration of both homodimeric forms of **1** to the U-N heterodimer **1**·**2** was observed with $^1\text{H-NMR}$. In order to gain more insight into the mechanism of hetero-complexation, $^1\text{H-NMR}$ equilibration measurements were conducted at three different equimolar concentrations of **1** and **2** (5, 10 and 20 mM) at 25 $^\circ\text{C}$. Furthermore, the formation of the U-N hetero-complex was monitored from an equimolar mixture of **1** and **2** at a concentration of **2** of 0.025 mM using UV-Vis spectroscopy. Formation of the heterodimers from the enol dimer (present in 10%) was too fast to be studied with the equilibration measurements at all concentrations. In fact, all enol dimer had completely disappeared after 18 s when data collection was started.²⁶ The kinetics of this exchange process were therefore studied with a different technique (*vide infra*). Conversion of the keto dimer on the other hand could be followed conveniently using the 1:1 equilibration experiments.

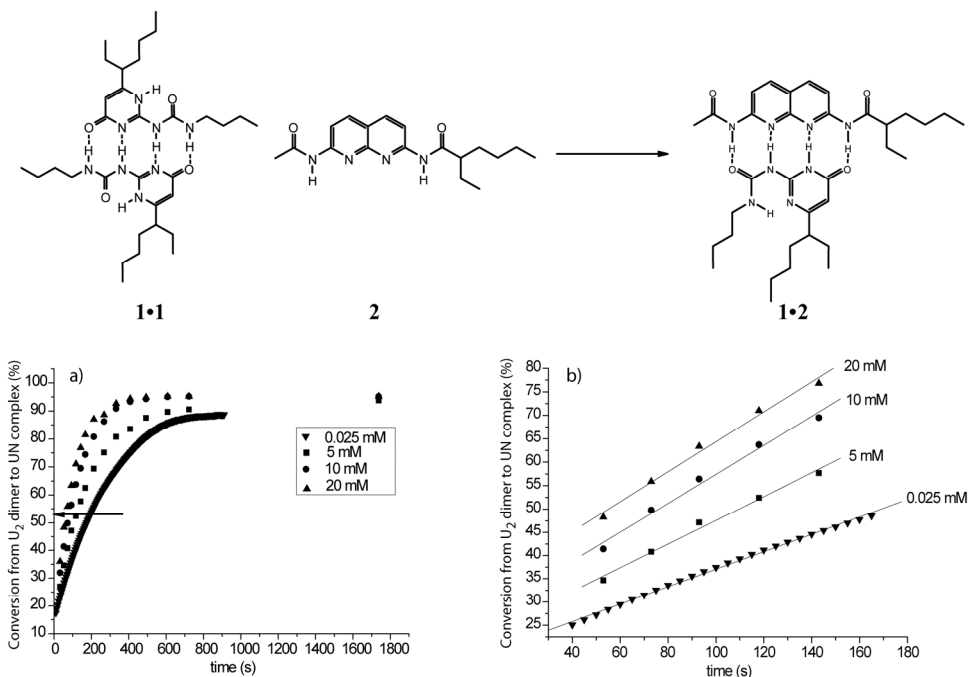


Figure 4.1: a) Conversion from DDAA dimers to U·N hetero-complex **1·2** as a function of time after injection of 1 eq of **1** for several total concentrations of **1** + **2** in toluene-*d*₈ at 25 °C as determined with ¹H-NMR (5, 10 and 20 mM) and UV-Vis spectroscopy (0.025 mM). The arrow indicates an increase in the total concentration of **1** and **2**. b) Expansion of the conversion-time plot displaying the increase of the initial conversion rate upon increasing the total concentration.

As is evident from the graph in Figure 4.1 the initial conversion rate of the hetero-complex increases with concentration implying that the overall order in reactants is higher than 1.

Guided by this important observation, possible dissociative kinetic mechanisms were simulated using the kinetic simulation program Gepasi.²⁷ The first minimalist kinetic representation that was considered to accurately include the essential features of the dynamic system as depicted in Scheme 4.1, corresponds to a mechanism in which the tautomerization from the 2-ureido-4[1H]-pyrimidinone monomeric form (U_g) to the 2-ureido-6[1H]-pyrimidinone monomeric form (U_h) is a unimolecular event (Figure 4.2a). As expected, simulation of the conversion of U·N complex as a function of total concentration in equimolar mixtures of **1** and **2** using this kinetic model reveals that the initial conversion rate becomes lower at higher concentrations, in sharp contrast with the experimental results. This concentration dependence results from the fact that in a completely unimolecular tautomerization mechanism as depicted in Figure 4.2a, the order in total ureido-pyrimidinone concentration (U_{tot}) is 0.5 when quasi-steady state

conditions are assumed, since nearly all U is present in dimers (see Appendix A for the derivation).

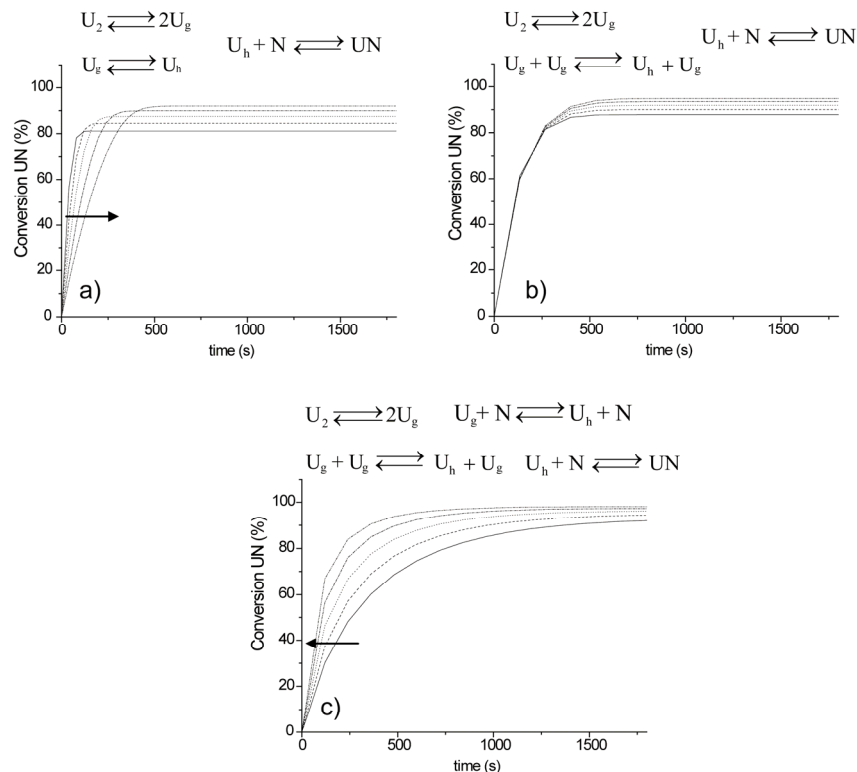


Figure 4.2: Simulated plots of U·N hetero-complex conversion vs. time at different concentrations (from 0.05 to 50 mM) for 1:1 mixtures of **1** and **2** for: a) Unimolecular tautomerization model. b) Bimolecular U assisted tautomerization. c) N and U assisted bimolecular tautomerization. The arrow indicates an increase in the total concentration of **1** and **2**.

A recent theoretical study²⁸ has shown that tautomerization via intermolecular double proton transfer has a lower energy barrier compared to a stepwise intramolecular proton transfer. The intermolecular process is facilitated by intermolecular hydrogen bonding. To study the influence of a bimolecular tautomerization event the conversion-time plots for different total concentrations of **1** and **2** in 1:1 mixtures were simulated according to the kinetic scheme depicted in Figure 4.2b. In this mechanism, tautomerization of the 2-ureido-4[1H]-pyrimidinone monomer (U_g) to the 2-ureido-6[1H]-pyrimidinone (U_h) monomeric form occurs via a bimolecular transition state.

Simulation of the conversion-time plots using this mechanism shows that the initial rate of conversion of U·N is independent of the total concentration in 1:1 mixtures of **1** and **2** as expected from a mechanism in which the order in U_{tot} is exactly one (again assuming quasi-steady state conditions, see Appendix A). Since the experimental results show that

the initial conversion rate becomes higher at higher concentration this kinetic model is inappropriate to describe the experimental data as well.

To account for the lower initial conversion rate of U·N at lower total concentrations there are two possibilities. Firstly, if formation of the U·N heterocomplex from the free 6[1H] monomer (U_h) and N is the rate determining step, the initial conversion rate will decrease upon decreasing the concentration. However, it has been shown by Hammes²⁹ that the association rate constant of double and triply hydrogen bonded complexes in organic solvents is a diffusion controlled process. Therefore the tautomerization from U_g to U_h is the rate determining step in the complexation between U homo dimers and N. In order to account for the lower initial rate at lower concentrations it is proposed that the tautomerization of the 2-ureido-4[1H]-pyrimidinone monomeric form (U_g) to the 2-ureido-6[1H]-pyrimidinone monomeric form (U_h) is also catalyzed by free N. Analysis of this kinetic scheme assuming steady state conditions (see Appendix A) reveals that the initial rate becomes larger as the total concentration in 1:1 mixtures is increased. Further simulation of this kinetic model without any explicit steady-state assumption using Gepasi (Figure 4.2c), shows that the initial conversion rate of U_2 to U·N increases as the total concentration of **1** and **2** is increased only if N catalyzed tautomerization is sufficiently fast compared to the U catalyzed tautomerization step.

Using this kinetic model the experimental conversion of U_2 to U·N hetero-complex as a function of time was fitted using an evolutionary programming algorithm present in Gepasi. Previously, it has been argued²⁰ that the association rate constant (k_2) of the 2-ureido-4[1H] pyrimidinone monomeric form (U_g) to the 2-ureido-4[1H] pyrimidinone dimeric form is a diffusion controlled process occurring with a rate constant close to $10^{10} \text{ M}^{-1} \text{ s}^{-1}$ in toluene- d_8 and a dissociation rate constant (k_1) of 1 s^{-1} .²⁰ Following the results obtained by Hammes²⁹ and by Söntjens²⁰ it is assumed that the association rate constant of formation of the U·N complex (k_6) from the 6[1H]-pyrimidinone monomeric form (U_h) with free N is also a diffusion controlled parameter ($k_6 = 10^{10} \text{ M}^{-1} \text{ s}^{-1}$ for toluene³⁰). The values of the rate constants k_1 , k_2 and k_6 were used as fixed parameters while the estimated values of the dimerization constant (defined as: $K_{\text{dim}} = [U_2]/[U_g]^2$) of **1** in toluene (between $1 \times 10^8 \text{ M}^{-1}$ and $7 \times 10^8 \text{ M}^{-1}$) and the association constant (defined as: $K_a = [UN]/([N] \times [U_h])$) of **1** with **2** (between 1×10^7 and $5 \times 10^8 \text{ M}^{-1}$) were used as constraints in the non-linear curve fitting of the kinetic data (Figure 4.3).

Because the rate determining tautomerization step occurs via two different routes, a large number of combinations of k_3 , k_4 , k_7 and k_8 are able to describe the experimental data. This results in a considerable negative covariance³¹ between the different

parameters and consequently results in large standard deviations. However, to test whether the mixed tautomerization model is correct we fitted the experimental UV-Vis data to a reduced model in which k_3 and k_4 were set to a fixed value of $0 \text{ M}^{-1} \text{ s}^{-1}$ (no U assisted tautomerization).

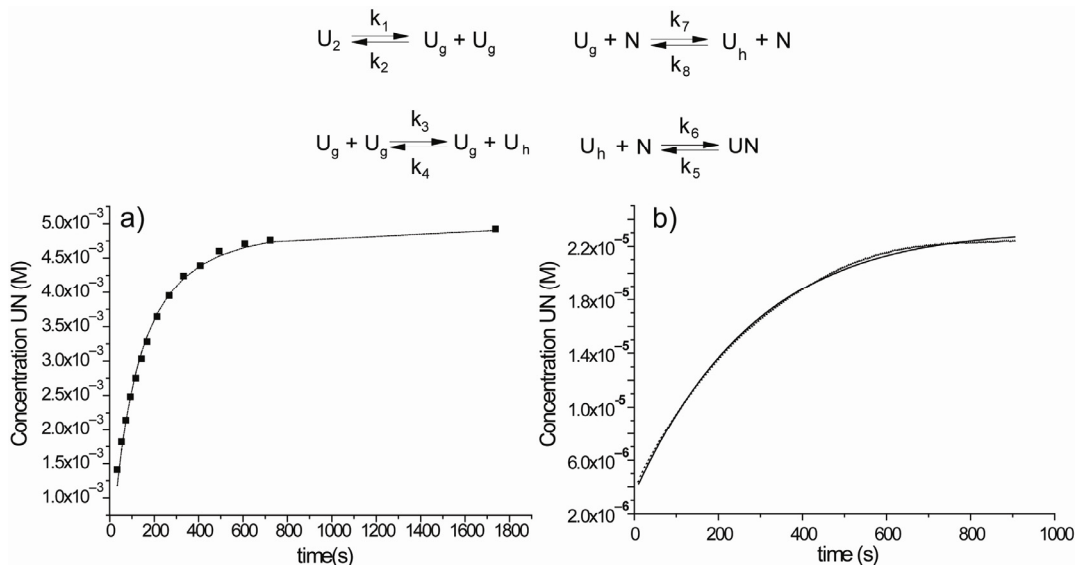


Figure 4.3: a) Concentration of $U \cdot N$ heterocomplex upon injection of 1 eq of **1** in toluene- d_8 to 1 mL of a 5 mM solution of **2** as calculated from the $^1\text{H-NMR}$ integrals. The dotted line represents the best fitted curve ($K_{dim} = 1 \times 10^8 \text{ M}^{-1}$, $K_a = 9 \times 10^7 \text{ M}^{-1}$) using the kinetic model as depicted in Figure 4.2c. b) Concentration of $U \cdot N$ heterocomplex upon titration of 1 eq of **1** in toluene to 2 mL of a 0.025 mM solution of **2** calculated from the absorption at 357 nm as a function of time. The dotted line represents the best fitted curve ($K_{dim} = 1 \times 10^8 \text{ M}^{-1}$, $K_a = 9 \times 10^7 \text{ M}^{-1}$) using the kinetic model as depicted in Figure 4.2c.

An extra sum of squares test³² revealed that the full model describes the data significantly better ($P < 0.0001$ for a significance level of 0.05) compared to the reduced model³³ indicating that both U and N contribute significantly to the tautomerization catalysis.

4.3 Kinetics of enol dimers

To compare the diamido-naphthyridine association kinetics of 2-ureido-4[1H]-pyrimidinone dimers with 2-ureido-pyrimidin-4-ol dimers kinetic experiments were conducted on dibutylamino substituted UPy **3**.

In sharp contrast to the association kinetics of 4[1H]-pyrimidinone dimer **1**, the kinetics of formation of the $U \cdot N$ heterocomplex **2·3** could not be followed by $^1\text{H-NMR}$ equilibration experiments due to the extremely rapid formation of the heterocomplex after injection of a solution of **3** in toluene- d_8 to a solution of **2** in the same solvent. As the $U \cdot N$ complex **2·3** and the ureido-pyrimidinone dimer **3·3** are in slow exchange on

the $^1\text{H-NMR}$ timescale in this solvent, 2D-EXSY^{34,35} experiments were conducted on solutions containing **3** and **2** in a 2:1 ratio (resulting in approximately equimolar amounts of **3·3** and **2·3**) at several concentrations of **3**.³⁶ The transfer functions³⁷, calculated from the volume integrals of the alkylidene protons of dimer **3·3** and U·N hetero-dimer **2·3** were fitted as a function of mixing time (τ_{mix}) according to the equation $\phi = k_{\text{ex}}\tau_{\text{mix}}$ for all three concentrations, resulting in the pseudo-first order rate constant k_{ex} for the exchange process (Figure 4.4). As can be deduced from Figure 4.4, the pseudo-first order rate constant increases by 45% as the total concentration of **2** and **3** in 1:2 mixtures is increased by a factor of 4. This suggests that the kinetic pathway for association of **3·3** with **2** is similar to the association of **1·1** with **2** where tautomerization is catalyzed by monomeric components.

Interestingly, addition³⁸ of 16 mole % (with respect to **3**) of benzoic acid to a solution containing 10 mM of **2** and 20 mM of **3** in toluene- d_8 resulted in an increase in the pseudo-first order rate constant from 10 s^{-1} to a value of almost 40 s^{-1} . The catalytic influence of benzoic acid on the exchange between the **3·3** and the U·N complex **2·3** is most probably the result of a decrease in the activation barrier of the [1,3] prototropic shift by formation of an intermolecular complex between the carboxylic acid and the 2-ureido-pyrimidin-4-ol monomer. Indeed, quantum mechanical calculations on the activation barrier for tautomerization between 2-pyridone and 2-hydroxy-pyridine have indicated that the activation energy is substantially decreased by the complexation with formic acid and double proton transfer occurs by a concerted mechanism.³⁹

The fact that the kinetics of diamido-naphthyridine association are much faster for 2-ureido-pyrimidin-4-ol dimers (**DADA** array) than for 2-ureido-4[1H]-pyrimidinone dimers (**DDAA** array) strongly suggests that a dissociative mechanism as drawn in Scheme 4.1 is operative in the formation of U·N hetero-complexes. The differences in complexation kinetics are the result of one or more of the following features. Firstly, the dissociation rate constant of **3·3** is most probably higher than the dissociation rate constant of **1·1** (1 s^{-1}). Secondly, the activation barrier of the [1,3] prototropic shift in the 2-ureido-4[1H]-pyrimidinone tautomer probably is substantially higher than the activation barrier of the [1,3] prototropic shift in the 2-ureido-pyrimidin-4-ol tautomer. Finally, and most importantly, association of 2-ureido-4[1H] pyrimidinone dimers with N might be slow because it requires a conformational change of the ureido group that involves the breakage of an intramolecular hydrogen bond (Scheme 4.1).

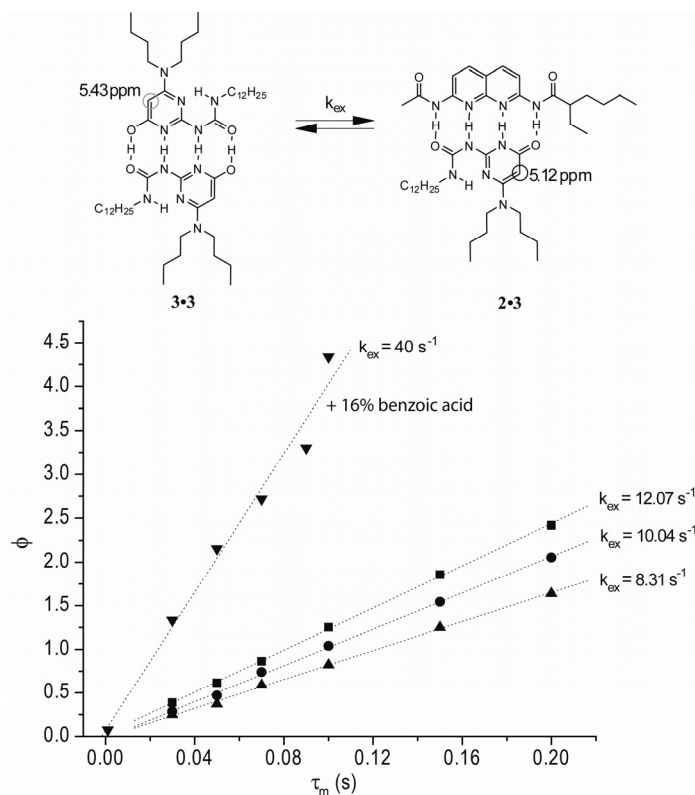


Figure 4.4: Plot of the transfer function ϕ vs. mixing time for 1:2 mixtures of 2 and 3 at three different concentrations (\blacktriangle = 5 mM 2 and 10 mM 3, \bullet = 10 mM 2 and 20 mM 3, \blacksquare = 20 mM 2 and 40 mM 3, \blacktriangledown = 10 mM 2, 20 mM 3 and 16 mole % benzoic acid). The dotted line represents the best fitted curve according to the equation $\phi = k_{ex} \tau_{mix}$ ($R^2 = 0.999$ in the first three cases) in which ϕ represents the transfer function³⁷, k_{ex} the pseudo-first order rate constant for the exchange process and τ_{mix} represents the mixing time during the EXSY experiment.

4.4 Kinetic product formation in mixtures of hydrogen bonded dimers

Using the insights gathered into the association kinetics of 1·1 and 3·3 with 2 in combination with the mechanistic scheme depicted in Scheme 4.1 it can be predicted that the thermodynamically disfavored heterodimer 1·3 can be obtained as kinetic product when 1 is present as a heterodimer with 2 (Figure 4.5). Because both the dissociation rate of U·N complex 1·2 as well as the dissociation rate of 3·3 are high, rapid exchange from 1·2 to 3·2 upon titration of 2 eq of 3 will take place. This results in the release of monomeric 1 in its *cis,trans* 6[1H]-pyrimidinone tautomeric form. When 3 is added in excess, the *cis,trans* 6[1H]-pyrimidinone tautomeric form of 1 can rapidly form the heteromeric enol dimer 1·3 via a fast [1,3] shift, while formation of the 4[1H] pyrimidinone homo-dimer 1·1 is slow because it requires both a [1,3] prototropic shift and a slow breakage of an intramolecular hydrogen bond. If the thermodynamic stability of homodimer 1·1 is higher than the heteromeric ureido-pyrimidinone complex

1·3, initial kinetic self-sorting^{2f} of **1** in **1·3** will be followed by slow equilibration to the homo-dimer **1·1**.

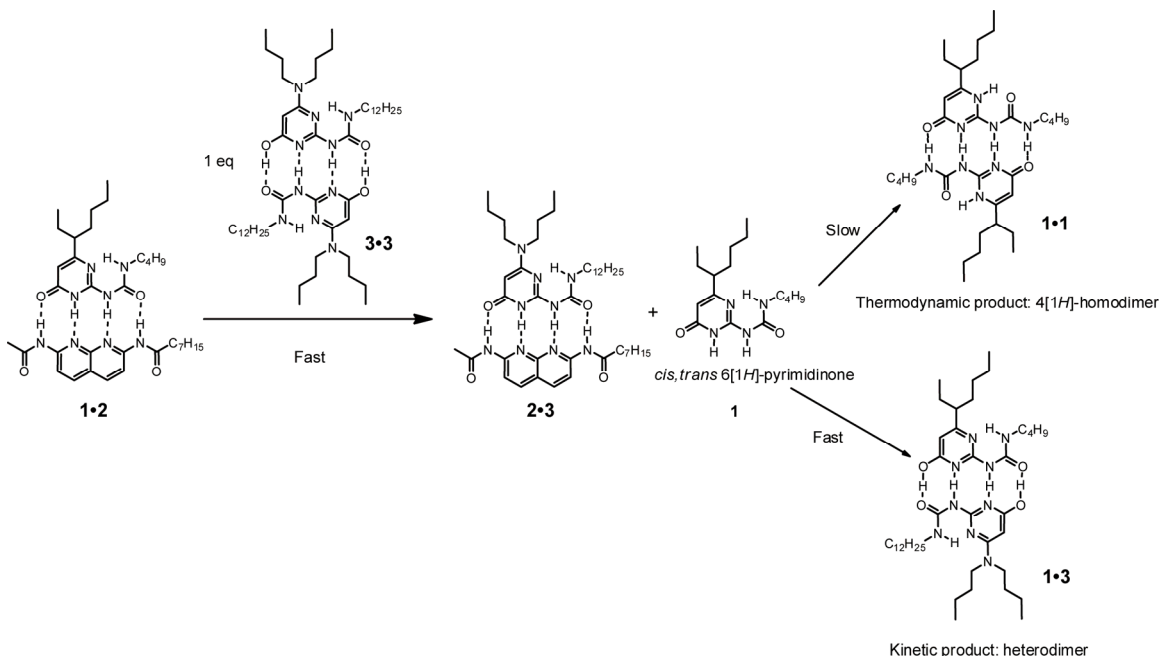


Figure 4.5: Kinetic and thermodynamic product formation in a system containing ureido-pyrimidinones **1**, **3** and diamido-naphthyridine **2**.

Injection of 50 μL of a 200 mM solution of **3** in toluene- d_8 to a solution containing 10 mM U·N complex **1·2** in the same solvent indeed result in rapid formation of the enol heterodimer **1·3**. After 18 s, the kinetic product (**1·3**) was formed with a yield of 65%. This was followed by a slow decrease of this complex accompanied by slow formation of ureido-pyrimidinone homodimers **1·1** and **3·3** to yield an equilibrium product mixture containing 41% homodimer **1·1** and 35% heterodimer **1·3** (Figure 4.6). Although the yield of the kinetic product is high, the selectivity for the formation of the thermodynamic product is limited, because there is only a small difference in free energy between keto and enol dimers of **1** in apolar solvents.^{40,41} The $^1\text{H-NMR}$ spectrum of a 1:1 mixture of **1** and **3** in toluene- d_8 at equilibrium indeed reveals that approximately 33% of the total amount of **1** is incorporated in the enol heterodimer **1·3**. However, the experiment clearly shows the validity of the dissociative mechanism proposed in Scheme 4.1.

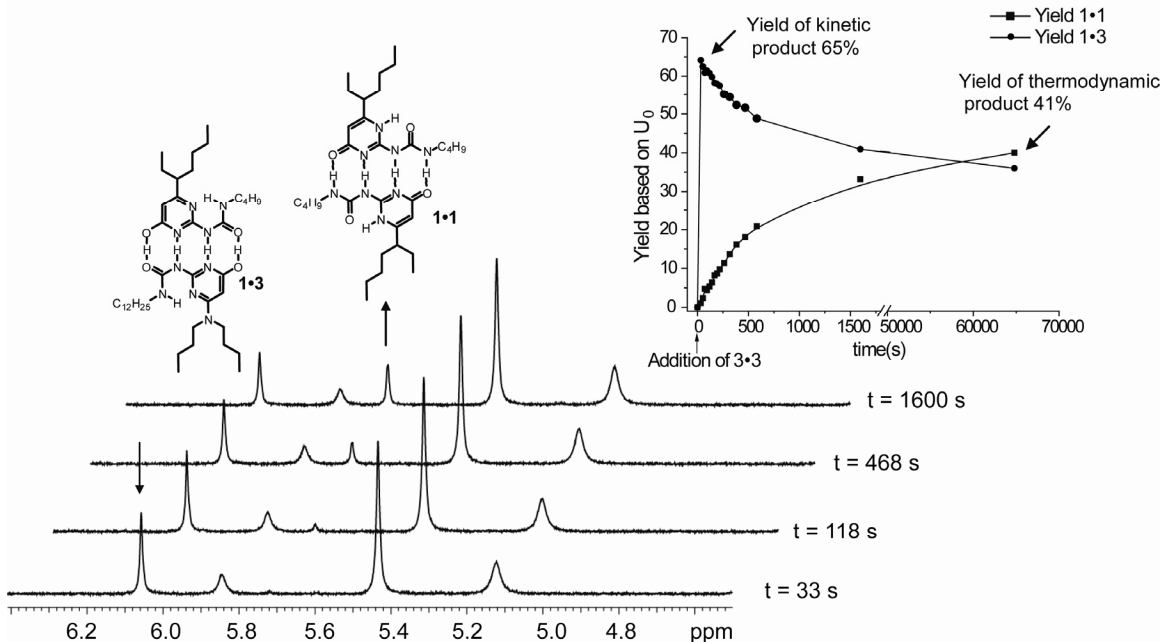


Figure 4.6: ¹H-NMR spectra (500 MHz, toluene-d₈) obtained at regular time intervals after injection of 2 eq of **3** to a solution containing 10 mM **1•2**. Fraction of the analytical concentration of **1** (U_0) present in the enol heterodimer **1•3** and homodimer **1•1** as a function of time (inset). The solid line is served to guide the eye.

4.5 Summary and conclusions

In summary, the kinetics of self-complementary quadruple hydrogen bonded 2-ureido-4[1H]-pyrimidinone and 2-ureido-pyrimidin-4-ol dimers with 2,7-diamido-1,8-naphthyridine follow a dissociative pathway in which the tautomerization step is catalyzed in a bimolecular process. Furthermore, kinetic product formation in a three-component supramolecular system is reported. The analysis presented here illustrates the prominent role of kinetic product formation in supramolecular assemblies and may aid in the understanding of the relation between complexation dynamics and the mechanical properties of supramolecular polymers based upon the interaction between ureido-pyrimidinones and 2,7-diamido-1,8-naphthyridine.

4.6 Experimental section

General Methods

See General Methods Chapter 2. 2,7-Diamido-1,8-naphthyridine **2** was synthesized according to the method of Ligthart et al.⁴² 2-Ureido-pyrimidinone **1** was synthesized according to Keizer.⁴³

Two dimensional NMR (EXSY)

All two dimensional NMR spectra were recorded on a 500 MHz NMR (Varian Unity Inova) by means of a 5 mm ¹H/X Inverse Detection probe equipped with gradient capabilities at 25 °C. For all EXSY measurements the 90° ¹H pulse width was calibrated. 2D EXSY experiments were performed using a relaxation delay time of 3 s (approximately 4-5 times T₁) for each mixing time. Unwanted XY magnetization was removed by a homospoil-90-homospoil preceding d₁. 2D-data were collected in the phase-sensitive mode using the States-Haberkmorn method. A total of 400 FIDs of 2 K complex data points were collected in t₂ with 16 scans per increment and zero-filling was applied in both dimensions before Fourier transformation. These data were then processed with shifted sine-bell window functions in both dimensions. Volume integrals were determined in VNMR using the *ll2d* routine available in Varian VNMR 6.1C.

Kinetic experiments

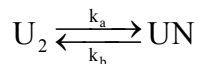
Keto dimers

Standard solutions of 5 mM, 10 mM and 20 mM **2** in toluene-d₈ were prepared for the kinetic experiments. The components were mixed by injection of 50 µL of 1 equivalent ureido-pyrimidinone **1** solution in toluene-d₈ (100 mM, 200mM and 400 mM respectively) which was equilibrated at the temperature of the measurement. Data acquisition was automatically performed using an acquisition delay. The exchange was monitored by ¹H NMR (500 MHz) with the probe maintained at constant temperature (25 °C). The fraction of hetero-complex **1·2** was determined from ¹H-NMR integration of the signals. To check the reproducibility of this method we performed each experiment in *triplo* and fitted the appearance of U·N with a simple first order model: $UN(t) = f_{\max} (1 - e^{-k_{\text{obs}}t})$. Analysis of the error revealed it to be small (5%). For the kinetic experiment conducted at low concentration 2 mL of a 0.025 mM solution of **2** in toluene was prepared in a standard 1 cm quartz cuvette. To this solution 50 µL of a 1.01 10⁻³ M solution of **1** in toluene-d₈ was added and the absorbance at 357 nm was followed as a function of time. The fraction of heterocomplex was calculated using the extinction coefficient of the U·N complex at 357 nm (31594 L mol⁻¹ cm⁻¹). This extinction coefficient was obtained from a separate titration experiment conducted in toluene by fitting the absorbance at 357 nm as a function of added **1** to a 1:1 binding model in which one of the components can self-associate. This titration also gave an estimate of the K_a in this solvent (between 10⁷ and 5 × 10⁸ M⁻¹).⁴⁴

Enol dimers

Standard solutions in toluene- d_8 were prepared for the kinetic measurements. Three different solutions were prepared containing 5 mM, 10 mM and 20 mM **2** and 10 mM, 20 mM and 40 mM **3** respectively (1:2 ratio of 2,7-diamido-naphthyridine and ureido-pyrimidinone).

In an EXSY experiment the observed rate constants are defined as follows:



In a simple two-site exchange system with sites A and B of equal longitudinal relaxation times⁴⁵ ($T_{1,A} = T_{1,B}$), the peak volumes determined in the EXSY experiment (I_{AA} and I_{BB} for diagonal peaks; I_{AB} and I_{BA} for cross-peaks) are converted into the exchange rate constant (defined³⁴ as $k_{ex} = k_a + k_b$) via the relation in equation (1):

$$k_{ex} = \tau_m^{-1} \ln \left(\frac{r+1}{r-1} \right) \quad (1)$$

as a function of mixing time, where r is the ratio between the diagonal and the cross-peaks:

$$r = 4X_A X_B \left(\frac{I_{AA} + I_{BB}}{I_{AB} + I_{BA}} \right) - (X_A - X_B)^2 \quad (2)$$

In which X_A and X_B represent the mole fractions of populations A and B, respectively. In a 1:2 mixture of ureido-pyrimidinone and 2,7-diamido-1,8-naphthyridine, $X_a = X_b = 0.5$, hence:

$$r = \left(\frac{I_{AA} + I_{BB}}{I_{AB} + I_{BA}} \right) \quad (3)$$

The logarithmic term in eq (1) is often referred to as the transfer function ϕ . The exchange rate constant can therefore easily be determined as the slope in a plot of ϕ as a function of τ_m .

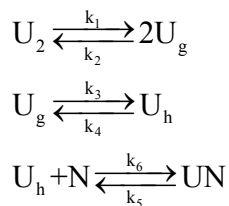
Acid catalyzed kinetics between 3·3 and 3·2

A solution containing 10 mM **2**, 20 mM **3** and 16 mole % of benzoic acid (0.12 mg) in toluene- d_8 was prepared. The ¹H-NMR spectrum of this solution did not show any evidence of protonation of either the ureido-pyrimidinone dimer or the U·N hetero-complex.

4.7 Appendices**Appendix A**

Analytical expressions for the kinetics of the three different dissociative mechanisms were derived.

The first mechanism investigated is a mechanism in which the tautomerization from the 2-ureido-4[1H]-pyrimidinone monomeric form (U_g) to the 2-ureido-6[1H]-pyrimidinone monomeric form (U_h) is a unimolecular event. The following expressions were derived using Maple 11, Maplesoft inc. 2007.



$$\frac{dUN}{dt} = k_6[N][U_h] - k_5[UN] \quad (4)$$

$$\frac{dU_2}{dt} = -k_1[U_2] + k_2[U_g][U_g] \quad (5)$$

$$\frac{d[U_g]}{dt} = 2k_1[U_2] - 2k_2[U_g]^2 + k_4[U_h] - k_3[U_g] \quad (6)$$

$$\frac{d[U_h]}{dt} = k_3[U_g] - k_4[U_h] + k_5[UN] - k_6[N][U_h] \quad (7)$$

Furthermore, we can write for the equilibrium concentrations of U_g and U_2 :

$$K_{\text{dim}} = \frac{[U_2]_e}{[U_g]_e^2} = \frac{k_2}{k_1} \quad (8)$$

At $t = 0$ the concentration of U_2 can be expressed in terms of the total analytical ureido-pyrimidinone concentration (U_{tot}) and the extent of the reaction (x):

$$[U_2] = \frac{1}{2}U_{\text{tot}} - \frac{1}{2}xU_{\text{tot}} \quad (9)$$

While the amount of 4[1H] pyrimidinone monomer (U_g) at $t = 0$ is approximately equal to:

$$[U_g] = \frac{1}{2} \frac{\sqrt{-2K_{\text{dim}}U_{\text{tot}}(-1+x)}}{K_{\text{dim}}} \quad (10)$$

If k_4 and $k_3 < k_2$ and k_6 (the rate constants k_6 and k_2 are assumed to be diffusion controlled), $k_2 > k_1$, $k_6 > k_5$ the concentrations of U_h and U_g will always be low and hence the quasi-steady state approximation (QSSA) is readily applicable. Setting $dU_h/dt = 0$ we can write:

$$k_3[U_g] - k_4[U_h] + k_5[UN] - k_6[N][U_h] = 0 \quad (11)$$

Solving for U_h in eq (11) gives:

$$[U_h] = \frac{k_3[U_g] + k_5[UN]}{k_4 + k_6[N]} \quad (12)$$

If it is assumed that the backward tautomerization reaction is slow, $k_6 \cdot N > k_4$ we can write:

$$[U_h] = \frac{k_3[U_g] + k_5[UN]}{k_6[N]} \quad (13)$$

Substitution of eq (10) in eq (13) gives:

$$[U_h] = \frac{\frac{1}{2} \frac{k_3 \sqrt{-2K_{\text{dim}}U_{\text{tot}}(-1+x)}}{K_{\text{dim}}} + k_5[UN]}{k_6[N]} \quad (14)$$

Further substitution of eq (14) in eq (4) gives after rearrangement:

$$\frac{d[UN]}{dt} = \frac{1}{2} \frac{k_3 \sqrt{-2K_{\text{dim}}U_{\text{tot}}(-1+x)}}{K_{\text{dim}}} \quad (15)$$

For small values of x , we can write:

$$\frac{d[\text{UN}]}{dt} = \frac{1}{2} \frac{k_3 \sqrt{2K_{\text{dim}} U_{\text{tot}}}}{K_{\text{dim}}} \quad (16)$$

The initial conversion rate is defined as:

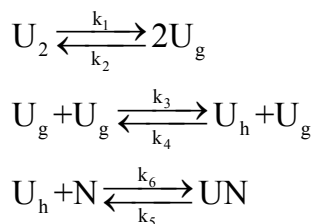
$$V_{\text{ini}} = \frac{d[\text{UN}]}{U_{\text{tot}} dt} \quad (17)$$

Hence, the expression for the initial conversion rate of [UN] becomes:

$$V_i = \frac{1}{2} \frac{k_3 \sqrt{2}}{\sqrt{K_{\text{dim}} * U_{\text{tot}}}} \quad (18)$$

From eq (18) it follows that the initial conversion rate of UN scales with $(U_{\text{tot}})^{-1/2}$ and hence becomes larger at lower total concentrations of ureido-pyrimidinone in this mechanism.

The second mechanism of U·N formation is a mechanism in which the tautomerization from the 2-ureido-4[1H]-pyrimidinone monomeric form (U_g) to the 2-ureido-6[1H]-pyrimidinone monomeric form (U_h) is a bimolecular event. The following expressions were derived using Maple 11, Maplesoft inc. 2007.



$$\frac{d[\text{UN}]}{dt} = k_6[\text{N}][U_h] - k_5[\text{UN}] \quad (19)$$

$$\frac{d[U_2]}{dt} = -k_1[U_2] + k_2[U_g][U_g] \quad (20)$$

$$\frac{d[U_g]}{dt} = 2k_1[U_2] - 2k_2[U_g]^2 + k_4[U_g][U_h] - k_3[U_g][U_g] \quad (21)$$

$$\frac{d[U_h]}{dt} = k_3[U_g][U_g] - k_4[U_g][U_h] + k_5[\text{UN}] - k_6[\text{N}][U_h] \quad (22)$$

Furthermore, we can write for the equilibrium concentrations of U_g and U_2 :

$$K_{\text{dim}} = \frac{[U_2]_e}{[U_g]_e^2} = \frac{k_2}{k_1} \quad (23)$$

At $t = 0$ we can express the concentration of U_2 in terms of the total analytical ureido-pyrimidinone concentration (U_{tot}) and the extent of the reaction (x):

$$[U_2] = \frac{1}{2} U_{\text{tot}} - \frac{1}{2} x U_{\text{tot}} \quad (24)$$

While the amount of 4[1H] pyrimidinone monomer (U_g) at $t = 0$ is approximately equal to:

$$U_g = \frac{1}{2} \frac{\sqrt{-2K_{\text{dim}} U_{\text{tot}} (-1+x)}}{K_{\text{dim}}} \quad (25)$$

If k_4 and $k_3 < k_2$ and k_6 (the rate constants k_6 and k_2 are assumed to be diffusion controlled), $k_2 > k_1$, $k_6 > k_5$ the concentrations of U_h and U_g will always be low and hence the quasi-steady state approximation (QSSA) is readily applicable. Setting $dU_h/dt = 0$ we can write:

$$k_3[U_g][U_g] - k_4[U_g][U_h] + k_5[UN] - k_6[N][U_h] = 0 \quad (26)$$

Solving for U_h in eq (26) gives:

$$[U_h] = \frac{k_3[U_g][U_g] + k_5[UN]}{k_4[U_g] + k_6[N]} \quad (27)$$

Because, $k_6 * N \gg k_4 * U_g$ eq (27) can be written as:

$$[U_h] = \frac{k_3[U_g][U_g] + k_5[UN]}{k_6[N]} \quad (28)$$

Substitution of eq (28) in eq (19) gives after rearrangement:

$$\frac{d[UN]}{dt} = k_3[U_g]^2 \quad (29)$$

Substitution of eq (25) in eq (29) yields:

$$\frac{d[UN]}{dt} = -\frac{1}{2} \frac{k_3 U_{tot} (-1 + x)}{K_{dim}} \quad (30)$$

For small values of x , we can write:

$$\frac{d[UN]}{dt} = \frac{1}{2} \frac{k_3 U_{tot}}{K_{dim}} \quad (31)$$

The initial conversion rate is defined as:

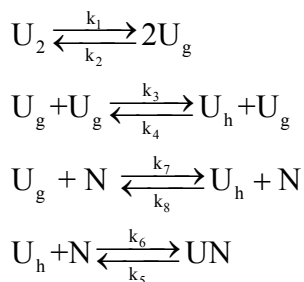
$$V_{ini} = \frac{d[UN]}{U_{tot} dt} \quad (32)$$

Hence, the expression for the initial conversion rate of UN becomes:

$$V_{ini} = \frac{1}{2} \frac{k_3}{K_{dim}} \quad (33)$$

Which is independent of the total ureido-pyrimidinone concentration.

The third mechanism that will be evaluated is a mechanism in which the tautomerization from the 2-ureido-4[1H]-pyrimidinone monomeric form (U_g) to the 2-ureido-6[1H]-pyrimidinone monomeric form (U_h) is a bimolecular event in U and is also catalyzed by N . The following expressions were derived using Maple 11, Maplesoft inc. 2007.



$$\frac{d[UN]}{dt} = k_6[N][U_h] - k_5[UN] \quad (34)$$

$$\frac{d[U_2]}{dt} = -k_1[U_2] + k_2[U_g][U_g] \quad (35)$$

$$\frac{d[U_g]}{dt} = 2k_1[U_2] - 2k_2[U_g]^2 + k_4[U_g][U_h] - k_3[U_g][U_g] + k_8[N][U_k] - k_7[U_g][N] \quad (36)$$

$$\frac{d[U_h]}{dt} = k_3[U_g][U_g] - k_4[U_g][U_h] + k_5[UN] - k_6[U_h][N] - k_8[U_h][N] + k_7[U_g][N] \quad (37)$$

As has been shown before, at $t = 0$ we can write for small values of x :

$$[U_g] = \frac{1}{2} \frac{\sqrt{2K_{\text{dim}} U_{\text{tot}}}}{K_{\text{dim}}} \quad (38)$$

Furthermore, at $t = 0$ the concentration of free N will be approximately equal to the total analytical ureido-pyrimidinone concentration:

$$N = U_{\text{tot}} \quad (39)$$

Again we assume the concentrations of U_h and U_g always to be low and hence the quasi-steady state approximation (QSSA) is applicable. Setting $dU_h/dt = 0$ we can write:

$$k_3[U_g][U_g] - k_4[U_g][U_h] + k_5[UN] - k_6[U_h][N] - k_8[U_h][N] + k_7[U_g][N] = 0 \quad (40)$$

Solving for U_h gives:

$$[U_h] = \frac{k_3[U_g][U_g] + k_5[UN] + k_7[U_g][N]}{k_6[N] + k_8[N] + k_4[U_g]} \quad (41)$$

In the beginning of the reaction the concentration of U_g is much lower than the concentration of free N. Hence, $(k_6 \cdot N + k_8 \cdot N) \gg k_4 \cdot U_g$ and we can write:

$$[U_h] = \frac{k_3[U_g][U_g] + k_5[UN] + k_7[U_g][N]}{(k_6 + k_8)[N]} \quad (42)$$

Furthermore, $k_6 \gg k_8$ and hence we can write:

$$[U_h] = \frac{k_3[U_g][U_g] + k_5[UN] + k_7[U_g][N]}{k_6[N]} \quad (43)$$

This last assumption is based on the fact that k_6 is diffusion controlled (in the order of $1 \times 10^{10} \text{ M}^{-1} \text{ s}^{-1}$) while the backward bimolecular tautomerization reaction has a substantial activation barrier.²⁸

Substitution of eq (43) into eq (34) gives after rearrangement:

$$\frac{d[UN]}{dt} = k_3[U_g]^2 + k_7[U_g][N] \quad (44)$$

Substitution of eq (38) and eq (39) into eq (44) gives:

$$\frac{dUN}{dt} = \frac{1}{2} \frac{k_7 \cdot \sqrt{2} \cdot \sqrt{K_{\text{dim}} \cdot U_{\text{tot}}} \cdot U_{\text{tot}}}{K_{\text{dim}}} + \frac{1}{2} \frac{k_3 \cdot U_{\text{tot}}}{K_{\text{dim}}} \quad (45)$$

We again define the initial conversion rate as:

$$V_{\text{ini}} = \frac{d[UN]}{dt} \cdot \frac{1}{U_{\text{tot}}} \quad (46)$$

Hence, the expression for the initial conversion rate of UN becomes:

$$V_{\text{ini}} = \frac{1}{2} \frac{k_7 \sqrt{2} \sqrt{K_{\text{dim}} U_{\text{tot}}}}{K_{\text{dim}}} + \frac{1}{2} \frac{k_3}{K_{\text{dim}}} \quad (47)$$

Based on the value of k_7 and k_3 there are two possibilities on how the initial rate scales with the total concentration. If k_7 is approximately equal or bigger than k_3 the initial rate will be higher as the total ureido-pyrimidinone concentration is increased. However, if $k_3 \gg k_7$ the initial conversion rate will be independent of the total ureido-pyrimidinone concentration. Using Gepasi, the influence of the magnitude of k_7 and k_3 on the initial conversion rate while keeping k_2 , k_1 , k_4 , k_5 and k_6 constant was studied. The value of k_1 was set to be 1 s^{-1} as determined previously and both k_2 and k_6 were set to a value of $10^{10} \text{ M}^{-1} \text{ s}^{-1}$ (these two rate constants are diffusion controlled). Furthermore the values of k_3 and k_4 were set to $10^8 \text{ M}^{-1} \text{ s}^{-1}$ and $10^7 \text{ M}^{-1} \text{ s}^{-1}$ respectively and k_5 to a value of 200 s^{-1} (in agreement with the fact that U·N and free N are in fast exchange on the NMR timescale). The following simulations were performed using the program Gepasi. In the first simulation the values of k_7 and k_8 were chosen to be low ($10^{-4} \text{ M}^{-1} \text{ s}^{-1}$ and $10^{-5} \text{ M}^{-1} \text{ s}^{-1}$ respectively) compared to the values of k_3 and k_4 . This corresponds to a mechanism in which ureido-pyrimidinone tautomerization mainly occurs via bimolecular collisions between two ureido-pyrimidinone monomers. As expected the initial conversion rate in this mechanism is independent (Figure A1a) of the starting concentration ureido-pyrimidinone and N in 1:1 mixtures. During the simulation it was made sure that the values of K_{dim} and K_a corresponded to the measured values in a diluted toluene solution ($K_{\text{dim}} \approx 10^8 \text{ M}^{-1}$ and K_a between $10^7 - 5 \times 10^8 \text{ M}^{-1}$). In the second simulation the values of k_7 and k_8 were chosen to be high ($10^5 \text{ M}^{-1} \text{ s}^{-1}$ and $10^4 \text{ M}^{-1} \text{ s}^{-1}$ respectively) compared to the values of k_4 and k_3 . This corresponds to a mixed mechanism in which ureido-pyrimidinone tautomerization occurs via bimolecular collisions between two ureido-pyrimidinone monomers and via a bimolecular collision between an ureido-pyrimidinone and a diamido-naphthyridine monomer. As expected the initial conversion rate in this mechanism is dependent (Figure A1b) on the starting concentration of U and N in the 1:1 equilibration experiments.

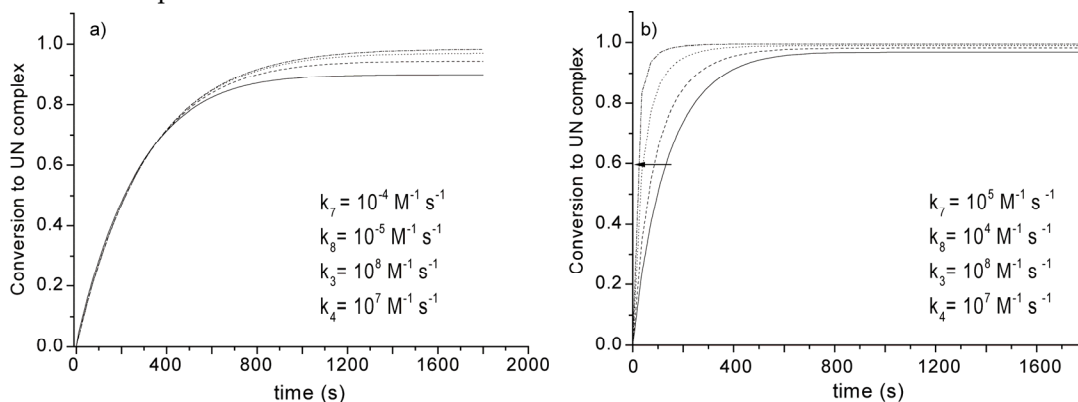


Figure A1: a) Conversion of U·N complex vs. time for a 1:1 association experiment using $k_7 = 10^{-4} \text{ M}^{-1} \text{ s}^{-1}$, $k_8 = 10^{-5} \text{ M}^{-1} \text{ s}^{-1}$, $k_3 = 10^8 \text{ M}^{-1} \text{ s}^{-1}$ and $k_4 = 10^7 \text{ M}^{-1} \text{ s}^{-1}$. b) Conversion of U·N complex vs. time for a 1:1 association experiment using $k_7 = 10^5 \text{ M}^{-1} \text{ s}^{-1}$, $k_8 = 10^4 \text{ M}^{-1} \text{ s}^{-1}$, $k_3 = 10^8 \text{ M}^{-1} \text{ s}^{-1}$ and $k_4 = 10^7 \text{ M}^{-1} \text{ s}^{-1}$. The arrow denotes an increase in the total concentration of U and N in 1:1 mixtures.

4.8 References

- 1) a) Lohr, A.; Lysetska, M.; Würthner, F. *Angew. Chem. Int. Ed.* **2005**, *44*, 5071. b) Jyothish, K.; Hariharan, M.; Ramaiah, D. *Chem. Eur. J.* **2007**, *13*, 5944. c) Jonkheijm, P.; Miura, A.; Zdanowska, M.; Hoeben, F. J. M.; De Feyter, S.; Schenning, A. P. H. J.; De Schyver, F. C.; Meijer, E. W. *Angew. Chem. Int. Ed.* **2004**, *43*, 74.
- 2) (a) Mathias, J. P.; Seto, C. T.; Simanek, E. E.; Whitesides, G. M. *J. Am. Chem. Soc.* **1994**, *116*, 1725. b) Mathias, J. P.; Simanek, E. E.; Seto, C. T.; Whitesides, G. M. *Angew. Chem., Int. Ed.* **1993**, *32*, 1766. c) Prins, L. J.; De Jong, F.; Timmerman, P.; Reinhoudt, D. N. *Nature* **2000**, *408*, 181. d) Prins, L. J.; Neuteboom, E. E.; Paraschiv, V.; Crego-Calama, M.; Timmerman, P., Reinhoudt, D. N. *J. Org. Chem.* **2002**, *67*, 4808. e) Paraschiv, V.; Crego-Calama, M.; Ishi-i, T.; Padberg, C. J.; Timmerman, P.; Reinhoudt, D. N. *J. Am. Chem. Soc.* **2002**, *124*, 7638. f) Mukhopadhyay, P.; Zavalij, P. Y.; Isaacs, L. *J. Am. Chem. Soc.* **2006**, *128*, 14093. g) Oshikiri, T.; Takashima, Y.; Yamaguchi, H.; Harada, A. *J. Am. Chem. Soc.* **2005**, *127*, 12186. h) Dyck, A. S. M.; Kisiel, U.; Bohne, C. *J. Phys. Chem. B* **2003**, *107*, 11652. i) Nordel, P.; Westerlund, F.; Wilhelmsson, M.; Nordén, B.; Lincoln, P. *Angew. Chem. Int. Ed.* **2007**, *46*, 2203. j) Badjić, J. D.; Cantrill, S. J.; Stoddart, J. F. *J. Am. Chem. Soc.* **2004**, *126*, 2288.
- 3) a) Ercolani, G. *J. Phys. Chem. B* **1998**, *102*, 5699. b) Ercolani, G. *J. Phys. Chem. B* **2003**, *107*, 5052.
- 4) Although there is no complete theory that describes kinetic product formation in general, there are models that explain kinetic product formation in individual cases as for example in the self-assembly of a virus capsid: Zlotnick, A.; Johnson, J. M.; Wingfield, P. W.; Stahl, S. J.; Endres, D. *Biochemistry* **1999**, *38*, 14644.
- 5) Johnson, R. S.; Yamazaki, T.; Kovalenko, A.; Fenniri, H. *J. Am. Chem. Soc.* **2007**, *129*, 5735.
- 6) Prins, L. J.; Timmerman, P.; Reinhoudt, D. N. *J. Am. Chem. Soc.* **2001**, *123*, 10153.
- 7) a) Hopfield, J. J. *Proc. Natl. Acad. Sci. USA* **1974**, *71*, 4135. b) Yamane, T.; Hopfield, J. J. *Proc. Natl. Acad. Sci. USA* **1977**, *74*, 2246.
- 8) Brunsveld, L.; Folmer, B. J. B.; Meijer, E. W.; Sijbesma, R. P. *Chem. Rev.* **2001**, *101*, 4071.
- 9) Lehn, J.-M., *Supramolecular Chemistry*. Wiley-VCH: 1995.
- 10) Ciferri, A., *Supramolecular Polymers*. Marcel Dekker: New York, 2000.
- 11) Zimmerman, N.; Moore, J. S.; Zimmerman, S. C. *Chem. Ind.* **1998**, 604.
- 12) Ciferri, A. *J. Macromol. Sci. Polym. Rev.* **2003**, *43*, 271.
- 13) Castellano, R. K.; Clark, R.; Craig, S. L., Nuckolls, C.; Rebek, J. Jr. *Proc. Natl. Acad. Sci. USA* **2000**, *97*, 12418.
- 14) Gibson, H. W., Yamaguchi, N.; Jones, J. W. *J. Am. Chem. Soc.* **2003**, *125*, 3522.
- 15) a) Arnaud, A.; Bellény, J.; Boué, F.; Bouteiller, L.; Carrot, G.; Wintgens, V. *Angew. Chem. Int. Ed.* **2004**, *43*, 1718. b) Arnaud, A.; Bouteiller, L. *Langmuir* **2004**, *20*, 6858.
- 16) Sijbesma, R. P.; Beijer, F. H.; Brunsveld, L.; Folmer, B. J. B.; Hirschberg, J. H. K. K.; Lange, R. F. M.; Lowe, J. K. L.; Meijer, E. W. *Science* **1997**, *278*, 1601.
- 17) Serpe, M. J.; Craig, S. L. *Langmuir* **2007**, *23*, 1626.
- 18) a) Yount, W.C.; Juwarker, H.; Craig, S. L. *J. Am. Chem. Soc.* **2003**, *125*, 15302. b) Yount, W.C.; Loveless, D. M.; Craig, S. L. *Angew. Chem. Int. Ed.* **2005**, *44*, 2746. c) Loveless, D. M.; Jeon, S. L.; Craig, S. L. *Macromolecules* **2005**, *38*, 10171.
- 19) Selected examples discussing the importance of kinetics in supramolecular chemistry: *General*: a) Davis, A. V.; Yeh, R. M.; Raymond, K. N. *Proc. Natl. Acad. Sci. USA* **2002**, *99*, 4793. b) Nau, W. M.; Wang, X. *Chem. Phys. Chem* **2002**, *3*, 393. *Organogels*: c)

- Huang, X.; Terech, P.; Raghavan, S. R.; Weiss, R. G. *J. Am. Chem. Soc.* **2005**, *127*, 4336. *Host-guest*: d) Palmer, L. C., Rebek, J. Jr. *Org. Biomol. Chem.* **2004**, *2*, 3051. e) Rudkevich, D. M.; Hilmersson, G.; Rebek, J. Jr. *J. Am. Chem. Soc.* **1997**, *41*, 9911. f) Castellano, R. K.; Craig, S. L.; Nuckolls, C.; Rebek, J. Jr. *J. Am. Chem. Soc.* **2000**, *122*, 7876. g) Goshe, A. J.; Steele, I. M.; Ceccarelli, C.; Rheingold, A. L.; Bosnich, B. *Proc. Natl. Acad. Sci. USA* **2002**, *99*, 4823. h) Gibb, C. L. D.; Li, X.; Gibb, B. C. *Proc. Natl. Acad. Sci. USA* **2002**, *99*, 4857. *Nucleation-elongation*: i) Oosawa, F.; Kasai, M. *J. Mol. Biol.* **1962**, *4*, 10. j) Pasternack, R. F.; Gibbs, E. J.; Collings, P. J.; dePaula, J. C.; Turzo, L. C.; Terracina, A. *J. Am. Chem. Soc.* **1998**, *120*, 5873. *Hydrogen bonded complexes*: k) Prins, L. J.; Neuteboom, E. E.; Paraschiv, V.; Crego-Calama, M.; Timmerman, P.; Reinhoudt, D. N. *J. Org. Chem.* **2002**, *67*, 4808. l) Mogck, O.; Pons, M.; Böhmer, V.; Vogt, W. *J. Am. Chem. Soc.* **1997**, *119*, 5706. m) Das, G.; Talukdar, P.; Matile, S. *Science* **2002**, *298*, 1600. *Self-replicating peptides*: n) Kennan, A. J.; Haridas, V.; Severin, K.; Lee, D. H.; Ghadiri, M. R. *J. Am. Chem. Soc.* **2001**, *123*, 1797. *Metallic helicates*: o) Elhabiri, L.; Hamacek, J.; Bünzli, J.-C. G.; Albrecht-Gary, A. M. *Eur. J. Inorg. Chem.* **2004**, 51. *Other*: p) Milic, T. N.; Chi, N.; Yablon, D. G.; Flynn, G. W.; Batteas, J. D.; Drain, C. M. *Angew. Chem. Int. Ed.* **2002**, *41*, 2117.
- 20) Söntjens, S. H. M.; Sijbesma, R. P.; van Genderen, M. H. P.; Meijer, E. W. *J. Am. Chem. Soc.* **2000**, *122*, 7487.
- 21) For a review on the mechanisms of a variety of prototropic tautomerizations believed to be intermolecular see: Kereselidze, J. A.; Zarqua, T. Sh.; Kikalishvili, T. J.; Churgulia, E. J.; Makaridze, M. C. *Russ. Chem. Rev.* **2002**, *71*, 993.
- 22) Nagy, P. I.; Tejada, F. R.; Messer, W. S., Jr. *J. Phys. Chem. B* **2005**, *109*, 22588.
- 23) Chou, P. -T.; Wei, C. -Y.; Hung, F. -T. *J. Phys. Chem. B* **1997**, *101*, 9119.
- 24) Freeman, F.; Po, H. N. *J. Phys. Chem. A* **2006**, *110*, 7904.
- 25) Yang, Z.; Rodgers, M.T. *Phys. Chem. Chem. Phys.* **2004**, *6*, 2749.
- 26) This can more clearly be observed from the experimental data in Figure 4.1 which shows that extrapolation to $y=0$ results in an intercept with the negative x -axis, indicating a faster process preceding the complexation of keto dimers of **1** with **2**. Therefore, we are specifically monitoring the formation of the U-N hetero-complex from DDAA dimers in the 1:1 kinetic equilibration experiments.
- 27) Mendes, P. *Trends Biochem. Sci.* **1997**, *22*, 361.
- 28) Padermshoke, A; Katsumoto, Y.; Aida, M. *J. Phys. Chem. B* **2006**, *110*, 26388.
- 29) a) Hammes, G. G., Spivey, H. O. *J. Am. Chem. Soc.* **1966**, *88*, 1621. b) Hammes, G. G.; Park, A. C. *J. Am. Chem. Soc.* **1969**, *91*, 956. c) Hammes, G. G.; Park, A.C. *J. Am. Chem. Soc.* **1968**, *90*, 4151.
- 30) The diffusion controlled rate constant was calculated using the viscosity of toluene at 293 K ($\eta = 5.58 \times 10^{-4} \text{ kg m}^{-1} \text{ s}^{-1}$) using the formula $k_{diff} = \frac{8 * R * T}{3 * \eta}$ resulting in a value of k_{diff} of $1.18 \times 10^{10} \text{ M}^{-1} \text{ s}^{-1}$.
- 31) Negative covariance indicates that higher than average values of one variable are tend to be paired with lower than average values of the other variable.
- 32) *Fitting Models to Biological Data using Linear and Nonlinear Regression*, Motuslky, H.; Christopoulos, A. Available at www.graphpad.com.
- 33) Full model: residual sum of squares = 4.6×10^{-12} , 174 degrees of freedom. Reduced model: residual sum of squares = 4.52×10^{-11} , 176 degrees of freedom.
- 34) Perrin, C. L.; Dwyer, T. J. *Chem. Rev.* **1990**, *90*, 935.

- 35) Jeener, J.; Meier, B. H.; Bachmann, P.; Ernst, R. R. *J. Chem. Phys.* **1979**, *71*, 4546.
- 36) 2D-EXSY measurements on a solution of 4[1H]-pyrimidinone dimer **1·1** and **1·2** in the same molar ratio did not result in cross-peaks between the diagonal peaks of the alkylidene proton of the ureido-pyrimidinone dimer and the alkylidene proton of the hetero-complex even at high mixing times ($\tau_{\text{mix}} > 1$ s). This indicates that the site to site rate constant of this process is lower than 10^{-1} s^{-1} (see reference 34) in agreement with ^1H -NMR equilibration experiments.
- 37) Under the conditions that the mol fraction of U·N complex is equal to the mole fraction of U_2 dimer the transfer function takes the following form: $\phi = \ln(r + 1/r - 1)$ where $r = (I_{\text{AA}} + I_{\text{BB}})/(I_{\text{AB}} + I_{\text{BA}})$, the ratio of diagonal- and cross-peak intensities.
- 38) The ^1H -NMR spectrum of this solution did not show any evidence of protonation of either the U_2 dimer or the U·N complex **2·3**.
- 39) Hazra, M. K.; Chakraborty, T. *J. Phys. Chem. A.* **2006**, *110*, 9130.
- 40) Beijer, F. H.; Sijbesma, R. P.; Kooijman, H.; Spek, A. L.; Meijer, E. W. *J. Am. Chem. Soc.* **1998**, *120*, 6761.
- 41) The ^1H -NMR spectrum of a 1:1 solution of **1** and **3** (5 mM each) in the more polar solvent CDCl_3 reveals that approximately 14% of the total concentration of **1** is incorporated in the ureido-pyrimidinone hetero-dimeric form **1·3** (see Chapter 2).
- 42) Ligthart, G. B. W. L.; Ohkawa, H.; Sijbesma, R. P.; Meijer, E. W. *J. Org. Chem.* **2006**, *71*, 375.
- 43) Keizer, H. M.; Sijbesma, R. P.; Meijer, E. W. *Eur. J. Org. Chem.* **2004**, *12*, 2553.
- 44) Due to the high K_{dim} of **1** and high K_{a} of **1·2** in toluene it proved difficult to obtain a good fit around the equivalence point. A titration performed at a concentration of **2** of $1 \times 10^{-5} \text{ M}$ gave a K_{a} of $3.4 (\pm 1.7) \times 10^8 \text{ M}^{-1}$ while the same titration performed at a concentration of **2** of $2.5 \times 10^{-6} \text{ M}$ gave a value of $7 (\pm 3) \times 10^7 \text{ M}^{-1}$. Due to the difficulty of obtaining reproducible data at this concentration a reliable estimate of the K_{a} of **1·2** in toluene is therefore $10^7 - 5 \times 10^8 \text{ M}^{-1}$.
- 45) T_1 relaxation measurements conducted on a solution containing 10 mM **2** and 20 mM **3** in toluene- d_8 showed that the T_1 relaxation time of the alkylidene proton of **3₂** (0.82 s^{-1}) is almost equal to the T_1 relaxation time of the alkylidene proton of the U·N complex **2·3** (0.81 s^{-1}).

5

Self-assembly of UPy dimers into one-dimensional stacks via lateral hydrogen bonding in solution

Abstract

Chiral UPy dimers substituted with an additional urea functionality self-assemble into one-dimensional stacks via lateral non-covalent interactions in various solvents. $^1\text{H-NMR}$ and DOSY studies in CDCl_3 suggest the formation of short stacks (< 10) whereas temperature dependent CD (circular dichroism) studies in heptane show the formation of much larger stacks. Analysis of the concentration dependent chemical shift evolution in CDCl_3 and the temperature dependent CD effect in heptane suggest that this self-assembly process follows an isodesmic pathway in both solvents. Furthermore, the length of the aggregates can be controlled by variation of the substituent attached to the urea functionality. In sharp contrast, UPy dimers carrying an additional urethane group do not self-assemble into ordered stacks as is evident from the absence of a CD effect in heptane and a concentration independent chemical shift of the alkylidene proton of the pyrimidinone ring in CDCl_3 . Finally, mixing experiments of UPy-urea dimers with UPy dimers suggest the formation of UPy / UPy-urea heterodimers which self-assemble into larger aggregates at high concentrations.

5.1 Introduction

The N,N'-disubstituted urea moiety is often used in the construction of hydrogen bonded supramolecular polymers¹, organogelators², foldamers³ or novel crystalline frameworks.⁴ Urea groups are known to associate strongly via bifurcated hydrogen bonds,⁵ whose strength exceeds that of amide and urethane hydrogen bonds.⁶ The aggregation of N,N'-disubstituted urea groups leads to the formation of linear chains in the solid state⁷ as well as in solution.⁸ FTIR measurements in CCl₄ have shown that the self-assembly of N,N'-dialkyl substituted urea groups into linear chains in solution is a cooperative process⁸ as a result of the polarization of the urea function prior to dimerization.⁹

Due to the aggregation of urea groups into linear chains, incorporation of these groups in covalent polymers has led to the formation of thermoplastic elastomers in which cross linking between the chains occurs via non-covalent interactions.¹⁰ Due to the combination of strongly interacting segments alternating with weakly interacting segments, microphase-separated materials with a soft block/hard block morphology are obtained. When the hard blocks contain urethane and/or urea groups, strong and specific hydrogen-bonding interactions lead to useful properties, such as a high modulus for a given hard block content.^{6,11}

Recently, Kautz *et al.* investigated¹² the effect of lateral hydrogen bonding *via* urea and urethane hydrogen bonding on a series of telechelic 2-ureido-pyrimidinone (UPy) substituted poly(ethylene butylene) polymers. Specifically, it has been shown that directional lateral aggregation in these supramolecular polymers results in 1-D aggregation of the dimerized UPy end groups in long fibers. Atomic force microscopy (AFM) on these polymers revealed marked differences between the urea and urethane substituted UPy polymers. Whereas lateral hydrogen bonding *via* the urea moiety resulted in the formation of micrometer long fibers, lateral hydrogen bonding *via* the urethane moiety resulted in a much smaller and less densely packed morphology than the urea substituted polymers indicating that aggregation is not complete. Furthermore, tensile testing showed that the material properties of these polymers were superior compared to the same supramolecular polymer lacking additional lateral hydrogen bonding. Interestingly, differential scanning calorimetry (DSC) showed that the fibers display a first order melting transition at high temperatures while temperature dependent FTIR measurements have shown that this first order phase transition is directly associated with the breakup of the UPy-urea aggregates.¹²

In this Chapter, several discrete UPy monomers bearing urea and urethane groups will be prepared and their self-assembly in solution will be investigated in various solvents using concentration dependent ¹H-NMR and temperature dependent circular dichroism.

5.2 Design and synthesis

The design of the UPy monomers is apparent in Chart 5.1a. Each UPy monomer consists of the following parts:

1) *The UPy group capable of quadruple hydrogen bonding.*

By dimerization of the two pyrimidinone rings ($K_{\text{dim}} = 6 \times 10^7 \text{ M}^{-1}$ in CHCl_3), a flat aromatic surface is created which enhances aromatic π - π interactions between two hydrogen bonded dimers.¹³ This additional interaction is important because it results in the preference of *longitudinal* self-assembly over *lateral* self-assembly of the UPy-urea dimers (Chart 5.1b).²¹

2) *Chiral groups attached to the C₆ position of the pyrimidinone group.* By attaching chiral groups to this position, the possible formation of helical aggregates can be biased by perturbation of the equilibrium between P and M type helical aggregates.¹⁴ As a result of this perturbation, the self-assembly of the UPy dimers into ordered aggregates can be conveniently followed using temperature dependent circular dichroism (CD).

3) *A urea or urethane functionality to induce lateral hydrogen bonding between UPy dimers.* Because hydrogen bonding *via* the urea group is much stronger than hydrogen bonding *via* the urethane group, variation at this position will greatly influence the lateral association of UPy dimers into 1-D aggregates.

4) *Additional solubilizing groups attached to urea or urethane moiety.* By variation of the R substituent, the self-assembly of UPy dimers equipped with lateral interacting groups can be studied in a wide range of solvents. Moreover, by introducing an electron-withdrawing aromatic substituent at this position the intermolecular association between the urea groups is expected to strengthen.¹⁵

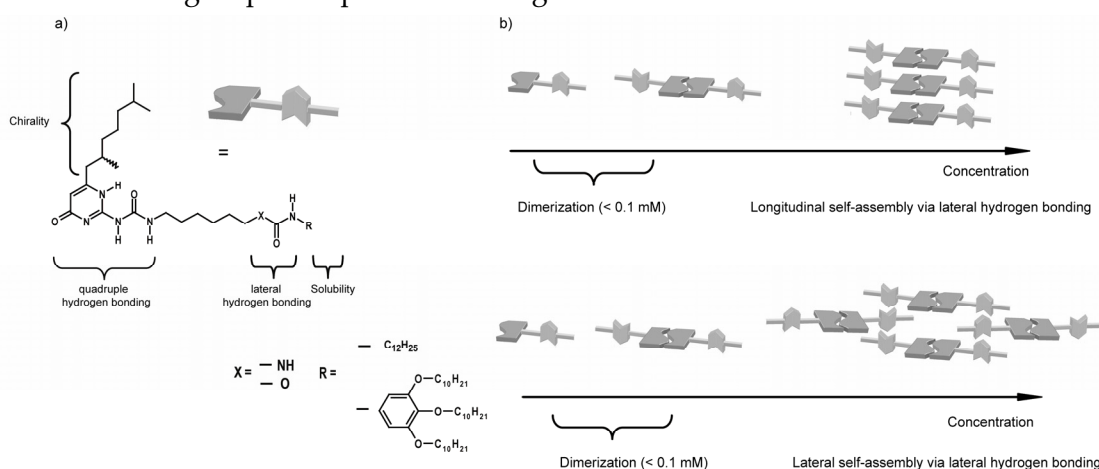
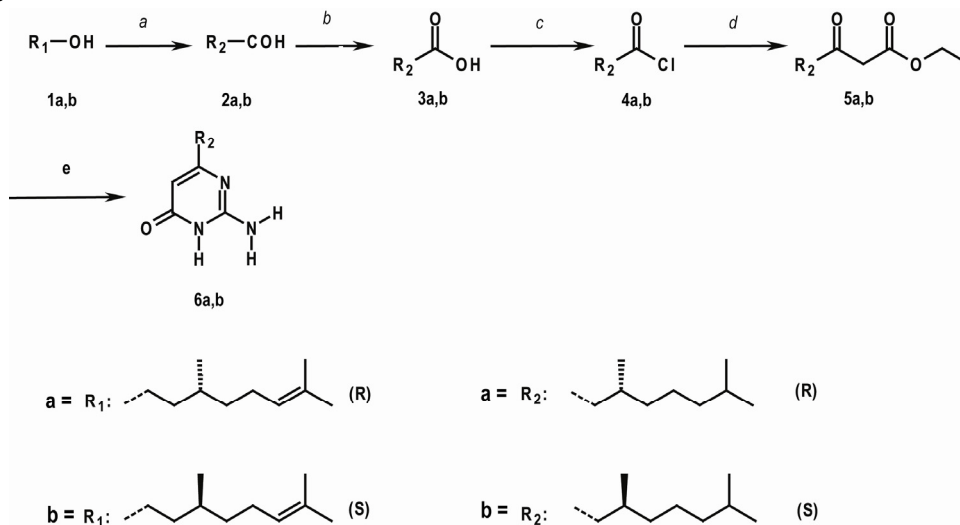


Chart 5.1: a) Design and structure of UPy monomers bearing additional laterally interacting urea or urethane substituents. b) Longitudinal and lateral self-assembly of UPy-urea dimers.

The synthesis of chiral isocytosines **6a** and **6b** is depicted in Scheme 5.1. The synthetic route towards isocytosines **6a** and **6b** was adapted from a previously established route for converting acyl chlorides into isocytosines.¹⁶ The corresponding chiral acyl chlorides **4a** and **4b** were synthesized from commercially available¹⁷ (*R*)-3,7-dimethyl-6-octen-1-ol **1a** and (*S*)-3,7-dimethyl-6-octen-1-ol **1b** by reducing the double bond using Pd/C and hydrogen and subsequent oxidation of alcohols **2a** and **2b** in the presence of periodic acid¹⁸ and a catalytic amount of pyridinium chlorochromate to the corresponding carboxylic acids.



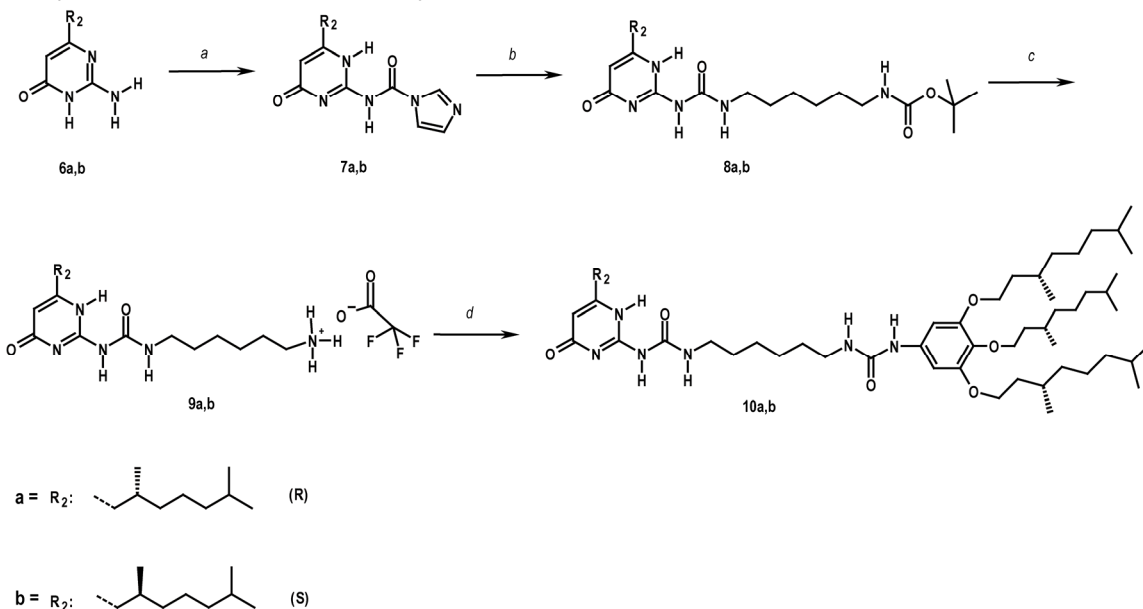
Scheme 5.1: Synthetic route towards chiral isocytosines, **6a** and **6b**: a) Pd/C, H₂, ethyl acetate, 24 h, RT, 98%; b) periodic acid, 2% pyridinium chlorochromate, acetonitrile, 3 h, 0–25 °C; c) oxalyl chloride, dimethylformamide (cat), dichloromethane, 3–12 h, 0–25 °C; d) ethyl potassium malonate, MgCl₂, Et₃N, acetonitrile, 25 h, 0–25 °C; e) guanidinium carbonate, potassium *tert*-butoxide, ethanol, 43–65 h, reflux.

Isocytosines **6a** and **6b** were activated¹⁹ using 1,1'-carbonyldiimidazole and further reacted with mono-Boc protected 1,6-hexanediamine in CHCl₃. Deprotection of the Boc group using trifluoroacetic acid resulted in chiral ammonium salts **9a** and **9b** (Scheme 5.2). Chiral synthons **9a** and **9b** serve as convenient intermediates in the synthesis of various chiral UPy-urea monomers.

Preliminary studies on the UPy-urea system performed by W. Appel²⁰ have shown that linear as well as branched aliphatic chains attached to the urea functionality (R group in Chart 5.1) are not sufficient to solubilise these molecules in apolar solvents such as heptane. Therefore, it was decided to attach a chiral 3,4,5-tris(3(*S*),7-dimethyloctyloxy)-phenyl group to this position to ensure solubility in apolar solvents. By introduction of this substituent, two different diastereomers are created (*R*, *S*, *S*, *S* **10a** and *S*, *S*, *S*, *S* **10b**).

Chiral UPy-urea monomer **13** (*R* chirality) bearing an aliphatic substituent was synthesized in two steps from **9a** (Scheme 5.3). The solubility of **13** in apolar solvents such as heptane and cyclohexane was found to be extremely low, however in CDCl₃ chiral UPy-urea **13** was found to be soluble up to a concentration of 20 mM.

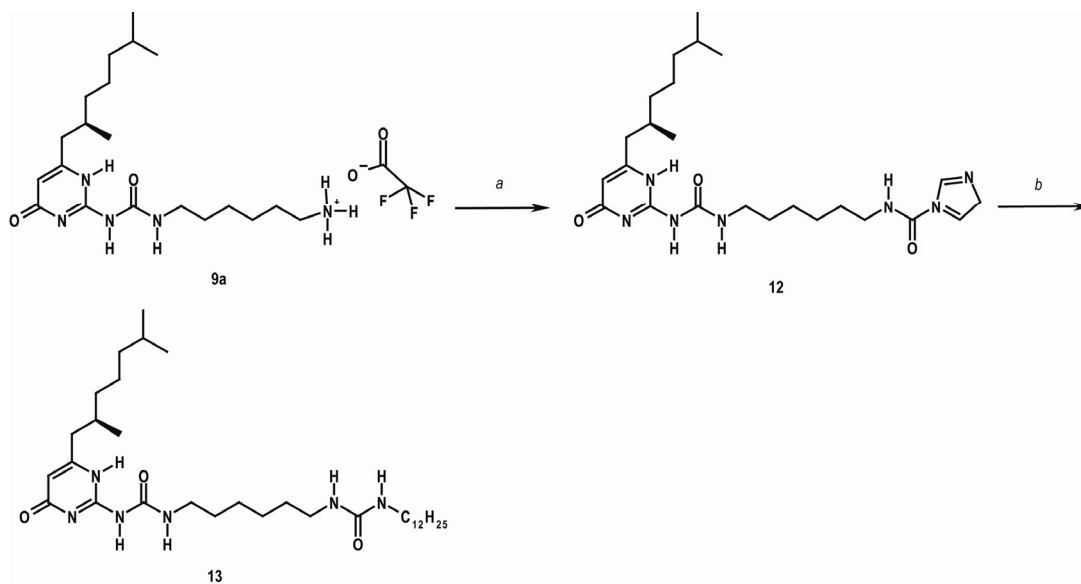
Finally, *S, S, S, S* chiral UPy-urethane **15** was synthesized in two steps from isocytosine **6b** (Scheme 5.4) by reaction of the isocytosine with 6-isocyanato-1-hexanol at elevated temperatures in DMF. Reaction of UPy **14** with 3,4,5-tris(3(*S*),7-dimethyloctyloxy)-phenyl isocyanate resulted in chiral UPy-urethane **15**.



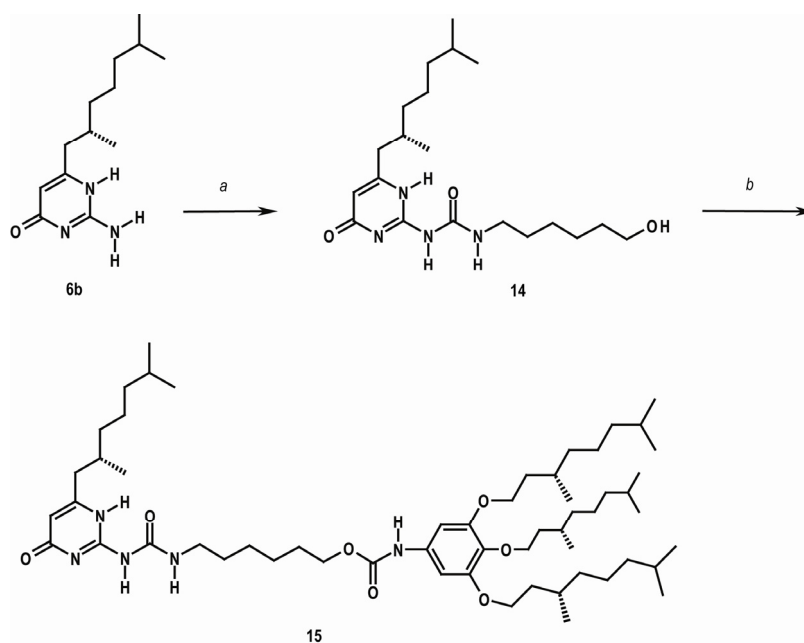
Scheme 5.2: Synthetic route towards chiral UPy-urea monomers **10a** and **10b** bearing a chiral gallic wedge at the urea functionality: a) 1,1'-carbonyldiimidazole, CHCl₃, 4–12 h, 50 °C; b) mono-Boc protected 1,6-hexanediamine, CHCl₃, 17 h, 50 °C; c) trifluoroacetic acid, dichloromethane, 4–13 h, RT; d) 3,4,5-tris(3(*S*),7-dimethyloctyloxy)-phenyl isocyanate (**11**), triethylamine, CHCl₃, 48 h, 50 °C.

5.3 Self-assembly of UPy-urea and UPy-urethane dimers in CDCl₃

Concentration dependent ¹H-NMR measurements in CDCl₃ were performed on UPy-urea **10a** at concentrations where all monomeric **10a** is present as dimers (>0.1 mM).²¹ These measurements show a downfield shift of both urea NH protons at higher concentrations (Figure 5.1a) accompanied by an upfield shift of the alkylidene proton located at the pyrimidinone ring and significant line broadening. The upfield shift of the proton located on the pyrimidinone ring is typical for self-assembled structures resulting from close contact of aromatics.²²



Scheme 5.3: Synthetic route towards chiral UPy-urea monomer **13** (*R* enantiomer) bearing an aliphatic substituent at urea functionality: a) 1,1'-carbonyldiimidazole, CHCl_3 , 4 h, 50°C , 95%; b) *n*-dodecylamine, CHCl_3 , 48 h, 55°C , 73%.



Scheme 5.4: Synthetic route towards chiral UPy-urethane monomer **15** bearing a chiral gallic wedge at the urethane functionality: a) di-*tert*-butyl tricarbonate, 6-amino-1-hexanol, dichloromethane, 0.5 h, RT then **6b**, dimethylformamide, 4.5 h, 90°C , 56%; b) tris(3(*S*),7-dimethyloctyloxy)-phenyl isocyanate **11**, dibutyltin dilaurate, CHCl_3 , 48 h, 60°C , 34%.

Calculations on stacked cytosine assemblies have shown that ring-current effects due to intermolecular interactions result in a small upfield shift (between 0.1 and 0.3 ppm).²³ Moreover, the downfield shift of both NH protons indicate that these protons are involved in the formation of hydrogen bonds²⁴ at higher concentrations. The downfield shift of both NH protons and the concomitant upfield shift of the alkylidene proton suggest the formation of a larger aggregate in which both urea NH protons are hydrogen bonded and the pyrimidinone rings of two UPy dimers are in close contact. To further gain prove of aggregation of these molecules, concentration dependent DOSY measurements were performed on solutions of **10a** in CDCl₃ (Figure 5.1b). These measurements (Figure 5.1b) show that the viscosity corrected²⁶ diffusion constant becomes smaller at higher concentrations, indicative of the formation of an aggregate consisting of multiple dimers of **10a**.

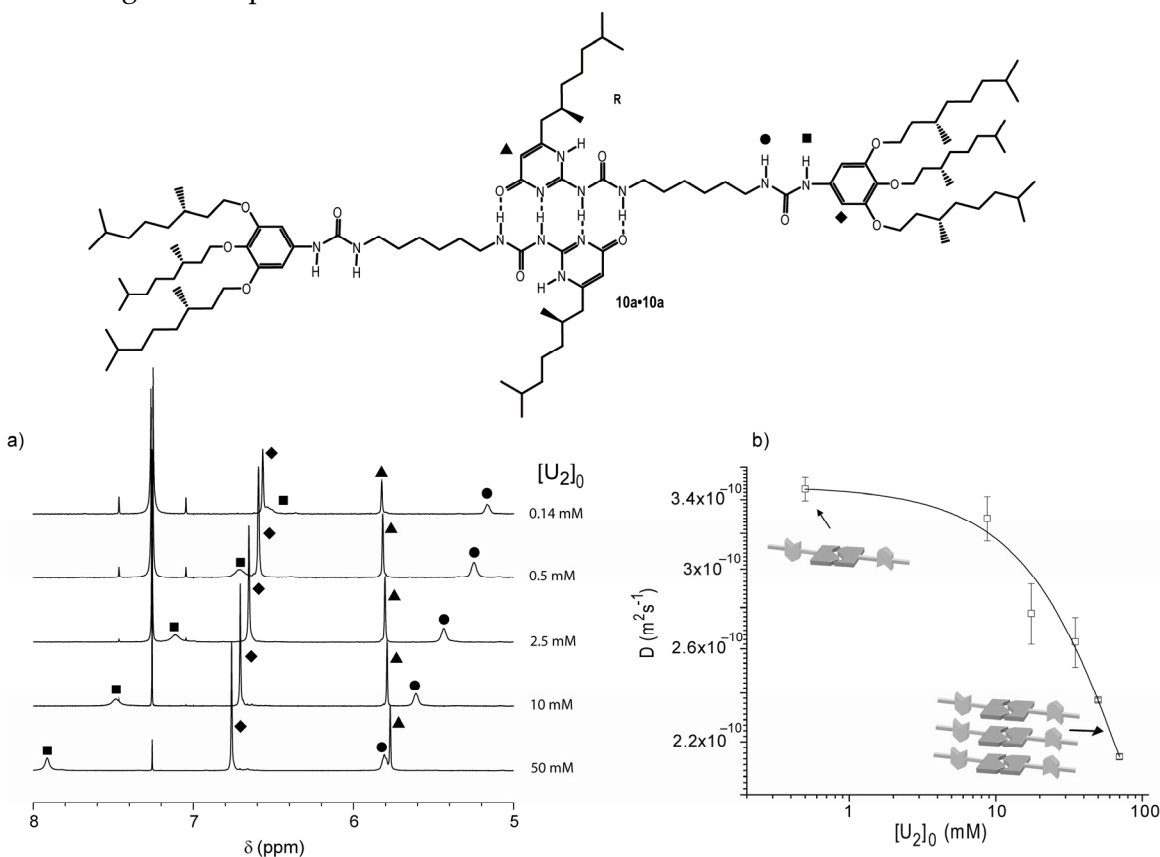


Figure 5.1: a) Concentration dependent ¹H-NMR of UPy-urea dimer **10a·10a** in CDCl₃ at 25 °C. b) Concentration dependent average diffusion constant for **10a·10a** in CDCl₃ at 25 °C calculated using the measured diffusion constants of the signals depicted in part a. The diffusion constants of all signals were calculated using the bipolar pulse pair stimulated echo sequence with convection compensation.²⁵ The solid line is served to guide the eye.

In order to gain additional insight into the self-assembly process of UPy-urea dimer **10a-10a**, the concentration dependent chemical shift of all protons were fitted according to a three parameter isodesmic (equal K), self-association model (Appendix A, eq (21)) using the Levenberg-Marquardt algorithm.²⁷ In this way, the isodesmic equilibrium constant (K), the chemical shift of protons in the unaggregated UPy-urea dimer and the limiting value of the chemical shift of the protons within the stack are obtained (Table 5.1).

Table 5.1: Isodesmic equilibrium constants determined by dilution of UPy-urea dimer **10a-10a** using $^1\text{H-NMR}$.

Proton	K (M^{-1})
Urea NH ●	329 ± 40
Urea NH ■	322 ± 38
Gallic Aryl ◆	387 ± 41
Alkylidene ▲	254 ± 40

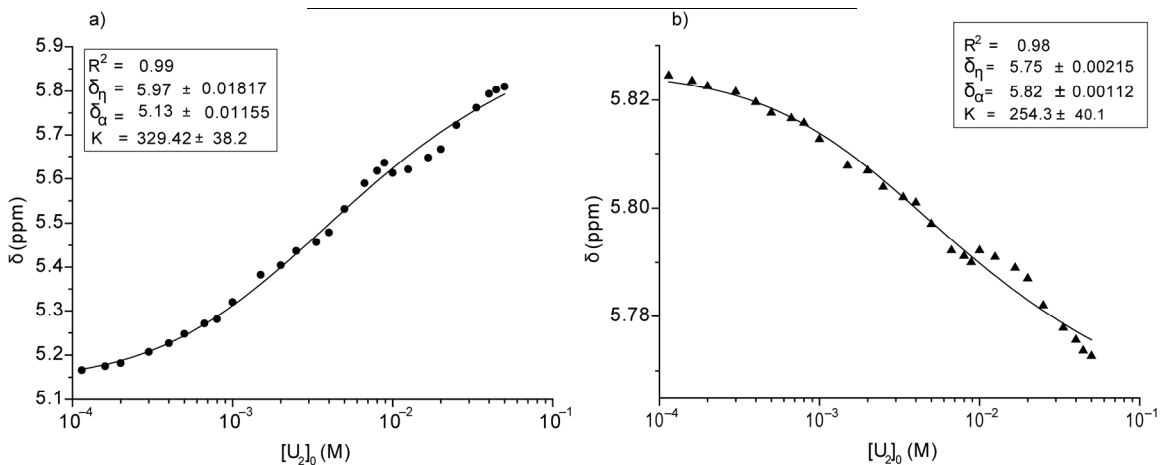


Figure 5.2: Concentration dependent chemical shift of UPy-urea dimer **10a-10a**: a) Concentration dependent chemical shift of the urea NH proton (●). b) Concentration dependent chemical shift of the alkylidene proton. The curves represent the best fit of the data to the isodesmic model of indefinite association.

Figure 5.2a and b display the concentration dependent chemical shift data of UPy-urea dimer **10a-10a** as well as the best fitted curves according to an isodesmic self-assembly model. As can be observed from Figure 5.2a, the concentration dependent chemical shift evolution of the urea NH proton (■) is accurately described by the indefinite isodesmic self-assembly model. Fitting of the concentration dependent chemical shift evolution of the second urea NH proton (●) and the aromatic proton located on the gallic wedge (◆) to the same isodesmic self-assembly model showed that the chemical shift evolution of

these protons is also well described by this model. The isodesmic equilibrium constant (K) of these three protons as determined by non-linear least-square fitting are in the range of 322-387 M⁻¹ (Table 5.1). However, fitting of the concentration dependent chemical shift evolution of the alkylidene proton (Figure 5.2b) shows that the isodesmic self-assembly model is inappropriate to describe the experimental data, especially in the high concentration regime. The isodesmic equilibrium constant of this proton was determined to be 254 M⁻¹. The differences between the isodesmic equilibrium constant of the urea NH protons and the alkylidene proton can be attributed to one of the two following effects. Firstly, the error in the determination of the exact chemical shift value is much higher for the alkylidene proton as compared to the urea NH protons as the first only shifts by a value of 0.1 ppm while the latter shifts by a value of almost 1 ppm. Secondly, the difference in isodesmic equilibrium constant between the two protons can be the result of the fact that the self-assembly of UPy-urea dimer **10a·10a** is hierarchical. At low concentrations, hydrogen bonding of the urea NH protons results in the formation of a hydrogen bonded aggregate in which the pyrimidinone rings are not stacked on top of each other. Only at higher concentrations, additional stabilisation of the aggregate due to π - π aromatic interactions occur.

¹H-NMR dilution of UPy-urea dimer **13·13**, substituted with a linear aliphatic substituent, resulted in a concentration dependent chemical shift of both urea NH protons and the alkylidene proton (Appendix B) in CDCl₃. Fitting of the concentration dependent data to a three parameter isodesmic self-assembly model resulted in the isodesmic equilibrium constants for all three protons. As can be observed from Table 5.2, the average isodesmic equilibrium constant of **13·13** is an order of a magnitude lower compared to the value of UPy dimer **10a·10a**. As already mentioned, this lowering is most probably the result of the decreased acidity of the urea NH protons in **13** compared to the urea protons in **10a**. Also in the case of UPy-urea dimer **13·13**, the isodesmic equilibrium constant obtained from the concentration dependent chemical shift data of the alkylidene proton is lower than the isodesmic equilibrium constant of the urea NH protons.

Finally, dilution studies were performed on UPy-urethane dimer **15·15** in CDCl₃. In sharp contrast to the urea functionalised ureido-pyrimidinones **10a** and **13**, no concentration dependent chemical shift was observed for the alkylidene proton, indicating the absence of aromatic stacking interactions even at high concentrations. Fitting of the concentration dependent chemical shift of the NH proton to a four parameter²⁸ indefinite isodesmic self-assembly model resulted in an isodesmic equilibrium constant of only 4.2 M⁻¹ (Table 5.2).

Table 5.2: *Isodesmic equilibrium constants as determined via dilution in CDCl₃ at 25 °C for UPy-urea dimer 13·13 and UPy-urethane dimer 15·15. The protons are marked according to the symbols used in Appendix B and C.*

UPy dimer	Urea NH ●	Urea/ Urethane NH ■	Gallic Aryl ◆	Alkyldiene ▲
13·13	14.9 M ⁻¹	14.6 M ⁻¹	-	5 M ⁻¹
15·15	-	4.2 M ⁻¹	-	-

5.4 Heteromeric self-assembly of UPy/UPy-urea dimers in CDCl₃

The ¹H-NMR spectrum of a solution of 2 eq of UPy **16** and 1 eq of UPy-urea **10a** at a total analytical concentration of **10a** of 35 mM in CDCl₃ showed two sets of signals corresponding to the UPy-urea homo-dimer **10a·10a** and the UPy/UPy-urea heterodimer **10a·16** (Figure 5.3). Because the UPy-urea homodimer **10a·10a** and the UPy / UPy-urea heterodimer **10a·16** are in slow exchange on the ¹H-NMR timescale up to the final analytical concentration of **10a** of 0.83 mM, the equilibrium composition of the mixture could be determined by integration of the corresponding signals (see Appendix D). Furthermore, the signals corresponding to the UPy/UPy-urea heterodimer **10a·16** showed concentration dependent chemical shifts, indicating that the UPy/UPy-urea heterodimer **10a·16** aggregates in CDCl₃. In principle, several different possibilities for the aggregation of the UPy/UPy-urea heterodimer **10a·16** are possible (Figure 5.4). The first possibility consists of incorporation of the mixed UPy/UPy-urea heterodimer **10a·16** into the UPy-urea homodimer aggregates, resulting in the formation of mixed aggregates of UPy dimers **10a·16** and **10a·10a**. The second possibility is the formation of two separate aggregates, *i.e.* one aggregate consisting of only UPy-urea homodimers and one aggregate consisting only of UPy/UPy-urea heterodimers. In order to differentiate between the two possibilities, the concentration dependent ¹H-NMR chemical shifts of NH proton (■) present in the UPy-urea homodimer in the “pure” (containing only **10a**, Figure 5.2a) and in the “mixed” solution (containing both **10a** and **16**) were compared (Figure 5.4).

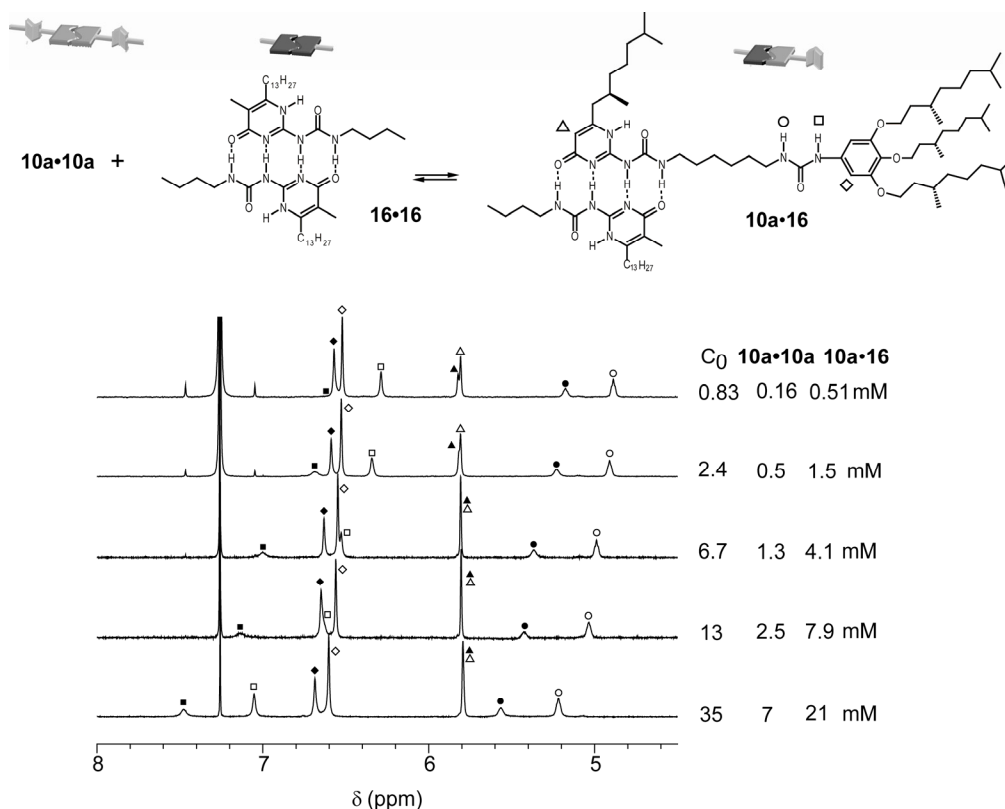


Figure 5.3: Concentration dependent $^1\text{H-NMR}$ of a solution of 1 eq **10a** (C_0) and 2 eq of **16** in CDCl_3 at a temperature of 25 °C. The closed symbols denote the signals corresponding to the UPy-urea homodimer **10a·10a** and the open symbols denote the signals arising from the UPy/UPy-urea heterodimer **10a·16**. The calculated equilibrium concentrations of homodimer **10a·10a** and heterodimer **10a·16** based on the experimentally determined integral ratio are depicted in the table next to the spectra.

As can be observed from the two curves in Figure 5.4, the presence of **16** has no effect on the longitudinal self-assembly of UPy dimer **10a·10a** as the chemical shift evolution of the NH proton of **10a·10a** in a solution which also contains **16** is the same as in the solution containing no **16**. This behaviour can be rationalised by either of the following possibilities:

- 1) The two aggregates effectively self-sort into two aggregates consisting of UPy-urea homodimer **10a·10a** and UPy/UPy-urea heterodimer **10a·16** (Figure 5.4).
- 2) The formation of a hetero-aggregate of **10a·16** and **10a·10a** in which long blocks of $(10a \cdot 16)_n$ and $(10a \cdot 10a)_i$ are present. This can occur if the association constant between the homodimer **10a·10a** and the heterodimer **10a·16** is much lower than the association constants of homodimer **10a·10a** and heterodimer **10a·16** for formation of long stacks. However, this second possibility is highly unlikely as the number average degree of the supramolecular polymers at the highest concentration is roughly 10.

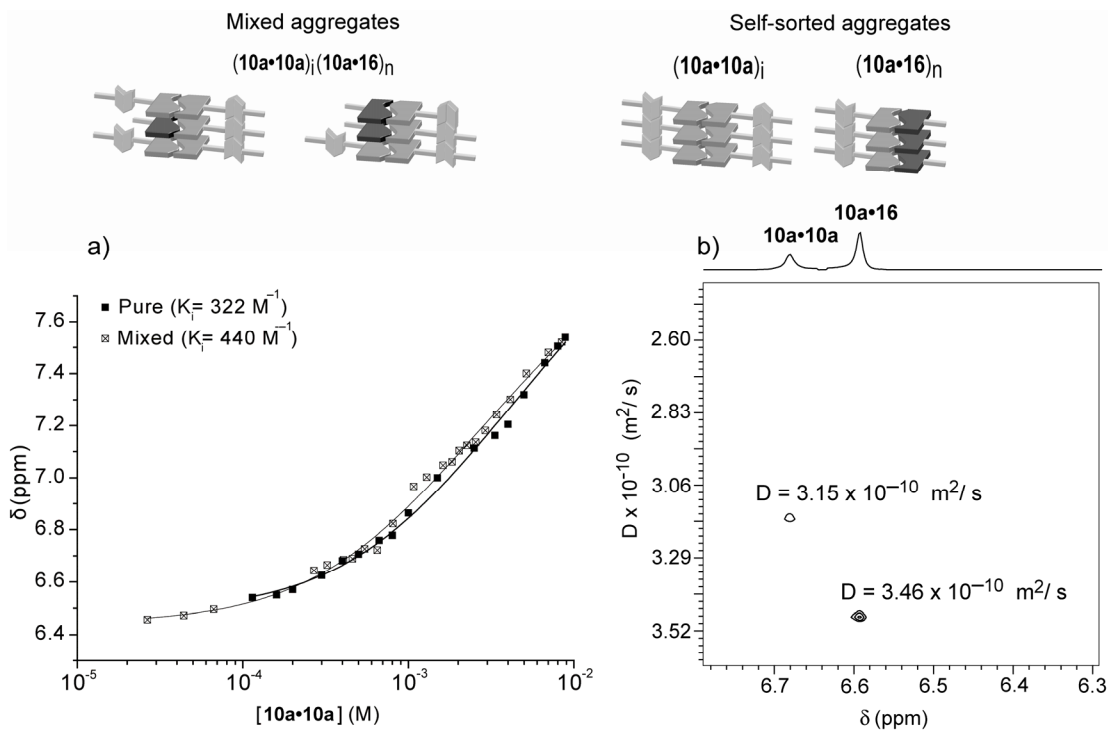


Figure 5.4: a) Concentration dependent chemical shift of the urea NH proton of UPy-urea homodimer **10a·10a** (■, Figure 5.1) in a solution containing only **10a** and in a solution containing **10a** and **16**. The equilibrium concentration of **10a·10a** in the mixture was calculated as outlined in Appendix D. The solid line is the best fitted curve according to a three parameter isodesmic self-assembly model. b) Partial 2D-DOSY spectrum of a mixture of **10a** and **16** in CDCl_3 at a temperature of 25 °C. The equilibrium concentration of UPy-urea dimer **10a·10a** was calculated to be 5 mM.

A 2D-DOSY spectrum (Figure 5.4b) of a mixture of **10a** and **16** at a total analytical concentration of **10a** of 26 mM shows that the corrected diffusion constant for the signals corresponding to UPy-urea homodimer **10a·10a** and UPy / UPy-urea heterodimer **10a·16** are different, indicating that they do not belong to the same chemical species. The corrected diffusion constant of the UPy-urea homodimer aggregate in the mixture of **10a** and **16** was found to be $3.15 \times 10^{-10} \text{ m}^2/\text{s}$ which is close to the value of $3.3 \times 10^{-10} \text{ m}^2/\text{s}$ obtained by extrapolation of the corrected diffusion constants in a solution containing only **10a** (Figure 5.1b). Although these results suggest the formation of two distinct, self-sorted aggregates, care must be taken in the interpretation of the diffusion coefficient obtained by DOSY as they represent a weighted average of the diffusion coefficient of the monomer and the stack.

Fitting of the concentration dependence of the urea protons of the mixed UPy/ UPy-urea heterodimer **10a·16** in the mixture containing **10a** and **16** showed that the isodesmic equilibrium constant of the heterodimer aggregates (21 and 25 M^{-1} at $T = 25 \text{ }^\circ\text{C}$

respectively) is approximately the square root of the isodesmic equilibrium constant of the aggregates formed by UPy-urea dimer **10a**·**10a** (Figure 5.5). From this square root dependence it can be concluded that the free energy gain *per* urea group in aggregates consisting of UPy-urea dimer **10a**·**10a** is equal.

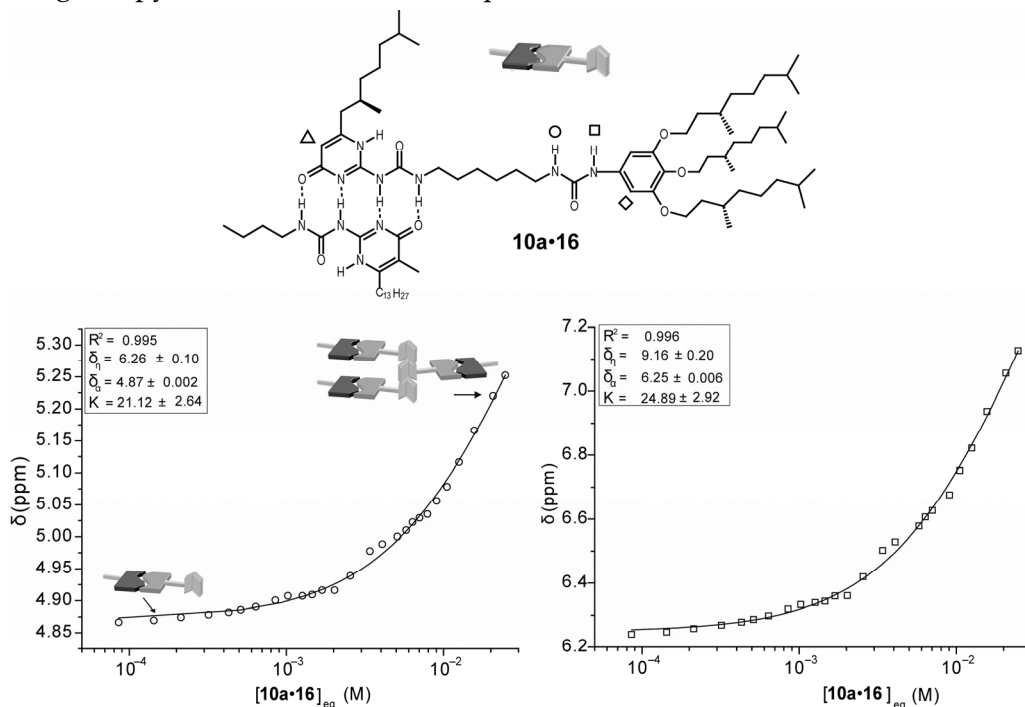


Figure 5.5: Concentration dependent chemical shift of the two urea protons (marked as \square and \circ) of **10a**·**16** in a mixture further containing aggregates of **10a**·**10a** and dimers of **16**·**16** in CDCl_3 at 25 °C. The equilibrium concentration of **10a**·**16** was calculated using the experimentally determined integrals. The solid line is the best fitted curve according to a three parameter isodesmic self-assembly model.

5.5 Self-assembly of UPy-urea and UPy-urethane dimers in heptane

Because UPy-urea dimers **10a**·**10a** and **10b**·**10b** are chiral, the self-assembly of these compounds could be studied with circular dichroism (CD). Indeed, CD spectroscopy performed on solutions of **10a** and **10b** at a concentration of 3.5×10^{-5} M (UPy dimer concentration = 1.75×10^{-5} M) in heptane at room temperature showed the appearance of a Cotton effect, indicating the formation of an ordered, helical aggregate in this solvent (Figure 5.6a and 5.6b).²⁹ The reversibility of the aggregation process was further elucidated using temperature dependent CD spectroscopy. At high temperatures, the Cotton effect disappeared indicating the formation of unaggregated UPy-urea monomers or dimers while the Cotton effect reappeared at lower temperatures. At 20 °C, the Cotton effects of **10a** and **10b** at 220 nm are opposite in sign while the absolute value of the Cotton effects are 15.35 mdeg for UPy-urea **10a** (*R, S, S, S*) and 14.63 mdeg for

UPy-urea **10b** (*S, S, S, S*). As this small difference can be explained by the chiral purity¹⁷ of the starting material, it can be concluded that the chirality of the aliphatic chain directly attached to the pyrimidinone ring determines the helicity of the aggregates formed by UPy-urea dimers **10a**·**10a** and **10b**·**10b**.

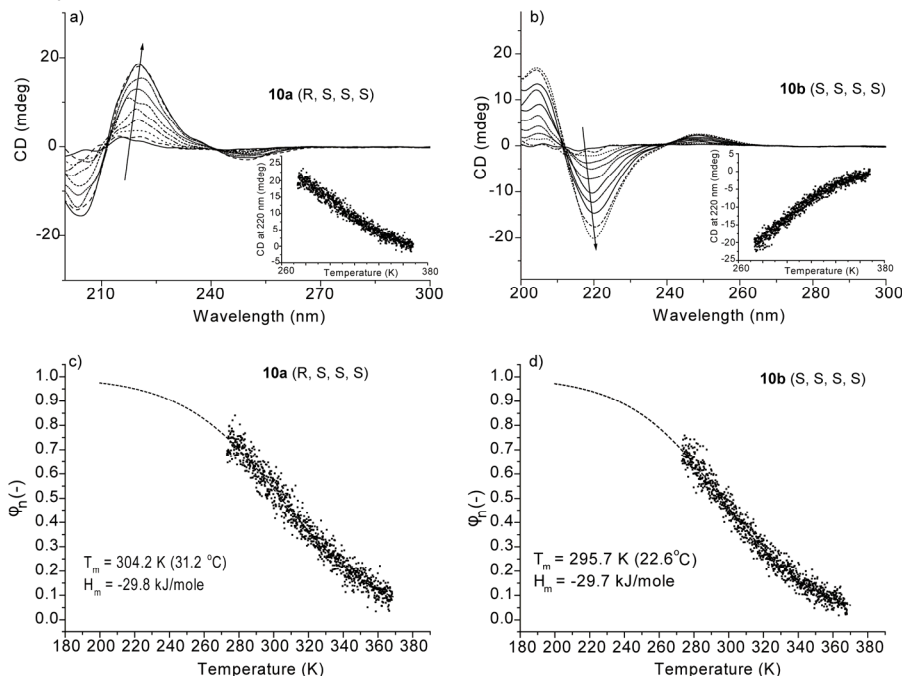


Figure 5.6: a) CD spectra of **10a** (*R, S, S, S*) in heptane (3.5×10^{-5} M) at temperatures between 0 and 90 °C with 10 °C intervals (arrow indicates increasing temperature). Inset shows the molar ellipticity at 220 nm as a function of temperature for the same solution. b) CD spectra of **10b** (*S, S, S, S*) in heptane (3.5×10^{-5} M) at temperatures between 0 and 90 °C with 10 °C intervals (arrow indicates increasing temperature). Inset shows the molar ellipticity at 220 nm as a function of temperature for the same solution. c) Normalized degree of aggregation for **10a**. d) Normalized degree of aggregation for **10b**. The solid lines in c and d are the best fitted curves using a temperature dependent isodesmic self-assembly model.

The cooling curves obtained from the temperature dependent changes of the Cotton effect at 220 nm for UPy-urea **10a** and **10b** are clearly sigmoidal (Figure 5.6a and b, inset) indicating that the self-assembly of the UPy-urea dimers into helical aggregates occurs via an isodesmic (equal K) self-assembly mechanism. Fitting of the normalized degree of aggregation using a temperature dependent isodesmic self-assembly model³⁰ showed a good correlation with the experimental data (Figure 5.6c and d). Using this model, the “melting” temperature of the stack (defined as the temperature at which $\phi_n = 0.5$) and the molecular enthalpy release due to noncovalent interactions (H_m) were obtained. Using the calculated fraction of aggregated material, an isodesmic equilibrium constant of 4.5×10^5 M⁻¹ at $T = 25$ °C for UPy-urea dimer **10a**·**10a** in heptane was calculated (Appendix E).

In contrast with the behaviour observed in heptane, a solution of **10a** in the more polar solvent isopropanol, at the same concentration in which a solution of **10a** in heptane showed the formation of a Cotton effect, did not show a Cotton effect, indicating that an ordered aggregate is not present in this solvent. From these results it can be concluded that intermolecular hydrogen bonding of the urea functionality plays an important role in the stabilization of the helical aggregate formed by UPy-urea dimer **10a·10a** as isopropanol is expected to compete with the intermolecular hydrogen bonds between UPy-urea dimers. This notion was further confirmed by temperature dependent CD measurements performed on UPy-urethane dimer **15·15** in heptane at an analytical concentration of **15** (*S, S, S, S*) of 2.5×10^{-5} M. The absence of a Cotton effect for UPy-urethane dimer **15·15**, while UPy-urea dimer **10a·10a** displays a Cotton effect at approximately the same concentration, clearly shows the necessity of strong intermolecular hydrogen bonding in the formation of ordered aggregates consisting of stacked UPy dimers.

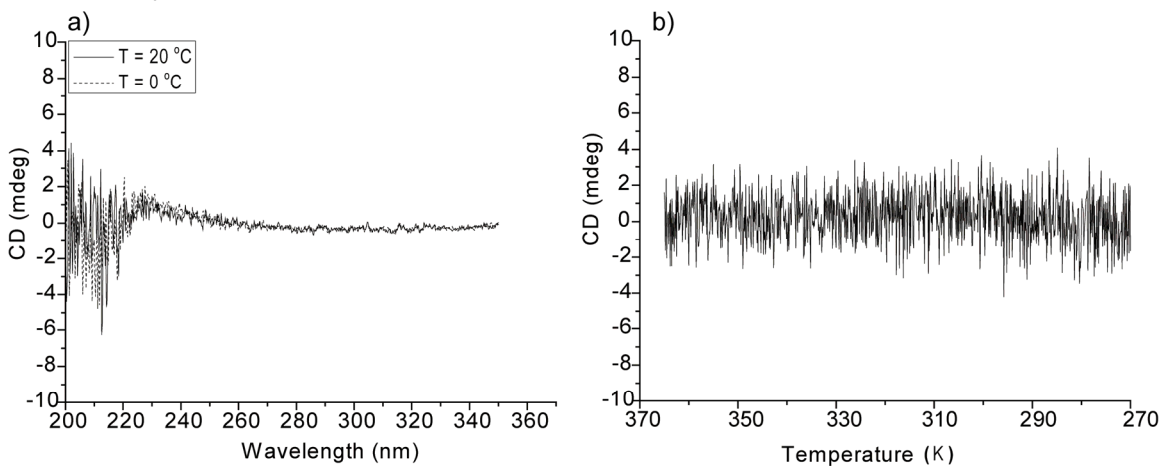


Figure 5.7: a) CD spectra of **15** (*R, S, S, S*) in heptane (2.5×10^{-5} M) at temperatures of $20\text{ }^\circ\text{C}$ and $0\text{ }^\circ\text{C}$. b) Molar ellipticity at 220 nm as a function of temperature for the same solution.

5.6 Discussion and conclusion

In this Chapter, the self-assembly of UPy dimers substituted with additional urea and urethane functionality has been studied in various solvents. $^1\text{H-NMR}$ dilution of UPy-urea dimer **10a·10a** in CDCl_3 showed concentration dependent chemical shifts for both urea protons as well as the alkylidene proton on the pyrimidinone ring. At high concentrations, the chemical shift of the two NH protons of the urea functionality shift downfield, indicative of the formation of a hydrogen bonded aggregate, while the chemical shift of the alkylidene proton shifts upfield, indicative of close contact between aromatic surfaces at high concentrations.

The concentration dependent chemical shifts were fitted with an isodesmic self-assembly model. The isodesmic self-assembly model assumes that each steps in the aggregation process occurs with the same thermodynamic constant, K . It should be noted however, that the equations that describe the concentration dependent chemical shift evolution as a result of dimerization and isodesmic aggregation are algebraically identical apart from a factor of 2.²⁷ Therefore, the quality of the fits cannot be used to distinguish between the two possible mechanisms. Recently, it has been shown that either a Van 't Hoff plot or the concentration dependence of the diffusion coefficient can be used to distinguish between the two possible mechanisms.³¹ However, fitting of the concentration dependent diffusion data of UPy-urea dimer **10a·10a** obtained by PGSE NMR, using a monomer-dimer model and assuming spherical aggregates clearly shows that this model is inappropriate to describe the concentration dependence of the diffusion constant (Appendix F). Hence, it can be concluded that the self-assembly of the UPy-urea dimer **10a·10a** in CDCl_3 occurs via an isodesmic mechanism. This notion is further confirmed by CD measurements performed in the apolar solvent heptane. In heptane, **10a** displays a temperature dependent Cotton effect, indicative of the formation of an ordered helical aggregate. Using the temperature dependent Cotton effect, the fraction of aggregated material at each temperature could be determined allowing the determination of the isodesmic equilibrium constant at room temperature ($4.5 \times 10^5 \text{ M}^{-1}$), while fitting of this value to a temperature dependent isodesmic aggregation model allowed for the determination of the molecular enthalpy release due to noncovalent interactions. Good agreement between the temperature dependent isodesmic self-assembly model and the fraction of aggregated molecules was found indicating that also in heptane the self-assembly of UPy-urea dimer **10a·10a** occurs in a stepwise manner.

The value of K in heptane is more than 1000 times higher than in CDCl_3 , as a result of stronger hydrogen bonds and stronger π - π interactions in the more apolar solvent heptane. In contrast to CDCl_3 , heptane is unable to disrupt the proposed one dimensional hydrogen bond array formed by the urea protons of aggregated **10a·10a**.³² Furthermore, aromatic-aromatic interactions present between UPy-urea dimers **10a·10a** are stronger in apolar solvents compared to halogenated solvents, such as chloroform as these compete with the π electrons of the aromatic group.³³

In contrast to the urea substituted UPy dimers, the urethane substituted UPy dimer **15·15** only display a small downfield shift of the NH proton and no upfield shift of the alkylidene proton in CDCl_3 . This behavior is translated to the more apolar solvent heptane as no Cotton effect is observed for **15·15** even at the lowest temperature. The lack of Cotton effect of Upy urethane dimer **15·15** in heptane shows that strong lateral

hydrogen bonding between the UPy dimers is necessary in order to form an ordered aggregate consisting of several UPy dimers.

The isodesmic self-assembly of UPy-urea aggregates in solution raises an interesting question on the melting behavior of UPy-urea substituted polymers in the bulk. In the bulk, a first order melting transition has been measured at high temperatures and it has been shown that this first order phase transition is directly associated with the breakdown of the UPy-urea aggregates.¹² How is then possible that a noncooperative growth process in dilute solution results in a first order phase transition in the bulk? Recent Monte Carlo simulations on isodesmic supramolecular polymers reveal that a nucleated first order phase transition is possible when a single supramolecular polymer condenses into a fibril consisting of multiple polymeric chains.³⁵ Hence, the first order melting transition of UPy-urea substituted polymers in the bulk is most probably the result of melting of fibers consisting of multiple UPy-urea aggregates associating via weak interactions.

Finally, by addition of monomeric UPy to a solution of UPy-urea **10a-10a**, the self-assembly of mixed UPy/UPy-urea heterodimers could be studied in CDCl₃ as the homo and hetero-dimers are in slow exchange on the ¹H-NMR timescale. Just as the UPy-urea homodimer, the mixed UPy/UPy-urea heterodimer aggregates in CDCl₃ as is evident by the concentration dependent chemical shift of the NH proton. The isodesmic equilibrium constant of the UPy/UPy-urea heterodimer in CDCl₃ is close to the square root of the isodesmic equilibrium constant of the UPy-urea homodimer indicating that the two urea groups in the homodimer do not act in a cooperative fashion during the self-assembly of UPy-urea homodimers into larger aggregates.

5.7 Experimental section

General Methods

See General Methods Chapter 2 and 3. All reactions were performed under an atmosphere of Argon. Dichloromethane was distilled over P₂O₅. Triethylamine was dried over KOH. Optical rotations were measured on a Jasco DIP-370 digital polarimeter at a wavelength of 589 nm (NaD line) and a temperature of 25 °C. 3,4,5-Tris[(S)-3,7-dimethyloctyloxy]aniline was prepared as previously reported by Van Gorp.^{3a}

Synthesis of 3(R),7-dimethyl-octanol (2a)

3(R),7-Dimethyl-6-octen-1-ol **1a** (10.40 g, 66.6 mmol) was dissolved in ethyl acetate (75 mL) and bubbled through by argon for 15 min. Pd/C (0.5 g) was added and the solution was catalytically hydrogenated in a Parr apparatus and after 24 h no more H₂ was taken up. The suspension was filtered over Celite and washed with ethyl acetate (20 mL). After evaporation *in vacuo* pure 3(R),7-

dimethyl-octanol **1a** was obtained as an colourless oil (9.71 g, 61.43 mmol). Yield: 92%. ¹H-NMR (CDCl₃): δ = 3.67-3.58 (m, 2H, CH₂-OH), 1.62-1.47 (m, 3H, -CH₂-, (CH₂)₂CHCH₃), 1.39-1.06 (m, 7H, -CH₂-, (CH₂)₂CH(CH₃)₂), 0.89 (d, 3H, CHCH₃), 0.87 (d, 6H, CH(CH₃)₂). ¹³C-NMR (CDCl₃): δ = 60.0 (C-OH), 39.9, 39.2, 37.3, 29.5, 27.9, 24.6, 22.6 (-CH₂-), 22.5 (CHCH₃), 19.6 (CH(CH₃)₂). IR (ATR): ν = 3324, 2954, 2926, 2870, 1464, 1383, 1366, 1052, 1010, 966 cm⁻¹. $[\alpha]_D^{25} = +3.734$ (neat).

Synthesis of 3(R),7-Dimethyl-octanoic acid (3a)

Periodic acid (31.15 g, 136.8 mmol) was dissolved in acetonitrile (500 mL) and the mixture was vigorously stirred at room temperature for 40 min. The solution was cooled on an ice bath and a solution of 3(R),7-dimethyl-octanol **2a** (9.71 g, 61.3 mmol) and acetonitrile (125 mL) was added dropwise. Pyridinium chlorochromate (0.272 g, 1.27 mmol) was added and the solution was stirred for an additional 15 min. The reaction mixture was stirred for 3 h at room temperature after which the acetonitrile was evaporated *in vacuo* and ethyl acetate (1000 mL) was added and extracted with H₂O:brine 1:1 v/v (600 mL), saturated NaHSO₃ (1000 mL) and brine (1000 mL), respectively. The organic layer was dried over anhydrous MgSO₄, filtered and evaporated *in vacuo*. Kügel-Rohr distillation (1 mbar, 120 °C) yielded the pure acid as yellow oil (8.54 g, 49.57 mmol). Yield: 81%. ¹H-NMR (CDCl₃): δ = 12.0 (s, 1H, C-OH), 2.36-2.31 (dd, 1H, CH₂COOH), 2.15-2.10 (dd, 1H, CH₂COOH), 1.97-1.93 (m, 1H, (CH₂)₂CHCH₃), 1.55-1.48 (m, 1H, CH₂CH(CH₃)₂), 1.31-1.12 (m, 6H, -CH₂-), 0.95 (d, 3H, CHCH₃), 0.86 (d, 6H, CH(CH₃)₂). ¹³C-NMR (CDCl₃): δ = 180.3 (COOH), 41.7 ((C=O)CH₂), 39.0, 36.9, 30.1, 27.9, 24.6, 22.6 (-CH₂-), 22.5 (CHCH₃), 19.6 (CH(CH₃)₂). IR (ATR): ν = 2956, 2928, 2870, 2678, 1705, 1463, 1410, 1293, 1220, 936 cm⁻¹. $[\alpha]_D^{25} = +4.61$ (neat).

Synthesis of 3(S),7-dimethyl-octanoic acid (3b)

Periodic acid (15.24 g, 66.9 mmol, 2.2 eq) was dissolved in acetonitrile (240 mL) during 30 min. The solution was cooled on an ice bath and a solution of 3(S),7-dimethyloctanol (**2b**) (4.7502 g, 30.0 mmol) in acetonitrile (60 mL) was added dropwise. Pyridinium chlorochromate (0.1330 g, 0.62 mmol) was added and an additional 15 min was stirred. After stirring at room temperature for 3.5 h, ethyl acetate (600 mL) was added and the organic layer was extracted with H₂O:brine 1:1 v/v (600 mL), saturated NaHSO₃ (500 mL) and brine (500 mL). Column chromatography (SiO₂, CHCl₃/EtOH 100:0 to 95:5 v/v) yielded the pure acid as a colorless oil (2.76 g, 16.00 mmol). Yield: 54%. ¹H-NMR (CDCl₃): δ = 2.35 (dd, 1H, CH₂COOH), 2.15 (dd, 1H, CH₂COOH), 1.98-1.93 (m, 1H, (CH₂)₂CHCH₃), 1.56-1.47 (m, 1H, CH₂CH(CH₃)₂), 1.35-1.12 (m, 6H, -CH₂-), 0.98 (d, 3H, CHCH₃), 0.86 (d, 6H, CH(CH₃)₂). ¹³C-NMR (CDCl₃): δ = 179.4 (COOH), 41.5 ((C=O)CH₂), 39.0, 36.9, 30.2, 27.9, 24.6, 22.6 (-CH₂-), 22.5 (CHCH₃), 19.7(CH(CH₃)₂). IR (ATR): ν = 2957, 2929, 2871, 2672, 1709, 1464, 1411, 1384, 1294, 1221, 937 cm⁻¹. $[\alpha]_D^{25} = -4.36$ (neat).

Synthesis of 3(R),7-dimethyl octanoic acid chloride (4a)

Under an argon atmosphere 3(R),7-dimethyl octanoic acid **3a** (8.54 g, 49.51 mmol) was dissolved in distilled dichloromethane (100 mL). The solution was cooled on an ice bath and a drop of dimethylformamide was added. A solution of oxalyl chloride (5.3 mL, 59.41 mmol) in dry dichloromethane (60 mL) was added dropwise and the solution was stirred at room temperature overnight. Evaporation of the solvent and excess oxalyl chloride followed by flushing with

toluene, yielded a yellow oil (8.50 g, 44.57 mmol). Yield: 90%. ¹H-NMR (CDCl₃): δ = 2.90-2.85 (dd, 1H, (COOH)CH₂), 2.70-2.64 (dd, 1H, (COOH)CH₂), 2.16-2.07 (m, 1H, (CH₂)₂CHCH₃), 1.56-1.50 (m, 1H, CH₂CH(CH₃)₂), 1.34-1.13 (m, 6H, -CH₂-), 0.98 (d, 3H, CHCH₃), 0.88 ((d, 6H, CH(CH₃)₂). ¹³C-NMR (CDCl₃): δ = 173.0 (C=O), 54.2 ((COOH)CH₂), 38.8, 36.3, 30.7, 27.8, 24.5, 22.6 (-CH₂-), 22.5 (CHCH₃), 19.2 (CH(CH₃)₂). IR (ATR): ν = 2957, 2930, 2871, 1798, 1464, 1385, 985, 967, 929, 724 cm⁻¹.

Synthesis of 3(S),7-dimethyl-octanoic acid chloride (4b)

3(S),7-dimethyl-octanoic acid **3b** (2.76 g, 16.00 mmol) was dissolved in dry dichloromethane (30 mL) under an argon atmosphere and cooled on an ice bath. A solution of oxalyl chloride (1.65 mL, 19.22 mmol, 1.2 eq) in dry dichloromethane (20 mL) was added dropwise and the solution was stirred under an argon atmosphere at room temperature for an additional 3 h. Evaporation of the solvent and the excess oxalyl chloride *in vacuo* yielded a yellow oil (2.78 g, 14.6 mmol) which was used as such. Yield: 92%. ¹H-NMR (CDCl₃): δ = 2.88 (dd, 1H, (COOH)CH₂), 2.71 (dd, 1H, (COOH)CH₂), 2.10-2.08 (m, 1H, (CH₂)₂CHCH₃), 1.59-1.51 (m, 1H, CH₂CH(CH₃)₂), 1.36-1.14 (m, 6H, -CH₂-), 1.00 (d, 3H, CHCH₃), 0.89 (d, 6H, CH(CH₃)₂). ¹³C-NMR (CDCl₃): δ = 173.2 (C=O), 54.2 ((COOH)CH₂), 38.9, 36.3, 30.7, 27.9, 24.5, 22.6 (-CH₂-), 22.5 (CHCH₃), 19.2 (CH(CH₃)₂). IR (ATR): ν = 2957, 2930, 2870, 1799, 1464, 1384, 985, 967, 929 cm⁻¹.

Synthesis of 5(R),9-dimethyl-3-oxo-decanoic acid ethyl ester (5a)

Potassium ethyl malonate (11.8 g, 66.8 mmol) and dry ethyl acetate (100 mL) were transferred to a round bottom flask. The mixture was cooled on an ice bath under an argon atmosphere. To this mixture was added Et₃N (12.1 g, 119.5 mmol) followed by dry MgCl₂ (5.46 g, 57.4 mmol). The mixture was heated at 35 °C for 6 h and subsequently cooled on an ice bath and a solution of 3(R),7-dimethyl octanoic acid chloride **4a** (8.3 g, 43.5 mmol) in dry ethyl acetate (35 mL) was added dropwise. The mixture was allowed to stir at room temperature for 19 h and then cooled down on an ice bath adding 13% HCl (120 mL) carefully while keeping the temperature below 25°C. The aqueous layer was separated and then back extracted with CHCl₃: ethyl acetate 1:1 v/v (65 ml). The combined organic layers were washed with 13% HCl (2x 65 mL), followed by H₂O (70 mL), brine (70 mL) and 5 wt% KHCO₃ (150 mL). The organic layer was dried over sodium sulfate, filtered and evaporated *in vacuo*. Column chromatography (SiO₂, CHCl₃:methanol 100:0 to 98:2 v/v), yielded the pure product as a yellow oil (7.4 g, 30.53 mmol). Yield: 70%. ¹H-NMR (CDCl₃): δ = 4.22-4.16 (d, 2H, OCH₂CH₃), 3.41 (s, 2H, (C=O)CH₂(COOEt)), 2.54-2.49 (dd, 1H, CH₂(C=O)(COOEt)), 2.36-2.30 (dd, 1H, CH₂(C=O)(COOEt)), 2.02-1.81 (m, 1H, (CH₂)₂CHCH₃), 1.55-1.48 (m, 1H, CH₂CH(CH₃)₂), 1.33-1.10 (m, 6H, -CH₂-), 0.91-0.85 (m, 12H, -CH₃). ¹³C-NMR (CDCl₃): δ = 202.4 (C=O), 167.0 ((O=C)O), 61.1(OCH₂), 50.3 ((C=O)CH₂(COOEt)), 49.6 ((C=O)CH₂), 38.9, 36.9, 28.8, 27.8, 24.5, 22.5, 22.4, 19.6 (-CH₂-), 19.3 (CHCH₃), 14.0 (CH(CH₃)₂). IR (ATR): ν = 2956, 2929, 2871, 1744, 1716, 1647, 1630, 1465, 1367, 1315, 1232, 1150, 1096, 1030 cm⁻¹. $[\alpha]_D^{25} = +2.332$ (neat).

Synthesis of 5(S),9-dimethyl-3-oxo-decanoic acid ethyl ester (5b)

Ethyl potassium malonate (3.81 g, 22.38 mmol, 1.4 eq) was dissolved in dry ethyl acetate (35 mL) and cooled on an ice bath under an argon atmosphere. Et₃N (4.05 g, 40.02 mmol, 2.5 eq) and dry

MgCl₂ (1.83 g, 19.22 mmol, 1.2 eq) were added and stirred at 35 °C for 6.5 h. The suspension was cooled on an ice bath and a solution of 3(S),7-dimethyl octanoic acid chloride **4b** in dry ethyl acetate (10 mL) was added dropwise. The suspension was stirred at room temperature for 19 h, after which it was cooled on an ice bath and 13% HCl (40 mL) was gently added. The solution was stirred at room temperature for 15 min after which the layers were separated. The aqueous layer was extracted with CHCl₃:ethyl acetate 1:1 *v/v* (20 mL). The combined organic layers were extracted with 13% HCl (2 x 20 mL), H₂O (20 mL) and brine (20 mL). Additional washing with 5 wt% KHCO₃ removed the unreacted ethyl potassium malonate present. The organic layer was dried over sodium sulfate and removal of the solvent *in vacuo* yielded the product (3.35 g, 13.83 mmol) as an orange oil. Yield: 96%. ¹H-NMR (CDCl₃): δ = 4.28-4.12 (q, 2H, OCH₂CH₃), 3.44 (s, 2H, (C=O)CH₂(COOEt)), 2.50 (dd, 1H, CH₂(C=O)(COOEt)), 2.37 (dd, 1H, CH₂(C=O)(COOEt)), 2.08-1.97 (m, 1H, (CH₂)₂CHCH₃), 1.53 (m, 1H, CH₂CH(CH₃)₂), 1.35-1.11 (m, 6H, -CH₂-), 0.93-0.87 (m, 12H, -CH₃). ¹³C-NMR (CDCl₃): δ = 202.7 (C=O), 167.2 ((O=C)O), 61.3 (OCH₂), 50.4 ((C=O)CH₂(COOEt)), 49.8 ((C=O)CH₂), 39.0, 37.0, 36.9, 29.0, 27.9, 24.6, 22.6, 22.5, 19.7 (-CH₂-), 19.7 (CHCH₃), 14.1 (CH(CH₃)₂). IR (ATR): ν = 2956, 2939, 2871, 1743, 1716, 1647, 1465, 1411, 1367, 1315, 1233, 1151, 1096, 1031 cm⁻¹. [α]_D²⁵ = -1.56 (neat).

Synthesis of 2-amino-6-(2(R),6 dimethylheptyl)-6[1H]-pyrimidinone (6a)

5(R),9-dimethyl-3-oxo-decanoic acid ethyl ester **5a** (7.4 g, 30.53 mmol), guanidinium carbonate (3.364 g, 40.30 mmol, 1.3 eq) and potassium *tert*-butoxide (3.43 g, 30.53 mmol) were dissolved in ethanol (120 mL) and stirred at reflux temperature for 65 h. The solvent was evaporated *in vacuo* and CHCl₃ (400 mL) was added. The organic layer was extracted with 10% citric acid (2x 200 mL), saturated KHCO₃ (2x 200 mL) and brine (2x 200 mL). The organic layer was dried over sodium sulfate. The product was concentrated *in vacuo* and precipitated in pentane. Column chromatography (SiO₂, CHCl₃:EtOH 100:0 to 95:5 *v/v*) yielded the pure isocytosine (4.45 g, 18.73 mmol) as a slightly yellow solid, mp: 201.9-208.7 °C. Yield: 61%. ¹H-NMR (CDCl₃): δ = 7.00 (bs, 3H, NH), 5.56 (s, 1H, C=CH), 2.42-2.37 (dd, 1H, (CH=C)-CH₂CH(CH₃)(CH₂), 2.14-2.09 (dd, 1H, (CH=C)-CH₂CH(CH₃)(CH₂)), 1.83 (m, 1H, (CH₂)₂CHCH₃), 1.53-1.46 (m, 1H, CH₂CH(CH₃)₂), 1.31-1.10 (m, 6H, -CH₂-), 0.89-0.84 (m, 9H, -CH₃). ¹³C-NMR (CDCl₃): δ = 38.9, 36.8, 27.7, 24.5, 22.5 (-CH₂-), 22.3 (CHCH₃), 19.1 (CH(CH₃)₂) (incomplete). IR (ATR): ν = 3320, 3104, 2953, 2926, 2869, 2742, 1645, 1612, 1520, 1467, 1384 cm⁻¹. MALDI-TOF-MS (m/z): 237.18. Observed: 238.27 (MH⁺). Anal. Calcd for C₁₃H₂₃N₃O: C 65.79, H 9.77, N 17.70. Found: C 66.12, H 9.78, N 17.85. [α]_D²⁵ = +0.031 (0.02 g/mL CHCl₃).

Synthesis of 2-amino-6-(2(S),6-dimethylheptyl)-6[1H]-pyrimidinone (6b)

5(S),9-dimethyl-3-oxo-decanoic acid ethyl ester **5b** (3.263 g, 13.46 mmol), guanidinium carbonate (1.60 g, 17.76 mmol, 1.3 eq) and potassium *tert*-butoxide (1.51 g, 13.46 mmol) were dissolved in ethanol (50 mL) and stirred at reflux temperature for 43 h. The solvent was evaporated *in vacuo* and CHCl₃ (50 mL) was added. The organic layer was extracted with saturated KHCO₃ (2x 30 mL) and brine (2x 30 mL). The organic layer was dried over sodium sulphate. The product was concentrated *in vacuo* and precipitated in pentane. Column chromatography (SiO₂, CHCl₃:EtOH

100:0 to 95:5 *v/v*) yielded the pure isocytosine (0.903 g, 3.79 mmol) as a slightly yellow solid, mp: 203 °C. Yield: 30%. ¹H-NMR (CDCl₃): δ = 6.93 (bs, 3H, NH), 5.61 (s, 1H, C=CH), 2.39 (dd, 1H, (CH=C)-CH₂CH(CH₃)(CH₂), 2.14 (dd, 1H, (CH=C)-CH₂CH(CH₃)(CH₂), 1.84 (m, 1H, (CH₂)₂CHCH₃), 1.52 (m, 1H, CH₂CH(CH₃)₂), 1.33-1.13 (m, 6H, -CH₂-), 0.90-0.81 (m, 9H, -CH₃). ¹³C-NMR (CDCl₃): δ = 39.1, 37.0, 32.2, 27.9, 24.7, 22.7 (-CH₂-), 22.6 (CHCH₃), 19.3 (CH(CH₃)₂) (incomplete). IR (ATR): ν = 3334, 3070, 2955, 2929, 2869, 1655, 1480, 1376, 1284, 1171, 825, 767 cm⁻¹. MALDI-TOF-MS (m/z): 237.18. Observed: 238.08 (MH⁺). Anal. Calcd for C₁₃H₂₃N₃O: C 65.79, H 9.77, N 17.70. Found: C 65.73, H 9.72, N 17.58. $[\alpha]_D^{25} = -0.028$ (0.02 g/mL CHCl₃).

Synthesis of 2-(1-imidazolylcarbonylamino)-6-(2(R),6-dimethylheptyl)-4[1H]-pyrimidinone (7a)
2-amino-6-(2(R),6 dimethylheptyl)-6[1H]-pyrimidinone **6a** (1.5 g, 6.31 mmol) and 1,1'-carbonyldiimidazole (1.24 g, 7.58 mmol) were dissolved in dry CHCl₃ (20 mL) under an argon atmosphere at 50 °C and stirred overnight. CHCl₃ (50 mL) was added and the organic layer was extracted with H₂O (2x 35 ml) and brine (2 x 35 ml). The organic layer was dried over magnesium sulphate and evaporated *in vacuo*. Trituration in diethyl ether (20 mL) yielded the product as a white solid (1.62 g, 4.89 mmol). Yield: 77%. ¹H-NMR (CDCl₃): δ = 12.01-11.86 (bs, 2H, NH), 8.86 (s, 8.86, N-CH=N), 7.64 (s, 1H, (C=O)N-CH=CH), 7.02 (s, 1H, (C=O)N-CH=CH), 5.79 (s, 1H, C=CH), 2.63-2.60 (dd, 1H, (CH=C)-CH₂CH(CH₃)(CH₂), 2.46-2.41 (dd, 1H, (CH=C)-CH₂CH(CH₃)(CH₂)), 1.97-2.00 (m, 1H, (CH₂)₂CHCH₃), 1.54-1.51 (m, 1H, CH₂CH(CH₃)₂), 1.44-1.15 (m, 6H, -CH₂-), 1.00-0.86 (m, 9H, -CH₃).

Synthesis of 2-(1-imidazolylcarbonylamino)-6-(2(S),6-dimethylheptyl)-4[1H]-pyrimidinone (7b)

2-Amino-6-(2(S),6-dimethylheptyl)-6[1H]-pyrimidinone **6b** (0.526 g, 2.21 mmol) and 1,1'-carbonyldiimidazole (0.396 g, 2.44 mmol, 1.2 eq) were dissolved in dry CHCl₃ (3 mL) under an argon atmosphere and stirred at 50 °C for 4 h. CHCl₃ (10 mL) was added and extracted with H₂O (2 x 15 mL) and brine (15 mL). The organic layer was dried over sodium sulphate. Evaporation of the solvent *in vacuo* yielded the product (0.693 g, 2.08 mmol) as a yellow solid. Yield: 94%. ¹H-NMR (CDCl₃): δ = 8.85 (s, 1H, N-CH=N), 7.65 (s, 1H, (C=O)N-CH=CH), 7.03 (s, 1H, (C=O)N-CH=CH), 5.79 (s, 1H, C=CH), 2.62 (dd, 1H, (CH=C)-CH₂CH(CH₃)(CH₂)), 2.44 (dd, 1H, (CH=C)-CH₂CH(CH₃)(CH₂)), 1.99 (m, 1H, (CH₂)₂CHCH₃), 1.56-1.13 (m, 7H, -CH₂-), 1.01 (d, 3H, -CH₃), 0.86 (d, 6H, -CH₃). ¹³C-NMR (CDCl₃): δ = 199.6, 161.0, 157.6, 157.1, 155.9, 138.3, 128.2, 118.0, 105.4, 90.3, 57.5, 41.0, 39.4, 37.2, 32.6, 28.3, 24.9, 23.0, 22.8, 19.5. IR (ATR): ν = 3165, 3070, 2953, 2927, 2868, 1708, 1654, 1599, 1465, 1363, 1317, 1274, 1231, 1221, 1182, 1093, 1060, 1030, 986 cm⁻¹.

Synthesis of 2-(6-[t-butoxycarbonylamino]-hexylureido)-6-(2(R),6-dimethylheptyl)-4[1H]-pyrimidinone (8a)

2-(1-Imidazolylcarbonylamino)-6-(2(R),6-dimethylheptyl)-4[1H]-pyrimidinone **7a** (1.60 g, 4.83 mmol) and mono-BOC protected 1,6-hexanediamine (1.25 g, 5.77 mmol) were dissolved in dry CHCl₃ (20 mL) under an argon atmosphere and stirred at 50 °C for 17 h. CHCl₃ (100 mL) was added and the solution was extracted with 1 M HCl (60 mL), saturated NaHCO₃ (60 mL) and brine (60 mL). The organic layer was dried over magnesium sulfate, filtered and evaporated *in*

vacuo. This yielded the product as a white solid (2.17 g, 4.52 mmol), mp: 122.0-123.1 °C Yield: 94%. ¹H-NMR (CDCl₃): δ = 13.18 (s, 1H, C=C-NH-C), 11.87 (s, 1H, C-NH-(C=O)), 10.17 (s, 1H, (C=O)NH-CH₂), 5.82 (s, 1H, C=CH), 4.64 (s, 1H, NH-BOC) 3.32-3.19 (q, 2H, NH-CH₂-CH₂), 3.17-3.08 (q, 2H, CH₂CH₂-NH-BOC), 2.51-2.39 (dd, 1H, (CH=C)-CH₂CH(CH₃)(CH₂)), 2.32-2.16 (dd, 1H, (CH=C)-CH₂CH(CH₃)(CH₂)), 1.82 (m, 1H, (CH₂)₂CHCH₃), 1.61 (m, 1H, CH₂CH(CH₃)₂), 1.60-1.03 (m, 23H, -CH₂-, -CH₃), 0.99-0.65 (m, 9H, -CH₃). ¹³C-NMR (CDCl₃): δ = 173.1, 156.6, 155.9, 154.7, 151.5, 106.8, 78.9 (OC(CH₃)₃), 40.4, 39.7, 38.9, 16.6, 31.9, 29.8, 29.3, 28.4, 27.8, 26.4, 26.2, 24.5, 22.6, 22.5, 19.2. IR (ATR): ν = 3217, 1954, 2929, 2868, 1698, 1659, 1585, 1525, 1462, 1390, 1365, 1251, 1172, 1140, 801 cm⁻¹. Anal. Calcd for C₂₅H₄₅N₅O₄: C 62.60, H 9.46, N 14.60. Found: C 62.37, H 9.44, N 14.66. MALDI-TOF-MS (m/z): 479.35. Observed = 480.22 (MH⁺), 502.21 (MNa⁺). [α]_D²⁵ = +0.48 (50 mg/mL CHCl₃).

Synthesis of 2-(6-[*t*-butoxycarbonylamino]-hexylureido)-6-(2(*S*),6-dimethylheptyl)-4[1*H*]-pyrimidinone (8b)

2-(1-Imidazolylcarbonylamino)-6-(2(*S*),6-dimethylheptyl)-4[1*H*]-pyrimidinone **7b** (0.619 g, 1.87 mmol) and mono-BOC protected 1,6-hexanediamine (0.495 g, 2.29 mmol, 1.2 eq) were dissolved in dry CHCl₃ (14 mL) under an argon atmosphere and stirred at 52 °C for 17 h. CHCl₃ (30 mL) was added and the solution was extracted with 1 M HCl (25 mL), saturated NaHCO₃ (25 mL) and brine (25 mL). The organic layer was dried over sodium sulfate. Evaporation of the solvent *in vacuo* yielded the product (0.553 g, 1.15 mmol) as a white solid, mp: 122 °C. Yield: 62%. ¹H-NMR (CDCl₃): δ = 13.17 (s, 1H, C=C-NH-C), 11.87 (s, 1H, C-NH-(C=O)), 10.17 (s, 1H, (C=O)NH-CH₂), 5.82 (s, 1H, C=CH), 4.64 (s, 1H, NH-BOC), 3.24 (q, 2H, NH-CH₂-CH₂), 3.09 (q, 2H, CH₂CH₂-NH-BOC), 2.44 (dd, 1H, (CH=C)-CH₂CH(CH₃)(CH₂)), 2.24 (dd, 1H, (CH=C)-CH₂CH(CH₃)(CH₂)), 1.83 (m, 1H, (CH₂)₂CHCH₃), 1.63-1.12 (m, 24H, -CH₂-, -CH₃), 0.94 (d, 3H, -CH₃), 0.86 (d, 6H, -CH₃). ¹³C-NMR (CDCl₃): δ = 173.2, 156.6, 156.0, 154.7, 151.5, 106.9, 79.0 (OC(CH₃)₃), 40.5, 39.8, 39.0, 36.7, 31.9, 29.9, 29.4, 28.4, 27.9, 26.4, 26.3, 24.5, 22.7, 22.5, 19.3. IR (ATR): ν = 3372, 3216, 2955, 2928, 2858, 1698, 1683, 1645, 1578, 1519, 1463, 1446, 1365, 1249, 1170, 804 cm⁻¹. MALDI-TOF-MS (m/z): 479.35. Observed m/z = 480.26 (MH⁺), 502.26 (MNa⁺). Anal. Calcd for C₂₅H₄₅N₅O₄: C 62.60, H 9.46, N 14.60. Found: C 62.69, H 9.45, N 14.50. [α]_D²⁵ = -0.52 (50 mg/mL CHCl₃).

Synthesis of 2-(6-Amino-hexylureido)-6-(2(*R*),6-dimethylheptyl)-4[1*H*]-pyrimidinone (9a)

2-(6-[*t*-Butoxycarbonylamino]-hexylureido)-6-(2(*R*),6-dimethylheptyl)-4[1*H*]-pyrimidinone **8a** (2.17 g, 4.52 mmol) was stirred in distilled dichloromethane (200 mL). Trifluoroacetic acid (TFA) (65 mL, 30 eq) was added at room temperature and the mixture was stirred for 13 h. Afterwards, trifluoroacetic acid and dichloromethane were evaporated *in vacuo* and the remaining solid was flushed several times with toluene. Trituration with diethyl ether (25 mL) yielded the product as a white solid (1.96 g, 3.97 mmol), mp: 123.4-130.3 °C. Yield: 88%. ¹H-NMR (DMSO-d₆): δ = 10.6-8.4 (bs, 2H, C-NH-(C=O), (C=O)NH-CH₂), 7.73 (s, 1H, CH₂-NH₃⁺), 7.61 (s, 1H, C=C-NH-C), 5.76 (s, 1H, C=CH), 3.17-3.12 (q, 2H, NH-CH₂-CH₂), 2.80-2.75 (q, 2H, CH₂CH₂-NH₃⁺), 2.38-2.30 (dd, 1H, (CH=C)-CH₂CH(CH₃)(CH₂)), 2.17-2.12 (dd, 1H, (CH=C)-CH₂CH(CH₃)(CH₂)), 1.90-1.78 (m, 1H, (CH₂)₂CHCH₃), 1.55-1.44 (m, 1H, CH₂CH(CH₃)₂), 1.39-1.09 (m, 14H, -CH₂-), 0.87-0.79 (m, 9H, -

CH_3). ^{13}C -NMR (DMSO- d_6): $\delta = 167.6, 162.7, 155.7, 152.5, 106.1, 44.9, 39.7, 39.5, 37.3, 32.4, 29.9, 28.3, 27.9, 26.7, 26.4, 25.1, 23.5, 23.4, 20.2$. IR (ATR): $\nu = 2934, 2866, 1698, 1640, 1575, 1526, 1465, 1435, 1251, 1202, 1182, 1133, 835, 798, 722\text{ cm}^{-1}$. MALDI-TOF-MS (m/z): 379.29, Observed: 380.41 (MH^+), 402.40 (MNa^+). Anal. Calcd for $\text{C}_{22}\text{H}_{39}\text{F}_3\text{N}_5\text{O}_4$: C 53.54, H 7.76, N 14.19. Found: C 52.50, H 7.40, N 13.75 (0.15 eq TFA).

Synthesis of 2-(6-amino-hexylureido)-6-(2(S),6-dimethylheptyl)-4[1H]-pyrimidinone (9b)

2-(6-[*t*-Butoxycarbonylamino]-hexylureido)-6-(2(S),6-dimethylheptyl)-4[1H]-pyrimidinone **8a** (2.40 g, 5.0 mmol) was stirred in distilled dichloromethane (140 mL). Trifluoroacetic acid (TFA) (12 mL) was added dropwise during 1 h at room temperature and the mixture was stirred for an additional 3 h. Afterwards, the trifluoroacetic acid and dichloromethane were evaporated *in vacuo* and the oil was repeatedly dissolved in toluene and evaporated *in vacuo* to yield a brown oil which slowly solidified (2.41 g, 4.88 mmol). Yield: 98%. ^1H -NMR (CDCl_3): $\delta = 5.95$ (s, 1H, C=CH), 4.93 (s, 3H, $\text{CH}_2\text{-NH}_3^+$), 3.24 (q, 2H, $\text{NH-CH}_2\text{-CH}_2$), 2.92 (t, CH_2NH_2), 2.54 (dd, 1H, (CH=C)- $\text{CH}_2\text{CH}(\text{CH}_3)(\text{CH}_2)$), 2.34 (dd, 1H, (CH=C)- $\text{CH}_2\text{CH}(\text{CH}_3)(\text{CH}_2)$), 1.88 (m, 1H, $(\text{CH}_2)_2\text{CHCH}_3$), 1.68-1.15 (m, 15H, $-\text{CH}_2-$), 0.93 (d, 3H, $-\text{CH}_3$), 0.88 (d, 6H, $-\text{CH}_3$). ^{13}C -NMR (DMSO- d_6): $\delta = 167.0, 162.3, 155.1, 152.0, 105.5, 44.3, 39.1, 38.6, 36.7, 31.9, 29.4, 27.8, 27.4, 26.2, 25.8, 24.6, 23.0, 22.8, 19.6$. IR (ATR): $\nu = 3279, 2957, 2934, 2871, 2555, 1687, 1637, 1545, 1369, 1255, 1179, 1142\text{ cm}^{-1}$. MALDI-TOF-MS (m/z): 379.29. Observed: 380.44 (MH^+), 402.43 (MNa^+). Anal. Calcd for $\text{C}_{22}\text{H}_{39}\text{F}_3\text{N}_5\text{O}_4$: C 53.54, H 7.76, N 14.19. Found: C 50.14, H 7.12, N 12.90 (0.5 eq TFA).

Synthesis of 2-{6-(3,4,5-tris(3(S),7-dimethyloctyoxo)-phenylureido)-hexylureido-6-(2(R), 6-dimethylheptyl)-4[1H]-pyrimidinone (10a)

2-(6-Amino-hexylureido)-6-(2(R),6-dimethylheptyl)-4[1H]-pyrimidinone **9a** (0.50 g, 1.01 mmol) was dissolved in dry Et_3N (0.11 g, 1.11 mmol, 1.1 eq) and distilled CHCl_3 (20 mL). 3,4,5-tris(3(S),7-dimethyloctyoxo)-phenyl isocyanate **11** (0.71 g, 1.22 mmol, 1.2 eq) was added and the mixture stirred under argon atmosphere at 50 °C, during a period of 48 hours. Afterwards, CHCl_3 (15 mL) was added and the organic layer was extracted with NaHCO_3 (25 ml), citric acid (25 mL, pH 3~4) and brine (25 mL). The organic layer was dried over magnesium sulfate and evaporated *in vacuo*. The pure product was obtained after column chromatography (SiO_2 , CHCl_3 :ethanol, 98:2 to 95:5, v/v) and precipitation in cold acetonitrile (40 mL) as an off white solid (0.43 g, 0.44 mmol), mp: 99.8-102.9 °C. Yield: 45%. ^1H -NMR (CDCl_3): $\delta = 13.32$ (s, 1H, C-NH-C), 11.75 (s, 1H, C-NH-C=O), 10.03 (s, 1H, O=C-NH- CH_2), 7.74 (s, 1H, O=C-NH- C_{arom}), 6.74 (s, 2H, CH_{arom}), 5.78 (s, 1H, C=CH), 5.73 (s, 1H, $\text{CH}_2\text{-NH-C=O}$), 3.99-3.86 (m, 6H, O- CH_2-), 3.25-3.17 (m, 4H, HN- $\text{CH}_2\text{-CH}_2$), 2.51-2.45 (dd, 1H, (CH=C)- $\text{CH}_2\text{CH}(\text{CH}_3)(\text{CH}_2)$), 2.25-2.19 (dd, 1H, (CH=C)- $\text{CH}_2\text{CH}(\text{CH}_3)(\text{CH}_2)$), 1.85-1.11 (m, 46H, alkyl-H), 0.97-0.84 (m, 36H, $-\text{CH}_3$). ^1H -NMR (DMF- d_6): $\delta = 12.08$ -11.72 (bs, 1H, C-NH-C), 10.04-9.63 (bs, 1H, C-NH-C=O), 8.53 (s, 1H, O=C-NH- C_{arom}), 8.03-7.81 (bs, 1H, O=C-NH- CH_2), 7.07 (s, 2H, CH_{arom}), 6.35 (s, 1H, $\text{CH}_2\text{-NH-C=O}$), 5.96 (s, 1H, C=CH), 4.20-4.01 (m, 6H, O- CH_2-), 3.44-3.32 (m, 4H, HN- $\text{CH}_2\text{-CH}_2$), 2.61-2.57 (dd, 1H, (CH=C)- $\text{CH}_2\text{CH}(\text{CH}_3)(\text{CH}_2)$), 2.37-2.32 (dd, 1H, (CH=C)- $\text{CH}_2\text{CH}(\text{CH}_3)(\text{CH}_2)$), 2.03-1.26 (m, 46H, alkyl-H), 1.21-1.01 (m, 36H, $-\text{CH}_3$). ^{13}C -NMR (CDCl_3): $\delta = 173.5, 156.3, 156.2, 154.8, 153.3, 152.3, 135.5, 133.4, 106.4, 98.2, 71.8, 67.3, 40.4, 39.4, 39.4, 39.0, 37.6, 37.4, 37.3, 36.8, 36.4, 32.0, 29.8, 29.7, 29.4, 29.1, 28.0, 27.9, 25.8, 25.6, 24.7, 24.5, 22.7, 22.6,$

22.6, 22.6, 22.5, 19.6, 19.5, 19.5, 19.2. IR (ATR): $\nu = 3333, 2954, 2927, 2869, 1656, 1583, 1504, 1464, 1423, 1250, 1227, 1114, 907 \text{ cm}^{-1}$. MALDI-TOF-MS (m/z): 966.78. Observed: 967.72 (MH⁺). Anal. Calcd for C₅₇H₁₀₂N₆O₆: C 70.76, H 10.63, N 8.69. Found: 70.97, H 10.67, N 8.73. $[\alpha]_D^{25} = +1.32$ (25 mg/mL CHCl₃).

Synthesis of 2-{6-(3,4,5-tris(3(S),7-dimethyloctyoxo)-phenylureido)-hexylureido-6-(2(S), 6-dimethylheptyl)-4[1H]-pyrimidinone (10b)

2-(6-Amino-hexylureido)-6-(2(S),6-dimethylheptyl)-4[1H]-pyrimidinone **9b** (0.53 g, 1.07 mmol) was dissolved in dry Et₃N (0.12 g, 1.18 mmol, 1.1 eq) and distilled CHCl₃ (20 mL). 3,4,5-tris(3(S),7-dimethyloctyoxo)-phenyl isocyanate **11** (0.78 g, 1.33 mmol, 1.2 eq) was added and the mixture stirred under argon atmosphere at 50 °C, during a period of 48 hours. CHCl₃ (15 mL) was added and the organic layer was extracted with NaHCO₃ (25 mL), citric acid (25 mL, pH 3~4) and brine (25 mL). The organic layer was dried over magnesium sulfate and evaporated *in vacuo*. The pure product was obtained after column chromatography (SiO₂, CHCl₃:ethanol, 98:2 to 95:5, v/v) followed by precipitation in cold acetonitrile (60 mL) as an off white solid (0.67 g, 0.695 mmol), mp: 99.6-101.8 °C. Yield: 65%. ¹H-NMR (CDCl₃): $\delta = 13.33$ (s, 1H, C-NH-C), 11.75 (s, 1H, C-NH-C=O), 10.03 (s, 1H, O=C-NH-CH₂), 7.73 (s, 1H, O=C-NH-C_{arom.}), 6.74 (s, 2H, CH_{arom.}), 5.80 (s, 1H, C=CH), 5.75 (s, 1H, CH₂-NH-C=O), 3.99-3.86 (m, 6H, O-CH₂-), 3.25-3.17 (m, 4H, HN-CH₂-CH₂), 2.51-2.46 (dd, 1H, (CH=C)-CH₂CH(CH₃)(CH₂)), 2.25-2.19 (dd, 1H, (CH=C)-CH₂CH(CH₃)(CH₂)), 1.85-1.08 (m, 46H, alkyl-H), 0.97-0.80 (m, 36H, -CH₃). ¹H-NMR (DMF-d₆): $\delta = 11.96$ -11.53 (bs, 1H, C-NH-C), 9.78-9.52 (bs, 1H, C-NH-C=O), 8.37 (s, 1H, O=C-NH-C_{arom.}), 7.93-7.59 (bs, 1H, O=C-NH-CH₂), 6.89 (s, 2H, CH_{arom.}), 6.18 (s, 1H, CH₂-NH-C=O), 5.80 (s, 1H, C=CH), 4.03-3.86 (m, 6H, O-CH₂-), 3.28-3.15 (m, 4H, HN-CH₂-CH₂), 2.44-2.39 (dd, 1H, (CH=C)-CH₂CH(CH₃)(CH₂)), 2.21-2.18 (dd, 1H, (CH=C)-CH₂CH(CH₃)(CH₂)), 1.89 (m, 46H, alkyl-H), 1.06-0.92 (m, 36H, -CH₃). ¹³C-NMR (CDCl₃): $\delta = 173.5, 156.3, 156.2, 154.8, 153.3, 152.3, 135.5, 133.4, 106.4, 98.2, 71.8, 67.3, 40.4, 39.4, 39.3, 39.0, 37.6, 37.4, 37.3, 36.8, 36.4, 32.0, 29.8, 29.7, 29.4, 29.1, 28.0, 27.9, 25.8, 25.6, 24.7, 24.5, 22.7, 22.6, 22.6, 22.6, 22.5, 19.6, 19.5, 19.5, 19.2$. IR (ATR): $\nu = 3319, 2953, 2926, 2869, 1702, 1638, 1593, 1564, 1530, 1464, 1423, 1255, 1230, 1113, 801 \text{ cm}^{-1}$. MALDI-TOF-MS (m/z): 966.78. Observed: 967.74 (MH⁺). $[\alpha]_D^{25} = -3.84$ (25 mg/mL CHCl₃). Anal. Calcd for C₅₇H₁₀₂N₆O₆: C 70.76, H 10.63, N 8.69.

Measured: C 70.37, H 10.56, N 8.56.

Synthesis of 3,4,5-tris(3(S),7-dimethyloctyoxo)-phenyl isocyanate (11)

Under argon atmosphere, a solution of 3,4,5-tris(3(S),7-dimethyloctyoxo) aniline (0.69 g, 1.23 mmol) in distilled toluene (25 mL) was added to a solution of phosgene in toluene (20% w/w in toluene) (2.43 g, 12.9 mL, 24.56 mmol, 20 eq) and stirred at room temperature. After 3 h the excess of phosgene and solvent was evaporated *in vacuo*. This yielded the pure compound as brown oil. (0.71 g, 1.21 mmol). Yield: 98%. ¹H-NMR (CDCl₃): $\delta = 6.29$ (s, 2H, C=CH-C), 3.98-3.91 (m, 6H, O-CH₂-), 1.86-1.13 (m, 30H, H-alkyl), 0.95-0.91 (d, 9H, CHCH₃), 0.88-0.86 (d, 18H, CH(CH₃)₂). IR (ATR): $\nu = 2954, 2927, 2870, 2264, 1588, 1436, 1384, 1227, 1117 \text{ cm}^{-1}$. MALDI-TOF-MS (m/z): 587.49. Observed: 587.43 (M⁺).

Synthesis of 2-(6-[1-imidazolylcarbonylamino]-hexylureido-6-(2(R),6-dimethylheptyl)-4[1H]pyrimidinone (12)

In a 10 mL flask, a mixture of **9a** (1.00 g, 2.0 mmol), 1,1'-carbonyldiimidazole (0.39 g, 2.4 mmol) and dry triethylamine (0.30 g, 3 mmol) in 5 mL dry CHCl₃ was stirred for 4 hours at 50 °C under an atmosphere of argon, until the mixture became clear. After evaporation of the solvent *in vacuo*, the residue was transferred to a glass filter with 3 × 5 mL acetone, filtered, rinsed with 3×5 mL acetone and 5 mL diethylether and dried *in vacuo* at 50 °C. The product was obtained as an off-white powder (0.9 g, 1.9 mmol). Yield: 95%. ¹H-NMR (CDCl₃): δ = 13.33 (s, 1H, NH), 11.85 (s, 1H, NH), 10.02 (s, 1H, NH), 8.20 (s, 1H, imidazole CH), 7.47 (s, 1H, imidazole CH), 7.05 (s, 1H, imidazole CH) 5.64 (s, 1H, O=C-CH=C-CH₂), 3.47-3.25 (m, 4H, NH-CH₂-CH₂), 2.46-2.36 (dd, 1H, CH=C-CH₂-CH(CH₃)-CH₂), 2.24-2.13 (dd, 1H, CH=C-CH₂-CH(CH₃)-CH₂), 1.69-1.11 (m, 17H, -CH₂- and CH₂-CH(CH₃)₂), 0.90 (d, 3H, -CH₃), 0.86 (d, 6H, -CH₃). ¹³C-NMR (CDCl₃): δ = 173.6, 156.4, 154.7, 152.3, 149.1, 136.0, 130.0, 116.1, 106.3, 40.4, 40.0, 38.9, 38.8, 36.6, 31.9, 29.1, 28.4, 27.8, 25.2, 25.1, 24.5, 22.6, 22.5, 19.1 ppm. IR (ATR): ν = 3219, 3029, 2929, 2867, 1743, 1698, 1656, 1581, 1523, 1479, 1466, 1381, 1365, 1315, 1284, 1249, 1138, 1101, 1062, 1017, 953, 913, 838, 73 cm⁻¹.

Synthesis of 2-(6-[2-dodecylureido]-hexyl)-ureido-6-(2(R),6-dimethylheptyl)-4[1H]pyrimidinone (13)

Activated UPy **12** (0.20 g, 0.42 mmol) and *n*-dodecyl amine (0.12 g, 0.65 mmol) were added to dry CHCl₃ (5 mL) and stirred at 55 °C for 2 days under an atmosphere of argon. After cooling to room temperature, 25 mL CHCl₃ was added, and the mixture was extracted 3 times with 15 mL 0.1 M HCl (aq), neutralized with 20 mL saturated NaHCO₃ (aq) and washed with 20 mL brine. After drying with MgSO₄ the solvent was removed by evaporation *in vacuo*, resulting in the crude 2-ureido-pyrimidinone. Further purification by recrystallization from 2-propanol, resulted in pure **13** as a white powder (0.18 g, 0.30 mmol), mp: 155 °C (degr). Yield: 73%. ¹H-NMR (CDCl₃): δ = 13.22 (s, 1H, NH), 11.85 (s, 1H, NH), 10.10 (s, 1H, NH), 5.82 (s, 1H, O=C-CH=C-CH₂), 4.64 (t, 1H, NH), 4.42 (t, 1H, NH), 3.25 (m, 2H, NH-CH₂-CH₂), 3.18-3.11 (m, 4H, NH-CH₂-CH₂), 2.50-2.45 (dd, 1H, CH=C-CH₂-CH(CH₃)-CH₂), 2.27-2.21 (dd, 1H, CH=C-CH₂-CH(CH₃)-CH₂), 1.83 (m, 1H, CH=C-CH₂-CH(CH₃)-CH₂), 1.61-1.12 (m, 35H, -CH₂- and CH₂-CH(CH₃)₂), 0.95-0.86 (m, 12H, -CH₃) ppm. ¹³C-NMR (CDCl₃): δ = 173.3, 158.5, 156.5, 154.8, 151.8, 106.7, 40.54, 40.48, 40.1, 39.6, 39.0, 36.7, 32.0, 31.9, 30.3, 29.71-29.60 (m), 29.38, 29.34, 29.23, 27.9, 26.9, 26.2, 26.1, 24.5, 22.67, 22.66, 22.5, 19.2, 14.1. IR (ATR): ν = 3317, 3222, 2954, 2923, 2853, 1699, 1655, 1627, 1575, 1527, 1482, 1462, 1378, 1366, 1320, 1307, 1294, 1256, 1179, 1135, 1098, 1019, 941, 907, 892, 860, 801, 769, 742 cm⁻¹. MALDI-TOF-MS (m/z): 591.50. Observed: 591.54 (MH⁺), 613.50 (MNa⁺), 629.47 (MK⁺). Anal. Calcd for C₃₃H₆₂N₆O₃: C 67.08, H 10.58, N 14.22. Found: C 66.45, H 10.87, N 14.05.

Synthesis of 2-(6-hydroxy-hexylureido)-6-(2(S),6-dimethylheptyl)-4[1H]-pyrimidinone (14)

To a solution of di-*t*-butylcarbonate (1.37 g, 5.25 mmol, 1.2 eq) in dry dichloromethane (10 mL) was added a solution of 6-amino-1-hexanol (0.56 g, 4.81 mmol, 1.1 eq) in distilled dichloromethane (15 mL) at room temperature under argon atmosphere. The reaction mixture showed immediate gas evolution (CO₂) indicating the formation of the isocyanate. Stirring was continued for 1 h. This reaction mixture was slowly added to a solution of 2-amino-6-(2(S)-

dimethylheptyl)-4[1H]-pyrimidinone **6b** (1.04 g, 4.38 mmol) in dry dimethylformamide (20 mL) at 90 °C under an argon atmosphere. The reaction mixture was stirred for 4.5 h, after which it was cooled. The solvent was evaporated *in vacuo* and the remaining solid was recrystallized from cold acetone (30 mL), filtered and washed with cold diethyl ether. Column chromatography (SiO₂, CHCl₃:ethanol 93:7 v/v), yielded the pure product as a white solid (0.94 g, 2.47 mmol), mp: 99.9-101.7 °C. Yield: 56%. ¹H-NMR (CDCl₃): δ = 13.20 (s, 1H, C=C-NH-C), 11.86 (s, 1H, C-NH-(C=O)), 10.11 (s, 1H, (C=O)NH-CH₂), 5.84 (s, 1H, C=CH), 3.64-3.61 (q, 2H, CH₂-CH₂-OH), 3.30-3.25 (q, 2H, NH-CH₂-CH₂), 2.49-2.44 (dd, 1H, (CH=C)-CH₂CH(CH₃)(CH₂), 2.27-2.21 (dd, 1H, (CH=C)-CH₂CH(CH₃)(CH₂)), 1.78-1.67 (m, 1H, (CH₂)₂CHCH₃), 1.65-1.51 (m, 1H, CH₂CH(CH₃)₂), 1.48-1.11 (m, 14H, -CH₂-), 0.96-0.84 (m, 9H, -CH₃). ¹³C-NMR (CDCl₃): δ = 173.4, 156.6, 154.7, 151.7, 106.8, 62.0, 40.4, 39.3, 39.0, 36.7, 32.5, 31.9, 29.3, 27.9, 25.8, 24.6, 24.5, 22.6 (CH(CH₃)₂), 22.5 (CH(CH₃)₂), 19.2 (CH(CH₃)₂), 19.1 (CHCH₃). IR (ATR): ν = 3021, 2955, 2929, 2855, 1702, 1655, 1562, 1527, 1463, 1251, 1055, 798, 750, 740 cm⁻¹. MALDI-TOF-MS (m/z): 380.28. Observed: 381.13 (MH⁺), 403.12 (MNa⁺). Anal. Calcd for C₂₀H₃₆N₄O₃: C 63.13, H 9.54, N 14.72. Found: C 62.97, H 9.56, N 14.52.

Synthesis of 2-{6-(3,4,5-tris(3(S),7-dimethyloctyloxy)-phenylurethane)-hexylureido-6-(2(S), 6-dimethylheptyl)-4[1H]-pyrimidinone (15)}

2-(6-hydroxy-hexylureido)-6-(2(S),6-dimethylheptyl)-4[1H]-pyrimidinone **14** (0.50 g, 1.31 mmol) was dissolved in distilled CHCl₃ (20 mL). 3,4,5-Tris(3(S),7-dimethyloctyloxy)-phenyl isocyanate **11** (0.93 g, 1.58 mmol, 1.2 eq) and a drop of dibutyl-tin-dilaurate (cat.) were added to the solution and the mixture stirred under argon atmosphere at 60 °C during a period of 48 hours. CHCl₃ (20 mL) was added and the organic layer was extracted with NaHCO₃ (25 mL), citric acid (25 mL, pH 3-4) and brine (25 mL). The organic layer was dried over magnesium sulfate and evaporated *in vacuo*. The pure product was obtained after column chromatography (SiO₂, CHCl₃:ethanol, 98:2, v/v) (SiO₂, ethyl acetate:heptane, 4:6, v/v) and precipitation in cold acetonitrile (25 mL) as an off white solid (0.42 g, 0.434 mmol), mp: 79.9- 82.0 °C. Yield: 34%. ¹H-NMR (CDCl₃): δ = 13.17 (s, 1H, C-NH-C), 11.88 (s, 1H, C-NH-C=O), 10.20 (s, 1H, O=C-NH-CH₂), 6.69 (s, 1H, O=C-NH-C_{arom.}), 6.66 (s, 2H, CH_{arom.}), 5.80 (s, 1H, C=CH), 4.15-4.12 (s, 2H, CH₂-CH₂-O), 4.00-3.88 (m, 6H, O-CH₂-), 3.28-3.23 (m, 4H, HN-CH₂-CH₂), 2.46-2.43 (dd, 1H, (CH=C)-CH₂CH(CH₃)(CH₂), 2.25-2.23 (dd, 1H, (CH=C)-CH₂CH(CH₃)(CH₂)), 1.86-1.14 (m, 46H, alkyl-H), 0.93-0.84 (m, 36H, -CH₃). ¹³C-NMR (CDCl₃): δ = 173.2, 156.6, 154.7, 153.7, 153.3, 151.6, 134.1, 133.7, 106.8, 97.6, 71.7, 67.3, 65.2, 40.4, 39.9, 39.4, 39.3, 39.0, 37.5, 37.4, 37.3, 36.7, 36.4, 31.9, 29.8, 29.7, 29.3, 28.6, 28.0, 27.9, 26.6, 25.6, 24.7, 24.5, 22.7, 22.6, 22.6, 22.6, 22.5, 19.6, 19.5, 19.2. IR (ATR): ν = 2954, 2927, 2869, 1699, 1657, 1581, 1525, 1506, 1463, 1428, 1247, 1216, 1116, 908, 730 cm⁻¹. Anal. Calcd for C₅₇H₁₀₁N₅O₇: C 70.69, H 10.51, N 7.23. Found: C 70.90, H 10.75, N 6.78. MALDI-TOF-MS (m/z): 967.77. Observed: 968.78 (MH⁺).

¹H-NMR titrations

¹H-NMR dilution experiments on **10a** in CDCl₃ were performed on a Varian Unity Inova, 500 MHz equipped with a 5mm ¹H/X Inverse Detection probe equipped with gradient capabilities at 25 °C. Typical procedure: 56.9 mg of compound **10a** was dissolved in 1 mL CDCl₃ resulting in a

100 mM solution, of which 0.6 mL was injected into the NMR tube. This was then diluted to a final concentration of 0.1 mM.

DOSY-NMR titrations

135 mg of compound **10a** was dissolved in 1.0 mL dry CDCl₃ resulting in a 140 mM solution (70 mM in **10a**·**10a**). This was then diluted to a final concentration of 0.5 mM. At each concentration, a 2D-DOSY spectrum was recorded using the DOSY bipolar pulse pair stimulated echo with convection compensation (*Dbppste_cc* in the Varian DOSY package) sequence for the determination of the self-diffusion of the different components at a temperature of 25 °C. The self-diffusion constant was calculated as the average of the values obtained for the signals of the protons located on the gallic wedge, the alkylidene proton and the -OCH₂- protons of the citronellol chains attached to the gallic wedge and were corrected for changes in the viscosity.²⁶ See Chapter 3 for further details on the procedure.

Mixed ¹H-NMR titration

203 mg (0.500 mmol) of compound **16** was dissolved in 6 mL CDCl₃. Of this solution, 1 mL was added to compound **10a** (40.2 mg, 41.7 μmol) resulting in a solution containing 41.7 mM **10a** and 83.3 mM **16**, of which 0.6 mL was injected into the NMR tube and diluted at a constant temperature of 25 °C. The 2D-DOSY experiment was performed on the solution that was obtained after two dilution steps (analytical concentration of **10a** of 26 mM) at a temperature of 25 °C and the obtained diffusion constants were corrected using the residual solvent peak of CHCl₃ in the mixture. All experiments were performed on a Varian Unity Inova, 500 MHz equipped with a 5mm ¹H/X Inverse Detection probe with gradient capabilities.

UV-vis and Circular Dichroism measurements

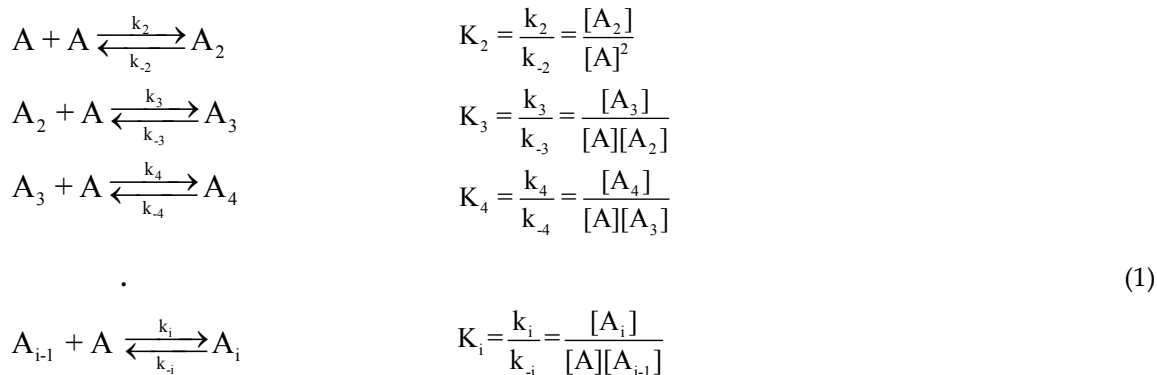
UV-vis and Circular Dichroism measurements were performed on a Jasco J-815 spectropolarimeter where the sensitivity, time constant and scan rate were chosen appropriately. Corresponding temperature dependent measurements were performed with a PFD-425S/15 Peltier-type temperature controller with a temperature range of 263–383 K and adjustable temperature slope.

5.8 Appendices

Appendix A

Mathematical treatment of an isodesmic polymerization in solution and expression of the $^1\text{H-NMR}$ chemical shift evolution under fast exchange.

Consider the reversible polymerization of monomer [A] in solution:



According to eq (1), the molar concentration of all molecules with different degree of polymerization (i) at equilibrium can be written as:

$$[\text{A}_i] = K_i[\text{A}_{i-1}][\text{A}] = K_i \dots K_3 K_2 [\text{A}]^i = [\text{A}]^i \prod_{j=2}^i K_j \tag{2}$$

The initial total concentration of monomer (c_t) is defined as:

$$c_t = \sum_{i=1}^{\infty} i[\text{A}_i] \tag{3}$$

The total concentration of all i-mers including free monomer (c_p) is defined as:

$$c_p = \sum_{i=1}^{\infty} [\text{A}_i] \tag{4}$$

In an isodesmic, infinite reversible polymerization, the equilibrium constants for all monomer additions are identical ($K_2 = K_3 = \dots = K_i \dots = K$). Therefore, eq (2) reduces too:

$$[\text{A}_i] = K^{-1} (K[\text{A}])^i \tag{5}$$

And the mole fraction of species i is defined as:

$$x_i = \frac{i[\text{A}_i]}{c_t} \tag{6}$$

Due to eq (5), the initial monomer concentration can be written as:

$$c_t = \sum_{i=1}^{\infty} i K^{-1} (K[\text{A}])^i \tag{7}$$

If $K[\text{A}] < 1$ this sum can be conveniently written as:

$$c_t = \frac{[\text{A}]}{(1-K[\text{A}])^2} \tag{8}$$

and c_p is written as:

$$c_p = \frac{[A]}{(1-K[A])} \quad (9)$$

If the total concentration c_t is known, the free monomer concentration $[A]$ can be isolated from eq (8):

$$[A] = \frac{1}{2} \frac{2c_t K + 1 - \sqrt{4c_t K + 1}}{c_t K^2} \quad (10)$$

Given a value of K and the initial total concentration, the corresponding concentration of free monomer (A) can be calculated as well as the mole fraction of each i -mer.

The weight average degree of polymerization (DP_w) is defined by eq (11).

$$DP_w = \frac{\sum_{i=1}^{\infty} i^2 N_i}{\sum_{i=1}^{\infty} i N_i} \quad (11)$$

The numerator of eq (11) is proportional to the summation of the molar concentrations of all the i -mers multiplied by i^2 , whereas the denominator is proportional to the initial monomer concentration, c_t . In other words, eq (11) can be rewritten as eq (12):

$$DP_w = \frac{\sum_{i=1}^{\infty} i^2 A^i}{c_t} = \frac{\sum_{i=1}^{\infty} i^2 K^{-1} (K[A])^i}{c_t} = \frac{1 + K[A]}{1 - K[A]} \quad (12)$$

The number average degree of polymerization (DP_n) is defined by eq (13).

$$DP_n = \frac{\sum_{i=1}^{\infty} i N_i}{\sum_{i=1}^{\infty} N_i} \quad (13)$$

where N_i is the number of molecules of a given i -mer. Now the numerator of eq (13) is proportional to the initial monomer concentration, c_t , whereas the denominator is proportional to the summation of the molar concentrations of all the i -mers. In other words eq (13) can be rewritten as eq (14):

$$DP_n = \frac{c_t}{\sum_{i=1}^{\infty} [A_i]} = \frac{1}{1 - K[A]} \quad (14)$$

The observed chemical shift under fast exchange can be written as:

$$\delta_{\text{obs}} = f_{\alpha} \delta_{\alpha} + f_{\lambda} \delta_{\lambda} + f_{\eta} \delta_{\eta} \quad (15)$$

In which f_{α} represents the mole fraction of monomer, f_{λ} represents the molfraction of molecules at stack ends and f_{η} represents the mole fraction of molecules in a stack interior. In this equation δ_{α} , δ_{λ} and δ_{η} denote the chemical shift of the monomer, the chemical shift of molecules at the stack end and the chemical shift of molecules in the interior of the stack.

From eq (10) the molfraction of monomer is obtained:

$$f_{\alpha} = \frac{1}{2} \frac{2c_t K + 1 - \sqrt{4c_t K + 1}}{c_t K^2} \quad (16)$$

The molfraction of molecules at the end of a stack (f_{λ}) can be written as:

$$f_{\lambda} = \frac{2[A_2] + 2[A_4] + 2[A_6] + \dots + 2[A_i]}{c_t} = \frac{2 \sum_2^{\infty} A_i}{c_t} = \frac{2K^{-1} \sum_2^{\infty} (KA)^i}{c_t} \quad (17)$$

This last sum can be written as:

$$f_{\lambda} = \frac{2K^{-1} \sum_2^{\infty} (KA)^i}{c_t} = \frac{2KA^2}{(1-KA)c_t} \quad (18)$$

The mole fraction of molecules in the interior of a stack can be written as:

$$f_{\eta} = \frac{[A_3] + 2[A_4] + 3[A_5] + \dots + (i-2)[A_i]}{c_t} = \frac{K^{-1} \sum_3^{\infty} (i-2)A_i}{c_t} = \frac{K^{-1} \sum_3^{\infty} (i-2)(KA)^i}{c_t} \quad (19)$$

The last sum can be written as:

$$f_{\eta} = \frac{K^{-1} \sum_3^{\infty} (i-2)(KA)^i}{c_t} = \frac{K^2 A^3}{(1-KA)^2 c_t} \quad (20)$$

Substitution of eq (10) into eq (20) and eq (18) gives expressions for f_{λ} and f_{η} as a function of c_t and K . Substitution of these expressions into eq (15) gives an expression for P as a function of four parameters (K , δ_{α} , δ_{λ} and δ_{η}) and the known total concentration (c_t) and the measured chemical shift. This expression can be used to fit the experimental data. However, often the number of parameters is reduced to three by assuming that the chemical shift of a molecule at a stack end is given by the average of monomer and interior stack:

$$\delta_{\lambda} = \frac{\delta_{\alpha} + \delta_{\eta}}{2} \quad (21)$$

Using eq (21) in combination with eq (10), eq (15), eq (16), eq (18) and eq (20) the following expression is obtained:

$$\delta_{\text{obs}} = \delta_{\alpha} + (\delta_{\eta} - \delta_{\alpha}) \left(1 + \frac{1 - \sqrt{4Kc_t + 1}}{2Kc_t} \right) \quad (22)$$

By fitting the concentration dependent chemical shift data to eq (22), values for K , δ_{α} and δ_{η} are obtained.

Appendix B

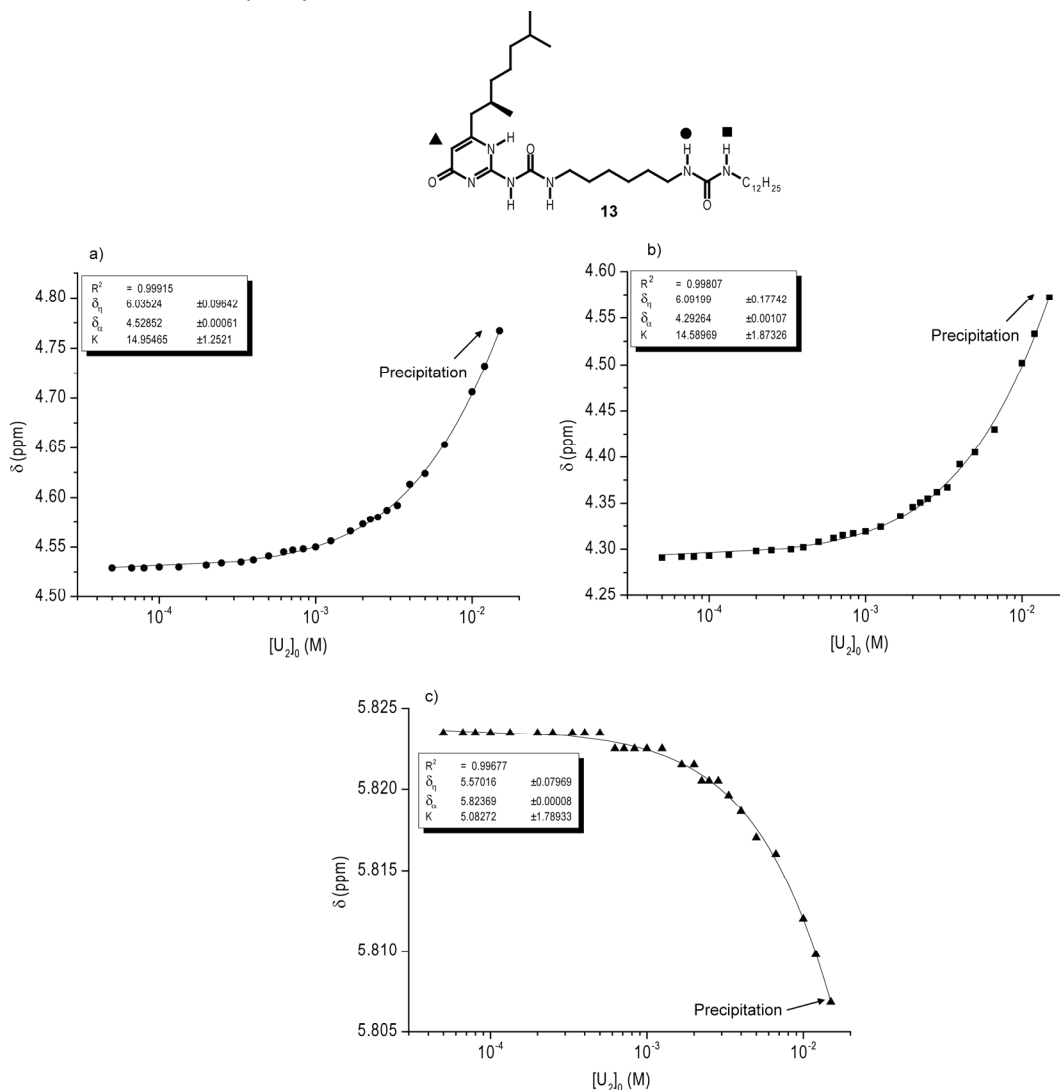
¹H-NMR dilution curves of UPy-urea dimer **13** in CDCl₃ at 25 °C.

Figure A1: Concentration dependent chemical shifts of UPy-urea dimer **13** in CDCl₃ at 25 °C: a) urea NH proton (●); b) urea NH proton (■); c) alkylidene proton (▲). The solid line represents the best fitted curve according to a three parameter isodesmic model for self-assembly.

Appendix C

$^1\text{H-NMR}$ dilution curves of UPy-urethane dimer **15**•**15** in CDCl_3 at 25 °C.

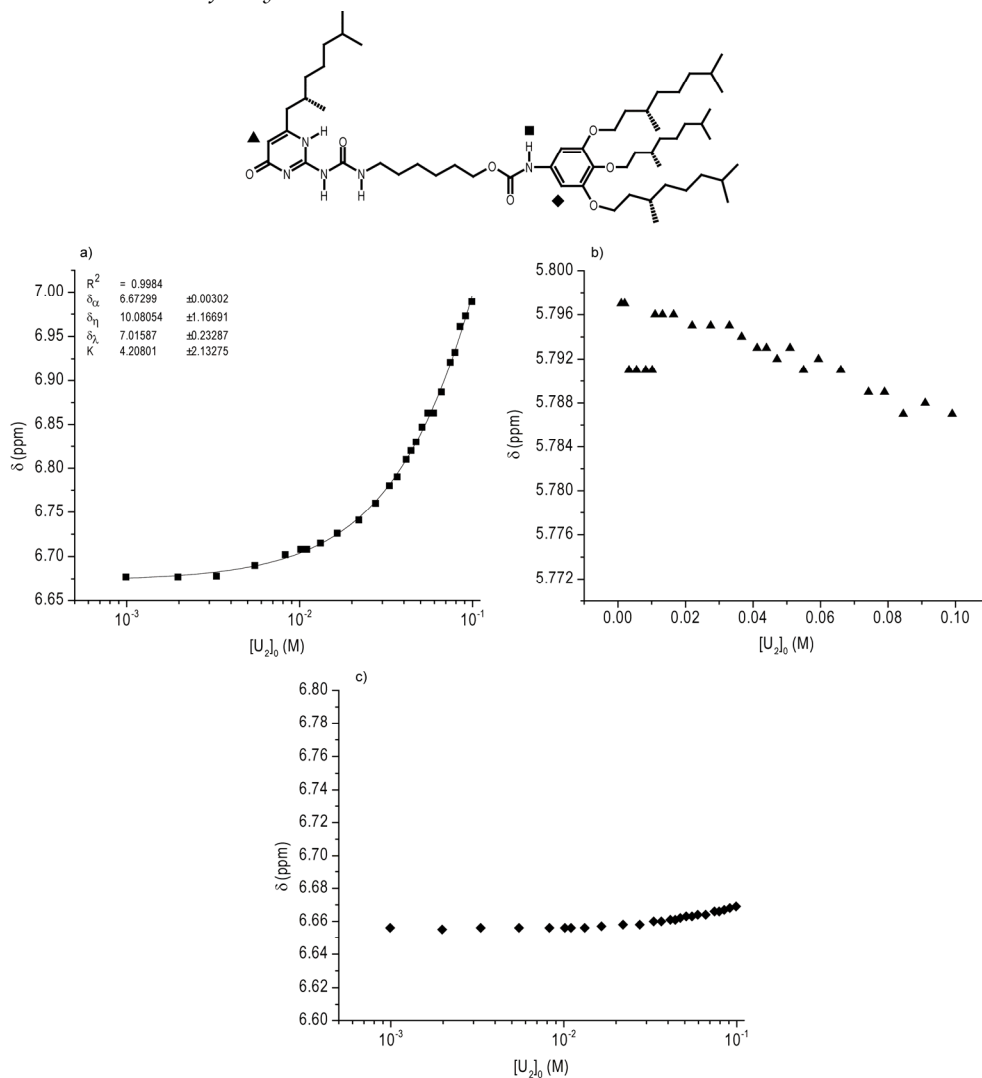
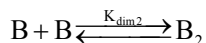
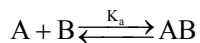
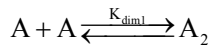


Figure A2: Concentration dependent chemical shifts of UPy-urethane dimer **15**•**15** in CDCl_3 at 25 °C: a) urethane NH proton (\blacksquare); b) alkylidene proton (\blacktriangle); c) aromatic proton (\blacklozenge). The solid line represents the best fitted curve according to a four parameter isodesmic model for self-assembly.

Appendix D

Calculation of the equilibrium concentration of UPy-urea homodimers and UPy/ UPy-urea heterodimers based on the measured $^1\text{H-NMR}$ integrals.

Consider the following equilibria:



In which A_2 represents the concentration of UPy-urea homodimer, AB represents the concentration of UPy / UPy-urea heterodimer and B_2 represents the concentration of UPy dimer. The mass balances for the total analytical concentration of A (C_A) and B (C_B) are given by:

$$C_A = 2[\text{A}_2] + [\text{AB}] + [\text{A}] \quad (23)$$

$$C_B = 2[\text{B}_2] + [\text{AB}] + [\text{B}] \quad (24)$$

Because the dimerization constant of 2-ureido-pyrimidinones are $> 10^6 \text{ M}^{-1}$ in CDCl_3 , the concentration of monomer is negligible even at the lowest concentrations at which the $^1\text{H-NMR}$ measurements were performed. Hence eq (23) and eq (24) reduce to:

$$C_A = 2[\text{A}_2] + [\text{AB}] \quad (25)$$

$$C_B = 2[\text{B}_2] + [\text{AB}] \quad (26)$$

The integrals in the $^1\text{H-NMR}$ spectrum of the UPy / UPy-urea mixture are proportional to the total concentrations of A_2 and AB dimers, regardless of whether these dimers are aggregated or not.

Because all the species are in slow exchange on the $^1\text{H-NMR}$ timescale, the integrals of the various species A_2 , B_2 and AB can be readily obtained.

In such a case the integrals of A_2 (I_{A_2}) and AB (I_{AB}) are proportional to the concentration of A and AB:

$$I_{\text{A}_2} = 2f_{\text{A}_2}[\text{A}_2] \quad (27)$$

$$I_{\text{AB}} = f_{\text{AB}}[\text{AB}] \quad (28)$$

The factor 2 is due to the fact that each UPy-urea homodimer A_2 contains twice as much A as heterodimer AB .

The ratio of these integrals is defined as:

$$y = \frac{I_{\text{AB}}}{I_{\text{A}_2}} \quad (29)$$

By substitution of equations (27) and (28) into equation (29), and assuming the proportionality constants f are equal, we obtain:

$$[\text{AB}] = 2y[\text{A}_2] \quad (30)$$

Substitution of eq (30) into mass balance eq (25) results in expressions for the equilibrium concentrations of A_2 and AB given the analytical concentration of species A.

$$[\text{A}_2] = \frac{C_A}{2(y+1)} \quad (31)$$

$$[AB] = \frac{y}{y+1} C_A \quad (32)$$

For the mass balance of B, we can write:

$$[B_2] = \frac{C_B - [AB]}{2} \quad (33)$$

For the titrations described in this Chapter, $C_B = 2C_A$. Taken into account eq (32), eq (33) can be written as:

$$[B_2] = \frac{(y+2)}{2(y+1)} C_A \quad (34)$$

Using eq (31), eq (32) and eq (34), the equilibrium concentration of all species can be calculated using the integral ratio of any given proton that is part of either A_2 , AB or B_2 .

Appendix E

Calculation of the isodesmic equilibrium constant using temperature dependent CD.

The temperature dependent isodesmic self-assembly model has the following form³⁰:

$$\phi_n(T) = \frac{1}{1 + \exp\left[-0.908\Delta H \frac{T - T_m}{RT_m^2}\right]} \quad (35)$$

In which R represents the universal gas constant (8.3144 J K⁻¹ mol⁻¹), ϕ_n represents the fraction of aggregated material (Defined as: $\phi_n = (c_t - A)/c_t$), T_m represents the temperature (in Kelvin) at which $\phi_n = 0.5$ and ΔH is the molecular enthalpy release (J mol⁻¹).

Using eq (10), eq (14) and the definition of ϕ_n it can be shown that the following relation holds, which links the number average degree of polymerization (DP_n) to the fraction of aggregated material, ϕ_n :

$$DP_n(T) = \frac{1}{\sqrt{1 - \phi_n(T)}} \quad (36)$$

Which agrees with the expression given by van der Schoot.³⁴

Furthermore, the number-averaged degree of polymerization is also related to the total concentration of molecules, c_t , and the isodesmic equilibrium constant, K_i via:

$$DP_n(T) = \frac{1}{2} + \frac{1}{2} \sqrt{4K_i(T)c_t + 1} \quad (37)$$

Equating eq (36) and eq (37) the following relation is obtained which describes the relation between the isodesmic equilibrium constant, c_t and the fraction of aggregation (ϕ_n):

$$K_i(T) = \frac{-1 + \sqrt{1 - \phi_n(K)}}{c_t(-1 + \phi_n(K))} \quad (38)$$

Using the known concentration of UPy-urea dimer **10a-10a** (1.75×10^5 M⁻¹) and the fraction of aggregated material as determined by spectroscopic methods, the isodesmic equilibrium constant can be calculated at each temperature when $\phi_n < 1$.

Appendix F

Equations for fitting the concentration dependence of the diffusion constant to a monomer-dimer equilibrium.

The observed diffusion coefficient D_{obs} is the weighted average of the diffusion constants of the different aggregates present in solution:

$$D_{\text{obs}} = \sum_{i=1}^{i=\infty} x_i \cdot D_i \quad (39)$$

With x_i the fraction of compound present in the form of i -mers and D_i the diffusion coefficients for these i -mers. The diffusion coefficients for different i -mers depend on both aggregate size and aggregate shape. Assuming spherical aggregates, diffusion coefficients are calculated directly from the hydrodynamic radius:

$$D_i = \frac{k \cdot T}{6 \cdot \pi \cdot \eta \cdot r_i} \quad (40)$$

With k the Boltzmann constant ($1.38065 \times 10^{-23} \text{ J}\cdot\text{K}^{-1}$), T the temperature (in Kelvin) and η the viscosity of the solvent. For spherical aggregates consisting of monomers with molecular volume V_1 , the hydrodynamic radius increases roughly with the cube root of the aggregation number i , *i.e.* the volume increases linearly with aggregation number:

$$r_i = \sqrt[3]{\left\{ \frac{\frac{3}{4} \cdot i \cdot V_1}{\pi} \right\}} \quad (41)$$

Fractional contributions of i -mers x_i to the total concentration can be calculated³¹ from the equations describing equilibrium conditions for dimerization:

$$x_i = i \cdot \left(\frac{\left\{ K_{\text{dim}}^{i-1} \cdot \left(\frac{(-1 + \sqrt{(1 + 8 \cdot K_{\text{dim}} \cdot c_t)})}{(4 \cdot K_{\text{dim}})} \right)^i \right\}}{c_t} \right) \quad (42)$$

In which K_{dim} represents the dimerization constant and c_t the total analytical concentration of UPy-urea dimer **10a**.

Combination of eq (39), (40), (41) and (42) gives the following expression for the observed diffusion constant:

$$D_{\text{obs}} = \sum_{i=1}^{n=i} (x_i \cdot D_i) = \frac{k \cdot T}{6 \cdot \pi^{0.666} \cdot \eta \cdot (\frac{3}{4} \cdot 1 \cdot V_1)^{0.333}} \cdot \left(\frac{\left(\frac{(-1 + \sqrt{(1 + 8 \cdot K_{\text{dim}} \cdot c_t)})}{(4 \cdot K_{\text{dim}})} \right)}{c_t} \right) \quad (43)$$

$$+ \frac{k \cdot T}{6 \cdot \pi^{0.666} \cdot \eta \cdot (\frac{3}{4} \cdot 2 \cdot V_1)^{0.333}} \cdot 2 \cdot \left(\frac{\left\{ K_{\text{dim}} \cdot \left(\frac{(-1 + \sqrt{(1 + 8 \cdot K_{\text{dim}} \cdot c_t)})}{(4 \cdot K_{\text{dim}})} \right)^2 \right\}}{c_t} \right)$$

Using this equation the concentration dependent viscosity corrected diffusion constants obtained from the PGSE NMR measurements were fitted using the known value of η for CHCl_3 at 298.15 K (5.42×10^{-4} Pa·s). As can be observed from the Figure A3, the monomer-dimer model is inappropriate to describe the concentration dependence of the diffusion coefficient of UPy-urea dimer **10a·10a** in CDCl_3 at 25 °C. Hence it can be concluded that the self-assembly of the UPy-urea dimer **10a·10a** occurs via a stepwise (equal K) mechanism.

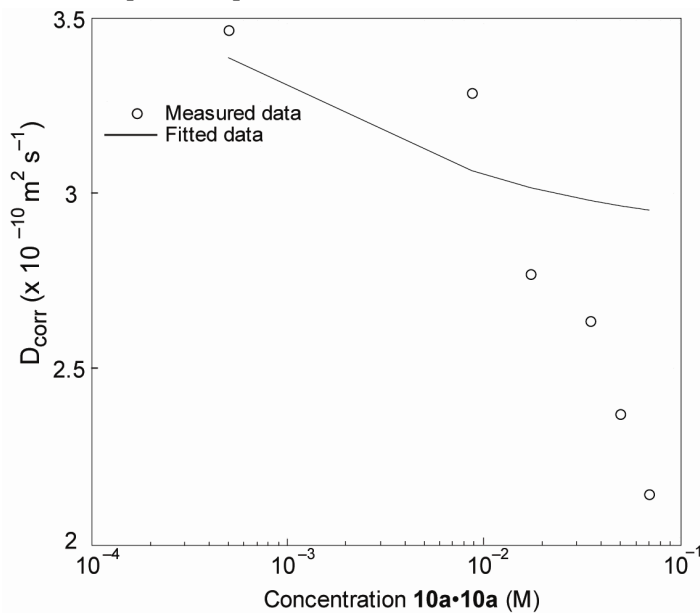


Figure A3: Viscosity corrected diffusion coefficient for **10a·10a** in CDCl_3 at 25 °C as a function of concentration. The solid line represents the least-square fits to a dimerization model ($K_{\text{dim}} = 700 \text{ M}^{-1}$).

5.9 References

- Lortie, F.; Boileau, S.; Bouteiller, L.; Chassenieux, C.; Demé, B.; Ducouret, G.; Jalabert, M.; Lauprêtre, F.; Terech, P. *Langmuir* **2002**, *18*, 7218.
 - Boileau, S.; Bouteiller, L.; Lauprêtre, F.; Lortie, F. *New J. Chem.* **2000**, *24*, 845.
 - Obert, E.; Bellot, M.; Bouteiller, L.; Andrioletti, F.; Lehen-Ferrenbach, C.; Boue, F. *J. Am. Chem. Soc.* **2007**, *129*, 15601.
 - Simic, V.; Bouteiller, L.; Jalabert, M. *J. Am. Chem. Soc.* **2003**, *125*, 13148.
 - Shikata, T.; Nishida, T.; Isare, B.; Linares, M.; Lazzaroni, R.; Bouteiller, L. *J. Phys. Chem. B.* **2008**, *112*, 8459.
 - van Gorp, J. J.; Vekemans, J. A. J. M.; Meijer, E. W. *J. Am. Chem. Soc.* **2002**, *124*, 14759.
 - Shimizu, L. S.; Smith, M. D.; Hughes, A. D.; Shimizu, K. D. *Chem. Commun.* **2001**, 1592.
 - Liu, Y.; Li, Y.; Jiang, L.; Gan, H.; Liu, H.; Li, Y.; Zhuang, J.; Lu, F.; Zhu, D. *J. Org. Chem.* **2004**, *69*, 9049.
- Hanabusa, K.; Shimura, K.; Hirose, K.; Kimura, M.; Shirai, H. *Chem. Lett.*, **1996**, 885.
 - de Loos, M.; van Esch, J.; Kellogg, R. M.; Feringa, B. L. *Angew. Chem.* **2001**, *113*, 633.
 - van Esch, J.; Schoonbeek, F.; de Loos, M.; Kooijman, H.; Spek, A. L.; Kellogg, R. M.; Feringa, B. L. *Chem. Eur. J.* **1999**, *5*, 937.
 - van Esch, J.; De Feyter, S.; Kellogg, R. M.; De Schryver, F.; Feringa, B. L. *Chem. Eur. J.* **1997**, *3*, 1238.
 - de Loos, M.; van Esch, J.; Kellogg, R. M.; Feringa, B. L. *Tetrahedron* **2007**, *63*, 7285.
 - de Loos, M.; Friggeri, A.; van Esch, J.; Kellogg, R. M.; Feringa, B. L. *Org. Biomol. Chem.* **2005**, *3*, 1631.
 - Estroff, L. A.; Hamilton, A. D. *Angew. Chem., Int. Ed.* **2000**, *39*, 3447.
 - Wang, G.; Hamilton, A. D. *Chem. Eur. J.*

- 2002, 8, 1954. i) Yabuuchi, K.; Marfo-Owusu, E.; Kato, T. *Org. Biomol. Chem.* **2003**, 1, 3464. j) Piepenbrock, M. M.; Lloyd, G. O.; Clarke, N.; Steed, J. W. *Chem. Commun.* **2008**, 2644. k) Avalos, M.; Babiano, R.; Cintas, P.; Gomez-Carretero, A.; Jimenez, J. L.; Lozano, M.; Ortiz, A. L.; Palacios, J. C.; Pinazo, A. *Chem. Eur. J.* **2008**, 14, 5656. l) Baddeley, C.; Yan, Z.; King, G.; Woodward, P. M.; Badjic, J. D. *J. Org. Chem.* **2007**, 72, 7270.
- 3) a) van Gorp, J. J.; Vekemans, J. A. J. M.; Meijer, E. W. *Chem. Commun.* **2004**, 60. b) Zhang, A. M.; Han, Y. H.; Yamato, K.; Zeng, X. C.; Gong, B. *Org. Lett.* **2006**, 8, 803. c) Rodriguez, J. M.; Hamilton, A. D. *Angew. Chem., Int. Ed.* **2007**, 46, 8614. d) Corbin, P. S.; Zimmerman, S. C.; Thiessen, P. A.; Hawryluk, N. A.; Murray, T. J. *J. Am. Chem. Soc.* **2001**, 123, 10475. e) Ricks, H. L.; Shimizu, L. S.; Smith, M. D.; Bunz, U. H. F.; Shimizu, K. D. *Tetrahedron* **2004**, 45, 3229.
- 4) Custelcean, R. *Chem. Commun.* **2008**, 295 and references therein.
- 5) Etter, M. C.; Urbanczyk-Lipkowska, Z.; Zia-Ebrahimi, M.; Panunto, T. W. *J. Am. Chem. Soc.* **1990**, 112, 8415.
- 6) For a comparison between urea and urethane hydrogen bonding: Yilgör, E.; Burgaz, E.; Yurtsever, E.; Yilgör, I. *Polymer* **2000**, 41, 849.
- 7) a) Zhao, X.; Chang, Y. L.; Fowler, F. W.; Lauher, J. W. *J. Am. Chem. Soc.* **1990**, 112, 6627. b) Chang, Y. L.; West, M. A.; Fowler, F. W.; Lauher, J. W. *J. Am. Chem. Soc.* **1993**, 115, 5991.
- 8) a) Jadzyn, J.; Stockhausen, M.; Zywucki, B. *J. Phys. Chem.* **1985**, 91, 754. b) Lortie, F.; Boileau, S.; Bouteiller, L. *Chem. Eur. J.* **2003**, 9, 3008.
- 9) Masunov, A.; Dannenberg, J. J. *J. Phys. Chem. B* **2000**, 104, 806.
- 10) a) Heikens, D.; Meijers, A.; Reth, P. H. v. *Polymer* **1968**, 9, 15. b) Musselman, S. G.; Santosusso, T. M.; Barnes, J. D.; Sperling, L. H. *J. Polym. Sci.* **1999**, 37, 2586. c) Beck, R. A.; Truss, R. W. *Polymer* **1999**, 40, 307. d) Shirasaka, H.; Inoue, S. I.; Asai, K.; Okamoto, H. *Macromolecules* **2000**, 33, 2776. e) Garrett, J. T.; Siedlecki, C. A.; Runt, J. *Macromolecules* **2001**, 34, 7066. f) Garrett, J. T.; Lin, J. S.; Runt, J. *Macromolecules* **2002**, 35, 161. g) Legge, N. R.; Holden, G.; Quirk, R. P. *Thermoplastic Elastomers*, 2nd ed.; Hanser Publishers: Munich, 1996.
- 11) a) Klinedinst, D. B.; Yilgor, E.; Yilgor, I.; Beyer, F. L.; Wilkes, G. L. *Polymer* **2005**, 46, 10191. b) Versteegen, R. M.; Sijbesma, R. P.; Meijer, E. W. *Macromolecules* **2005**, 38, 3176.
- 12) Kautz, H.; van Beek D. J. M.; Sijbesma, R. P.; Meijer, E. W. *Macromolecules* **2006**, 39, 4265.
- 13) Guo, D.; Sijbesma, R. P.; Zuilhof, H. *Org. Lett.* **2004**, 6, 3667.
- 14) Examples: a) Hirschberg, J. H. K. K.; Brunsveld, L.; Ramzi, A.; Vekemans, J. A. J. M.; Sijbesma, R. P.; Meijer, E. W. *Nature* **2000**, 407, 167. b) Jonkheijm, P.; van der Schoot, P.; Schenning, A. P. H. J.; Meijer, E. W. *Science* **2006**, 313, 80. c) Brunsveld, L.; Schenning, A. P. H. J.; Broeren, M. A. C.; Janssen, H. M.; Vekemans, J. A. J. M.; Meijer, E. W. *Chem. Lett.* **2000**, 292. d) Green, M. M.; Peterson, N. C.; Sato, T.; Teramoto, A.; Cook, R.; Lifson, S. *Science* **1995**, 268, 1860.
- 15) Kozlova, T. V.; Zharkov, V. V. *Zh. Prikl. Spektrosk.* **1981**, 35, 303.
- 16) Hirschberg, J. H. K. K.; Koevoets, R. A.; Sijbesma, R. P.; Meijer, E. W. *Chem. Eur. J.* **2003**, 9, 4222.
- 17) (R)-3,7-dimethyl-6-octen-1-ol **1a** and (S)-3,7-dimethyl-6-octen-1-ol **1b** were purchased from Sigma-Aldrich. The purity of these compounds was investigated using chiral GC/MS. (R)-3,7-dimethyl-6-octen-1-ol was found to contain no impurities whereas (S)-3,7-dimethyl-6-octen-1-ol contained 1.5% of the R enantiomer.
- 18) Hunsen, M. *Synthesis* **2005**, 15, 2487.
- 19) Keizer, H. M.; Sijbesma, R. P.; Meijer, E. W. *Eur. J. Org. Chem.* **2004**, 2553.

- 20) Appel, W.P.J. *Lateral interactions in the UPy-urea motif*, Graduation report, Eindhoven University of Technology, **2006**.
- 21) Because the dimerization constant of 2-ureido-pyrimidinones are $> 10^6 \text{ M}^{-1}$ in CDCl_3 , the concentration of monomer is negligible even at the lowest concentrations at which the $^1\text{H-NMR}$ measurements are performed.
- 22) Examples: a) Zhao, D.; Moore, J. S. *J. Org. Chem.* **2002**, *67*, 3548. b) Kraft, A.; Osterod, F.; Frohlich, R. *J. Org. Chem.* **1999**, *64*, 6425. c) Nakade, H.; Jordan, B. J.; Xu, H.; Han, G.; Srivastava, S.; Arvizo, R. R.; Cooke, G.; Rotello, V. M. *J. Am. Chem. Soc.* **2006**, *128*, 14924.
- 23) Giessner-Prettre, C.; Pullman, B. *J. Theor. Biol.* **1970**, *27*, 87.
- 24) A downfield shift of both urea protons has also been observed for a bisurea based low molecular weight gelator under dilute conditions, see reference 2i.
- 25) Jerschow, A.; Muller, N. *J. Magn. Reson.* **1997**, *125*, 372.
- 26) The viscosity corrected diffusion constants are determined using the following formula: $D_c = D_{\text{meas}} \times (D_{\text{sol, pure}} / D_{\text{sol, meas}})$ where D_{meas} and $D_{\text{sol, meas}}$ are the measured values for the solute and the residual solvent peak (CHCl_3) respectively and $D_{\text{sol, pure}}$ is the diffusion constant measured for the residual CHCl_3 in pure CDCl_3 .
- 27) Martin, R. B. *Chem. Rev.* **1996**, *96*, 3043.
- 28) Fitting of the concentration dependent data to a three parameter indefinite isodesmic self-assembly model resulted in an unrealistic value of δ_η . Therefore, the data were fitted to a four parameter isodesmic self-assembly model as is described in Appendix A.
- 29) For an excellent review on the use of CD spectroscopy in the study of chiral self-assemblies: Gottarelli, G.; Lena, S.; Masiero, S.; Pieraccini, S.; Spada, G. P. *Chirality* **2008**, *20*, 471.
- 30) The temperature dependent isodesmic self-assembly model has the following form:
- $$\phi_n(T) = \frac{1}{1 + \exp\left[-0.908\Delta H \frac{T - T_m}{RT_m^2}\right]}$$
- In which R represents the universal gas constant ($8.3144 \text{ J K}^{-1} \text{ mol}^{-1}$), ϕ_n represents the fraction of aggregated material, T_m represents the temperature at which $\phi_n = 0.5$ and ΔH is the molecular enthalpy release (J mol^{-1}). See: Smulders, M. M. J.; van der Schoot, P. P. A. M.; Schenning, A. P. H. J.; Meijer, E. W. Paper in preparation.
- 31) Buurma, N. J.; Haq, I. J. *Mol. Biol.* **2008**, *281*, 607.
- 32) Chloroform has good H-bond-donor but relatively weak H-bond-acceptor properties. On the other hand, heptane is neither a good H-bond donor nor H-bond acceptor. For a discussion on the competitive effect of solvents on hydrogen bonded assemblies, see: Hunter, C. A. *Angew. Chem. Int. Ed.* **2004**, *43*, 5310.
- 33) Dissolution of benzene in chloroform is exothermic as was first found by Tamres in 1952 (*J. Am. Chem. Soc.* **1952**, *74*, 3375). It is now generally believed that this exothermicity is a result of a weak hydrogen bond between the CH proton of chloroform and the pi-electrons of the aromatic. Because of this solvent-solute interactions, the solute-solute interactions are weakened resulting in a lower equilibrium constant.
- 34) van der Schoot, P. P. A. M. *Theory of Supramolecular Polymerization in Supramolecular Polymers*; Second Edition; Taylor & Francis Group 2005.
- 35) Huisman, B. A. H.; Bolhuis, P. G.; Fasolino, A. *Phys. Rev. Lett.* **2008**, *100*, 188301.

6

The influence of polar side chains on the thermodynamics of 2-ureido-pyrimidinone based self-assemblies in apolar solvents

Abstract

The thermodynamic strength of 2-ureido-pyrimidinone based self-assemblies substituted with polar side chains is investigated in CHCl₃ using a variety of techniques. Substitution of the UPy unit with polar side chains containing hydrogen bond donors or acceptors results in a large decrease in the dimerization constant (K_{dim}) of UPy dimers, the association constant (K_a) of UPy·NaPy dimers and the isodesmic equilibrium constant (K_i) of UPy-urea based stacks (see Chapter 5). In this chapter, the influence of two different polar side chains will be investigated i.e. side chains containing different numbers of ethylene oxide (EO) units and a polyacrylate side chain. Using ¹H-NMR, DOSY, FT-IR and UV-Vis spectroscopy it is found that the reduction of both K_{dim} and K_a is primarily dependent on the length of the aliphatic spacer connecting the hydrogen bonds with the polar side chain.

Part of this work has been published:

a) Feldman, K. E.; Kade, M. J.; de Greef, T. F. A.; Meijer, E. W.; Kramer, E. J.; Hawker, C. J. *Macromolecules* **2008**, *41*, 4694-4700. b) de Greef, T. F. A.; Nieuwenhuizen, M. M. L.; Stals, P. J. M.; Fitié, C. F. C.; Palmans, A. R. A.; Sijbesma, R. P.; Meijer, E. W. *Chem. Commun.* **2008**, 4306.

6.1 Introduction

Polar side chains such as oligo ethylene oxide (EO) are widely employed as solubilizing chains for the construction of supramolecular assemblies in water.¹ Supramolecular polymers² and networks³ based on hydrogen bonding have been created using a combination of polar and apolar polymers which serve both as linking units to physically connect the associating end groups as well as structurally organizing units due to the incompatibility of hydrophilic and hydrophobic chains.⁴ Due to its low toxicity and excellent biocompatibility, EO chains are also applied in the design of low-molecular-weight hydrogelators⁵ and multivalent ligands for biomedical applications.⁶ However, substitution of supramolecular assemblies with polar oligomers and polymers can lead to unexpected results. For example, Kaifer⁷ reported a generation dependent drop in the dimerization constant of ureido-pyrimidinone dimers substituted with polar Newkome type oligoamide dendrons. The large drop in dimerization strength on going from the first (G_1 , $K_{\text{dim}} > 10^6 \text{ M}^{-1}$) to the third generation (G_3 , $K_{\text{dim}} = 2.6 \text{ M}^{-1}$) dendron was attributed to either an increase in the steric hindrance exerted by the larger dendritic component or by the increase in the relative microenvironment polarity created by the dendritic wedge. In sharp contrast to the results obtained by Kaifer, Chow and co-workers⁸ reported a generation independent (G_1 - G_3) dimerization constant of 2-ureido-pyrimidinones equipped with less polar Fréchet type oligo aryether dendrons.⁸ Because the oligoamide G_3 dendron is approximately similar in size compared to the oligo aryether G_3 dendron these authors conclude that the decrease in K_{dim} is a result of an increase in the polarity of the microenvironment which directly influences the strength of the individual hydrogen bonds. Although the increase in the polarity of the microenvironment seems a plausible explanation for the observed decrease in K_{dim} it must be noted that a generation dependent increase in the polarity of the microenvironment has been measured for oligo aryether dendrons.⁹ An alternative explanation for the decrease in K_{dim} , which has not been noted by the authors, is back folding of the polar side chains to the polar groups of the 2-ureido-pyrimidinone moiety resulting in stabilization of the monomer. Hydrogen bond induced back-folding of end groups is commonly observed in various polar dendrimers such as PPI and PAMAM dendrimers in both apolar and polar solvents.¹⁰ In this respect, the decrease in K_{dim} can be either explained by the more flexible character of the oligoamide dendrons compared to the rigid character of the polyaryl ether dendrons or due to the fact that the oligoamide dendron contains stronger hydrogen bond donors and acceptors.

Another example of the remarkable effect of short polar side chains on the thermodynamics of host-guest complexes was noted by Stoddart and co-workers in their

investigation on the complexation of cyclobis(paraquat-*p*-phenylene) with an 1,4-dioxybenzene-based acyclic guest. The values of the association constants (K_a) of the corresponding complexes varied significantly depending on the nature of the substituents attached to the aromatic ring of the 1,4-dioxybenzene guest. Attachment of long EO chains resulted in a significant increase (10^2) in K_a compared to short EG chains presumably due to favorable [CH \cdots O] interactions between the polyether oxygen atoms and acidic hydrogen atoms located on the bipyridinium units of the host.¹¹

These examples clearly demonstrate the remarkable effect of the attachment of short polar chains on the thermodynamics of supramolecular assemblies.¹² Because the 2-ureido-pyrimidinone is used in the construction of supramolecular materials where it serves as a physical chain-extending and cross-linking moiety, it is of utmost importance to characterize the conditions by which polar oligomers and polymers covalently attached to the UPy unit could enhance or decrease the material properties by changing the dimerization strength or association dynamics.

In this Chapter, a number of 2-ureido-pyrimidinone derivatives substituted with polar side chains are synthesized and their dimerization, association with 2,7-diamido-1,8-naphthyridine and their isodesmic self-assembly into one dimensional stacks is investigated and compared to their aliphatic analogues. In the first part of this Chapter the focus will be on the effect of short oligo EO chains carrying different numbers of polyether oxygen atoms. Furthermore, if any effect is observed it is highly likely that it depends on the length of the aliphatic linker connecting the EO chain with the urea functionality of the UPy unit. Therefore, several UPy derivatives have been synthesized having an equal amount of polyether oxygen atoms but with a different number of carbon atoms between the ureido nitrogen atom and the first oxygen of the EO chain. In the second part of this Chapter, several UPy based ATRP (Atom Transfer Radical Polymerization) initiators are synthesized and polymerized with *n*-butylacrylate. The dimerization strength of the resulting telechelic UPy polymers will then be probed with a variety of techniques (DOSY, ¹H-NMR, UV-Vis).

6.2 The effect of ethylene oxide chains on UPy based self-assemblies

6.2.1 Synthesis and design

To study the effect of EO chains on UPy dimerization a series of UPy monomers were synthesized (Chart 6.1). Each UPy monomer consists of the following parts:

1) *The UPy group, capable of quadruple hydrogen bonding interactions.*

Previously, the dimerization constant of this unit, substituted with aliphatic substituents at the ureido group, was determined to be $6 \times 10^7 \text{ M}^{-1}$ in CHCl_3 .¹³

2) *An apolar alkylene spacer linking the EO chain with the UPy group.*

Large alkylene spacers provide both a low polarity microenvironment as well as provide a significant entropic barrier for backfolding of the oxygen atoms of the EO chain to the acidic NH protons of the UPy unit. Intramolecular hydrogen bonding of the oxygen atoms of the EO chain to the acidic NH protons of the UPy unit will result in a loss of conformational freedom of the alkylene spacer which in turn results in an increasing conformational entropy across the series $m = 0, 1, 4$ (see Chart 6.1). It has been estimated by Page, Jencks¹⁴ and Mandolini¹⁵ that the entropy that is lost for freezing one methylene group is approximately 4-4.5 cal/K for non-substituted alkanes. Although entropic effects are important in reversible cyclizations, enthalpic effects such as the enthalpic contribution of the intramolecular hydrogen bond¹⁶ and torsional strain¹⁷ caused by an increase in the number of unfavorable gauche interactions upon backfolding of the alkylene spacer, are of equal importance.

3) *A hydrophilic ethylene oxide substituent containing various numbers of oxygen ether type hydrogen bond acceptors connected to the alkyl spacer.*

FT-IR measurements on the mono-alkyl ethers of ethylene glycol ($n = 0-3$) in CHCl_3 have shown that the number of conformations in which an intramolecular hydrogen bond is present between the free OH and the oxygen atoms increases as the number of ethylene oxide units is increased.¹⁸ Because the urea functionality contains two acidic NH protons capable of hydrogen bonding with the polyether oxygen hydrogen bond acceptors a large difference in K_{dim} is expected upon increasing n .

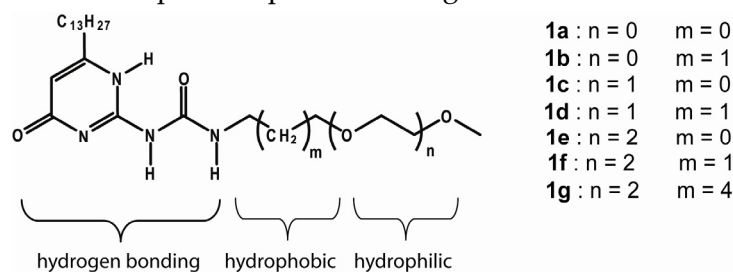
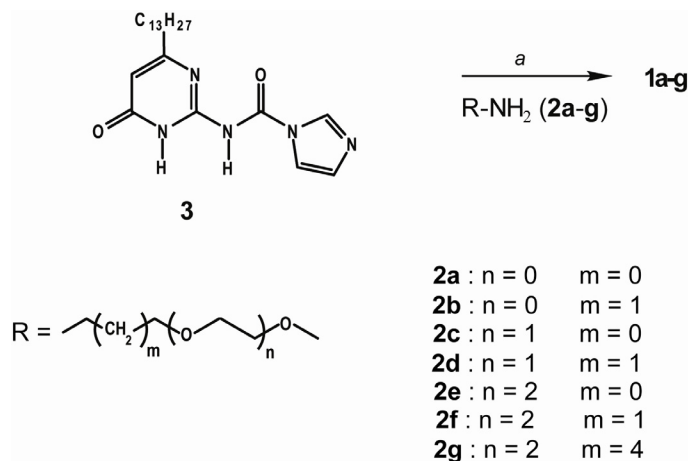


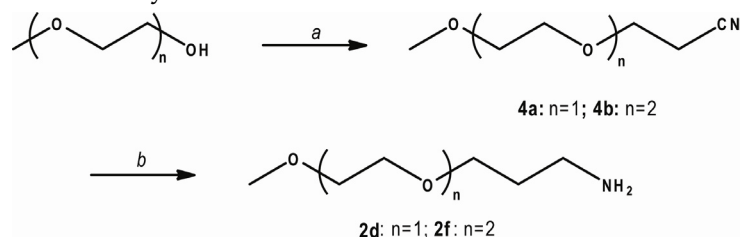
Chart 6.1: Design and structure of EO substituted 2-ureido-pyrimidinones **1a-1g**.

Straightforward coupling of amine terminated mono-methyl ethylene oxides **2a-2g** with CDI activated tridecyl pyrimidinone **3** resulted in the desired EO substituted 2-ureido-pyrimidinones **1a-g** (Scheme 6.1). Amine terminated mono-methyl ethylene oxides **2d** and **2f** ($m = 1$) were synthesized by Michael addition of the corresponding alcohol terminated mono-methyl ethylene oxides to acrylonitrile followed by reduction of the nitrile by borane in THF (see Scheme 6.2).



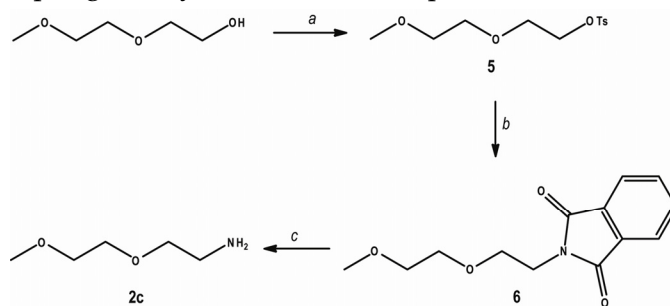
Scheme 6.1: Synthesis of EO substituted 2-ureido-pyrimidinones **1a-g**: a) amine terminated mono-methyl ethylene oxides **2a-2g**, CHCl₃, 48 h, 60 °C, NEt₃ (for **2g**).

Amino-diethylene glycol **2c** was synthesized by tosylation of the corresponding alcohol resulting in tosylate **5**. Reaction of tosylate **5** with potassium phthalimide and subsequent deprotection of phthalimide **6** by hydrazine monohydrate (see Scheme 6.3) resulted in **2c** in an overall yield of 27%.



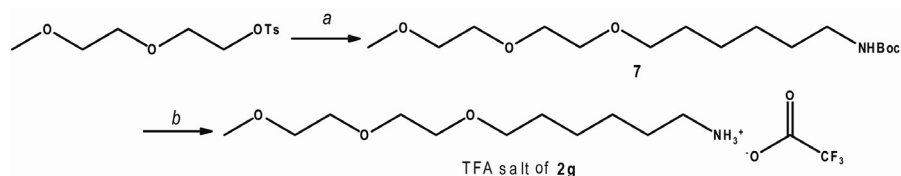
Scheme 6.2: Synthetic route toward amine terminated ethylene glycols **2d** and **2f**: a) acrylonitrile, KOH, 3 h, RT.; b) BH₃·THF, reflux overnight.

Finally, amino ethylene glycol **2g** in which a large hydrophobic spacer separates the oxygen atoms of the ethylene oxide chain from the amino group, could be synthesized by a Williamson coupling of tosylate **5** with N-Boc protected 6-aminohexanol.



Scheme 6.3: Synthetic route toward 2-(2-methoxyethoxy)ethyl amine **2c**: a) Tosyl chloride, tetrahydrofuran, 1 h, room temperature, 98%; b) potassium phthalimide, dimethylformamide, 4 h, 110 °C, 43%; c) N₂H₄/ethanol 1/1, 12 h, reflux, 64%.

Deprotection of the Boc group using trifluoroacetic acid in dichloromethane resulted in the TFA salt of amine **2g** (see Scheme 6.4).



Scheme 6.4: Synthetic route toward amine terminated ethylene glycol **2g**: a) *N*-Boc protected 6-aminohexanol, KOH, tetrahydrofuran, 24 h, reflux, 10%; b) trifluoroacetic acid, dichloromethane, 3 h, room temperature, 94%.

6.2.2 Assessment of dimerization strength using $^1\text{H-NMR}$

The dimerization strength of EO substituted 2-ureido-pyrimidinones **1a-g** was probed using $^1\text{H-NMR}$ dilution experiments in dry CDCl_3 . Upon dilution of tri-EO monomethyl ether substituted UPy **1e** (in which the EO chain is connected via a C_2 spacer) an additional signal at $\delta = 5.86$ ppm is found in the region of the $^1\text{H-NMR}$ spectrum where the signals of the alkylidene protons resonate (Figure 6.1a). At high concentrations only a single signal at $\delta = 5.82$ ppm is observed, the value of which corresponds¹⁹ to the alkylidene proton of the UPy dimer. Further examination of the ^1H -spectrum of **1e** in CDCl_3 showed concentration dependent changes in the region where the inter and intra molecular NH protons resonate (Figure 6.1b) as well as in the region where the methylene protons of the EO chain resonate (Figure 6.1c).

DOSY NMR on a solution of **1e** (0.5 mM in CDCl_3) shows that the second signal at $\delta = 5.86$ ppm belongs to a faster diffusing species (Appendix A). Based on the ratio of the two diffusion constants and assuming a spherical geometry²⁰ a molecular weight ratio of 1.85 was calculated, in close agreement²¹ with the fact that the additional signals originate from the 6[1H]-pyrimidinone monomeric form. Using the integral ratio between the monomeric and dimeric signals (see Appendix B) in the $^1\text{H-NMR}$ spectrum of **1e** at 25 °C, a K_{dim} of $3 (\pm 0.5) \times 10^4 \text{ M}^{-1}$ was calculated. This value of K_{dim} is approximately 1000 times lower than the dimerization constant of aliphatic substituted ureido-pyrimidinones.¹³

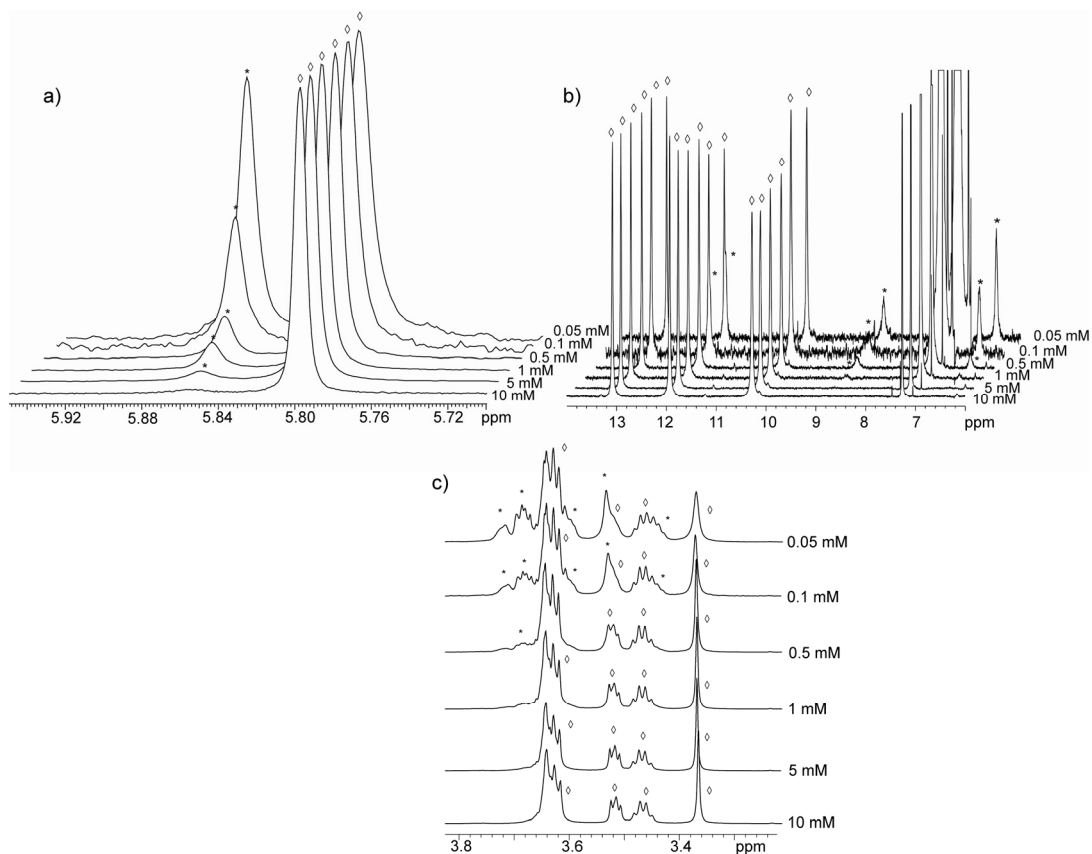


Figure 6.1: Partial ^1H -NMR spectra of **1e** in CDCl_3 ($T = 25\text{ }^\circ\text{C}$) at different total concentrations of UPy (abbreviated as U_0) showing: a) the changes in the region were the $\text{C}=\text{CH}$ proton on the ureido-pyrimidinone ring resonate. b) the changes in the region were the NH protons resonate, c) the changes in the region were the $\text{NHCH}_2\text{CH}_2\text{OCH}_2\text{CH}_2\text{OCH}_2\text{CH}_2\text{OCH}_3$ protons resonate. The symbols denote signals belonging to dimeric (\diamond) and monomeric ($*$) species. All spectra were normalized with respect to the peak at 5.82 ppm (a), 13.1 ppm (b) and 3.36 ppm (c).

In order to delineate the relation between the length of the aliphatic spacer (m) and the number of EO units (n), ^1H -NMR dilution experiments were performed on all UPy compounds **1a-g** in CDCl_3 up onto a concentration of 0.5 mM. Based on these titrations the K_{dim} value can be calculated if $K_{\text{dim}} < 10^6\text{ M}^{-1}$ (Table 6.1).²² From the data in Table 6.1 it can be concluded that the value of K_{dim} decreases as the number of EO units (n) is increased and within the series $n = 2$ increases as the total number of carbon atoms ($m + 2$) between the ureido NH proton and the first oxygen atom of the EO chain is increased from 2 to 6. For a shorter EO chain ($n = 1$) the situation is less straightforward as in this case the K_{dim} decreases upon going from $m = 0$ to $m = 1$ (*vide infra*).

Table 6.1: Dimerization constants for model compounds **1a-g** as determined by $^1\text{H-NMR}$ dilution experiments in CDCl_3 at 25 °C.

Compound	K_{dim} (M^{-1})
1a ($n = 0, m = 0$)	$>10^6$
1b ($n = 0, m = 1$)	$>10^6$
1c ($n = 1, m = 0$)	$>10^6$
1d ($n = 1, m = 1$)	$5 \times 10^5 \pm 1 \times 10^5$
1e ($n = 2, m = 0$)	$2.8 \times 10^4 \pm 0.2 \times 10^4$
1f ($n = 2, m = 1$)	$7.7 \times 10^4 \pm 0.6 \times 10^4$
1g ($n = 2, m = 4$)	$> 10^6 \text{ M}^{-1}$

6.2.3 Infrared spectroscopy

FT-IR spectroscopy is a powerful tool for the evaluation of the preferred conformation²³ of the terminal EO chains in UPy compounds **1a-g**. Previous FT-IR studies on mono-disperse EO chains in various solvents has shown that the *anti* and *gauche* conformations of the C-C and C-O bonds have different stretching vibrations.²⁴ Because backfolding of the EO chain to the acidic NH protons of the UPy motif results in a change of the EO chain from a linear to a bent conformation it is expected that this process can be conveniently monitored by FT-IR. In order to minimize the number of C-C bonds, FT-IR dilution experiments in CDCl_3 were performed on model compound **8** ($m = 0, n = 2$) bearing a methyl group on the pyrimidinone ring (see Figure 6.2). The dimerization constant of this compound was determined to be $1.2 \times 10^4 \text{ M}^{-1}$ based on the integrals of the monomer and dimer in the $^1\text{H-NMR}$ spectrum obtained at 0.1 mM and 0.05 mM. Unfortunately, the changes in the region between $1290\text{--}1360 \text{ cm}^{-1}$, characteristic for the changes in the C-C and C-O stretch vibrations, could not be followed at low concentrations due to the low intensity of the peaks in this region and the presence of artefacts caused by the high concentration of solvent.

However, it proved possible to probe the changes in the amide I and amide II region (between 1500 and 1750 cm^{-1}) as a function of concentration due to the higher intensity of the vibrations present in this region. Concentration dependent infrared measurements performed on a solution of **8** in CDCl_3 revealed significant changes in the amide I and amide II region, indicative of a rearrangement of the hydrogen bond array. As can be observed from Figure 6.2, the most pronounced changes can be observed in the bands between $1550\text{--}1590 \text{ cm}^{-1}$ and $1625\text{--}1675 \text{ cm}^{-1}$.

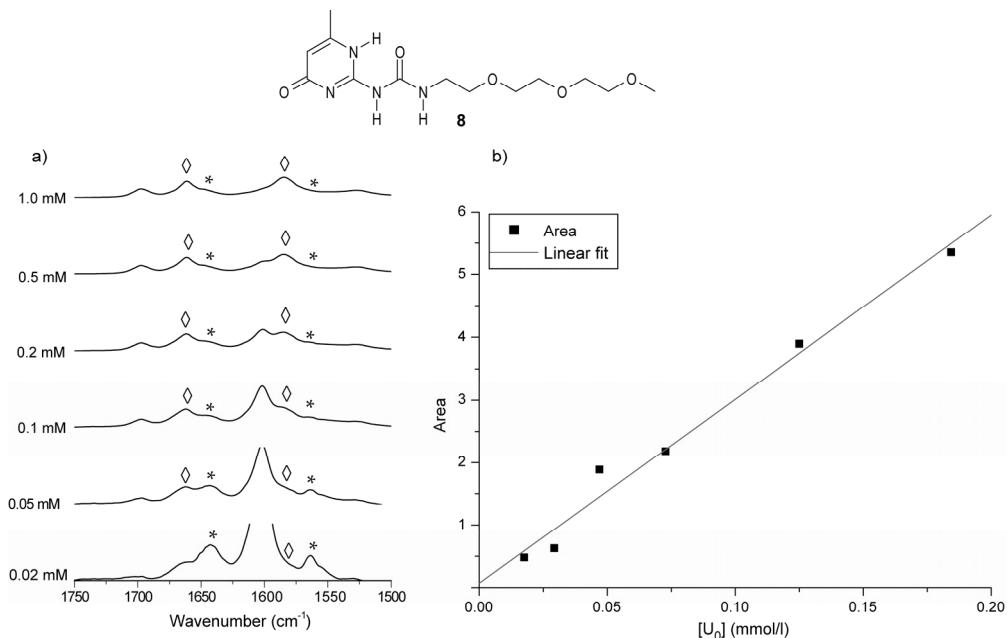


Figure 6.2: FT-IR dilution of **8** in CDCl₃ at room temperature: a) Amide I and amide II region of the FT-IR spectrum of **8** in CDCl₃ normalized for the concentration of UPy (U_0). The symbols denote signals belonging to dimeric (◇) and monomeric (*) species. The band at 1600 cm⁻¹ is assigned to residual water in the sample. b) Relative area of the IR band at 1560 cm⁻¹ obtained by deconvolution plotted against the calculated monomer concentration (U_0).

To allow for a quantitative analysis, the FT-IR spectrum between 1500 and 1710 cm⁻¹ at each concentration was deconvoluted into seven peaks using a Lorentzian²⁵ lineshape (Figure 6.2b). A plot of the relative area of the band at 1560 cm⁻¹ (corrected for the concentration) against the calculated monomer concentration reveals that this band indeed originates from monomeric ureido-pyrimidinone.

In order to further prove the claim that the K_{dim} of **1g** ($m = 4$, $n = 2$) is indeed much higher than that of **8** ($m = 0$, $n = 2$) concentration dependent FT-IR measurements were also conducted on **1g** in CDCl₃. As can be observed from the concentration dependent FT-IR spectra (Figure 6.3) no spectral changes on diluting from 1 mM to 0.04 mM occur, in agreement with the much higher K_{dim} value of **1g** ($> 10^6$ M⁻¹) as found using ¹H-NMR.

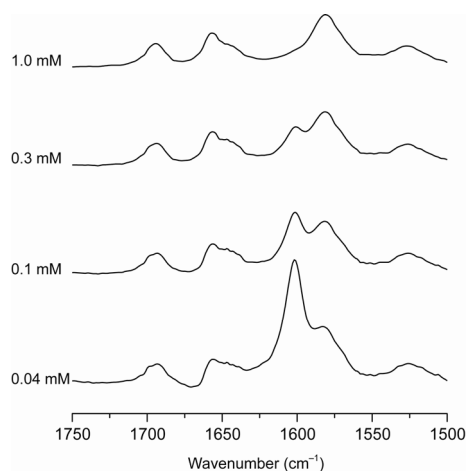


Figure 6.3: Amide I and amide II region of the FT-IR spectrum at various concentrations of **1g** in CDCl_3 at room temperature. The band at 1600 cm^{-1} is assigned to residual water in the sample.

6.2.4 UV-Vis spectroscopy

UV-Vis spectroscopy provides a convenient tool to evaluate the tautomeric preference of the pyrimidinone ring.²⁶ More specifically, it has been shown that the 4[1H] pyrimidinone tautomer has an absorption maximum at 260 nm while the 6[1H] tautomer has an absorption maximum at 285 nm. Because no experimental data is available for the enol tautomer a theoretical study on the various monomeric pyrimidinone tautomers using TDDFT (time dependent DFT) was performed. The time-dependent density functional theory is well-known as a rigorous formalism for the treatment of excitation energies within the DFT framework.²⁷ The combination of efficiency as well as precision makes TDDFT very attractive and as a result it has been applied for the calculation of excitation energies of simple molecules²⁸ and large systems.²⁹ The TD-DFT calculations on 2-ureido-pyrimidinone monomers **9a-c** were performed using the hybrid PBE0 functional³⁰ in conjunction with the standard 6-311++G(2d,p) triple split basis set³¹ using the Gaussian03 suite of programs.³² The effect of solvent (CHCl_3) on the excitation energies was taken into account using the polarizable continuum model (PCM) of nonequilibrium solutions.³³

As can be observed from the calculated oscillator strengths of the three different tautomeric forms (Figure 6.4a), the 6[1H] tautomer has an absorption at high wavelengths which is not present in the two other tautomeric forms. Figure 6.4b shows the measured UV-Vis spectra of 0.05 mM solutions of **1a-f** in CHCl_3 . The extinction coefficient at 285 nm, corresponding to the 6[1H] tautomer, is largest for the compounds with the lowest K_{dim} indicating that the fraction present as the 6[1H] is the largest for

these. Moreover, the values of the extinction coefficient nicely follow the order of K_{dim} as determined by the $^1\text{H-NMR}$ experiments.

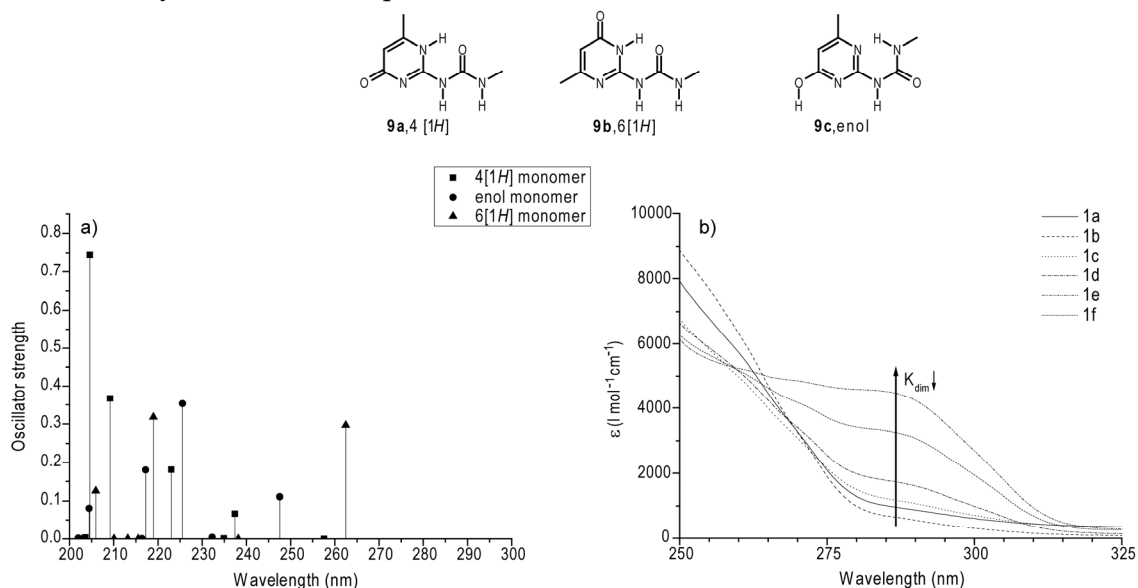


Figure 6.4: a) Calculated oscillator strength stick spectra of 2-ureido-pyrimidinone tautomers **9a-c** at 0 K. b) Partial UV-Vis spectra of 0.05 mM solutions of compounds **1a-f** in CHCl_3 ($T = 25^\circ\text{C}$).

6.2.5 $^1\text{H-NMR}$ coupling constant analysis

In order to gain more insight into the cause of the reduced K_{dim} of UPy compounds **1e** and **1f** ($n = 2$), a 2D NOESY experiment was conducted on a 0.5 mM solution of **1f** in CHCl_3 . Molecular models of **1f** in the *transoid*, *transoid* 6[1H] tautomeric form indicate that the distance between the ureido-NH protons and the closest methylene protons of the EO chain should be within 4 Å when the polyether oxygen atoms are hydrogen bonded to the NH protons of the urea functionality. Unfortunately, no NOe contact between these protons could be observed at a concentration of 0.5 mM, most possibly due to the low fraction of the 6[1H] tautomer at this concentration. 2D NOESY experiments conducted at lower concentration also failed due to the low signal to noise ratio as a result of the low sensitivity of the 2D NOESY sequence.

$^1\text{H-NMR}$ coupling constant analysis is a common technique for the evaluation of conformational equilibria in molecules. The relation between the $^3J_{\text{HH}}$ coupling constant and the dihedral torsion angle was first described by Karplus³⁴ and later generalized by Haasnoot and Altona.³⁵ In general, the coupling constants are largest for dihedral angles close to 180° (*anti* conformation). As previously mentioned two sets of signals, corresponding to the 4[1H] UPy dimer and the 6[1H] UPy monomer, are visible at low concentrations of **1f** in CDCl_3 . Unfortunately, $^1\text{H-NMR}$ coupling constant analysis on the $-\text{O}-\underline{\text{CH}_2}-\underline{\text{CH}_2}-\text{O}-$ protons could not be performed due to the overlapping peaks of

monomer and dimer in the region between 3-3.8 ppm. However, $^1\text{H-NMR}$ coupling constant analysis of the central methylene protons in the C_3 spacer of **1f** revealed that the two multiplets have different coupling constants *i.e.* 6.6 Hz for the dimer and 5.4 Hz for the monomer (Figure 6.5). The decrease of the coupling constant can be explained by an increase in the fraction of C-C bonds adopting a *gauche* conformation in the C_3 spacer of the monomer compared to the dimer (Figure 6.5). Hence, it can be concluded that the C_3 chain connecting the EO chain with 2-ureido-pyrimidinone ring undergoes a conformational change as the UPy tautomerizes from the 4[1H] dimer to the 6[1H] monomer, in agreement with the backfolding hypothesis.

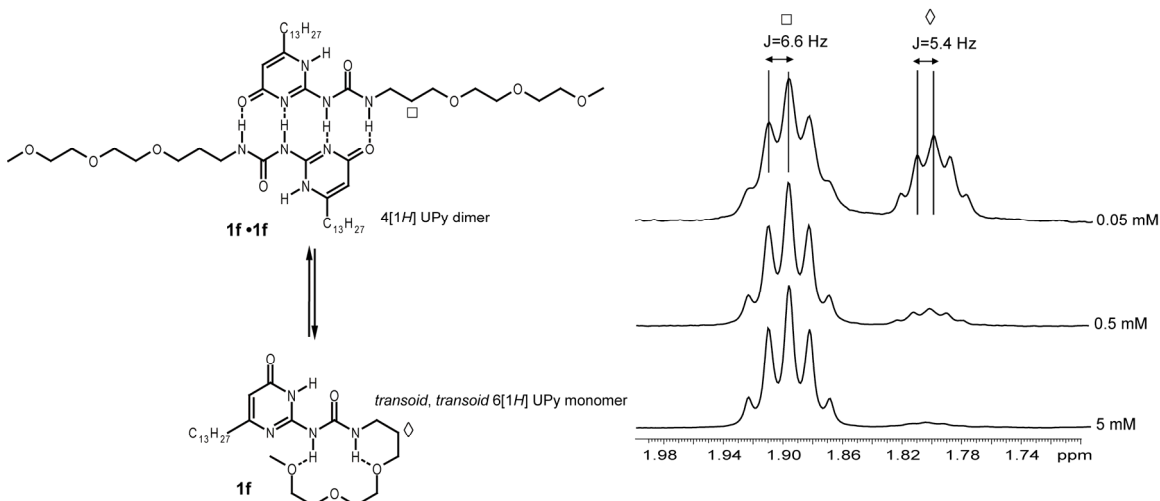


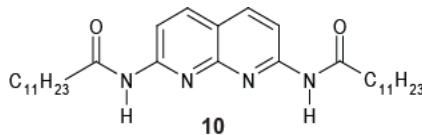
Figure 6.5: Partial $^1\text{H-NMR}$ spectrum of UPy **1f** in CDCl_3 ($T = 25\text{ }^\circ\text{C}$) showing the splitting pattern of the central methylene protons of the C_3 spacer. The left part of the picture displays the conformational changes in the C_3 spacer upon going from the 4[1H] UPy dimer to the 6[1H] UPy monomer, the latter in which the EO chain is hydrogen bonded to the oxygen atoms of the EO chain.

6.2.5 How is the association constant with 2,7-diamido-1,8-naphthyridine affected?

Based on the UV-Vis experiments described in the previous sections it can be concluded that the 6[1H] monomer becomes increasingly stabilized as the number of EO units is increased. As explained in Chapter 2, the fidelity of UPy·NaPy hetero-complex formation can be greatly increased if UPy dimerization is much weaker than the association strength of UPy·NaPy formation. Because the K_{dim} of **1e** and **1f** is precisely known, the K_a of **1e** and **1f** with NaPy **10** could be reliably obtained by UV-Vis titrations using the procedure as outlined in Chapter 2.

As is shown in Table 6.2, the K_a values of **1e** ($m = 0, n = 2$) and **1f** ($m = 1, n = 2$) with **10** are 50-80 times smaller compared to the value of K_a of **10** with 2-ureido-pyrimidinone substituted with an aliphatic substituent ($K_a \approx 5 \times 10^6 \text{ M}^{-1}$ in CHCl_3).

Table 6.2: UPy dimerization constant and UPy·NaPy association constant of UPy **1e**, **1f** and **1g** and NaPy **10** in CDCl₃ (K_{dim}) and CHCl₃ (K_a) at 25 °C.



Compound	K_{dim} (M ⁻¹)	K_a (M ⁻¹)
1e	$2.8 \pm 0.2 \times 10^4$	$9.6 \pm 0.2 \times 10^4$
1f	$7.7 \pm 0.6 \times 10^4$	$6.9 \pm 0.4 \times 10^4$
1g	$> 10^6$	$0.55\text{-}3.5 \times 10^6$

Given the fact that the K_{dim} of UPy **1g** ($m = 4$, $n = 2$) could not precisely be determined, the absorption data obtained from the titration of **1g** and **10** was fitted with two different values of K_{dim} corresponding to the lowest (10^6 M⁻¹) and highest (6×10^7 M⁻¹) estimate of K_{dim} . In this way, the value of K_a of **1g**·**10** was determined to be in the range of $0.55\text{-}3.5 \times 10^6$ M⁻¹ which is close to the value of 5×10^6 M⁻¹ found for 2-ureido-pyrimidinone molecules substituted with aliphatic substituents. From this data it can thus be concluded that substitution of tri EO chains ($n = 2$) to UPy compounds results in a loss of binding strength with 2,7-diamido-1,8-naphthyridine when short spacers are used to connect the EO chain to the urea functionality of the UPy unit.

6.2.6 Discussion and conclusion: the effect of short EO chains on the thermodynamics of UPy dimers in CDCl₃

The data as presented in the previous sections are significant for a number of reasons. Firstly, the results from the UV-Vis studies clearly show that the UPy compounds displaying a reduced K_{dim} , are present in their 6[1H] tautomeric form at low concentrations. Secondly, the FT-IR experiments show a rearrangement of the hydrogen bonding array as is evident by the large concentration dependent changes in the amide I and amide II region of the spectrum. Finally, although a NOe interaction between the ureido NH and the methylene groups of the EO chain could not be detected, analysis of the coupling constant of the central \underline{CH}_2 protons of the C₃ spacer in UPy compound **1f** did show evidence of backfolding of the EO chain in the monomeric form of **1f**.

Taken all the results into account two mechanisms can be thought to be responsible for the reduction of K_{dim} in EO substituted 2-ureido-pyrimidinones. 1) Hydrogen bonding of the ether oxygen atoms of the EO chain to the acidic NH protons of the urea in the *transoid*, *transoid* 6[1H] monomeric form causes an additional stabilization of this tautomer compared to the dimerizing 4[1H] tautomer. Because the measured K_{dim} is the product of the tautomerization constant *squared* (K_{taut} , defined as: $K_{taut} = \text{concentration}$

4[1H] monomer / concentration 6[1H] monomer) and the true dimerization constant of the 4[1H] monomer (K_{dim}^* defined as: concentration 4[1H] dimer / (concentration 4[1H] monomer)²) it can be easily recognized that an increase in the stability of the 6[1H] tautomer leads to a rapid decrease in the observed K_{dim} (Figure 6.6a) due to a decrease in K_{taut} . As was explained previously, the stabilizing effect of intramolecular hydrogen bonding of the EO chain on the 6[1H] monomer will be lower for longer spacers (increasing m) due to entropic effects while it will increase with the number of possible interactions (n). 2) Repulsive electrostatic interactions between the first oxygen of the EO chain and the carbonyl group of pyrimidinone ring (Figure 6.6b). In this case the K_{dim} is lowered due the fact that the UPy 4[1H] dimer is destabilized with respect to its aliphatic counterpart. For this interaction, the largest effect on K_{dim} is expected for the shortest spacer (small m).

As can be observed from Table 6.1 and Figure 6.4b, within the series $n = 2$, K_{dim} reduces as m is increased. As the EO chain for $n = 2$ is large enough to form intramolecular hydrogen bonds to both NH protons, this increase in K_{dim} as m grows larger is a direct result of an increasing entropic penalty for cyclization for larger aliphatic spacers. Furthermore, the number of unfavourable *gauche* interactions, induced in the aliphatic spacer as it bends back upon itself, also increases as m grows larger resulting in a higher enthalpic offset for back folding of the larger spacers. In addition to these effects, the effect of repulsive electrostatic interactions is the highest for $m = 0$.

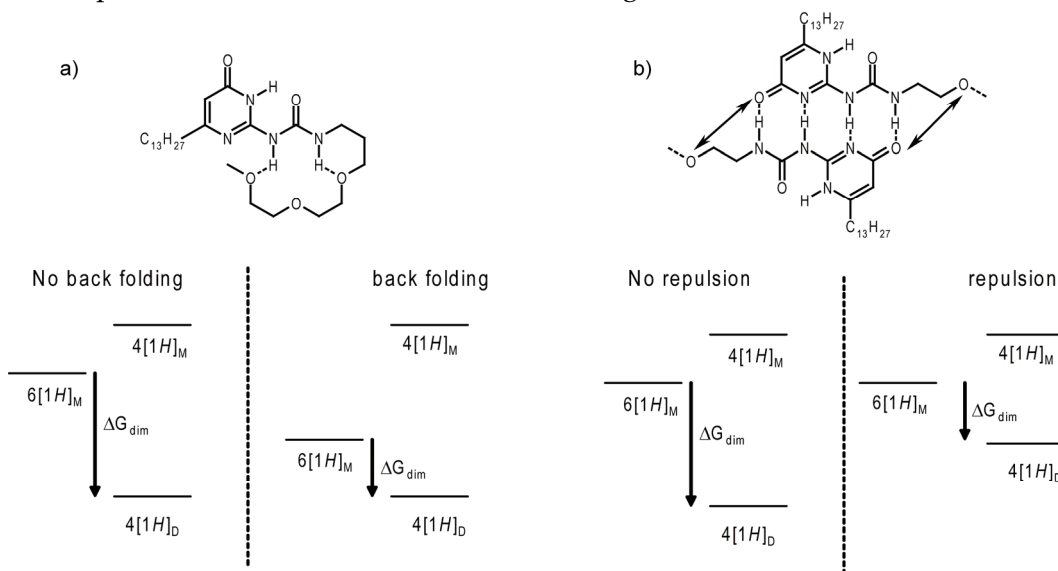


Figure 6.6: The effect of short EO chains on the thermodynamics of UPy dimerization. a) The effect of stabilization of the 6[1H] tautomer, resulting in a reduction in K_{dim} (and hence ΔG_{dim}). b) The effect of repulsive electrostatic interactions, resulting in destabilization of the 4[1H] dimer and subsequent reduction in K_{dim} . The subscripts M and D denote monomer and dimer respectively.

As already noted, within the series $n = 1$, the opposite behaviour is observed, *i.e.* upon increasing m from 0 to 1, K_{dim} decreases. To understand the cause of this effect, Monte Carlo conformational searching using the OPLS 2005 force field and the GB/SA solvation model (CHCl_3) was performed using Macromodel 9.5 on derivatives of **1c** and **1d** in which the tridecyl chain is substituted for a methyl group. Subsequently, the lowest energy conformers of **1c** and **1d** found using this procedure were optimized at the B3LYP//6-311G+(d,p)//PCM(CHCl_3) level of theory. Analysis of the hydrogen bond geometries of both conformers show that in the case of **1d** ($m = 1$) the hydrogen bond lengths are between 1.91 and 2.16 Å while the N-H \cdots O angles are 138° and 172° respectively. On the other hand, the hydrogen bond lengths in the folded conformation of **1c** are much larger, *i.e.* between 1.93 and 2.52 Å while the angles are 163° and 141° respectively (Figure 6.7). Statistical surveys of crystallographic data suggest that the optimum bond distances are approximately 1.9 Å for H \cdots O and that hydrogen bonding is strongest when the NH \cdots O angle approaches linearity.^{16,36,37} Taken into account these findings and the calculated hydrogen bond lengths and angles in the lowest energy conformers of **1c** and **1d** it can be concluded that the extent of intramolecular hydrogen bonding is much higher in monomeric **1d** compared to **1c** due to the fact that the longer aliphatic spacer in **1d** allows simultaneous binding of both NH protons to the ether oxygen atoms of the EO chain.

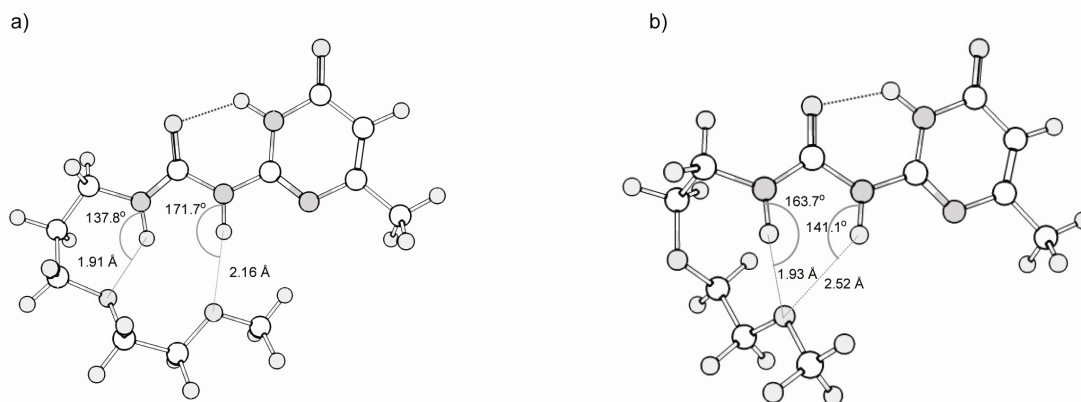


Figure 6.7: Energy minimized structures (DFT, B3LYP//6-311G+(d,p)//PCM(CHCl_3)) of: a) Transoid, transoid 2-ureido-6[1H]-pyrimidinone **1c** ($m = 1$, $n = 1$) b) Transoid, transoid 2-ureido-6[1H]-pyrimidinone **1d** ($m = 0$, $n = 1$). Note that the aliphatic tridecyl chain in **1c** and **1d** has been replaced by a CH_3 group to speed up calculations.

More importantly, the EO chain of **1d** can form multiple hydrogen bonds without violating stereochemical restrictions, *i.e.* all torsion angles C–C–O–C and C–O–C–C

along the polyether chain are *anti* (between 162° and 178°) while the angles O-C-C-O are *gauche* (60°), as is also observed in the crystal structure of a 1:1 complex of urea and bis[2-*o*-methoxyphenoxy]ethyl ether.³⁸

Although the present analysis has only taken into account the hydrogen bond geometry in the lowest energy conformers of **1c** and **1d**, similar effects are also expected in other conformers in which the conformation of the EO chain is different.

In comparison to the association constant (K_a) that has been reported for 2-ureido-pyrimidinones carrying aliphatic chains, the K_a of EO substituted 2-ureido-pyrimidinones with 2,7-diamido-1,8-naphthyridine is reduced by roughly two orders of magnitude. This reduction can also be attributed to back folding. As explained in Chapter 2, the *cisoid*, *transoid* 6[1H] tautomeric form can bind to 2,7-diamido-1,8-naphthyridine resulting in the formation of a **ADDA** hydrogen bond array. However, stabilization of this conformer by intramolecular hydrogen bonding of the ether oxygen atoms present in the EO chain is much less favorable compared to intramolecular hydrogen bonding of the EO chains in the *transoid*, *transoid* conformer (Figure 6.8). Hence, also in this case stabilization of the *transoid*, *transoid* 6[1H] monomer results in a perturbation of the equilibrium ultimately resulting in a decrease of K_a .

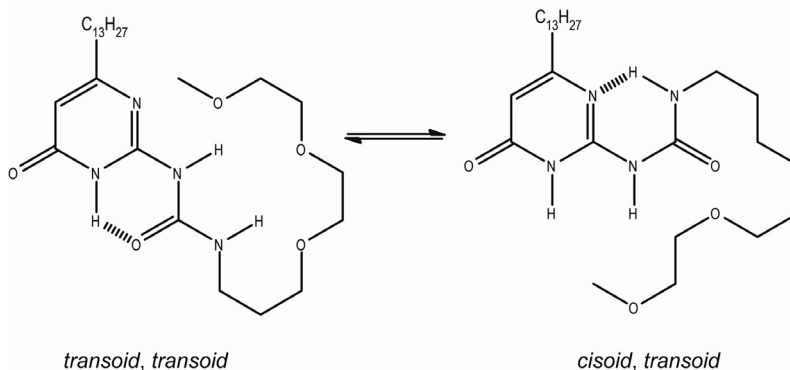
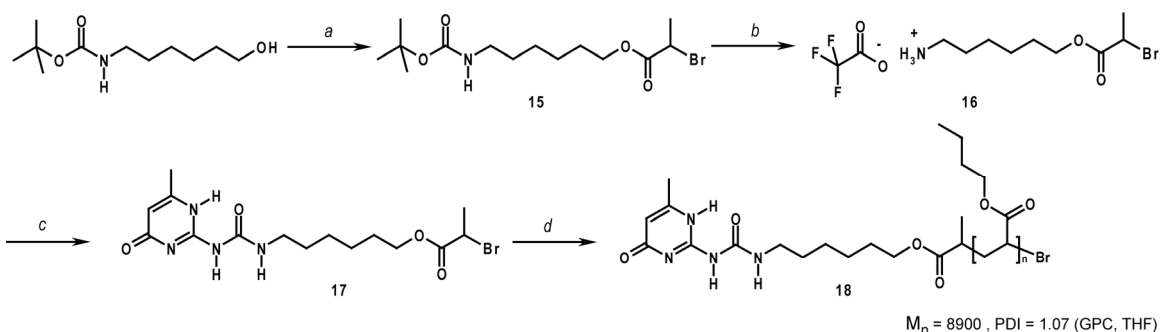


Figure 6.8: Conformational equilibria of the 2-ureido-6[1H]-pyrimidinone monomers of **1e**. Backfolding of the EO chains is geometrically much more feasible in the *transoid*, *transoid* conformer.

It is interesting to note that although UPy dimerization is lowered by a factor of 2000 for **1e**, the K_a of **1e**·**10** is only reduced by a factor of 60. The cause of this difference can be twofold. Firstly, backfolding of the EO chain to the intramolecular hydrogen bond of the UPy·NaPy complex **1e**·**10** can cause an increased stabilization of this complex. Secondly, repulsive electrostatic interactions between the oxygen atoms of the EO chain and the electronegative atoms constituting the hydrogen bond array are much less pronounced in the UPy·NaPy complex compared to the UPy·UPy complex.



Scheme 6.6: Synthetic route toward $P(nBA)_n\text{-C}_6\text{-UPy}$ **18**: a) 2-bromopropionyl bromide, pyridine, dichloromethane, 12 h, 0 °C then RT, 64%; b) trifluoroacetic acid, dichloromethane, 14 h, 0 °C then RT, 93%; c) 2-(1-imidazolylcarbonylamino)-6-methyl-4-[1H]-pyrimidinone, triethylamine, chloroform, 12 h, 50 °C, 50%; d) *n*-butyl-acrylate (*nBA*), PMDETA, CuBr, 3 h, 70 °C.

The $^1\text{H-NMR}$ spectra of $P(nBA)_n\text{-C}_2\text{-UPy}$ **14** and $P(nBA)_n\text{-C}_6\text{-UPy}$ **18** in CDCl_3 at a concentration of 10 mM clearly shows three sharp resonances in the downfield region (> 9 ppm) of the spectrum indicative of extensive dimerization via hydrogen bonding. Furthermore, the position of the alkylidene proton of the pyrimidinone ring for both UPy polymers at this concentration is indicative for the formation quadruple hydrogen bonded dimers.

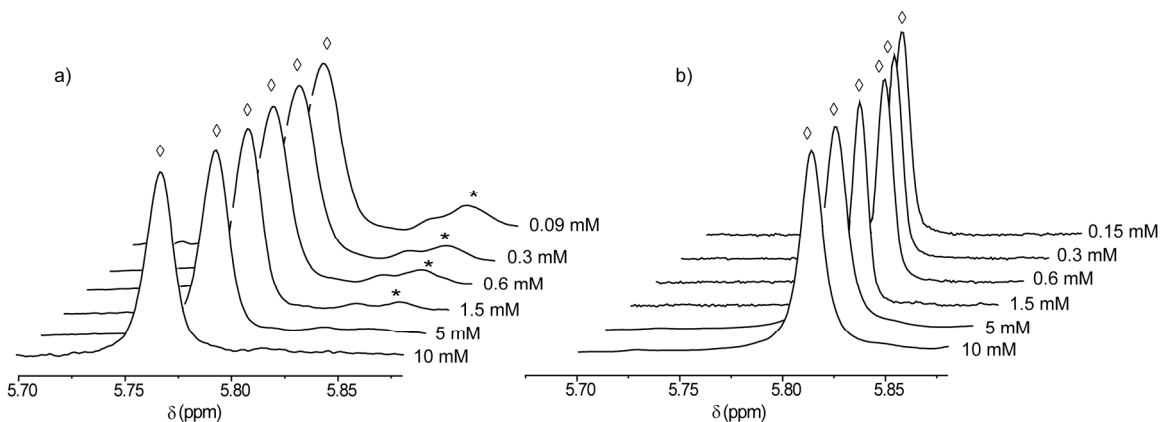


Figure 6.9: Partial $^1\text{H-NMR}$ spectra in CDCl_3 at 25 °C showing the concentration dependent changes in the region where the $\text{C}=\text{CH}$ proton of the ureido-pyrimidinone ring resonates for: a) $P(nBA)_n\text{-C}_2\text{-UPy}$ **14** in which a C_2 spacer connects the UPy end group with the $P(nBA)_n$. b) $P(nBA)_n\text{-C}_6\text{-UPy}$ **18** in which a C_6 spacer connects the UPy end group with the $P(nBA)_n$. The symbols denote signals belonging to dimeric (\diamond) and monomeric (*) species.

To investigate the dimerization constant of the two polymers in CDCl_3 , $^1\text{H-NMR}$ dilution experiments were performed on UPy polymers **14** and **18**. Figure 6.9 displays the partial $^1\text{H-NMR}$ spectra of the signals corresponding to the alkylidene proton of the pyrimidinone ring for both UPy polymers. Whereas no concentration dependent

changes are observed for $P(nBA)_n\text{-C}_6\text{-UPy}$ **18**, the $^1\text{H-NMR}$ spectrum of $P(nBA)_n\text{-C}_2\text{-UPy}$ **14** shows an additional signal, corresponding to monomeric 2-ureido-6[1H]-pyrimidinone at lower concentrations.

In order to confirm the lower dimerization constant of UPy polymer **14**, concentration dependent DOSY experiments were performed. As can be observed in Figure 6.10a, the viscosity corrected self-diffusion constant⁴¹ of the protons of $P(nBA)_n\text{-C}_2\text{-UPy}$ **14** becomes larger upon lowering the concentration, indicative of an increase in monomeric **14** at lower concentrations. In sharp contrast, the viscosity corrected self-diffusion constant of the protons of $P(nBA)_n\text{-C}_6\text{-UPy}$ **18** are concentration independent between 1 mM and 0.03 mM (Figure 6.10b) indicating that solutions of UPy polymer **18** mainly contain dimerized species in this concentration range (Figure 6.10b).

The transition from a concentration independent ($c < 0.1$ mM) to a concentration dependent regime ($c > 1$ mM) as is clearly observed for UPy polymer **18** can be attributed to the onset of domain overlap interactions occurring between the polymeric chains.

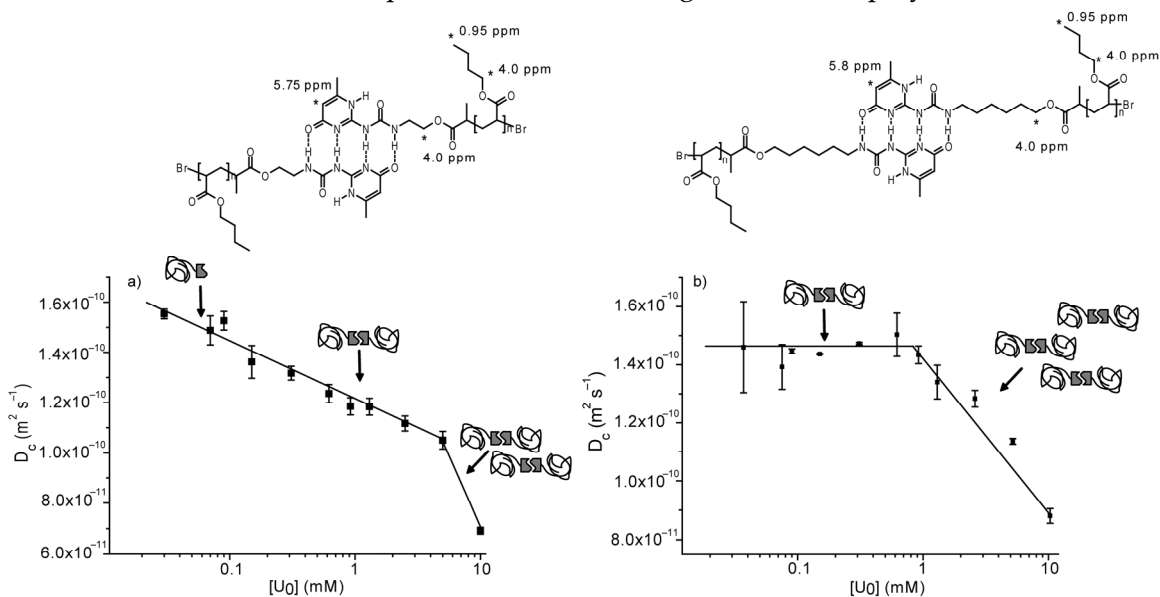


Figure 6.10: Concentration dependent diffusion constants in CDCl_3 at $25\text{ }^\circ\text{C}$ for: a) $P(nBA)_n\text{-C}_2\text{-UPy}$ **14** in which a C_2 spacer connects the UPy end group with the $P(nBA)_n$. b) $P(nBA)_n\text{-C}_6\text{-UPy}$ **18** in which a C_6 spacer connects the UPy end group with the $P(nBA)_n$. The diffusion constants were acquired using the bipolar pulse pair stimulated echo sequence with convection compensation.⁴² The calculated diffusion constant is the average diffusion constant determined for the protons marked with an asterisk.

Fitting of the non-corrected self-diffusion constant of **18** in the concentration range from 10 to 2 mM to a power law ($D_s \sim c^{-\nu}$) gives $\nu = 0.35$ ($R^2 = 0.93$) which deviates somewhat from the theoretical value of $\nu = 0.5$ found by Hess using a theory of phase-space distribution of polymer segments.⁴³ This discrepancy can be attributed to two effects.

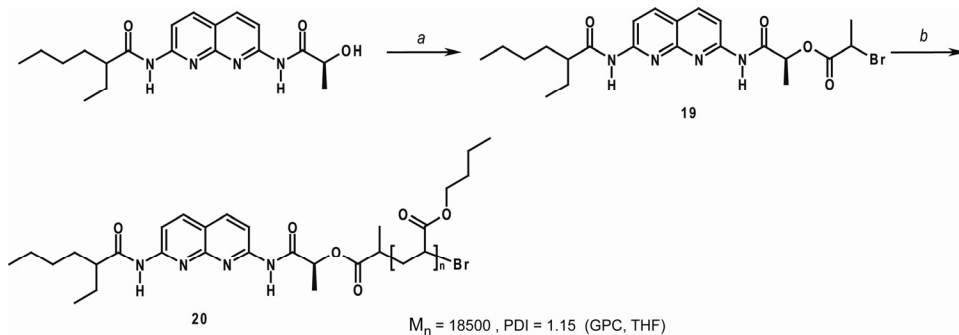
Firstly, the width of the crossover regime in which $D_s \sim c^{-0.5}$ holds is small as was also observed experimentally by fluorescence correlation spectroscopy on polystyrene chains.⁴⁴ Secondly, the theory of Hess does not take into account the fact that the individual polymer coils formed by dimeric **18** can exchange with each other due to the reversible nature of the hydrogen bonded end groups.

Based on the combined concentration dependent ¹H-NMR and DOSY study it can be concluded that the K_{dim} of $P(n\text{BA})_n\text{-C}_6\text{-UPy}$ **18** is much higher than $P(n\text{BA})_n\text{-C}_2\text{-UPy}$ **14** in accordance with the results obtained from the concentration dependent studies of EO substituted 2-ureido-pyrimidinones. Indeed, UV-Vis spectra of **14** and **18** in CHCl_3 at a concentration of 0.05 mM clearly show that the extinction coefficient of **14** at 285 nm is higher than the extinction coefficient of **18** at the same wavelength, indicating an increased fraction of monomeric UPy in the first (Appendix C).

The K_{dim} of UPy polymer **14** was calculated to be $1.7 \pm 0.3 \times 10^4 \text{ M}^{-1}$ based on the integral ratio between the signals corresponding to monomeric 2-ureido-6[1H]pyrimidinone and dimeric 2-ureido-4[1H]pyrimidinone in solutions of **14** at low concentration. Based on the lowest concentration of the DOSY experiments, the K_{dim} of **18** can be estimated to be $> 10^6 \text{ M}^{-1}$.

6.3.2 Hetero-dimerization strength

The synthesis of $P(n\text{BA})_n\text{-NaPy}$ **20** is depicted in Scheme 6.7. The association strength of UPy **14** and UPy **18** with NaPy polymer **20** was probed using UV-Vis titrations. Fitting of the absorption at 355 nm as a function of added **14** (Appendix D) using a K_{dim} of $1.7 \times 10^4 \text{ M}^{-1}$ for **14**·**14** resulted in a K_a of $1.2 \pm 0.4 \times 10^3 \text{ M}^{-1}$ for UPy·NaPy complex **14**·**20**.



Scheme 6.7: Synthetic route toward $P(n\text{BA})_n\text{-NaPy}$ **20**: a) 2-bromopropionyl bromide, triethylamine, tetrahydrofuran, 4 h, 0 °C then RT, 91%. b) *n*-butyl-acrylate (*nBA*), Me_6TREN , CuBr , 3 min, 70 °C.

Given the fact that the K_{dim} of UPy **18** could not precisely be determined, the absorption data obtained from the titration of **18** and **20** was fitted with different values of K_{dim} corresponding to the lowest (10^6 M^{-1}) and highest ($6 \times 10^7 \text{ M}^{-1}$) estimate of K_{dim} . In this

way, the value of K_a of **18·20** was determined to be in the range of $0.45\text{-}3 \times 10^6 \text{ M}^{-1}$ which is close to the value of $5 \times 10^6 \text{ M}^{-1}$ found for 2-ureido-pyrimidinone molecules substituted with aliphatic substituents. The dimerization constants and association constants of UPy polymers **14** and **18** and NaPy polymer **20** are summarized in Table 6.3.

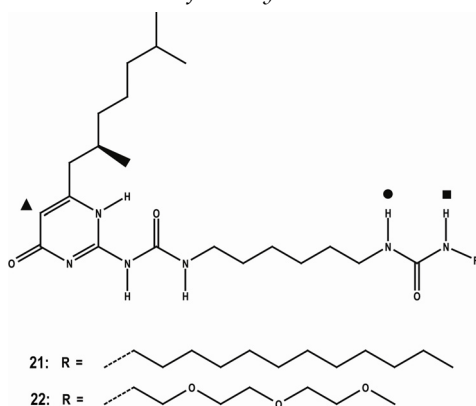
Table 6.3: UPy dimerization constant and UPy-NaPy association constant of UPy polymer **14** and **18** and NaPy polymer **20** in CDCl_3 (K_{dim}) and CHCl_3 (K_a) at 25 °C.

Compound	$K_{dim} (\text{M}^{-1})$	$K_a (\text{M}^{-1})$
14	$1.7 \pm 0.3 \times 10^4$	$1.2 \pm 0.4 \times 10^3$
18	$> 10^6$	$0.45\text{-}3 \times 10^6$

6.4 The effect of ethylene oxide chains on the self-association of UPy-urea dimers in CDCl_3

In Chapter 5, the self-association of UPy dimers bearing an additional urea functionality was discussed. Specifically, it has been shown that the dimer of UPy **21**, in which a linear alkyl substituent is attached to the urea functionality, forms small aggregates in CDCl_3 as is evident from the concentration dependent $^1\text{H-NMR}$ chemical shift of both NH protons as well as the alkylidene proton of the pyrimidinone ring. The concentration dependence of the chemical shift could be fitted using an isodesmic self-association model resulting in an equilibrium constant (K_i) between $5\text{-}15 \text{ M}^{-1}$ depending on the proton of interest (Table 6.4). To investigate the influence of EO chains on the self-association of UPy-urea dimers in solution, UPy **22** was synthesized via a previously established synthetic route (Chapter 5, Scheme 5.3).

$^1\text{H-NMR}$ dilution experiments on **22** in CDCl_3 and fitting of the resulting concentration dependent chemical shift to an isodesmic model (see Chapter 5 for details) resulted in an average K_i value of both NH protons of only 2.5 M^{-1} (see Appendix E for the data), a value eight times lower compared to the K_i value of **21·21**.

Table 6.4: *Isodesmic equilibrium constants (K_i) for UPy-urea dimers 21·21 and 22·22 in $CDCl_3$ at 25 °C.*

Compound	Urea NH ● (M^{-1})	Urea NH ■ (M^{-1})	Alkylidene ▲ (M^{-1})
21·21	14.9	14.6	5
22·22	2.4 ± 1.3	2.5 ± 0.5	a)

a) Although this signal showed an upfield shift, the changes were too small to be fitted in a reliable way.

6.5 Discussion and conclusion

As has been shown in this Chapter, substitution of hydrogen bond directed supramolecular assemblies with polar chains containing hydrogen bonding acceptors leads to a reduction of the association constant in apolar solvents, where the reduction of the association constant is dependent on the length of the aliphatic spacer connecting the hydrogen bonds and the polar side chain. Although in this Chapter only UPy based assemblies were investigated, it was recently found that substitution of a single alkyl chain with an EO chain severely reduces the association constant of the hydrogen bond induced supramolecular polymerization of N,N',N'' -trialkyl-benzene-1,3,5-tricarboxamides in apolar solvents.⁴⁵

Furthermore, the effect of short ethylene oxide monomethyl ether chains on two distinct supramolecular assemblies has been recently reported by Bouteiller⁴⁶ and Araki.⁴⁷ In both cases, the dominant secondary interaction responsible for the non-covalent assembly is hydrogen bonding. In the first report, Bouteiller discusses the influence of EO tails on the supramolecular polymerization of ethylene oxide substituted bis-ureas in polar and apolar solvents while in the second example Araki discusses the influence of EO tails on the formation of giant supramolecular vesicles composed of hydrogen-bonded sheet structures of guanosine derivatives. These two examples have in common that the microscopic (formation of vesicles) and macroscopic properties (viscosity) of the

thermodynamically formed supramolecular assembly are highly dependent on the creation of a hydrophobic pocket that shields the hydrogen bonds from the EO moiety. The results described in this Chapter illustrate the extreme sensitivity of non-covalent assemblies towards substitution with polar groups. As has been noted in the introduction, EO chains are commonly used in various applications in order to increase the solubility in water.⁴⁸ However, in almost all cases the influence of the EO chain on the properties of the conjugate is not compared to the properties of the unfunctionalized analogue. Although the effects of EO chains on non-covalent interactions in apolar solvents are relatively easy to understand, the situation in water is considerably more difficult due to additional hydrogen bonding of water with the EO chain. Recent experiments aiming to elaborate the effect of protein PEGylation have shown that substitution of proteins with EO chains can result in a decreased binding affinity due to intramolecular interactions between the EO chain and the active site of the protein.⁴⁹ These results seem to suggest that backfolding of EO chains can also occur in water, especially when electrostatic interactions are involved.

6.6 Experimental section

General Methods

See General Methods Chapter 2. All reactions were performed under an atmosphere of Argon unless noted otherwise. Size exclusion chromatography was carried out at room temperature on a Waters chromatograph connected to a Waters 410 differential refractometer and six Waters Styragel columns (five HR-5 μm and one HWM-20 μm) using THF as eluent (flow rate: 1 mL/min). A Waters 410 differential refractometer and a 996 photodiode array detector were employed. The molecular weights of the polymers were calculated relative to linear polystyrene standards. Tetrahydrofuran was dried using a Pure Solv-MD solvent purification system from Advanced Technology. *n*-Butyl acrylate (*n*BA) was purified by passing over neutral alumina.

2-[2-(2-Methoxyethoxy)ethoxy]ethyl amine (**2e**) was synthesized according to Scherman.⁵⁰ 2-(1-Imidazolylcarbonylamino)-6-methyl-4-[1H]-pyrimidinone (**11**) was prepared as reported by Keizer.⁵¹ 2-Ethyl-N-(7-((S)-2-hydroxypropanamido)-1,8-naphthyridin-2-yl)hexanamide was synthesized as described in Chapter 3. 2-(6-[1-Imidazolylcarbonylamino]-hexylureido-6-(2(R),6-dimethylheptyl)-4[1H]pyrimidinone was synthesized as described in Chapter 5.

Synthesis of 2-(2-methoxyethyl)-ureido-6-tridecyl-4[1H]pyrimidinone (**1a**)

Activated pyrimidinone **3** (1.94 g, 5.00 mmol) and 2-methoxyethyl amine **2a** (0.75 g, 10.00 mmol) were added to dry CHCl_3 (16 mL) and stirred at 60 °C for 2 days. After cooling to room temperature, 50 mL CHCl_3 was added, and the mixture was extracted 3 times with 15 mL aqueous 1 M HCl, neutralized with 20 mL saturated NaHCO_3 (aq) and washed with 20 mL brine. After drying with MgSO_4 the solvent was removed by evaporation *in vacuo*, resulting in the crude

ureido-pyrimidinone (1.66 g, 4.2 mmol). Further purification by silica filtration using 4% methanol in CHCl₃ as eluent, resulted in pure **1a** as a white powder (1.40 g, 3.5 mmol), mp: 118.5-119.8 °C. Yield: 71%. ¹H-NMR (CDCl₃): δ = 13.09 (s, 1H, NH), 11.95 (s, 1H NH), 10.33 (s, 1H, NH), 5.82 (s, 1H, O=C-CH=C-CH₂), 3.56 (m, 2H, NH-CH₂-CH₂-O), 3.48 (t, 2H, m, 2H, NH-CH₂-CH₂-O), 3.38 (s, 3H, O-CH₃), 2.45 (t, 2H, CH=C-CH₂-CH₂), 1.62 (m, 2H, CH=C-CH₂-CH₂-CH₂), 1.31-1.25 (m, 20H, -CH₂-), 0.87 (t, 3H, -CH₃). ¹³C-NMR (CDCl₃): δ = 173.1, 156.9, 154.6, 152.4, 105.9, 71.0, 58.8, 39.6, 32.7, 31.9, 29.6-28.8 (multiple signals), 27.0, 22.7, 14.1. IR (ATR): ν = 2953, 2918, 2850, 1698, 1660, 1582, 1524, 1467, 1438, 1310, 1258, 1212, 1199, 1137, 1124, 1088, 965, 943, 884, 810, 771, 743, 721 cm⁻¹. MALDI-TOF-MS (m/z): calcd: 394.29. Observed: 395.26 (MH⁺), 417.24 (MNa⁺). Anal. Calcd for C₂₁H₃₈N₄O₃: C 63.93, H 9.71, N 14.20. Found: C 64.12, H 9.94, N 14.45.

Synthesis of 2-(3-methoxypropyl)-ureido-6-tridecyl-4[1H]pyrimidinone (**1b**)

Activated pyrimidinone **3** (1.94 g, 5.00 mmol) and 3-methoxypropyl amine **2b** (0.89 g, 10.00 mmol) were added to dry CHCl₃ (16 mL) and stirred at 60 °C for 2 days. After cooling to room temperature, 50 mL CHCl₃ was added, and the mixture was extracted 3 times with 15 mL 1 M aqueous HCl, neutralized with 20 mL saturated NaHCO₃ (aq) and washed with 20 mL brine. After drying with MgSO₄ the solvent was removed by evaporation *in vacuo*, resulting in the crude ureido-pyrimidinone (1.90 g, 4.65 mmol). Further purification by silica filtration using 4% methanol in CHCl₃ as eluent, resulted in the pure product as a white powder (1.61 g, 3.95 mmol), mp: 89.3-89.9 °C. Yield: 79%. ¹H-NMR (CDCl₃): δ = 13.15 (s, 1H, NH), 11.91 (s, 1H, NH), 10.22 (s, 1H, NH), 5.81 (s, 1H, O=C-CH=C-CH₂), 3.45 (t, 2H, CH₂-CH₂-O), 3.35-3.32 (m, 5H, NH-CH₂-CH₂ and O-CH₃), 2.45 (t, 2H, CH=C-CH₂-CH₂), 1.88 (m, 2H, NH-CH₂-CH₂-CH₂-O), 1.62 (m, 2H, CH=C-CH₂-CH₂-CH₂), 1.31-1.25 (m, 20H, -CH₂-), 0.87 (t, 3H, -CH₃). ¹³C-NMR (CDCl₃): δ = 173.1, 156.7, 154.7, 152.4, 105.8, 70.1, 58.6, 37.0, 32.7, 31.9, 29.6-28.8 (multiple signals), 27.0, 22.6, 14.1. IR (ATR): ν = 2918, 2850, 1698, 1657, 1579, 1524, 1467, 1445, 1395, 1307, 1255, 1212, 1196, 1126, 1109, 946, 884, 813, 792, 771, 741, 722 cm⁻¹. MALDI-TOF-MS (m/z): calcd: 408.31. Observed: 409.42 (MH⁺), 431.40 (MNa⁺). Anal. Calcd for C₂₂H₄₀N₄O₃: C 64.67, H 9.87, N 13.71. Found: C 65.10, H 9.97, N 13.85.

Synthesis of 2-[2-(2-methoxyethoxy)ethyl]ureido-6-tridecyl-4[1H]pyrimidinone (**1c**)

Activated pyrimidinone **3** (0.428 g, 1.1 mmol) and 2-(2-methoxyethoxy)ethyl amine **2c** (0.20 g, 1.6 mmol) were added to dry CHCl₃ (4 mL) and stirred at 60 °C for 2 days. After cooling to room temperature, 50 mL CHCl₃ was added, and the mixture was extracted 3 times with 15 mL 1 M aqueous HCl, neutralized with 20 mL saturated NaHCO₃ (aq) and washed with 20 mL brine. After drying with MgSO₄ the solvent was removed by evaporation *in vacuo*, resulting in the crude ureido-pyrimidinone (0.44 g, 1.0 mmol). Further purification by recrystallization from 2-propanol, resulted in pure **1c** as a white powder (0.37 g, 0.85 mmol), mp: 92.7-93.1 °C. Yield: 78%. ¹H-NMR (CDCl₃): δ = 13.08 (s, 1H, NH), 11.94 (s, 1H, NH), 10.27 (s, 1H, NH), 5.80 (s, 1H, O=C-CH=C-CH₂), 3.67-3.64 (m, 4H, O-CH₂-), 3.54 (m, 2H, O-CH₂-), 3.47 (m, 2H, NH-CH₂-CH₂-O), 3.37 (s, 3H, O-CH₃), 2.45 (t, 2H, CH=C-CH₂-CH₂), 1.62 (m, 2H, CH=C-CH₂-CH₂-CH₂), 1.32-1.26 (m, 20H, -CH₂-), 0.88 (t, 3H, -CH₃). ¹³C-NMR (CDCl₃): δ = 173.0, 156.8, 154.6, 152.4, 105.8, 72.0, 70.5, 70.3, 69.4, 59.0, 39.5, 32.7, 31.9, 29.6-28.8 (multiple signals), 27.0, 22.7, 14.1. IR (ATR): ν = 2919, 2852, 1698, 1664, 1620, 1585, 1563, 1527, 1489, 1468, 1456, 1398, 1332, 1302, 1261, 1202, 1124, 1029, 983, 947, 884, 854,

808, 771, 744, 722 cm^{-1} . MALDI-TOF-MS (m/z): 438.32. Observed: 439.37 (MH^+), 461.62 (MNa^+). Anal. Calcd for $\text{C}_{23}\text{H}_{42}\text{N}_4\text{O}_4$: C 62.98, H 9.65, N 12.77. Found: C 62.51, H 9.69, N 11.70.

Synthesis of 2-[3-(2-Methoxyethoxy)propyl]ureido-6-tridecyl-4[1H]pyrimidinone (1d)

Activated pyrimidinone **3** (1.55 g, 4.0 mmol) and 3-(2-methoxyethoxy)propyl amine **2d** (0.955 g, 7.2 mmol) were added to dry CHCl_3 (15 mL) and stirred at 60 °C for 2 days. After cooling to room temperature, 150 mL CHCl_3 was added, and the mixture was extracted 3 times with 60 mL aqueous 0.1 M HCl (aq), neutralized with 150 mL saturated NaHCO_3 (aq) and washed with 150 mL brine. After drying with MgSO_4 the solvent was removed by evaporation *in vacuo*, resulting in the crude ureido-pyrimidinone (1.53 g, 3.4 mmol). Further purification by recrystallization from 2-propanol, resulted in pure **1d** as a white powder (0.958 g, 2.1 mmol), mp: 92.9-93.4 °C Yield: 53%. $^1\text{H-NMR}$ (CDCl_3): δ = 13.14 (s, 1H, NH), 11.90 (s, 1H, NH), 10.21 (s, 1H, NH), 5.79 (s, 1H, $\text{O}=\text{C}-\text{CH}=\text{C}-\text{CH}_2$), 3.60-3.52 (m, 6H, $\text{O}-\text{CH}_2$ -), 3.38 (s, 3H, $\text{O}-\text{CH}_3$), 3.36 (m, 2H, $\text{NH}-\text{CH}_2-\text{CH}_2$), 2.46 (t, 2H, $\text{CH}=\text{C}-\text{CH}_2-\text{CH}_2$), 1.91 (m, 2H, $\text{NH}-\text{CH}_2-\text{CH}_2-\text{CH}_2-\text{O}$), 1.63 (m, 2H, $\text{CH}=\text{C}-\text{CH}_2-\text{CH}_2-\text{CH}_2$), 1.32-1.21 (m, 20H, $-\text{CH}_2$ -), 0.88 (t, 3H, $-\text{CH}_3$). $^{13}\text{C-NMR}$ (CDCl_3): δ = 173.0, 156.7, 154.7, 152.4, 105.8, 72.0, 70.1, 68.9, 59.0, 37.1, 32.7, 31.9, 29.6-28.8 (multiple signals), 27.0, 22.7, 14.1. IR (ATR): ν = 2955, 2921, 2852, 1698, 1662, 1585, 1527, 1469, 1446, 1309, 1258, 1200, 1136, 1112, 1047, 947, 882, 849, 815, 792, 771, 742 cm^{-1} . MALDI-TOF-MS (m/z): 452.33. Observed: 453.38 (MH^+), 475.36 (MNa^+). Anal. Calcd for $\text{C}_{24}\text{H}_{44}\text{N}_4\text{O}_4$: C 62.21, H 9.61, N 11.61. Found: C 62.51, H 9.69, N 11.70.

Synthesis of 2-{2-[2-(2-methoxyethoxy)ethoxy]ethyl}ureido-6-tridecyl-4[1H] pyrimidinone (1e)

Activated pyrimidinone **3** (1.04 g, 2.68 mmol) and 2-(2-[2-methoxyethoxy]ethoxy)ethyl amine **2e** (0.889 g, 5.45 mmol) were added to dry CHCl_3 (9 mL) and stirred at 60 °C for 2 days. After cooling to room temperature, 25 mL CHCl_3 was added, and the mixture was extracted 3 times with 10 mL 0.1 M aqueous HCl, neutralized with 15 mL saturated NaHCO_3 (aq) and washed with 20 mL brine. After drying with MgSO_4 the solvent was removed by evaporation *in vacuo*, resulting in the crude ureido-pyrimidinone (1.1 g, 2.3 mmol). Further purification by recrystallization from 2-propanol, resulted in pure **1e** as a white powder (0.89 g, 1.8 mmol), mp: 82.6-83.0 °C. Yield: 69%. $^1\text{H-NMR}$ (CDCl_3): δ = 13.08 (s, 1H, NH), 11.93 (s, 1H, NH), 10.28 (s, 1H, NH), 5.80 (s, 1H, $\text{O}=\text{C}-\text{CH}=\text{C}-\text{CH}_2$), 3.64 (m, 8H, $\text{O}-\text{CH}_2$ -), 3.52 (m, 4H, $\text{O}-\text{CH}_2$ -), 3.47 (s, 3H, $\text{O}-\text{CH}_3$), 2.45 (t, 2H, $\text{CH}=\text{C}-\text{CH}_2-\text{CH}_2$), 1.63 (m, 2H, $\text{CH}=\text{C}-\text{CH}_2-\text{CH}_2-\text{CH}_2$), 1.28 (m, 20H, $-\text{CH}_2$ -), 0.87 (t, 3H, $-\text{CH}_3$). $^{13}\text{C-NMR}$ (CDCl_3): δ = 173.0, 156.8, 154.6, 152.4, 105.8, 72.0, 70.5, 70.3, 69.4, 59.0, 39.5, 32.7, 31.9, 29.6-28.8 (multiple signals), 27.0, 22.7, 14.1. IR (ATR): ν = 3216, 3135, 3030, 2955, 2918, 2873, 2853, 2817, 1702, 1676, 1641, 1620, 1594, 1562, 1470, 1456, 1418, 1400, 1333, 1280, 1262, 1202, 1186, 1122, 1045, 1028, 997, 982, 949, 937, 925, 866, 854, 827, 799, 791, 780, 772, 767, 742, 720, 708, 694 cm^{-1} . MALDI-TOF-MS (m/z): 482.35. Observed: 483.37 (MH^+), 505.34 (MNa^+). Anal. Calcd for $\text{C}_{25}\text{H}_{46}\text{N}_4\text{O}_5$: C 62.21, H 9.61, N 11.61. Found: C 62.51, H 9.69, N 11.70.

Synthesis of 2-{3-[2-(2-methoxyethoxy)ethoxy]propyl}ureido-6-tridecyl-4[1H] pyrimidinone (1f)

Activated pyrimidinone **3** (1.55 g, 4.00 mmol) and 3-(2-[2-methoxyethoxy]ethoxy)propyl amine **2f** (0.90 g, 5.08 mmol) were added to dry CHCl_3 (13 mL) and stirred at 60 °C for 2 days. After cooling to room temperature, 35 mL CHCl_3 was added, and the mixture was extracted 3 times with 15 mL 0.1 M aqueous HCl, neutralized with 20 mL saturated NaHCO_3 (aq) and washed with

20 mL brine. After drying with MgSO₄ the solvent was removed by evaporation *in vacuo*, resulting in the crude ureido-pyrimidinone (1.6 g, 3.2 mmol). Further purification by recrystallization from 2-propanol, resulted in pure **1f** as a white powder (1.3 g, 2.6 mmol), mp: 71.1-74.5 °C. Yield: 65%. ¹H-NMR (CDCl₃): δ = 13.14 (s, 1H, NH), 11.91 (s, 1H, NH), 10.20 (s, 1H, NH), 5.81 (s, 1H, O=C-CH=C-CH₂), 3.67-3.52 (m, 10H, O-CH₂-), 3.38 (s, 3H, O-CH₃), 3.33 (m, 2H, NH-CH₂-CH₂), 2.46 (t, 2H, CH=C-CH₂-CH₂), 1.90 (m, 2H, NH-CH₂-CH₂-CH₂-O), 1.63 (m, 2H, CH=C-CH₂-CH₂-CH₂), 1.31-1.26 (m, 20H, -CH₂-), 0.88 (t, 3H, -CH₃). ¹³C-NMR (CDCl₃): δ = 173.0, 156.5, 154.5, 152.3, 105.7, 71.8, 70.5, 70.4, 70.1, 68.7, 58.9, 37.0, 32.6, 31.8, 29.5-28.7 (multiple signals), 26.9, 22.5, 14.0. IR (ATR): ν = 2922, 2853, 2817, 1698, 1662, 1585, 1526, 1469, 1445, 1362, 1309, 1259, 1114, 1043, 991, 964, 948, 883, 816, 792, 771, 742 cm⁻¹. Anal. Calcd for C₂₆H₄₈N₄O₅: C 62.87, H 9.74, N 11.28. Found: C 62.96, H 9.76, N 11.37. MALDI-TOF-MS (m/z): 496.37. Observed: 497.29 (MH⁺), 519.26 (MNa⁺), 535.24 (MK⁺).

Synthesis of 2-{6-[2-(2-methoxyethoxy)ethoxy]hexyl}ureido-6-tridecyl-4[1H]-pyrimidinone (**1g**)

Activated pyrimidinone **3** (0.44 g, 1.13 mmol), 6-[2-(2-methoxyethoxy)ethoxy]hexyl ammonium trifluoroacetate **2g** (0.50 g, 1.58 mmol) and triethylamine (0.18 g, 1.80 mmol) were added to dry CHCl₃ (5 mL) and stirred at 55 °C for 2 days. After cooling, 25 mL CHCl₃ was added, and the mixture was extracted 3 times with 10 mL 0.1 M aqueous HCl, neutralized with 15 mL saturated NaHCO₃ (aq) and washed with 20 mL brine. After drying with MgSO₄ the solvent was removed by evaporation *in vacuo*, resulting in the crude ureido-pyrimidinone (0.53 g, 0.99 mmol). This was purified by recrystallization from 2-propanol, yielding the pure product as a white powder (0.46 g, 0.85 mmol), mp: 68.3-68.5 °C. Yield: 75%. ¹H-NMR (CDCl₃): δ = 13.17 (s, 1H, NH), 11.88 (s, 1H, NH), 10.18 (s, 1H, NH), 5.81 (s, 1H, O=C-CH=C-CH₂), 3.66-3.63 (m, 4H, O-CH₂-), 3.59-3.54 (m, 4H, O-CH₂-), 3.44 (t, 2H, O-CH₂-CH₂-CH₂), 3.38 (s, 3H, O-CH₃), 3.24 (m, 2H, NH-CH₂-CH₂), 2.46 (t, 2H, CH=C-CH₂-CH₂), 1.66-1.54 (m, 6H, NH-CH₂-CH₂-CH₂, O-CH₂-CH₂-CH₂ and CH=C-CH₂-CH₂-CH₂), 1.38-1.26 (m, 24H, -CH₂-), 0.88 (t, 3H, -CH₃). ¹³C-NMR (CDCl₃): δ = 173.2, 156.6, 154.7, 152.4, 105.8, 72.0, 71.4, 70.7, 70.5, 70.1, 59.0, 40.0, 32.7, 31.9, 29.6-28.9 (multiple signals), 27.0, 26.8, 25.8, 22.7, 14.1. IR (ATR): ν = 2922, 2850, 1698, 1662, 1579, 1526, 1466, 1438, 1307, 1259, 1203, 1124, 1005, 948, 885, 813, 771, 744 cm⁻¹. MALDI-TOF-MS (m/z): 538.42. Observed: 539.50 (MH⁺), 561.48 (MNa⁺), 577.45 (MK⁺). Anal. Calcd for C₂₉H₅₄N₄O₅: C 64.65, H 10.10, N 10.40. Found: C 64.44, H 10.30, N 10.63.

Synthesis of 2-(2-methoxyethoxy)ethyl amine (**2c**)

N-2-(2-methoxyethoxy)ethyl phthalimide **6** (2.60 g, 10.4 mmol) was dissolved in a 1/1 v/v% mixture of 9 mL hydrazine monohydrate and ethanol, followed by heating to reflux temperature (110 °C) while stirring vigorously during 16 h under an inert atmosphere. After cooling down to room temperature, the product was extracted with 4 times 30 mL toluene from the pale-yellowish precipitate. The combined organic layers were collected and evaporated to yield the title compound, **2c**, as a yellowish oil (0.80 g, 6.7 mmol). Yield: 64%. ¹H-NMR (CDCl₃): δ = 3.58-3.44 (m, 6H, O-CH₂), 3.33 (s, 3H, O-CH₃), 2.82 (m, 2H, CH₂-CH₂-NH₂), 1.30 (s, 2H, NH₂). ¹³C-NMR (CDCl₃): δ = 73.5, 71.8, 70.1, 58.9, 41.7. IR (ATR): ν = 3172, 3080, 2951, 2922, 2853, 2664, 1979, 1693, 1649,

1603, 1470, 1409, 1371, 1342, 1322, 1278, 1232, 1224, 1180, 1092, 1068, 1027, 979, 914, 874, 858, 805, 751 cm⁻¹.

Synthesis of 3-(2-methoxyethoxy)propyl amine (2d)

A solution of 3-(2-methoxyethoxy)propanenitrile **4a** (3.84 g, 29.8 mmol) in dry tetrahydrofuran (30 mL) was added dropwise to a 1 M BH₃·THF solution (134 mL) in a 250 mL round-bottom flask after which the mixture was refluxed overnight. After subsequent cooling, the flask was placed in an ice bath, and slowly 50 mL methanol and 5 drops of 37% aqueous HCl solution were added. This procedure was repeated twice. Co-evaporation with toluene *in vacuo* resulted in a yellowish oil which was dissolved in 200 mL dichloromethane and transferred to a separation funnel. To this solution, 1 M aqueous NaOH was added until the aqueous layer became basic (70 mL) and additionally 0.1 M aqueous NaOH until the aqueous layer became clear (200 mL). The aqueous layer was extracted 3 times with 200 mL dichloromethane, and the combined organic phases were dried with MgSO₄ and evaporated *in vacuo*. The resulting oil was co-evaporated with toluene to give the title compound as a yellow oil (1.56 g, 8.80 mmol). Yield: 38%. ¹H-NMR (CDCl₃): δ = 3.52-3.49 (m, 6H, O-CH₂), 3.34 (s, 3H, O-CH₃), 2.75 (t, 2H, O-CH₂-CH₂-NH₂), 1.70-1.61 (m, 4H, CH₂-CH₂-CH₂ + NH₂). ¹³C-NMR (CDCl₃): δ = 71.8, 69.9, 69.3, 58.9, 50.0, 39.4, 33.2. IR (ATR): ν = 3369, 3303, 2927, 2865, 1600, 1456, 1386, 1300, 1244, 1199, 1102, 1031, 926, 848, 773 cm⁻¹.

Synthesis of 3-[2-(2-methoxyethoxy)ethoxy]propyl amine (2f)

A solution of 3-[2-(2-methoxyethoxy)ethoxy]propanenitrile **4b** (4.00 g, 23.1 mmol) in dry tetrahydrofuran (25 mL) was added dropwise to a 1 M BH₃·THF solution (104 mL) in a 250 mL round-bottom flask and the mixture was refluxed overnight. After subsequent cooling, the flask was placed in an ice bath, and slowly 40 mL methanol and 4 drops of 37% aqueous HCl solution were added. Subsequently, the mixture was stirred at room temperature for 2 hours, after which the solvent was removed by evaporation under reduced pressure. This procedure was repeated 2 more times. The resulting oil was co-evaporated with toluene three times, dissolved in 250 mL dichloromethane and transferred to a separation funnel. To the solution, 1 M aqueous NaOH was added until the aqueous layer became basic (50 mL) and additionally 0.1 M aqueous NaOH until the aqueous layer became clear (200 mL). The aqueous layer was extracted with 3 times 250 mL dichloromethane, and the combined organic phases were dried with MgSO₄ and removed by evaporation *in vacuo*. The resulting oil was co-evaporated with toluene two times to give the title compound as a red/brown oil (1.30 g, 9.76 mmol). Yield: 33%. ¹H-NMR (CDCl₃): δ = 3.61-3.49 (m, 10H, O-CH₂ and CH₂-CH₂-NH₂), 3.33 (s, 3H, O-CH₃), 2.75 (t, 2H, O-CH₂-CH₂-CH₂), 1.68 (m, 2H, O-CH₂-CH₂-CH₂-NH₂), 1.48 (s, 2H, NH₂). ¹³C-NMR (CDCl₃): δ = 71.7, 70.4, 70.3, 69.9, 69.2, 58.8, 39.4, 33.2. IR (ATR): ν = 3365, 2870, 1640, 1574, 1471, 1386, 1351, 1304, 1248, 1199, 1099, 1027, 982, 940, 848, 820 cm⁻¹.

Synthesis of 6-[2-(2-Methoxy-ethoxy)-ethoxy]-hexylamine (obtained a TFA salt) (2g)

tert-Butyl-6-[2-(2-methoxyethoxy)ethoxy]-hexyl carbamate **7** (0.26 g, 0.81 mmol) was dissolved in 30 mL dichloromethane. Subsequently, 1.8 mL trifluoroacetic acid was added and the solution was stirred for 3 h at room temperature. After evaporation *in vacuo* and co-evaporation with toluene, the trifluoroacetate salt was obtained as a yellowish oil (0.24 g, 0.76 mmol). Yield: 94%.

$^1\text{H-NMR}$ (CDCl_3): $\delta = 7.90$ (s, 3H, NH_3), 3.66-3.55 (m, 8H, O-CH_2 -), 3.50 (t, 2H, $\text{O-CH}_2\text{-CH}_2\text{-CH}_2$), 3.39 (s, 3H, O-CH_3), 2.96 (m, 2H, $\text{CH}_2\text{-CH}_2\text{-NH}_3$), 1.72-1.34 (m, 8H, $-\text{CH}_2-$). $^{13}\text{C-NMR}$ (CDCl_3): $\delta = 71.6, 71.0, 70.1, 69.9, 69.7, 58.6, 39.6, 28.8, 26.9, 25.7, 25.0$. IR (ATR): $\nu = 3060, 2934, 2866, 1675, 1641, 1525, 1457, 1427, 1393, 1367, 1353, 1247, 1199, 1175, 1127, 1025, 983, 932, 870, 833, 798, 721, 706\text{ cm}^{-1}$.

Synthesis of 3-(2-methoxyethoxy)propanenitrile (4a)

A solution of 2-methoxyethanol (6.26 g, 82.3 mmol) in acrylonitrile (38.0 g, 0.716 mol) in a 250 mL round-bottom flask was placed in an ice bath. After cooling for 10 minutes, 0.4 g finely powdered KOH was added and the mixture was stirred at $0\text{ }^\circ\text{C}$ during 1.5 h. Subsequently, 4 drops of 37% aqueous HCl solution were added and the solvent was removed by evaporation *in vacuo* at room temperature. The residue was dissolved in 100 mL CHCl_3 , filtrated and the solvent was removed by evaporation *in vacuo* to give the title compound **4a** as a colorless oil (10.34 g, 80.02 mmol). Yield: 97% $^1\text{H-NMR}$ (CDCl_3): $\delta = 3.72$ (t, 2H, O-CH_2), 3.66 (t, 2H, O-CH_2), 3.56 (t, 2H, $\text{O-CH}_2\text{-CH}_2\text{-CN}$), 3.38 (s, 3H, O-CH_3), 2.62 (t, 2H, $\text{O-CH}_2\text{-CH}_2\text{-CN}$). $^{13}\text{C-NMR}$ (CDCl_3): $\delta = 117.7$ ($\text{C}\equiv\text{N}$), 71.4, 70.2, 65.6, 58.7, 18.5. IR (ATR): $\nu = 2881, 2830, 2251, 1456, 1416, 1387, 1359, 1331, 1300, 1245, 1225, 1199, 1099, 1026, 982, 962, 920, 850, 757\text{ cm}^{-1}$.

Synthesis of 3-[2-(2-methoxyethoxy)ethoxy]propanenitrile (4b)

A solution of diethylene glycol monomethyl ether (10.00 g, 83.22 mmol) in acrylonitrile (38.35 g, 0.722 mol) in a 250 mL round-bottom flask was placed in an ice bath. After cooling for 10 minutes, 0.3 g finely powdered KOH was added and the mixture was stirred at $0\text{ }^\circ\text{C}$ during 2 hours. Subsequently, 4 drops of 37% aqueous HCl solution were added and the solvent was removed by evaporation *in vacuo* at room temperature. The residue was dissolved in 100 mL CHCl_3 , filtrated and the solvent was removed by evaporation *in vacuo* to give the title compound **4b** as a colorless oil (13.86 g, 80.02 mmol, 96%). $^1\text{H-NMR}$ (CDCl_3): $\delta = 3.69$ (t, 2H, $\text{O-CH}_2\text{-CH}_2\text{-CN}$), 3.66-3.50 (m, 8H, $\text{O-CH}_2\text{-CH}_2\text{-O-CH}_2\text{-CH}_2\text{-O}$), 3.35 (s, 3H, O-CH_3), 2.59 (t, 2H, $\text{O-CH}_2\text{-CH}_2\text{-CN}$). $^{13}\text{C-NMR}$ (CDCl_3): $\delta = 118.1, 71.7, 70.4, 70.3, 65.7, 58.7, 18.6$. IR (ATR): $\nu = 2878, 2250, 1454, 1417, 1353, 1330, 1299, 1248, 1200, 1101, 1027, 933, 849\text{ cm}^{-1}$.

Synthesis of 2-(2-methoxyethoxy)ethyl tosylate (5)

A 250 mL three-necked round-bottom flask was charged with a solution of diethylene glycol monomethylether (10 g, 83.2 mmol) in 27.5 mL of tetrahydrofuran. Upon vigorous stirring at $0\text{ }^\circ\text{C}$, sodium hydroxide (6.75 g, 0.169 mol) dissolved in 27.5 mL of water was added. To this mixture, a solution of tosyl chloride (20.35 g, 0.157 mol) in 27.5 mL of tetrahydrofuran was added dropwise over 15 min at $0\text{ }^\circ\text{C}$. The reaction mixture was allowed to warm to room temperature and stirred for 1 h under an inert atmosphere of argon. Subsequently, 275 mL of diethyl ether was added and the organic layer was separated and washed with 1 M aqueous NaOH (3 x 35 mL) without shaking (shaking can lead to the formation of an inseparable emulsion due to the amphiphilicity of the product). Again, the organic layer was washed with water (2 x 50 mL), dried over MgSO_4 , followed by evaporation and drying *in vacuo*, to yield the title compound as a colorless liquid (22.35 g, 81.5 mmol). Yield: 98%. $^1\text{H-NMR}$ (CDCl_3): $\delta = 7.80$ (d, 2H, S-C=CH-CH), 7.30 (d, 2H, S-C=CH-CH), 4.17 (t, 2H, $\text{CH}_2\text{-CH}_2\text{-O-S}$), 3.69 (t, 2H, $\text{CH}_2\text{-CH}_2\text{-O-S}$), 3.59 (m, 2H, $\text{H}_3\text{C-O-CH}_2\text{-CH}_2\text{-O}$), 3.48 (m, 2H, $\text{H}_3\text{C-O-CH}_2\text{-CH}_2\text{-O}$), 3.35 (s, 3H, O-CH_3), 2.44 (s, 3H, C-CH_3). $^{13}\text{C-NMR}$ (CDCl_3): δ

= 144.6, 132.7, 129.6, 127.7, 71.5, 70.4, 69.1, 68.4, 58.8, 21.4. IR (ATR): ν = 3369, 3303, 2927, 2865, 1600, 1456, 1386, 1300, 1244, 1199, 1102, 1031, 926, 848, 773 cm^{-1} .

Synthesis of N-2-(2-methoxyethoxy)ethyl phthalimide (6)

A 100 mL three-necked round-bottom flask was charged with a solution of 2-(2-methoxyethoxy)ethyl tosylate **5** (10.01 g, 36.5 mmol) in 25 mL of DMF before potassium phthalimide (9.04 g, 48.8 mmol) was added. The mixture was stirred at 110 °C for 4 h under an inert atmosphere of argon. After cooling to room temperature, 175 mL of diethylether was added to facilitate the precipitation of excess phthalimide. The resulting precipitate was removed by filtration. The solution was washed with 2 times 30 mL 1 M aqueous NaOH and 30 mL brine, dried over MgSO_4 , and evaporated *in vacuo* to yield the phthalimide derivative (3.88 g, 15.6 mmol). Yield: 43%. $^1\text{H-NMR}$ (CDCl_3): δ = 7.84 (dd, 2H, phthalimide CH), 7.70 (dd, 2H, phthalimide CH), 3.91 (t, 2H, O- CH_2 - CH_2 -N), 3.75 (t, 2H, O- CH_2 - CH_2 -N), 3.64 (m, 2H, O- CH_2 - CH_2 -O), 3.50 (m, 2H, O- CH_2 - CH_2 -O), 3.31 (s, 3H, O- CH_3). $^{13}\text{C-NMR}$ (CDCl_3): δ = 167.3, 133.9, 123.2, 71.9, 69.9, 67.9, 59.0, 37.2. IR (ATR): ν = 2876, 2821, 1772, 1705, 1615, 1428, 1391, 1353, 1319, 1260, 1190, 1173, 1106, 1023, 1000, 927, 874, 850, 794, 717, 695 cm^{-1} .

Synthesis of *tert*-butyl 6-[2-(2-methoxyethoxy)ethoxy]hexyl carbamate (7)

2-[2-(2-Methoxyethoxy)]ethyl tosylate **5** (2.20 g, 8.0 mmol), N-Boc protected 6-aminohexanol (2.26 g, 10.4 mmol) and ground KOH (0.772 g, 13.6 mmol) were refluxed in 10 mL distilled tetrahydrofuran during 24 h. After subsequent cooling to room temperature 100 mL CHCl_3 was added, and the resulting solution was extracted with 100 mL 10% aqueous citric acid solution. The organic layer was then washed with 50 mL saturated NaHCO_3 (aq) and subsequently with 50 mL brine, dried over MgSO_4 and evaporated *in vacuo*. The crude product was purified using column chromatography using 1~4% methanol in CHCl_3 as eluent, yielding the pure product as a colorless oil (0.26 g, 0.81 mmol). Yield: 10%. $^1\text{H-NMR}$ (CDCl_3): δ = 3.66-3.53 (m, 8H, O- CH_2 -), 3.45 (t, 2H, O- CH_2 - CH_2 - CH_2), 3.38 (s, 3H, O- CH_3), 3.09 (m, 2H, NH- CH_2 - CH_2), 1.59-1.30 (m, 17H, C-(CH_3)₃ and - CH_2 -). $^{13}\text{C-NMR}$ (CDCl_3): δ = 156, 78.8, 71.8, 71.2, 70.5, 70.4, 69.9, 58.9, 40.4, 29.9, 29.4, 28.3, 26.5, 25.7. IR (ATR): ν = 3356, 2931, 2862, 1712, 1699, 1521, 1455, 1391, 1365, 1268, 1248, 1171, 1105, 1040, 1028, 983, 927, 853, 781, 757, 730, 664 cm^{-1} .

Synthesis of 1-(2-hydroxyethyl)-3-(6-methyl-4-oxo-1,4-dihydropyrimidin-2-yl)urea (12)

To a stirred suspension of 2-(1-imidazolylcarbonylamino)-6-methyl-4-[1H]-pyrimidinone (**11**) (20 g, 91.2 mmol) in DMF (450 mL) was added ethanolamine (8.36 g, 139 mmol) at room temperature. After 2 h, the mixture became homogeneous, and 1.5 L of acetone was added to triturate the product. The white solid was filtered and rinsed with water and then acetone. After drying under vacuum, the product **12** was obtained as a white powder (16.3 g), mp: 189 °C (degr.). Yield: 84%. $^1\text{H-NMR}$ ($\text{DMSO-}d_6$): δ = 8.19 (b, 1H), 5.73 (s, 1H, C_1H), 3.46 (t, 2H, O- CH_2), 3.22 (t, 2H, NH- CH_2), 3.05 (b, 1H, OH), 2.10 (s, 3H, CH_3). IR (ATR): ν = 3508, 3484, 3052, 2939, 2881, 1703, 1661, 1578, 1519, 1443, 1234, 1057 cm^{-1} . MALDI-TOF-MS (m/z): calcd: 212.10. Observed: 213.16 (MH^+), 235.16 (MNa^+). Anal. Calcd for $\text{C}_8\text{H}_{12}\text{N}_4\text{O}_3$: C 45.3, H 5.7, N 26.4; Found: C 45.2, H 5.52, N 27.14.

Synthesis of 2-(3-(6-methyl-4-oxo-1,4-dihydropyrimidin-2-yl)ureido)ethyl 2-bromopropanoate (13)

A solution of **12** (5.00 g, 23.6 mmol) and triethylamine (2.62 g, 25.9 mmol) in freshly distilled tetrahydrofuran (20 mL) was cooled to 0 °C, after which 2-bromopropionyl bromide (5.04 g, 23.6 mmol) was added dropwise via a syringe under an atmosphere of argon. The solution was stirred for 4 h under argon while it was allowed to cool to room temperature. Water (50 mL) was added to the mixture, which was extracted with dichloromethane. The organic fraction was washed with saturated NaHCO₃ (3 × 15 mL) and with 1 M HCl (3 × 15 mL). The organic layer was dried over MgSO₄ and evaporated to dryness. The resulting solid was purified by recrystallization from ethanol, giving the product as a white solid, mp: 183 °C (degr.). Yield: 55% yield (4.50 g). ¹H NMR (CDCl₃): δ = 12.94 (b, 1H, NH), 11.92 (b, 1H, NH), 10.45 (b, 1H, NH), 5.79 (s, 1H, C₁H), 4.48-4.27 (m, 3H, CH-Br + O-CH₂), 3.56 (m, 2H, NH-CH₂), 2.28 (s, 3H, CH₃), 1.82 (d, 3H, CH₃). ¹³C-NMR (CDCl₃): δ = 172.8, 170.4, 156.9, 154.4, 148.4, 106.9, 64.3, 40.1, 38.8, 21.7, 19.0. IR (ATR): ν = 2953, 1739, 1701, 1660, 1575, 1523, 1444, 1248, 1145 cm⁻¹. MALDI-TOF-MS (m/z): calcd: 346.04. Observed: 347.12 (MH⁺), 369.09 (MNa⁺). Anal. Calcd for C₁₁H₁₅BrN₄O₄: C 38.06, H 4.36, N 16.14. Found: C 37.61, H 4.08, N 16.09.

Synthesis of UPy end-functional poly(*n*-butyl acrylate), P(nBA)_n-C₂-UPy (14)

n-Butyl acrylate (nBA, 1.1 g, 8.6 mmol), UPy initiator **13** (30 mg, 0.086 mmol), PMDETA (30 mg, 0.172 mmol), and freshly distilled THF (1.1 g) were combined in a Schlenk flask and subjected to three freeze-pump-thaw cycles. CuBr (12 mg, 0.086 mmol) was added under flowing nitrogen, and the flask evacuated and backfilled with nitrogen twice. The flask was then sealed and placed in a 70 °C oil bath for 3 h before exposing to air and diluting with THF. The reaction mixture was passed over neutral alumina to remove the copper, concentrated, and precipitated into cold hexanes to give P(nBA)_n-C₂-UPy **14**. After drying, the resulting oil was dissolved in 50 mL CHCl₃ and the organic fraction was washed with an aqueous solution of 0.01 M EDTA (3 × 100 mL), saturated NaHCO₃ (2 × 50 mL) and brine (1 × 100 mL). Evaporation of the organic layer *in vacuo* resulted in a sticky oil which was dried over P₂O₅ *in vacuo* at a temperature of 50 °C. M_n = 9800 g/mol, PDI 1.08 (GPC, THF). ¹H-NMR (CD₂Cl₂): δ = 12.92, 11.91, 10.45, 5.77, 4.02, 2.26, 1.89, 1.60, 1.37, 0.94.

Synthesis of 6-(tert-butoxycarbonylamino)hexyl 2-bromopropanoate (15)

Boc protected 6-aminohexanol (4.4 g, 20 mmol) was dissolved in 40 mL dichloromethane and 1.87 mL (24 mmol, 1.92 g) pyridine was added and the solution cooled to 0 °C. After this, 2-bromopropionyl bromide (4.75 g, 22 mmol) was added dropwise via a syringe under an atmosphere of argon. The solution was stirred for 12 h under argon while it was allowed to cool to room temperature. The solution was transferred to a separation funnel and washed with 1 M HCl (3 × 500 mL), saturated NaHCO₃ (3 × 500 mL) and brine (1 × 100 mL) after which the organic layer was dried with MgSO₄ and evaporated *in vacuo*. Column chromatography (CHCl₃ as an eluent) afforded 4.5 g of **15** as a colorless oil. Yield: 64%. ¹H-NMR (CDCl₃): δ = 4.54 (b, 1H, NH), 4.34 (q, 1H, CH-Br), 4.16 (m, 2H, O-CH₂), 3.08 (m, 2H, CH₂-NH), 1.81 (d, 3H, CH-CH₃), 1.68-1.31 (m, 17H, CH₂ and CH₃). ¹³C-NMR (CDCl₃): δ = 170.2, 156.0, 79.0, 65.8, 40.4, 40.2, 29.9, 28.6, 28.4,

28.3, 27.8, 26.3, 25.4, 21.6. IR (ATR): $\nu = 3349, 2976, 2933, 2862, 1737, 1697, 1517, 1448, 1391, 1366, 1337, 1269, 1249, 1227, 1163, 1071, 991 \text{ cm}^{-1}$.

Synthesis of 6-aminohexyl 2-bromopropanoate (obtained as TFA salt) (16)

A solution of 6-(tert-butoxycarbonylamino)hexyl 2-bromo-propanoate (0.6 g, 1.7 mmol) in freshly distilled dichloromethane was cooled to 0 °C. Subsequently, 5 mL (1.48 g, 12.9 mmol of trifluoroacetic acid) of a 20 % (v/v) solution of trifluoroacetic acid (anhydrous) / dichloromethane (freshly distilled) was added dropwise via a syringe. The solution was allowed to cool to room temperature and stirred for an additional 12 h. Evaporation *in vacuo* and extensive drying resulted in 0.58 g of 16 as a colourless oil. Yield: 93%. $^1\text{H-NMR}$ (CDCl_3): $\delta = 7.73$ (b, 3H, NH_3^+), 4.36 (q, 1H, CH-Br), 4.16 (m, 2H, O-CH_2), 2.96 (b, 2H, $\text{CH}_2\text{-NH}_3^+$), 1.81 (d, 3H, CH-CH_3), 1.68-1.41 (m, 8H, CH_2). $^{13}\text{C-NMR}$ (CDCl_3): $\delta = 170.6, 65.5, 40.2, 39.9, 27.9, 27.2, 25.6, 24.9, 21.5$. IR (ATR): $\nu = 3450, 2940, 2866, 1779, 1734, 1672, 1529, 1469, 1447, 1431, 1392, 1381, 1337, 1276, 1199, 1133, 1063, 990.9 \text{ cm}^{-1}$.

Synthesis of 6-(3-(6-methyl-4-oxo-1,4-dihydropyrimidin-2-yl)ureido)hexyl-bromopropanoate (17)

To a solution of 2-(1-imidazolylcarbonylamino)-6-methyl-4-[1H]-pyrimidinone 11 (0.39 g, 1.90 mmol) and TFA salt 16 (0.58 g, 1.59 mmol) in 10 mL CHCl_3 was added 1 mL of triethylamine (0.72 g, 7.2 mmol). Subsequently, the solution was stirred for 12 h at a temperature of 45 °C after which the solution was cooled and 20 mL of CHCl_3 was added. The organic phase was washed with aqueous 1 M HCl (4 x 100 mL), saturated NaHCO_3 (2 x 70 mL) and brine (1 x 100 mL) and dried with MgSO_4 . Evaporation *in vacuo* and column chromatography (1 % MeOH/ CHCl_3 as an eluent) resulted in pure 17 as an off white solid, mp: 159 °C. Yield: 50%. $^1\text{H-NMR}$ (CDCl_3): $\delta = 13.11$ (b, 1H, NH), 11.86 (b, 1H, NH), 10.17 (b, 1H, NH), 5.82 (s, 1H, CH_1), 4.35 (q, 1H, CH-Br), 4.17 (m, 2H, O-CH_2), 3.25 (m, 2H, $\text{CH}_2\text{-NH}$), 2.23 (s, 3H, CH_3), 1.81 (d, 3H, CH-CH_3), 1.69-1.39 (m, 8H, CH_2). $^{13}\text{C-NMR}$ (CDCl_3): $\delta = 173.0, 170.3, 156.6, 154.7, 148.2, 106.7, 66.0, 40.2, 39.8, 29.4, 28.3, 26.5, 25.5, 21.7, 18.9$. IR (ATR): $\nu = 2937, 2856, 1735, 1698, 1666, 1582, 1525, 1445, 1338, 1307, 1257, 1227, 1163, 1138, 942 \text{ cm}^{-1}$. MALDI-TOF-MS (m/z): calcd: 402.09. Observed: 404.03 (MH^+), 425.02 (MNa^+). Anal. Calcd for $\text{C}_{15}\text{H}_{23}\text{BrN}_4\text{O}_4$: C 44.68, H 5.75, N 13.89; Found: 44.77, H 5.55, N 14.05.

Synthesis of UPy end-functional poly(n-butyl acrylate), P(nBA)_n-C₆-UPy (18)

n-Butyl acrylate (nBA, 3 g, 23.45 mmol), UPy initiator 17 (34.7 mg, 0.23 mmol), PMDETA (81 mg, 0.47 mmol) were combined in a Schlenk flask and subjected to three freeze-pump-thaw cycles. CuBr (12 mg, 0.24 mmol) was added under flowing nitrogen, and the flask evacuated and backfilled with nitrogen twice. The flask was then sealed and placed in a 70 °C oil bath for 3 h before exposing to air and diluting with THF. The reaction mixture was passed over neutral alumina to remove the copper, concentrated, and precipitated into cold hexanes to give P(nBA)_n-C₆-UPy 18. After drying, the resulting oil was dissolved in 50 mL CHCl_3 and the organic fraction was washed with an aqueous solution of 0.01 M EDTA (3 x 100 mL), saturated NaHCO_3 (2 x 50 mL) and brine (1 x 100 mL). Evaporation of the organic layer *in vacuo* resulted in a sticky oil which was dried over P_2O_5 *in vacuo* at a temperature of 50 °C. $M_n = 8900 \text{ g/mol}$, PDI 1.07 (GPC, THF). $^1\text{H-NMR}$ (CHCl_3): $\delta = 13.11, 11.85, 10.17, 5.81, 4.2-3.9, 3.2, 2.4-2.2, 1.90-0.79$.

(2S)-1-(7-(2-ethylhexanamido)-1,8-naphthyridin-2-ylamino)-1-oxopropan-2-yl-2-bromopropanoate (19)

A solution of 2-ethyl-N-(7-((S)-2-hydroxypropanamido)-1,8-naphthyridin-2-yl)hexanamide (1.00 g, 2.79 mmol) and triethylamine (0.295 g, 2.92 mmol) in tetrahydrofuran (5 mL) was cooled to 0° C, after which 2-bromopropionyl bromide (1.37 g, 6.35 mmol) was added dropwise via syringe. The solution was stirred for 4 hours. Dichloromethane (15 mL) was added to the mixture, which was washed with sat. NaHCO₃ (3 x 15 mL) and with 1 M HCl (3 x 15 mL). The organic layer was dried over MgSO₄ and evaporated to dryness. During purification, two diastereomers were separated by column chromatography eluting with 80/20 hexanes/ethyl acetate. These two products were analyzed (¹H NMR is listed for both below), but were recombined for polymerizations because the second stereocenter loses all stereochemical information upon abstraction of the bromine atom. The final product was a white solid, which is a mixture of the two diastereomers, mp: 110 °C. Yield: 91%. ¹H-NMR (CDCl₃): δ = 9.95 (b, 1H, NH), 8.55 (dd, 1H, *J*₁ = 9 Hz, *J*₂ = 3 Hz), 8.50 (b, 1H, NH), 8.44 (dd, 1H, *J* = 9 Hz), 8.15-8.19 (m, 2H, C₄H + C₁₀H), 5.77 (m, 1H, O=C-CH-O), 4.55 (q, 1H, CH-Br), 2.32 (m, 1H, C₁₅H), 1.94 (d, 3H, CH-CH₃), 1.5-1.8 (m, 11H, CH₂), 0.99 (t, 3H, CH₃), 0.89 (m, 3H, CH₃). ¹H-NMR (CDCl₃) for alternate diastereomer: δ = 9.69 (b, 1H, NH), 8.55 (dd, 1H, *J*₁ = 9 Hz, *J*₂ = 3 Hz), 8.50 (b, 1H, NH), 8.44 (dd, 1H, *J* = 9 Hz), 8.15-8.19 (m, 2H, C₄H + C₁₀H), 5.68 (m, 1H, O=C-CH-O), 4.55 (q, 1H, CH-Br), 2.32 (m, 1H, C₁₅H), 1.94 (d, 3H, CH-CH₃), 1.5-1.8 (m, 11H, CH₂), 0.99 (t, 3H, CH₃), 0.89 (m, 3H, CH₃). ¹³C-NMR (CDCl₃): δ = 175.7, 169.5, 169.2, 154.2, 153.7, 153.4, 139.3, 139.0, 118.6, 114.0, 71.8, 50.7, 39.3, 32.2, 29.7, 26.0, 22.8, 21.4, 17.7, 14.2, 11.9 ppm. IR (ATR): ν = 2931, 2873, 1706, 1685, 1607, 1542, 1499, 1389, 1311, 1134 cm⁻¹. MALDI-TOF-MS (m/z): calcd: 492.15. Observed: 494.13 (MH⁺), 515.08 (MNa⁺). Anal. Calcd for C₂₂H₂₉BrN₄O₄: C 53.56 H 5.92 N 11.36. Found: C 53.13, H 5.70 N 11.35.

Napy end-functional poly(*n*-butyl acrylate), P(nBA)_{*n*}-Napy (20)

n-Butyl acrylate (nBA, 1.95 g, 15.2 mmol), NaPy initiator **19** (150 mg, 0.3 mmol), and Me₆TREN (57 mg, 0.3 mmol) were combined in a Schlenk flask and subjected to three freeze-pump-thaw cycles. CuBr (44 mg, 0.3 mmol) was added under flowing nitrogen and the flask evacuated and backfilled with nitrogen twice. The flask was then sealed and placed in a 70°C oil bath for 30 minutes before exposing to air and diluting with THF. The reaction mixture was passed over neutral alumina to remove the copper, concentrated, and precipitated into cold hexanes. After drying, the resulting oil was dissolved in 50 mL CHCl₃ and the organic fraction was washed with an aqueous solution of 0.01 M EDTA (3 x 100 mL), saturated NaHCO₃ (2 x 50 mL) and brine (1 x 100 mL). Evaporation of the organic layer *in vacuo* resulted in a sticky oil which was dried over P₂O₅ *in vacuo* at a temperature of 50 °C to give P(nBA)_{*n*}-NaPy. M_n = 18500 g/mol, PDI 1.15 (GPC, THF). ¹H NMR (CDCl₃): δ = 8.71, 8.66, 8.43, 8.33, 5.33, 4.88, 4.02, 2.33, 1.91, 1.60, 1.38, 0.94.

Synthesis of 2-(6-[2-{2-(2-methoxyethoxy)ethoxy}ethylureido]-hexyl)-ureido-6-(2(R),6-dimethylheptyl)-4[1H]-pyrimidinone (22)

2-(6-[1-Imidazolylcarbonylamino]-hexylureido-6-(2(R),6-dimethylheptyl)-4[1H]pyrimidinone (0.20 g, 0.42 mmol) and 2-(2-[2-methoxyethoxy]ethoxy)ethyl amine (1.06 g, 0.65 mmol) were added to dry CHCl₃ (4 mL) and stirred at 55 °C for 2 days. After cooling to room temperature, 20

mL CHCl₃ was added, and the mixture was extracted 3 times with 10 mL aqueous 0.1 M HCl, neutralized with 15 mL saturated NaHCO₃ (aq) and washed with 15 mL brine. After drying with MgSO₄ the solvent was removed by evaporation *in vacuo*, resulting in the crude urea substituted 2-ureido-pyrimidinone. Further purification by recrystallization from 2-propanol, resulted in pure **22** as a white powder (0.20 g, 0.35 mmol), mp: 135.5 °C. Yield: 83%. ¹H-NMR (CDCl₃): δ = 13.18 (s, 1H, NH), 11.87 (s, 1H, NH), 10.16 (s, 1H, NH), 5.81 (s, 1H, O=C-CH=C-CH₂), 5.08 (t, 1H, NH), 4.98 (t, 1H, NH), 3.65-3.54 (m, 10H, O-CH₂-), 3.39-3.35 (m, 5H, O-CH₃ and NH-CH₂-), 3.24 (m, 2H, NH-CH₂-CH₂), 3.14 (m, 2H, NH-CH₂-CH₂), 2.50-2.45 (dd, 1H, CH=C-CH₂-CH(CH₃)-CH₂), 2.27-2.21 (dd, 1H, CH=C-CH₂-CH(CH₃)-CH₂), 1.83 (m, 1H, CH=C-CH₂-CH(CH₃)-CH₂), 1.61-1.12 (m, 15H, -CH₂- and CH₂-CH(CH₃)₂), 0.94 (d, 3H, -CH₃), 0.87 (d, 6H, -CH₃). ¹³C-NMR (CDCl₃): δ = 173.1, 158.6, 156.5, 154.7, 151.6, 106.7, 71.9, 70.6, 70.3, 70.1, 58.8, 40.4, 40.1, 39.8, 38.9, 36.6, 31.9, 30.1, 29.4, 27.8, 26.5, 26.4, 24.5, 22.6, 22.5, 19.2. IR (ATR): ν = 3340, 3220, 2929, 2958, 1700, 1655, 1624, 1572, 1527, 1483, 1463, 1382, 1366, 1351, 1294, 1255, 120, 1200, 1183, 1110, 1028, 1005, 941, 854, 801, 769, 743 cm⁻¹. MALDI-TOF-MS (m/z): 568.40. Observed: 569.46 (MH⁺), 591.44 (MNa⁺), 607.42 (MK⁺). Anal. Calcd. for C₂₈H₅₂N₆O₆: C 59.13, H 9.22, N 14.78. Found: C 59.48, H 9.35, N 14.74.

¹H-NMR dilution experiments and calculation of K_{dim}

Typical procedure: weighed amounts of 2-ureido-pyrimidinones **1a-g** or UPy polymers **14** and **18** were dissolved in 2.0 ml dry CDCl₃ (distilled over P₂O₅) resulting in a 10 mM solution, of which 0.6 ml was injected into the NMR tube. The sample was then diluted to 5, 1, 0.5, 0.1 and 0.05 mM (in the case of **1a-g**) at 25 °C respectively. The peaks in the alkylidene region were deconvoluted using an algorithm present in the Varian VNMR software. Since the UPy dimer and UPy monomer are in slow exchange on the ¹H-NMR timescale it is possible to calculate the molar concentration of monomer and dimer based on the integrals of the NMR signals, the ratio of which is defined as *y* (I_{mono}/I_{dimer}). From this ratio and the overall UPy concentration U₀, the dimerization constant (K_{dim}) can be calculated using the following equation (see Appendix B):

$$K_{\text{dim}} = \frac{y(y+1)}{2U_0} \quad (1)$$

Extreme care was taken to keep water levels in the samples as low as possible, since traces of water could lead to the formation of acid in the solution, which interferes with the hydrogen bonding and can lead to degradation of the model compounds. Therefore, all compounds and glassware were dried over P₂O₅ and CDCl₃ was distilled over P₂O₅ and stored over molsieves. With this procedure, water levels in the samples were below the detection limit of standard Karl-Fischer titrations.

Fourier transform infrared experiments (FT-IR)

Infrared (IR) spectra were recorded at room temperature on a Perkin Elmer Spectrum One FT-IR spectrometer with a Universal ATR sampling Accessory. Solutions of **1g** and **8** in CDCl₃ (free of

TMS) were loaded between a pair of KBr windows using a 1 mm (for 10^{-3} M solution) or 5 mm (for 10^{-5} - 10^{-4} M solutions) Teflon spacer contained in a demountable liquid cell. The absorbance due only to **1g** or **8** was obtained by subtracting the spectra measured for pure CDCl_3 under otherwise identical conditions. The resulting corrected spectra were flat in the region between 1800 - 1550 cm^{-1} . For each spectrum, a 128-scan interferogram was collected with 4-cm^{-1} resolution. Measurements were performed without active temperature control.

Computational procedure for DFT and TD-DFT calculations

Geometry optimizations of the 2-ureido-pyrimidinone tautomers **9a-c** in the ground state were performed at the B3LYP/6-311++G(d,p) level as implemented in the Gaussian03 package.³² The solvent (CHCl_3) is taken into account approximately, by employing the polarized continuum model (IEF-PCM) based on the integral equation formalism model.⁵² Using the PCM approach the solute molecule is placed into a cavity surrounded by the solvent considered as a continuum medium with certain dielectric constant. The charge distribution of the solute polarizes the dielectric medium, which generates surface charges around the cavity and hence in turn polarizes the solute. The optimized conformations were confirmed as true minima by vibrational analysis at the same level of theory as in all cases only real frequencies were found. Geometry optimization was performed using the Berny algorithm and normal convergence criteria were used (RMS force criterion 3×10^{-4}). All geometries were optimized without symmetry constraints. The size of the integration grid was set to default (pruned (75302) grid).

Time dependent DFT on the optimized geometries of **9a-c** was performed using the PBE0 functional in combination with the 6-311G++(d,p) basis set and the IEF-PCM was used to take into account solvent effects (CHCl_3). In these calculations the so-called non-equilibrium procedure for TD-DFT calculations was used as it has been specifically designed for the study of absorption processes.³³ The oscillator strength of each transition in **9a-c** was calculated by the dipole approximation while visualization of the electronic spectra was achieved using GaussSum.⁵³

In all calculations in which the PCM approach was used to model the effect of solvent, the cavity used for the PCM approach was constructed using the simple united atom topological model (UA0), in which the van der Waals surface was built by placing a sphere around each solute heavy atom while hydrogen atoms were enclosed in the sphere of the atom to which they are bonded.

Geometry optimization of **1c** and **1d** (in their 6[1H] tautomeric forms and the tridecyl chain replaced by a methyl group) was started by Monte Carlo conformational searching (using the OPLS 2005 forcefield⁵⁴) of **1c** and **1d** (in which the $\text{C}_{13}\text{H}_{27}$ chain was replaced with a CH_3 group) with the GB/SA solvation model (CHCl_3) as implemented in MacroModel 9.5. In this way 900 structures were generated by varying dihedral angles around all C-C and C-O bonds of the EO

chain. In both cases the coordinates of the lowest energy conformer were exported and further optimized at the B3LYP/6-311+G(d,p)//PCM(CHCl₃) level of theory using the Gaussian03 package.³² Geometry optimization was performed using direct inversion in the iterative subspace method (GDIIIS).⁵⁵

Diffusion ordered spectroscopy (DOSY)

See Chapter 3. CDCl₃ used during the concentration dependent DOSY studies on UPy polymers **14** and **18** was distilled over P₂O₅ prior to use. The NMR tubes (5 mm) used for the studies were dried over P₂O₅ under high vacuum. The temperature was actively controlled at 25 °C.

The viscosity corrected diffusion constants were calculated using the following equation:

$$D_c = D_{\text{meas}} \times \frac{D_{\text{sol,pure}}}{D_{\text{sol,meas}}} \quad (2)$$

In which D_{meas} and $D_{\text{sol, meas}}$ represent the measured values for the solute and the residual solvent peak (CHCl₃) respectively and $D_{\text{sol, pure}}$ is the diffusion constant measured for the residual CHCl₃ in pure CDCl₃.

UV-Vis titrations

UV/Vis spectra were recorded using 1 cm path length cells on a Perkin Elmer Lambda 40P equipped with a PTP-1 Peltier temperature control system. A series of spectra were obtained by the addition of μL amounts of a stock solution containing 25.7 μM of NaPy and 300 μM UPy in CHCl₃ to a cell containing 2.0 mL of a 25.7 μM solution of 2,7-diamido-1,8-naphthyridine **10**. All obtained traces were base-line corrected. The temperature was actively controlled at 25 °C.

6.7 Appendices

Appendix A

2D DOSY spectrum of **1e**.

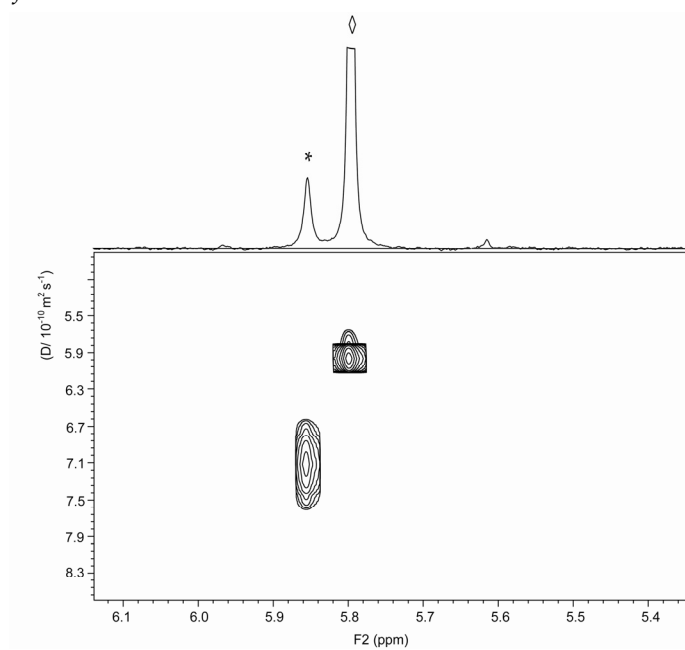


Figure A1: Partial 2D DOSY spectrum of **1e** in CDCl_3 at a concentration of 0.5 mM ($T = 25\text{ }^\circ\text{C}$). The symbols denote signals belonging to dimeric (\diamond) and monomeric ($*$) species

Appendix B*Calculation of K_{dim} based on 1H -NMR integrals*

Consider the following equilibrium (3)

which is governed by the equilibrium constant, K_{dim} :

$$K_{dim} = \frac{[U_2]}{[U]^2} \quad (4)$$

The mass balance equals

$$C_0 = 2[U_2] + [U] \quad (5)$$

The integrals are proportional to the amount of U present:

$$I_{U_2} = 2f_{U_2}[U_2] \quad (6)$$

$$I_U = f_U[U] \quad (7)$$

The ratio of both integrals can be defined as y :

$$y = \frac{I_{U_2}}{I_U} \quad (8)$$

Assuming that the proportionality constants are equal:

$$f_{U_2} = f_U \quad (9)$$

Substituting eq (6) and eq (7) into eq (8) yields:

$$2[U_2] = y[U] \quad (10)$$

Which can be substituted into eq (5)

$$U_0 = y[U] + [U] = (y+1)[U] \quad (11)$$

This yields a useful expression for $[U]$:

$$[U] = \frac{U_0}{y+1} \quad (12)$$

Substitution of this expression into eq (4) gives eq 1:

$$K_{dim} = \frac{[U_2]}{[U]^2} = \frac{[U_2]}{[U]} \cdot \frac{1}{[U]} = \frac{y}{2} \cdot \frac{y+1}{U_0} = \frac{y(y+1)}{2U_0} \quad (1)$$

Appendix C

UV-Vis spectra of UPy polymer **14** and **18** in CHCl_3 at a concentration of 0.05 mM ($T = 25^\circ\text{C}$)

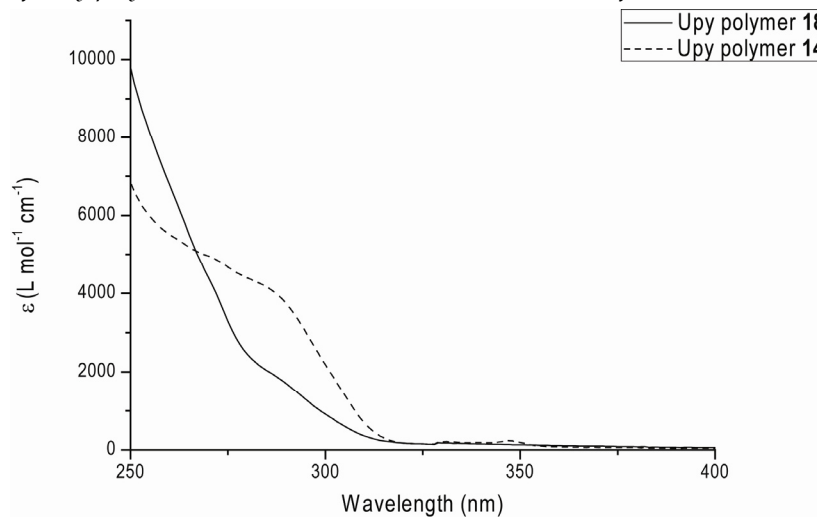


Figure A2: UV-Vis spectra of $\text{P}(\text{nBA})_n\text{-C}_2\text{-UPy}$ **14** and $\text{P}(\text{nBA})_n\text{-C}_6\text{-UPy}$ **18** in CHCl_3 at a concentration of 0.05 mM ($T = 25^\circ\text{C}$).

Appendix D

UV-Vis titrations of UPy polymers **14** and **18** with NaPy polymer **20** in CHCl_3 ($T = 25^\circ\text{C}$)

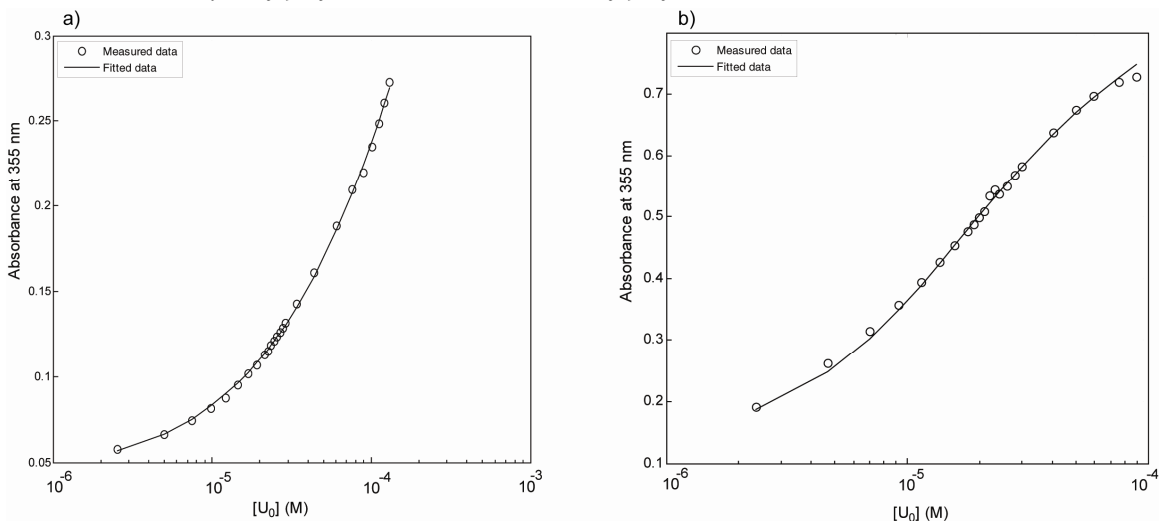


Figure A3: a) Plot of absorbance at 355 nm for a solution containing $2.53 \times 10^{-5} \text{ M}$ **20** vs. concentration of **14** in CHCl_3 at 25°C . The curve represents the best fit of the data ($K_a = 1.2 \pm 0.4 \times 10^3 \text{ M}^{-1}$) to the 1:1 binding model with one component self-associating ($K_{\text{dim}} = 1.7 \times 10^4 \text{ M}^{-1}$). b) Plot of absorbance at 355 nm for a solution containing $2.53 \times 10^{-5} \text{ M}$ **20** vs. concentration of **18** in CHCl_3 at 25°C . The curve represents the best fit of the data ($K_a = 3 \pm 0.6 \times 10^6 \text{ M}^{-1}$) to the 1:1 binding model with one component self-associating ($K_{\text{dim}} = 6 \times 10^7 \text{ M}^{-1}$).

Appendix E

Concentration dependent chemical shift data of UPy-urea dimer 22·22.

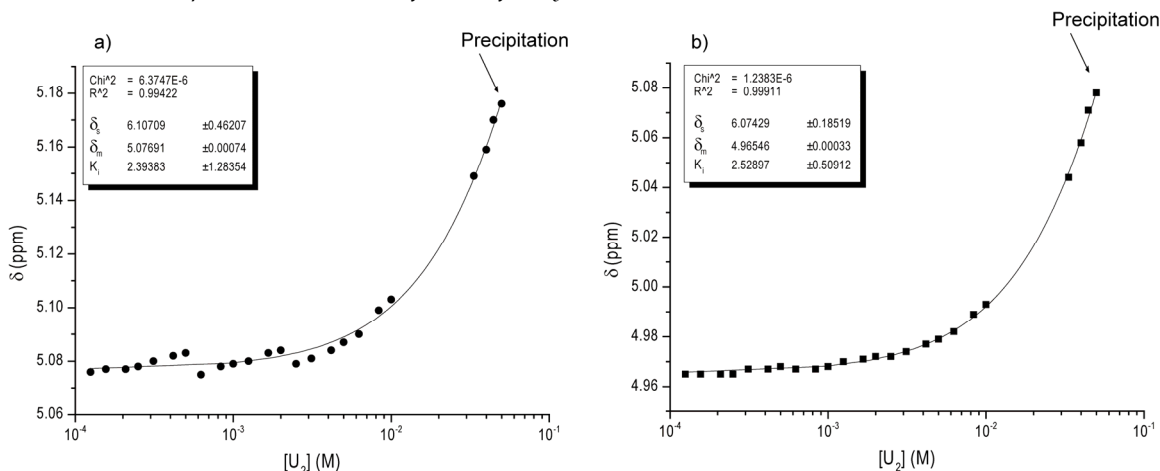


Figure A4: Concentration-dependent ^1H -NMR shift of the two urea NH protons of UPy dimer 22·22 in CDCl_3 at 25 °C. a) NH proton marked with ● in table 6.3. b) NH proton marked with ■ in table 6.3. The solid line corresponds to the best fitted values of K_i , $\bar{\delta}_m$ and $\bar{\delta}_s$ according to an isodesmic equilibrium model (see Chapter 5).

6.8 References

- Hirschberg, J. H. K.; Brunsveld, L.; Ramzi, A.; Vekemans, J. A. J. M.; Sijbesma, R. P.; Meijer, E. W. *Nature* **2000**, *402*, 167.
 - Brunsveld, L.; Vekemans, J. A. J. M.; Hirschberg, J. H. K.; Sijbesma, R. P.; Meijer, E. W. *Proc. Natl. Acad. Sci. U.S.A.* **2002**, *99*, 4977.
 - Brunsveld, L.; Lohmeijer, B. G. G.; Vekemans, J. A. J. M.; Meijer, E. W. *Chem. Commun.* **2000**, 2305.
 - Sinkeldam, R. W.; van Houtem, M. H. C. J.; Pieterse, K.; Vekemans, J. A. J. M.; Meijer, E. W. *Chem. Eur. J.* **2006**, *12*, 6129.
 - Mathews, J. R.; Goldoni, F.; Schenning, A. P. H. J.; Meijer, E. W. *Chem. Commun.* **2005**, 5503.
 - Kilbinger, A. F. M.; Schenning, A. P. H. J.; Goldoni, F.; Feast, W. J.; Meijer, E. W. *J. Am. Chem. Soc.* **2000**, *122*, 1820.
 - Wolffs, M.; Hoeben, F. J. M.; Beckers, E. H. A.; Schenning, A. P. H. J.; Meijer, E. W. *J. Am. Chem. Soc.* **2005**, *127*, 13484.
 - Arnaud, A.; Belleney, J.; Boué, F.; Bouteiller, L.; Carrot, G.; Wintgens, V. *Angew. Chem. Int. Ed.* **2004**, *43*, 1718.
 - Harada, A.; Cammas, S.; Kataoka, K. *Macromolecules* **1998**, *29*, 6183.
 - Scmuck, C.; Wienand, W. *J. Am. Chem. Soc.* **2003**, *125*, 452.
 - Scmuck, C.; Frey, P.; Heil, M. *ChemBioChem* **2005**, *6*, 628.
 - Schmuck, C.; Rehm, T.; Gröhn, F.; Klein, K.; Reinhold, F. *J. Am. Chem. Soc.* **2006**, *128*, 1430.
 - Inoue, Y.; Kuad, P.; Okumura, Y.; Takashima, Y.; Yamaguchi, H.; Harada, A. *J. Am. Chem. Soc.* **2006**, *129*, 6396.
 - Inoue, Y.; Miyauchi, M.; Nakajima, H.; Takashima, Y.; Yamaguchi, H.; Harada, A. *Macromolecules* **2007**, *40*, 3256.
 - Lee, M.; Lee, S.-J.; Jiang, L.-H. *J. Am. Chem. Soc.* **2004**, *126*, 12724.
 - Kim, B.-S.; Hong, D.-J.; Bae, J.; Lee, M. *J. Am. Chem. Soc.* **2005**, *127*, 16333.
 - Bae, J.; Choi, J.-H.; Yoo, Y.-S.; Oh, N.-K.; Kim, B.-S.; Lee, M. *J. Am. Chem. Soc.* **2005**, *127*, 9668.
 - Stone, M. T.; Moore, J. S. *Org. Lett.* **2004**, *6*, 469.
 - Ryu, J. -H.; Hong, D. -J.; Lee, M. *Chem. Commun* **2008**, 1043.
- Lafitte, V. G. H.; Aliev, A. E.; Horton, P. N.; Hursthouse, M. B.; Bala, K.; Golding P.; Hailes, H. C. *J. Am. Chem. Soc.* **2006**, *128*, 6544.

- 3) Binder, W. H. Petraru, L.; Roth, T.; Groh, P. W.; Pálfi, V.; Keki, S.; Ivan, B. *Adv. Funct. Mater.* **2007**, *17*, 1317.
- 4) a) Yang, X.; Hua, F.; Yamato, K.; Ruckenstein, E.; Gong, B.; Kim, W.; Ryu, C. Y. *Angew. Chem. Int. Ed.* **2004**, *43*, 6471. b) Feldman, K. E.; Kade, M. J.; de Greef, T. F. A.; Meijer, E. W.; Kramer, E. J.; Hawker, C. J. *Macromolecules* **2008**, *41*, 4694.
- 5) a) van Bommel, K. J. C.; van der Pol, C.; Muizebelt, I.; Friggeri, A.; Heeres, A.; Meetsma, A.; Feringa, B.; van Esch, J. *Angew. Chem. Int. Ed.* **2004**, *43*, 1663. b) Friggeri, A.; van der Pol, C.; van Bommel, K. J. C.; Heeres, A.; Stuart, M. C. A.; Feringa, B. L.; van Esch, J. *Chem. Eur. J.* **2005**, *11*, 5353.
- 6) a) Mammen, M.; Choi, S.-K.; Whitesides, G. M. *Angew. Chem. Int. Ed.* **1998**, *37*, 2755. b) Bilgicer, B.; Moustakas, D. T.; Whitesides, G. M. *J. Am. Chem. Soc.* **2007**, *129*, 3722. c) Krishnamurthy, V. M.; Semetey, V.; Bracher, P. J.; Shen, N.; Whitesides, G. M. *J. Am. Chem. Soc.* **2007**, *129*, 1312. d) Crespo-Biel, O.; Lim, C. W.; Ravoo, B. J.; Reinhoudt, D. N.; Huskens, J. *J. Am. Chem. Soc.* **2006**, *128*, 17024. e) Mulder, A.; Auletta, T.; Sartori, A.; Del Ciotto, S.; Casnati, A.; Ungaro, R.; Huskens, J.; Reinhoudt, D. N. *J. Am. Chem. Soc.* **2004**, *126*, 6627. f) Kiessling, L.; Gestwicki, J. E.; Strong, L. E. *Curr. Opin. Chem. Biol.* **2004**, *4*, 696.
- 7) Sun, H.; Kaifer, A. E. *Org. Lett.* **2005**, *7*, 3845.
- 8) Wong, C. -H.; Chow, H. -F.; Hui, S. -K.; Sze, K. -H. *Org. Lett.* **2006**, *8*, 1811.
- 9) Hawker, C. J.; Wooley, K. L.; Fréchet, J. M. J. *J. Am. Chem. Soc.* **1993**, *115*, 4375.
- 10) a) Chai, M.; Niu, Y.; Youngs, W. J.; Rinaldi, P. L. *J. Am. Chem. Soc.* **2001**, 4670. b) Lin, C.; Wu, K.; Sa, R.; Mang, C.; Liu, P.; Zhuang, B. *Chem. Phys. Lett.* **2002**, *363*, 343. c) Maiti, P. K.; Çağın, T.; Lin, S. -T.; Goddard III, W. A. *Macromolecules* **2005**, *38*, 979.
- 11) Gillard, R. E.; Raymo, F. M.; Stoddart, J. F. *Chem. Eur. J.* **1997**, *12*, 1933 and references therein.
- 12) Other examples on the effect of short EO chains on hydrogen bonding based self-assemblies: a) Nygaard, S.; Hansen, C. N.; Jeppesen, J. O. *J. Org. Chem.* **2007**, *72*, 1617. b) Hofacker, A. L.; Parquette, J. R. *Angew. Chem. Int. Ed.* **2005**, *117*, 1077.
- 13) Söntjens, S. H. M.; Sijbesma, R. P.; van Genderen, M. H. P.; Meijer, E. W. *J. Am. Chem. Soc.* **2000**, *122*, 7487.
- 14) a) Page, M. I.; Jencks, W. P. *Proc. Natl. Acad. Sci. U.S.A.* **1971**, *68*, 1678. b) Page, M. I. *Chem. Soc. Rev.* **1973**, *2*, 295.
- 15) Mandolini, L. *Adv. Phys. Org. Chem.* **1986**, *22*, 1.
- 16) The enthalpic contribution of the intramolecular hydrogen bond is largely dependent on the strength and spatial juxtaposition of the hydrogen bond donor and acceptor. The strength of the intramolecular hydrogen bond formed between the oxygen atoms of the EO chain and the urea NH proton is much lower compared to a normal amide-amide hydrogen bond due to the fact that the carbonyl group is a better electron donor for hydrogen bonding than the ether oxygen as a result of polarization effects. Previously it has been determined that amide-amide hydrogen bonding is strongest when the N-H...O hydrogen angle approaches linearity, see: Peters, D.; Peters, J. *J. Mol. Struct.* **1980**, *68*, 225.
- 17) The strain energy of cycloalkanes decreases from 27.5 kcal/mol for cyclopropane to 0.1 kcal/mol for cyclohexane and then increases to a value of 11.1 kcal/mol for cycloundecane after which it decreases again: Skinner, H. A.; Pilcher, G. *Quart. Rev.* **1963**, *17*, 264.
- 18) Singelenberg, F. A. J.; Lutz, E. T. G.; van der Maas, J. H. *J. Mol. Struct.* **1991**, *245*, 173.

- 19) Beijer, F. H.; Sijbesma, R. P.; Kooijman, H.; Spek, A. L.; Meijer, E. W. *J. Am. Chem. Soc.* **1998**, *120*, 6761
- 20) For perfectly spherical molecules it has been claimed that the ratio of the diffusion coefficients for two different molecular species is inversely proportional to the cubic root of the ratio of their molecular weights:
- $$\sqrt[3]{\frac{M_1}{M_2}} = \frac{D_2}{D_1} \quad (13)$$
- See: Waldeck, A. R.; Kuchel, P. W.; Lennon, A. J.; Capman, B. E. *Prog. Nucl. Magn. Reson. Spectrosc.* **1997**, *30*, 39.
- 21) The deviation from the expected value of 2 is most probably the result from the fact that the 4[1H] pyrimidinone dimer and the 6[1H] pyrimidinone monomer of **1e** are not in complete slow exchange on the DOSY time scale. For a discussion on the DOSY timescale, see: Cabritta, E. J.; Berger, S.; Bräuer, P.; Kärger, J. *J. Magn. Res.* **2002**, *157*, 124.
- 22) Under the assumption that at least 10% dissociation is required to be observable at the final concentration (0.05 mM), a lower limit on the dimerization constant can be placed: $K_{\text{dim}} > 1 \times 10^6 \text{ M}^{-1}$.
- 23) a) Wahab, S. A.; Matsuura, H. *Phys. Chem. Chem. Phys.* **2001**, *3*, 4689. b) Begum, R.; Yonemitsu, T.; Matsuura, H. *J. Mol. Struct.* **1998**, *447*, 111. c) Begum, R.; Matsuura, H. *J. Chem. Soc. Faraday Trans.* **1997**, *93*, 3839.
- 24) Key bands at 1355–1360 cm^{-1} and 1335–1320 cm^{-1} for the respective *gauche* and *anti* C-C conformations; while those at 1310–1297 cm^{-1} and 1290–1295 cm^{-1} for the *gauche* and *anti* C-O conformations, respectively.
- 25) Meier, R. *J. Vibrational Spectroscopy* **2005**, *39*, 266.
- 26) a) Morita, H.; Nagakura, S. *Theoret. Chim. Acta (Berl.)* **1968**, *11*, 279. b) Brown, D. J.; Teitei, T. *Aus. J. Chem.* **1965**, *18*, 559.
- 27) a) Gross, E. K. U.; Kohn, W. *Adv. Quantum. Chem.* **1990**, *21*, 255. b) Gross, E. K. U.; Dobson, J. F.; Petersilka, M. In *Density Functional Theory*; Nalewajski, R. F., Ed.; Springer Series "Topics in Current Chemistry"; Springer: Heidelberg, 1996; Vol. 81, p 81. c) Jamorski, C.; Casida, M. E.; Salahub, D. R. *J. Chem. Phys.* **1996**, *104*, 5134.
- 28) a) Improta, R.; Barone, V.; Santoro, F. *Angew. Chem. Int. Ed.* **2007**, *119*, 409. b) Santoro, F.; Barone, V.; Benzi, C.; Improta, R. *Theor. Chem. Acc.* **2007**, *117*, 1073. c) Jacquemin, D.; Perpète, E. A.; Scuseria, G. E.; Ciofini, I.; Adamo, C. *J. Chem. Theory Comput.* **2008**, *4*, 123.
- 29) a) Jödicke, C. J.; Lüthi, H. P. *J. Am. Chem. Soc.* **2003**, *125*, 252. b) Santoro, F.; Barone, V.; Improta, R. *Proc. Natl. Acad. Sci. U.S.A.* **2007**, *104*, 9931. c) van Gisbergen, S. J. A.; Schipper, P. R. T.; Gritsenko, O. V.; Baerends, E. J.; Snijders, J. G.; Champagne, B.; Kistman, B. *Phys. Rev. Lett.* **1999**, *83*, 694. d) Bauernschmitt, R.; Ahlrichs, R.; Hennrich, F. H.; Kappes, M. M. *J. Am. Chem. Soc.* **1998**, *120*, 5052.
- 30) a) Adamo, C.; Barone, V. *J. Chem. Phys.* **1999**, *110*, 6158. b) Perdew, J. P.; Burke, K.; Ernzerhof, M. *Phys. Rev. Lett.* **1996**, *77*, 3865.
- 31) The 6-311G++(2d,p) triple valence basis set was selected due to its good performance in a number of other TDDFT studies. See reference 28c and references therein.
- 32) Frisch, M. J.; Trucks, G.W.; Schlegel, H.B.; Scuseria, G.E.; Robb, M.A.; Cheeseman, J.R.; Zakrzewski, V.G.; Montgomery, J.A., Jr.; Stratmann, R.E.; Burant, J.C.; Dapprich, S.; Millam, J.M.; Daniels, A.D.; Kudin, K.N.; Strain, M. C.; Farkas, O.; Tomasi, J.; Barone, V.; Cossi, M.; Cammi, R.; Mennucci, B.; Pomelli, C.; Adamo, C.; Clifford, S.; Ochterski, J.; Petersson, G.A.; Ayala, P.Y.; Cui, Q.; Morokuma, K.; Malick, D.K.; Rabuck, A.D.; Raghavachari, K.; Foresman, J.B.; Cioslowski, J.; Ortiz, J. V.; Stefanov, B.B.; Liu, G.;

- Liashenko, A.; Piskorz, P.; Komaromi, I.; Gomperts, R.; Martin, R.L.; Fox, D.J.; Keith, T.; Al-Laham, M.A.; Peng, C.Y.; Nanayakkara, A.; Gonzalez, C.; Challacombe, M.; Gill, P. M. W.; Johnson, B. G.; Chen, W.; Wong, M.W.; Andres, J.L.; Head-Gordon, M.; Replogle, E.S.; Pople, J.A. Gaussian 03, Revision B.04; Gaussian, Inc.: Wallingford CT, 2003.
- 33) a) Cossi, M.; Barone, V. *J. Phys. Chem. A* **2000**, *104*, 10614. b) Aguilar, M. A. *J. Phys. Chem. A* **2001**, *105*, 10393.
- 34) a) Karplus, M.; *J. Chem. Phys.* **1959**, *80*, 11. b) Karplus, M.; *J. Am. Chem. Soc.* **1963**, *85*, 2870.
- 35) a) Haasnoot, C.A.G.; De Leeuw, F.A.A.M.; Altona, C. *Tetrahedron* **1980**, *36*, 2783.
- 36) Baker, E. N.; Hubbard, R. E. *Prog. Biophys. Mol. Biol.* **1984**, *44*, 97.
- 37) Mitchell, J. B. O.; Price, S. L. *Chem. Phys. Lett.* **1989**, *154*, 267.
- 38) Chacko, K. K.; Narasimhan, P. *Acta. Cryst.* **1984**, *C40*, 160.
- 39) Coessens, V.; Pintauer, T.; Matyjaszewski, K. *Prog. Polym. Sci.* **2001**, *26*, 337.
- 40) Huang, J. Y.; Pintauer, T.; Matyjaszewski, K. *J. Polym. Sci. Pol. Chem.* **2004**, *42*, 3285.
- 41) The corrected diffusion constants are determined using the following formula:
 $D_c = D_{\text{meas}} \times (D_{\text{sol, pure}} / D_{\text{sol, meas}})$ where D_{meas} and $D_{\text{sol, meas}}$ are the measured values for the solute and the residual solvent peak (CHCl_3) respectively and $D_{\text{sol, pure}}$ is the diffusion constant measured for the residual CHCl_3 in pure CDCl_3 .
- 42) Jerschow, A.; Muller, N. *J. Magn. Reson.* **1997**, *125*, 372.
- 43) a) Hess, W. *Macromolecules* **1986**, *19*, 1395. b) Hess, W. *Macromolecules* **1987**, *20*, 2587.
- 44) See: Liu, R.; Gao, X.; Adams, J.; Opperman, W. *Macromolecules*, **2005**, *38*, 8845.
- 45) de Greef, T. F. A.; Nieuwenhuizen, M. M. L.; Stals, P. J. M.; Fitié, C. F. C.; Palmans, A. R. A.; Sijbesma, R. P.; Meijer, E. W. *Chem. Commun.* **2008**, 4306.
- 46) Obert, E.; Bellot, M.; Bouteiller, L.; Andrioletti, F.; Lehen-Ferrenbach, C.; Boué, F. *J. Am. Chem. Soc.* **2007**, *129*, 15601.
- 47) Yoshikawa, I. Sawayama, J.; Araki, K. *Angew. Chem. Int. Ed.* **2008**, *47*, 1038.
- 48) For example, PEG chains are commonly used to study supramolecular assemblies in water. See: a) Oshovsky, G. V.; Reinhoudt, D. N.; Verboom, W. V. *Angew. Chem. Int. Ed.* **2007**, *46*, 2366 b) Ryu, J. -H.; Hong, D. -J.; Lee, M. *Chem. Commun* **2008**, 1043. c) Rehm, T.; Schmuck, C. *Chem. Commun* **2008**, 801.
- 49) a) Kubetzko, S.; Sarkar, C. A.; Plückthun, A. *Mol. Pharm.* **2005**, *68*, 1439. b) Kubetzko, S.; Balic, E.; Waibel, R.; Zangemesier-Wittke, Plückthun, A. *J. Biol. Chem.* **2006**, *281*, 35186. c) Das, R.; Baird, E.; Allen, S.; Baird, B.; Holowka, D.; Goldstein, B. *Biochemistry* **2008**, *47*, 1017.
- 50) Scherman, O.A.; Ligthart, G.B.W.L.; Ohkawa, H.; Sijbesma, R.P.; Meijer, E.W. *Proc. Natl. Acad. Sci. USA* **2006**, *103*, 11850.
- 51) Keizer, H. M.; Sijbesma, R. P.; Meijer, E. M. *Eur. J. Org. Chem.* **2004**, *12*, 2553.
- 52) Tomasi, J.; Mennucci, B.; Cancès, E. *J. Mol. Struct. (Theochem)* **1999**, *464*, 211
- 53) O'Boyle, N. M.; Tenderholt, A.L.; Langner, K. M. *J. Comp. Chem.* **2008**, *29*, 839.
- 54) Jorgensen, W. L.; Tirado-Rives, J. *Proc. Natl. Acad. Sci. U.S.A.* **2005**, *102*, 6665.
- 55) Csaszar, P.; Pulay, P. *J. Mol. Struct.* **1984**, *114*, 31.

Summary

In this thesis the mechanism by which quadruple hydrogen bonding systems based on the reversible dimerization of 2-ureido-pyrimidinone (UPy) and association of this unit with 2,7-diamido-1,8-naphthyridine (NaPy) is investigated.

In Chapter 1, a general overview of the different polymerization mechanisms of supramolecular polymers is given. By calculating various properties such as the degree of polymerization and the fraction of self-assembled material as a function of concentration or temperature, a clear distinction is made between supramolecular polymerizations occurring via an isodesmic (equal K) mechanism, a ring-chain mechanism or via a cooperative nucleation-elongation mechanism. Specifically, it is shown in the last two cases the mechanism exhibits a critical concentration or critical temperature where the self-assembly is initiated. An analogy is drawn between cooperative supramolecular polymerizations and phase transitions.

Due to the strong dimerization of the UPy unit the selectivity of the hetero-dimerization with 2,7-diamido-1,8-naphthyridine is concentration dependent. In Chapter 2, various new UPy monomers bearing electron-donating and electron-withdrawing units attached at the C₆ position of the pyrimidinone ring have been synthesized. The concentration dependent selectivity of these novel UPy monomers in the heteromeric recognition process with 2,7-diamido-1,8-naphthyridine is measured using UV-Vis spectroscopy. These experiments show that 2-ureido-pyrimidinones dimerizing *via* the enol tautomer have a much higher selectivity compared to 2-ureido-pyrimidinones dimerizing *via* the keto tautomer. The dimerization constant of one of the novel UPy monomers, bearing an electron-donating dibutyl-amino group at the C₆ position of the pyrimidinone ring, was measured using fluorescence spectroscopy and was found to be roughly 100 times lower compared to the keto dimer. UV-Vis titrations revealed that the association constant of the enol monomer with NaPy was the same as the association constant of the 4[1H] keto monomer. Hence, the decrease in K_{dim} results in an increased selectivity towards hetero-complexation with 2,7-diamido-1,8-naphthyridine.

In Chapter 3, the influence of the increased selectivity on the supramolecular polymerization of a UPy-NaPy AB type monomer was studied. To this end two UPy-NaPy monomers were synthesized bearing different UPy end groups. Although at high concentration the degree of polymerization (DP) of the more selective system was higher as expected, at lower concentration this was not the case. Using a mathematical model it is shown that the increase in selectivity of hetero-complexation also leads to an increase in the number of cyclic intermediates in the solution which ultimately results in lower

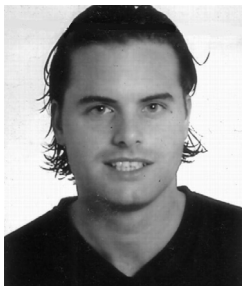
degrees of polymerization at lower concentrations. Furthermore, the mathematical model provided unique insights on the development of the polydispersity index at equilibrium of the resulting supramolecular polymers as a function of concentration.

To unravel the mechanism of the complexation of ureido-pyrimidinone dimers with 2,7-diamido-1,8-naphthyridine, kinetic experiments at various concentrations were performed and analyzed in Chapter 4. By analyzing various possible models for this complexation it is found that the prototropic shift of the UPy 4[1H] tautomer to the UPy 6[1H] tautomer is the rate determining step and that this step is bimolecular and catalyzed by free NaPy. By means of a carefully planned experiment, kinetic supramolecular assemblies in mixtures of hydrogen bonding assemblies could be detected.

Besides the formation of dimeric structures, UPy compounds with an additional urea functionality are also able to self-assemble into one dimensional stacks. In Chapter 5, concentration and temperature dependent measurements reveal that this self-assembly process in various solvents occurs via an isodesmic mechanism (*i.e.* it occurs with the same K value for each step).

In Chapter 6, the influence of polar side chains attached to the UPy unit is investigated. It is found that substitution of the UPy unit with various polar side chains resulted in a large decrease in the dimerization constant, in some cases as large as 10^3 . It is shown that the reduction in K_{dim} is directly related to the length of the aliphatic spacer connecting the UPy unit with the polar side chain. Although all data seems to suggest that intramolecular hydrogen bonding between the hydrogen bonding acceptors and donors in the polar side chain is the cause of the reduction in K_{dim} , direct evidence for this claim in the form of a NOe interaction could not be obtained.

Curriculum Vitae



Tom de Greef werd geboren op 5 april 1980 te Eindhoven. Na zijn VWO opleiding aan het Strabrecht College in Geldrop begon hij aan de studie Biomedische Technologie aan de Technische Universiteit te Eindhoven. De masterfase van deze studie werd in 2004 *cum laude* afgerond met een afstudeerproject bij de vakgroep Molecular Science and Technology onder leiding van dr. ir. J. J. van Gorp, dr. J. A. J. M. Vekemans en prof. dr. E. W. Meijer. Na een stage in de groep van dr. G. Tew aan de Universiteit van Massachusetts werd begonnen aan een promotiestudie op het gebied van supramoleculaire polymeren onder leiding van prof. dr. E. W. Meijer en prof. dr. R. P. Sijbesma. De belangrijkste resultaten van dit onderzoek zijn beschreven in dit proefschrift. Vanaf 15 november 2008 is hij werkzaam bij het Instituut voor Complexe Moleculaire Systemen (ICMS) gevestigd aan de Technische Universiteit van Eindhoven.

Tom de Greef was born on April 5th, 1980 in Eindhoven. After secondary education at the Strabrecht College in Geldrop, he started studying Biomedical Technology at the Eindhoven University of Technology. The master's program of this study was completed *cum laude* with a graduation project in the group Molecular Science and Technology under supervision of dr. ir. J. J. van Gorp, dr. J. A. J. M. Vekemans and prof. dr. E. W. Meijer. After an international internship in the group of dr. G. Tew at the University of Massachusetts he started as a PhD student in the area of supramolecular polymers under supervision of prof. dr. E. W. Meijer and prof. dr. R. P. Sijbesma. The most important results of this research are described in this thesis. As of November 15th he started working at the Institute for Complex Molecular Systems (ICMS) located at the Eindhoven University of Technology.

Publications

1. Insights into templated supramolecular polymerization: Binding of naphthalene derivatives to different ssDNA template lengths.
P. G. A. Janssen, S. Jabbari-Farouji, M. Surin, X. Vila, J. C. Gielen, T. F. A. de Greef, M. R. J. Vos, P. H. H. Bomans, N. A. J. M. Sommerdijk, P. C. M. Christianen, P. Leclère, R. Lazzaroni, P. van der Schoot, E. W. Meijer, A. P. H. J. Schenning *J. Am. Chem. Soc.*, in press.
2. The Influence of Selectivity on the Ring-Chain Equilibrium of Supramolecular AB type Polymers Capable of Both A·A and A·B Interactions.
T. F. A. de Greef, G. Ercolani, G. B. W. L. Ligthart, E. W. Meijer, R. P. Sijbesma *J. Am. Chem. Soc.* **2008**, *130*, 13755.
3. The Influence of Ethylene Glycol Chains on the Thermodynamics of Hydrogen-bonded Supramolecular Assemblies in Apolar Solvents.
T. F. A. de Greef, M. M. L. Nieuwenhuizen, P. J. M. Stals, C. F. C. Fitié, A. R. A. Palmans, R. P. Sijbesma, E. W. Meijer. *Chem. Commun.* **2008**, 4306.
4. Polymers with Multiple Hydrogen-Bonded End Groups and Their Blends.
K. E. Feldman, M. J. Kade, T. F. A. de Greef, E. W. Meijer, E. J. Kramer, C. J. Hawker *Macromolecules* **2008**, *41*, 4694-4700.
5. Supramolecular Polymers.
T.F.A. de Greef, E.W. Meijer *Nature* **2008**, *453*, 171-173.
6. The Mechanism of Ureido-Pyrimidinone:2,7-Diamido-Naphthyridine Complexation and the Presence of Kinetically Controlled Pathways in Multicomponent Hydrogen-Bonded Systems.
T. F. A. de Greef, G. B. W. L. Ligthart, M. Lutz, A. L. Spek, E. W. Meijer, R. P. Sijbesma *J. Am. Chem. Soc.* **2008**, *130*, 5479-5486.
7. Helicity Induction and Amplification in an Oligo(p-phenylenevinylene) Assembly through Hydrogen-Bonded Chiral Acids.
S. J. George, Z. Tomovic, M. M. J. Smulders, T. F. A. de Greef, P. E. L. G. Leclère, E. W. Meijer, A. P. H. J. Schenning *Angew. Chem.; Int. Ed. Engl.* **2007**, *46*, 8206-8211.
8. Towards poly(aminophthalimide), structures of Dimers and Trimers.
H. Katayama, T. F. A. de Greef, H. Kooijman, A. L. Spek, J. A. J. M. Vekemans, E. W. Meijer *Tetrahedron* **2007**, *63*, 6642-6653.
9. Solution ¹H NMR Confirmation of Folding in Short o-Phenylene Ethynylene Oligomers.
T. W. Jones, M. M. Slutsky, R. Laos, T. F. A. de Greef, G. N. Tew *J. Am. Chem. Soc.* **2005**, *127*, 17235-17240.

Dankwoord

Een proefschrift schrijven doe je nooit alleen. Daarom rest mij, als laatste taak naar vier jaar onderzoek, het bedanken van de vele mensen die zich met ongekend enthousiasme hebben ingezet om het onderzoek dat beschreven staat in dit proefschrift tot een goed einde te brengen.

Ik het geluk heb gehad om in de afgelopen vier jaar twee eerste promotoren te hebben, Bert Meijer en Rint Sijbesma die mij, met veel enthousiasme en daadkracht, de fijne kneepjes van het vak hebben geleerd. Bert, ik kijk met plezier terug aan de vele uren van discussies waarin we samen hebben gezocht naar de betekenis van het brede begrip “complexiteit” en tal van andere zaken zoals ring-keten evenwichten, coöperatieve polymerizaties en multivalente effecten. Verder was je er altijd om me we terug op aarde te roepen als ik me weer eens verloren had in de vele details waarin een promovendus verzeild raakt bij het doen van wetenschappelijk onderzoek. Je vermogen om boven alle details te staan, de grote lijnen te doorzien en je continue wens om van Eindhoven een chemische hoofdstad te maken zijn inspirerend. Rint, jouw enorme kennis en theoretisch inzicht hebben mij versteld doen staan. Meer dan eens kwam je met een suggestie voor een laatste experiment waarin alle voorgaande experimenten netjes op zijn plaats vielen. Grote bewondering heb ik ook voor de wijze waarop je zo snel je eigen groep hebt kunnen opbouwen met de daarbijhorende originele onderwerpen.

Minstens zo belangrijk als de promotoren zijn de studenten waar ik mee heb samengewerkt. Grote bewondering en waardering heb ik ook voor Marko Nieuwenhuizen. Marko, in de afgelopen twee jaar hebben we op een ongelooflijk leuke wijze met elkaar samengewerkt en veel van je werk heb ik kunnen opnemen in dit proefschrift. Je stond altijd open voor mijn ideeën en voordat ik het wist had je al wat moleculen in elkaar zitten en de nodige metingen gedaan. In de loop van de tijd begon ook bij jou de passie voor de fysische chemie te groeien met als gevolg het vele op en neer gestuur van nieuwe Matlab scriptjes. Je hebt gekozen voor een promotie binnen het ICMS en ik weet zeker dat we ook in de toekomst nog veel met elkaar te doen gaan krijgen, iets waar ik me erg op verheug. Ook afstudeerder Rob van de Bruggen heeft grote invloed gehad op de resultaten die behaald zijn tijdens de afgelopen vier jaar. Rob, jij kreeg het voor elkaar om samen met Jos Paulusse de chirale UPy-ureas die beschreven staan in hoofdstuk 5 zuiver in handen te krijgen. De ene kolom naar de andere, jij was er niet vies van!! Leuke herinneringen heb ik aan de stapavondjes op Stratumseind samen met Marko en jou. Als laatste wil ik ook afstudeerder Inge van der Meulen bedanken

voor het synthetiseren van de water oplosbare UPy moleculen. Peter Korevaar en Ivo Filot wil ik ontzettend veel succes wensen in hun aankomende afstudeerperiode.

Veel dank ben ik verschuldigd aan Ronald Ligthart en Jos Paulusse. Ronald, het enorme werk dat door jou verricht was aan de hetero-complementaire units bood aan mij een unieke kans om hier verder mee te gaan. Ook de gezellige etentjes samen met Ingrid van Baal en Jeroen Huijbers blijven mij bij. Jos wil ik bedanken voor de synthese van de chirale Upy moleculen en de leuke tijd in Santa Barbara. Ik wens je ontzettend veel succes in Wageningen. Maarten Smulders wil ik bedanken voor de hulp bij hoofdstuk 1 en de hulp bij de CD experimenten.

Joost van Dongen (mooie herinneringen aan een Valentijns feestje in de grotten van Amsterdam), Xianwen Lou en Ralf Bovee wil ik bedanken voor de praktische hulp bij het meten van GPC en de razendsnelle Maldi spectra die gemeten werden.

During the years that I have worked within MST I had the honour to work together with two real Japanese masters: Hiro Katayama and Haruki Ohkwama. Haruki, you taught me both the basics of synthetic organic chemistry and the joy of doing scientific research. Hiro, your synthetic work on the amino-phthalamide foldamers was impressive. I hope to see you both in Japan one day. I would also like to thank prof. Gianfranco Ercolani for his great help with the work described in Chapter 3 and for being a member in my defense ceremony. Your papers on cooperativity, ring-chain equilibria and multivalency have been a general guideline for people working in the field of supramolecular chemistry. Also I would like to thank prof. Lyle Isaacs for being a member in my defense ceremony. Your seminal work on self-sorting has inspired me alot. Ook wil ik dr. Marcel van Genderen bedanken voor het kritisch doorlezen van dit proefschrift en het plaatsnemen in mijn verdediging. Naast de leden van de leescommissie gaat mijn dank uit naar de totale promotiecommissie, gecompleteerd door prof. dr. Peter Hilbers en dr. Albert Schenning.

Thanks to Matt Kade, Katie Feldman, prof. Craig Hawker and prof. Ed Kramer my stay in Santa Barbara was one of the highlights of the last four years. Matt, special thanks to you for taking care of me and letting me live in your house.

Marcel van Genderen en Thomas Hermans wil ik bedanken voor de hulp bij vele NMR kwesties en de prettige samenwerking rondom de vele activiteiten die horen bij het zijn van "NMR verantwoordelijke". Ook wil ik Anja Palmans bedanken voor stimulerende discussies over de noodzaak van "computational chemistry" en de samenwerking betreffende het gedrag van ethyleen oxide gesubstitueerde self-assemblies. Natuurlijk kunnen we in deze lijst de synthetische vader van MST, Jef Vekemans niet vergeten. Bedankt voor het geduld dat je toonde tijdens mijn afstudeer periode en de vele

synthetische weetjes die later van pas kwamen. Voor een nuchtere en immers kritische kijk op de wetenschap kun je altijd even langs bij Appie “The Legend” Schenning die bovendien altijd in is voor een dolletje. I would also like to thank dr. Thorsten Felder and dr. Subi George for their collaborations on quadruple hydrogen bonding and OPV self-assemblies.

Freek Hoeben, Carel Fitié en Marko Nieuwenhuizen bedankt voor de leuke atmosfeer in de drukste kamer van MST! Ondanks het feit dat bijna alle ruimte in het kantoor ingenomen werd door mijn paperassen wisten jullie het altijd gezellig te maken en te houden. Mijn dank hiervoor!!

Wat is werken zonder dagelijkse afleiding? Hiervoor wil ik in het bijzonder het illustere Symochem duo Gaby van Gemert en Michel Fransen bedanken die altijd bereid waren om over de meest uiteenlopende zaken te kletsen.

Werken in een schoon en ordelijk lab helpt enorm in het doen van het dagelijkse werk. Hiervoor wil ik in het bijzonder Jolanda Spiering bedanken die hier vier jaar lang op bleef hameren. Furthermore, I would like to thank Evgeny Pidko for the help with all my questions regarding computational chemistry.

Met hulp van Hans Damen, Henk Eding, Angela Jones, Joke Rediker, Carine van der Vaart, Ingrid Dirkx en Hanneke Veldhoen was het bestellen van chemicaliën, het maken van elementanalyses, het regelen van postzaken, afspraken, reizen, computerzaken en vele andere kleine dingen altijd erg snel geregeld. Mijn dank hiervoor.

Papa en mama, bedankt voor alles! Jullie hebben mij altijd gesteund in alles wat ik deed. Pas als je ouder bent zie je dat het niet makkelijk is om iemand goed op te voeden maar ik kan met trots zeggen dat jullie het uitstekend gelukt is!!

Wat moet een mens zonder vrienden en familie? Ruud & Ilse, Pim & Eva, Sander & Kim, Bart, Roeland & Suus wil ik allemaal bedanken voor de vele avondjes gezelligheid in de afgelopen jaren. Ook de roemruchte jaren van Geldrop ‘t 9^e waarin de derde helft belangrijker was dan de eerste twee zijn niet te vergeten.

Lieve Marlies, jij kwam mijn leven binnen op een moment dat ik het totaal niet verwachtte. In een ontzettend korte tijd hebben we iets geweldigs opgebouwd met zijn tweetjes. Ook al was ik niet altijd even ontspannen in de afgelopen maanden, je stond altijd voor me klaar met veel geduld en een luisterend oor en hebt me menigmaal weer even met beide voeten op de grond gezet. Ik hou ontzettend veel van je en zal dat altijd blijven doen. Jij maakt mij ontzettend gelukkig!!

Tom